DISSERTATION

submitted to the

Combined Faculty of Natural Sciences and Mathematics

of the

Ruperto Carola University Heidelberg, Germany

for the degree of

Doctor of Natural Sciences

Presented by

M. Sc. Laura Llaó Cid

born in Sant Pere de Ribes, Spain

Oral examination: February 12th, 2021

CHARACTERIZATION OF THE T-CELL LANDSCAPE AND ITS FUNCTIONAL ROLE IN CHRONIC LYMPHOCYTIC LEUKEMIA

Referees:

Prof. Dr. Stefan Wiemann

Prof. Dr. Peter Lichter

‘*The great book, always open and which we should make an effort to read, is that of Nature*.’ - Antoni Gaudí i Cornet

Abstract

Chronic lymphocytic leukemia (CLL) is a lymphoid neoplasm characterized by an accumulation of mature B lymphocytes in blood and peripheral lymphoid organs which highly depend on a tumor-supportive microenvironment. Altered T-cell distribution and function have since long been observed in the CLL microenvironment, but the exact pathological role of the different T-cell subsets remains uncertain.

In the present work, the spectrum of CLL-associated T-cell phenotypes were investigated by using leading-edge single-cell technologies. Mass cytometry analyses of lymph nodes (LN), peripheral blood and bone marrow of CLL patients together with reactive lymph nodes (rLNs) of donors without cancer identified the CLL LN as a distinct niche, where $CD8^+$ effector memory T-cells with an exhausted phenotype accumulate. Single-cell transcriptome and TCR-clonality analyses of LN T-cells further revealed a clonal expansion restricted to effector memory $CD8^+$ T-cells, and enabled the characterization of the specific cross-talk between CLL cells and T-cell subsets. Besides, the single-cell transcriptome of T-cells from the Eμ-TCL1 mouse model of CLL was examined and shown to be similar to that of T-cells from CLL patients.

Since genome-wide association studies have identified that a single-nucleotide polymorphism affecting the T-cell master regulator *EOMES* is associated with CLL development, the role of this transcription factor in the disease was investigated. Epigenetic and single-cell RNA sequencing analyses revealed that *EOMES* is not expressed in CLL cells but in T-cells, and that its levels are highest in exhausted $CD8^+$ T-cells. Interestingly, *Eomes* deficiency in $CD8^+$ T-cells prevented their expansion and led to a decreased leukemia control in the TCL1 mouse model, providing a novel layer of evidence for an anti-tumor role of $CD8^+$ T-cells in CLL.

Furthermore, mass cytometry and single-cell RNA-sequencing analyses revealed an increase of T regulatory type 1 (T_R1) $CD4^+$ T-cells in CLL LNs compared to rLNs. Such accumulation was likewise confirmed in spleen of Eμ-TCL1 mice using flow cytometry. Strikingly, T_R1 cells failed to expand from *Eomes*-deficient $CD4^+$ T-cells adoptively transferred in leukemic mice, and consequently were less capable of controlling leukemia development. Moreover, T_R1 cell-mediated CLL control required IL-10 receptor signaling, as *Il10rb*$^{-/-}$ $CD4^+$ T-cells showed impaired anti-leukemia activity.

Taken together, the data generated herein comprehensively and deeply characterize the composition and phenotype of the T-cell compartment of CLL patients in comparison to individuals without cancer, and significantly improve our understanding of the function of distinct T-cell subsets in CLL.

Zusammenfassung

Chronisch lymphatische Leukämie (CLL) ist eine lymphoide Neoplasie, die durch eine Akkumulation reifer, maligner B-Lymphozyten charakterisiert ist, die stark von einer tumorunterstützenden Mikroumgebung abhängen. Eine veränderte T-Zellverteilung und funktionelle T-Zelldefekte wurden in der CLL-Mikroumgebung seit langem beobachtet, aber die spezifische pathologische Rolle der verschiedenen T-Zellsubpopulationen bleibt bisher unklar.

In der vorliegenden Arbeit wurde das Spektrum der CLL-assoziierten T-Zellphänotypen unter Verwendung modernster Einzelzellentechnologien analysiert. Massenzytometrieanalysen von Lymphknoten (LN), peripherem Blut und Knochenmark von Patienten mit CLL, sowie reaktiver Lymphknoten (rLNs) gesunder Spender charakterisierten die CLL LNs als eine spezifische Nische, in der sich $CD8^+$ Effektor-Gedächtnis-T-Zellen mit einem erschöpften Phänotyp ansammeln. Einzelzell-Transkriptom- und TCR-Zellrezeptor-Klonalitätsanalysen von Zellen aus LN zeigten, dass die klonale Expansion der $CD8^+$ T-Zellen auf die Effektor-Gedächtniszellen beschränkt ist, und ermöglichten die Charakterisierung der spezifischen Wechselwirkungen zwischen CLL-Zellen und den T-Zell-Subtypen. Außerdem wurde das Einzelzell-Transkriptom von T-Zellen aus dem Eμ-TCL1 Mausmodell für CLL untersucht und es wurde gezeigt, dass es dem von T-Zellen aus Patienten mit CLL ähnelt.

Da genomweite Assoziationsstudien gezeigt haben, dass ein Einzelnukleotid-Polymorphismus, der das T-Zell-Masterregulatorgen *EOMES* betrifft, mit der Entwicklung von CLL assoziiert ist, wurde die Rolle dieses Transkriptionsfaktors in CLL untersucht. Epigenetische Analysen und Einzelzell-RNA-Sequenzierungen ergaben, dass EOMES nicht in CLL-Zellen, sondern in T-Zellen exprimiert wird, und eine maximale Expression in erschöpften $CD8^+$ T-Zellen zeigt. Interessanterweise verhinderte das Fehlen von *Eomes* in $CD8^+$ T-Zellen deren Expansion im CLL-Mausmodell, was zu einer verminderten Leukämiekontrolle führte. Diese Daten unterstützen die Hypothese, dass $CD8^+$ T-Zellen eine Antitumor-Aktivität in CLL haben.

Darüber hinaus zeigten Massenzytometrie- und Einzelzell-RNA-Sequenzierungsanalysen eine Anhäufung von $CD4^+$ regulatorischen Typ 1 T-Zellen (T_R1) in CLL LNs im Vergleich zu rLNs. Eine solche Akkumulation wurde ebenfalls in der Milz von Eμ-TCL1 Mäusen unter Verwendung von Durchflusszytometrie bestätigt. Interessanterweise konnte keine Expansion von T_R1-Zellen aus *Eomes*-defizienten $CD4^+$ T-Zellen, die in Mäusen mit CLL injiziert wurden, beobachtet werden, was eine beschleunigte Leukämieentwicklung im Vergleich zu Tieren mit wildtyp T-Zellen zur Folge hatte. Darüber hinaus zeigten diese Studien, dass die T_R1-Zell-vermittelte Kontrolle von CLL im Mausmodell vom IL-10-Rezeptorsignalweg abhängt, da *Il10rb*-defiziente $CD4^+$ T-Zellen eine beeinträchtigte Anti-CLL-Aktivität aufwiesen.

Zusammengenommen charakterisieren die in dieser Arbeit generierten Daten in einer bisher nicht verfügbaren Tiefe und umfassenden Form die Zusammensetzung und den Phänotyp des T-Zell-Kompartiments bei CLL im Vergleich zu Individuen ohne Krebs und verbessern dadurch unser Verständnis der Funktion verschiedener T-Zell-Subpopulationen in CLL erheblich.

Table of contents

List of Figures

List of Tables

List of Abbreviations (A-Z)

AC	Absolute Counts
ADORA2A	Adenosine A2a Receptor
AKT1	AKT Serine/Threonine Kinase 1
APC	Antigen-Presenting Cell
APRIL	TNF Superfamily Member 13
AT	Adoptive Transfer
ATM	Ataxia Telangiectasia Mutated
BAFF	B-Cell Activating Factor
BCL-2	Selective B-Cell Lymphoma 2
BCR	B-Cell Receptor
BLIMP1	B Lymphocyte-Induced Maturation Protein 1
BM	Bone Marrow
BMSC	Bone Marrow Stromal Cell
BST2	Bone Marrow Stromal Cell Antigen 2
CAF	Cancer-Associated Fibroblast
CAR	Chimeric Antigen Receptor
CCL	C-C Motif Chemokine Ligand
CCR	C-C Chemokine Receptor Type
CD40L	CD40 Ligand
CDR3	Heavy Chain Complementarity-Determining Region 3
ChIP-seq	Chromatin Immunoprecipitation with Massively Parallel DNA Sequencing
CLL	Chronic Lymphocytic Leukemia
CMV	Cytomegalovirus
CTLA-4	Cytotoxic T-lymphocyte-Associated Protein 4
CXCL	C-X-C Motif Chemokine Ligand
CXCR	C-X-C Motif Chemokine Receptor
DC	Dendritic Cell
DMSO	Dimethyl Sulfoxide
DP	Double Positive
EBV	Epstein-Barr Virus
EOMES	Eomesodermin
FACS	Fluorescence-Activated Cell Sorting
FAS	Fas Cell Surface Death Receptor
FBS	Fetal Bovine Serum
FDC	Follicular Dendritic Cell
FMO	Fluorescence Minus One
FOXP3	Forkhead Box P3
FSC	Forward Sidescatter
GC	Germinal Genter
GEM	Gel Beads-in-Emulsion
GEX	5’ Gene Expression

GZM	Granzyme
HC	Healthy Control
HLA-DR	Human Leukocyte Antigen-DR Isotype
HSC	Hematopoietic Stem Cell
ICB	Immune Checkpoint Blockade
ICOS	Inducible T Cell Costimulator
ICOSL	ICOS Ligand
IDO1	Indoleamine 2,3-Dioxygenase 1
IFN	Interferon
Ig	Immunoglobulin
IGHV	Immunoglobulin Heavy Chain Variable Gene
IL	Interleukin
IL10R	IL-10 Receptor
IL4I1	Interleukin 4 Induced Gene 1
IL7R	IL-7 Receptor
IRF4	Interferon Regulatory Factor 4
KLRG1	Killer Cell Lectin Like Receptor G1
LAG3	Lymphocyte-Activation Gene
LAIR1	Leukocyte Associated Immunoglobulin Like Receptor 1
LILRB4	Leukocyte Immunoglobulin Like Receptor B4
LN	Lymph Node
MBL	Monoclonal B-Cell Lymphocytosis
MDSC	Myeloid-Derived Suppressor Cells
MFI	Mean Fluorescence Intensity
MHC	Major Histocompatibility Complex
MMP	Matrix Metalloproteinase
NCAM	Neural Cell Adhesion Molecule 1
NF-kB	Nuclear Factor-kB
NFAT	Nuclear Factor Of Activated T-Cells 1
NK	Natural Killer
NKG2D	Killer Cell Lectin Like Receptor K1
NLC	Nurse-Like Cell
NOTCH1	Notch Receptor 1
PB	Peripheral Blood
PBMC	Peripheral Blood Mononuclear Cells
PBS	Phosphate-Buffered Saline
PC	Principal Component
PCR	Polymerase Chain Reaction
PD-1	Programmed Cell Death 1
PDX	Patient-Derived Xenograft
PI3K	Phosphatidylinositol-3 Kinase
PMA	Phorbol Myristate Acetate
PRF1	Perforin 1
QC	Quality Control

ROS	Reactive Oxygen Species
RT	Reverse Transcription
SELL	Selectin L
SF3B1	Splicing Factor 3B Subunit 1
SIRPG	Signal Regulatory Protein Gamma
SLO	Secondary Lymphoid Organ
SNP	Single-Nucleotide Polymorphism
STAT3	Signal Transducer and Activator Of Transcription 3
t-SNE	T-Distributed Stochastic Neighbor Embedding
TAM	Tumor Associated Macrophages
TBET	T-box Transcription Factor 21
TCF7	Transcription Factor 7
TCL1	T-cell Leukemia/Lymphoma 1a
T_{CM}	Central Memory T-Cell
TCR	T-Cell Receptor
T_{EF}	Effector T-Cell
T_{EM}	Effector Memory T-Cell
T_{EX}	Exhausted T-Cell
TF	Transcription Factor
T_F	Follicular T-Cell
T_{FC}	Follicular $CD8^+$ T-Cell
T_{FH}	Follicular Helper $CD4^+$ T-Cell
TFS	Treatment-Free Survival
TGF	Tumor Growth Factor β
T_H	$CD4^+$ Helper T-Cell
T_{IFN}	Interferon-Responding T-Cell
TIGIT	T-Cell Immunoreceptor With Ig And ITIM Domains
TIM-3	T-Cell Immunoglobulin And Mucin-Domain Containing-3
TL	Tumor Load
T_M	Memory T-Cell
TME	Tumor Microenvironment
T_N	Naïve T-Cell
TNF	Tumor Necrosis Factor
TNFSF	Tumor Necrosis Factor Superfamily Member
TOX	Thymocyte Selection Associated High Mobility Group Box
T_R1	$CD4^+$ Type 1 Regulatory T-Cells
TRAIL	TNF-Related Apoptosis-Inducing Ligand
T_{TOX}	Cytotoxic T-Cell
UMI	Unique Molecular Identifier
VCAM1	Vascular Cell Adhesion Molecule 1
VEGF	Vascular Endothelial Growth Factor
WT	Wild Type
ZAP-70	Zeta Chain Of T-Cell Receptor Associated Protein Kinase 70

1 Introduction

1.1 The tumor microenvironment as a hallmark of cancer

Over the last decades, it became clear that the process of tumorigenesis not only encompasses cancer cells, but also the complex surrounding tissue, composed of multiple cell types. Consequently, in the revised description of the 'hallmarks of cancer' first proposed by Douglas Hanahan and Robert A. Weinberg, adaptations of the tumor microenvironment that help promote tissue inflammation and avoid immunosurveillance are also considered as part of the multistep process that enables tumor development and metastasis (Hanahan and Weinberg 2011).

The cells present in the tumor microenvironment (TME) can generally be divided into three types: infiltrating immune cells, cancer-associated fibroblasts (CAFs), and angiogenic vascular cells (comprising endothelial cells and pericytes) (Hanahan and Coussens 2012). Each group contributes to supporting tumor initiation, growth, and dissemination by helping sustain proliferative signaling, evading growth suppressors, inducing angiogenesis and metabolism reprogramming, activating invasion and metastasis, as well as escaping immune destruction (Hanahan and Coussens 2012). As an example, the mechanisms by which endothelial cells promote the formation of new blood vessels that help provide oxygen and nutrients to cancer cells has been extensively described (Folkman 1974; Folkman et al. 1989; Butler et al. 2010). Besides, while normal fibroblasts serve as epithelial tumor growth suppressors (Bissell and Hines 2011), CAFs promote loosening of cell-cell contacts and increase tumor cell motility that facilitates metastasis (Kalluri and Zeisberg 2006). Tumor-infiltrating immune cells operate in the TME in opposing ways, as leukocytes with both anti- and pro-tumorigenic properties can be found within the tumor. The major mechanisms by which immune cells and tumor cells interact and influence each other are summarized in the succeeding Sections 1.1.1 and 1.1.2.

1.1.1 Tumor-promoting inflammation

As part of the repair process in normal tissues, pro-inflammatory cues that promote cell proliferation are strictly followed by anti-inflammatory mechanisms ensuring homeostasis restoration (Medzhitov 2008). Instead, during chronic inflammation, the initiating factors persist and the mechanisms to resolve the inflammatory response fail, contributing to the onset of neoplastic lesions. In this line, under the observation that tumors are an aberrant and prolonged form of tissue growth and repair, Dvorak defined tumor as 'wounds that do not heal' (Dvorak 1986). Tumor development is, in fact, often linked to chronic infection, obesity, inhalation of pollutants, tobacco consumption or autoimmunity, conditions in which the underlying common factor is chronic inflammation (Jemal et al. 2010; Elinav et al. 2013). The

influence of inflammatory signals on carcinogenesis involves several processes that promote proliferation and survival signaling, as well as genomic destabilization. More specifically, cytokines secreted by infiltrating immune cells, including interleukin (IL) 6 (IL-6) and IL-1 together with tumor necrosis factor (TNF), induce signal transducer and activator of transcription 3 (STAT3) and nuclear factor-κB (NF-κB) respectively, thereby leading to cell cycle progression and inhibition of apoptosis (Greten et al. 2004; Pikarsky et al. 2004; Karin and Greten 2005; Yu et al. 2009; Grivennikov et al. 2010). At the same time, increased DNA damage can be induced by elevated levels of reactive oxygen species (ROS) and reactive nitrogen species (RNS), released by activated neutrophils and macrophages (Campregher et al. 2008). Similarly, several cytokines such as TNF, IL-1β, IL-4, IL-13, and tumor growth factor β (TGF-β) promote the ectopic expression of activation-induced cytidine deaminase (AID), which induces genomic instability and may entail mutations in critical cancer genes like *TP53* and *MYC* (Okazaki et al. 2007; Colotta et al. 2009; Takai et al. 2009). Besides, mismatch repair factors, that are necessary for DNA repair, can be repressed by hypoxia-inducible factor 1α (HIF-1α), the expression of which is induced by TNF, IL-1β and ROS (Colotta et al. 2009; Schetter et al. 2010).

Importantly, tumor cells themselves modulate their microenvironment via soluble mediators, thus shaping the inflammatory response. Recruited leukocytes, from both myeloid and lymphoid lineages are skewed to support cancer cell survival and proliferation, angiogenesis as well as metastasis, and at the same time suppress anti-tumor responses (Hanahan and Coussens 2012). For example, tumor associated macrophages (TAMs) – a significant component of the TME in many cancers – produce numerous angiogenic factors, like vascular endothelial growth factor (VEGF), implicated in vessel formation (Ono et al. 1999; Torisu et al. 2000). In addition, together with mast cells and neutrophils, they secrete matrix metalloproteinases (MMPs), which degrade components of the extracellular matrix and thus favor tumor spread and metastasis (Coussens et al. 2000; Egeblad and Werb 2002; Nozawa et al. 2006; Pahler et al. 2008).

1.1.2 Cancer immunosurveillance and immunoediting

As previously mentioned, infiltrating immune cells can also exert an anti-tumor response. Known as tumor immune surveillance, the process by which the immune system detects and eliminates tumor cells has been studied for decades (Burnet 1957; Burnet 1970; Dunn et al. 2002). Historically, the first evidence for the role of cellular immunity in preventing malignant growth came from the increased incidence of spontaneous tumors in immunodeficient mice as well as in immunosuppressed patients (Penn and Starzl 1970; Gatti and Good 1971; Sheil 1986; Shankaran et al. 2001; Street et al. 2001). Additionally, tumor infiltration by lymphocytes (particularly $CD8^+$ T-cells and natural killer (NK) cells) positively correlates with increased

patient survival in several tumor entities, such as melanoma, breast, bladder, colon and prostate cancer (Epstein and Fatti 1976; Clark et al. 1989; Rilke et al. 1991; Lipponen et al. 1992; Naito et al. 1998). The mechanism by which the immune system is able to recognize and kill tumor cells is based on the integrated response of both its innate and adaptive arms. This process is initiated when innate immune cells become 'alerted' to the presence of a growing tumor by inflammatory signals (Matzinger 1994; Smyth et al. 2006). NK cells, macrophages, $\gamma\delta^+$ T-cells, and NKT-cells are recruited to the tumor site and recognize molecules such as the stress-induced ligand for killer cell lectin like receptor K1 (also known as NKG2D) (Girardi et al. 2001; Gasser et al. 2005; Strid et al. 2008). This initial immune response is mediated and amplified via secretion of several cytokines, including IL-12 and interferon gamma (IFNγ) (Bancroft et al. 1991; Hodge-Dufour et al. 1997; MacMicking et al. 1997). The latter induces macrophages to express tumoricidal molecules like ROS, and activates NK cells, which in turn, kill tumor cells via TNF-related apoptosis-inducing ligand- (TRAIL) or perforin-dependent mechanisms (Schreiber et al. 1983; MacMicking et al. 1997; Smyth et al. 2001; Takeda et al. 2001; Hayakawa et al. 2002). In parallel, an adaptive immune response is driven by the presence of tumor antigens. These include differentiation antigens (like melanocyte differentiation antigen), products of mutated genes (such as *TP53*), overexpressed genes (like *HER2*), or carcinogenic infectious antigens (like human papillomavirus proteins) (Cheever et al. 2009; Schreiber et al. 2011). Cytokine-activated dendritic cells acquire and present these tumor antigens to T-cells in the lymph nodes (LNs) (Huang et al. 1994; Wculek et al. 2020). Upon antigen recognition, activated $CD4^+$ T helper cells 1 (T_H1) and cytotoxic $CD8^+$ T-cells subsequently participate in the killing of tumor cells. $CD4^+$ T_H1 cells achieve this by providing help in activating and polarizing other immune cells, whereas $CD8^+$ T-cells directly kill tumor cells inducing granule exocytosis- and death receptor-mediated apoptosis (de Visser et al. 2006; Zhu and Paul 2008; Halle et al. 2017).

The coexistence of tumor-promoting inflammation and protective tumor immunity can be explained as a dynamically interconnected process named 'cancer immunoediting' (Dunn et al. 2002) (Figure 1). In short, cancer immunoediting consists of three phases (elimination, equilibrium and escape), where tumor progression is promoted by either a Darwinian selection of the fittest tumor cells, and/or by establishing conditions in the TME that facilitate tumor outgrowth (Dunn et al. 2002). In the elimination phase, both innate and adaptive immunity cooperate to eliminate developing tumors. If a malignant cell escapes, it may enter an equilibrium phase, where the tumor is maintained in a state of dormancy, as its outgrowth is controlled by immunologic mechanisms (Aguirre-Ghiso 2007). In such a situation, which can be sustained for years, tumor editing occurs, eventually leading to a selection of tumor cells than can escape immune recognition, become insensitive to immune

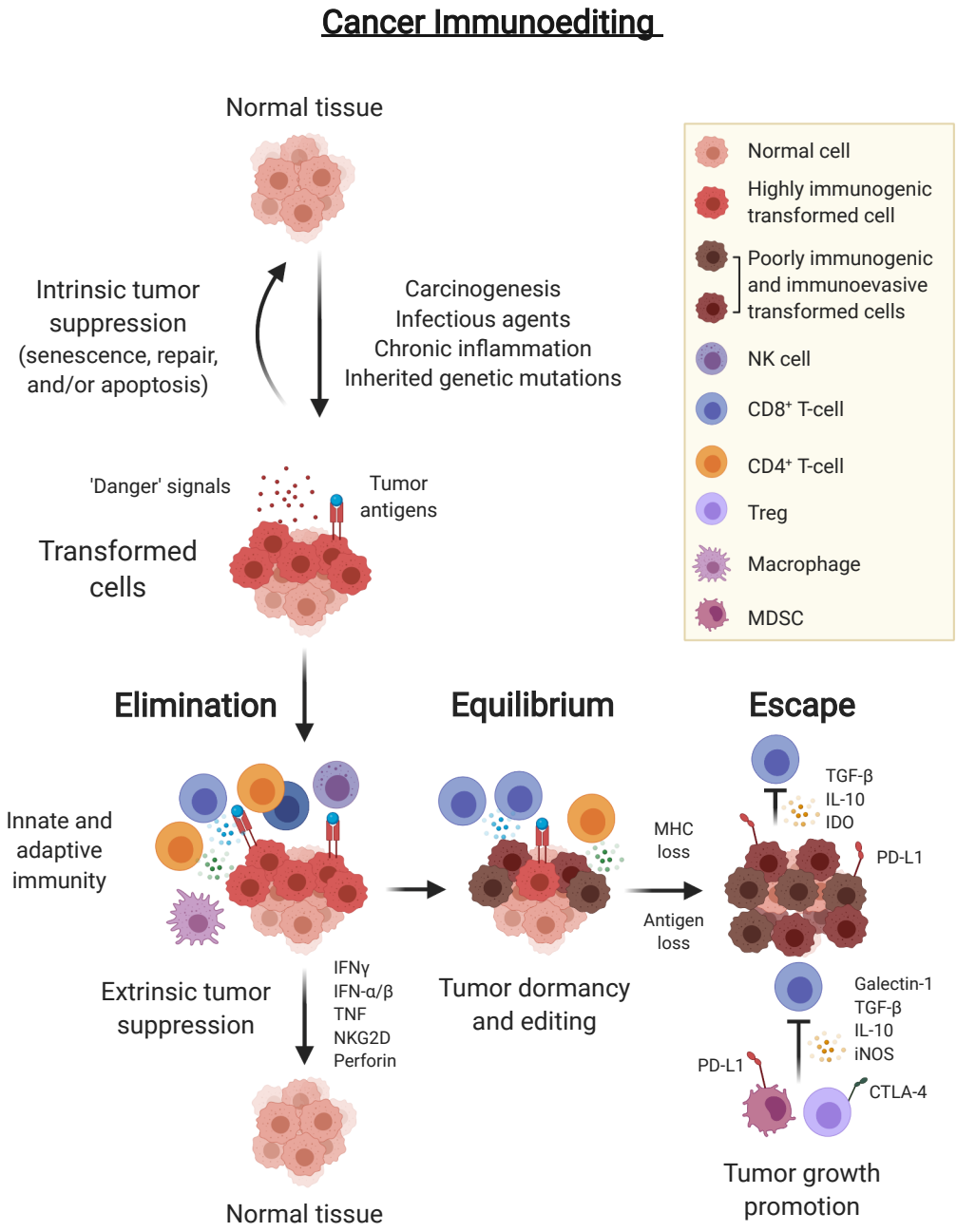

Figure 1: The three phases of cancer immunoediting. Normal cells can be transformed into tumor cells as a result of acquired oncogenic mechanisms and the failure of intrinsic tumor-suppressor mechanisms. In the elimination phase, previously known as cancer immunosurveillance, innate and adaptive immunity recognize and destroy tumor cells via secretion of effector molecules like IFNγ, IFN-α/β, TNF, NKG2D and perforin. However, if the elimination of tumor cells is incomplete, the tumor enters an equilibrium phase, where outgrowth is controlled by adaptive immunity and the tumor remains in state of dormancy. During this phase, tumor cells undergo a process of immunoediting, which eventually allows them to evade tumor recognition, killing or control by immune cells and become a progressive and clinically detectable tumor (the escape phase). CTLA-4 = cytotoxic T lymphocyte associated protein 4, IDO = indoleamine 2,3-deoxygenase, IFN = interferon, IL = interleukin, TNF = tumor necrosis factor, PD-L1 = programmed death-ligand 1, TGF-β = transforming growth factor β, iNOS = inducible nitric oxide synthase, NK = natural killer cell, MDSC = myeloid derived suppressor cell, Treg = regulatory T-cell. Figure modified from Vesely et al. 2011 using BioRender.com.

effector function, or induce immunosuppression within the TME. Upon acquisition of any of these abilities, the tumor enters the escape phase, and emerges as a progressively growing and visible tumor (Schreiber et al. 2011) (Figure 1).

Escaping tumor cells are able to interfere with the antitumor immune response via multiple mechanisms that ultimately allow them to evade cell killing and reprogram the immune cells into an immunosuppressive phenotype. Intrinsic mechanisms include the downregulation of major histocompatibility complex (MHC) molecules or upregulation of apoptosis inhibitors like B-cell lymphoma-extra large (BCL-XL) and CASP8 and FADD like apoptosis regulator (CFLAR) (Kataoka et al. 1998; Hinz et al. 2000). By secreting soluble factors like VEGF, they can also suppress dendritic cell maturation and thus prevent them to present tumor antigens in the LNs (Gabrilovich et al. 1999). In addition, secretion of immunosuppressive cytokines including TGF-β, galectin and IL-10, of other molecules like indoleamine 2,3-dioxygenase 1 (IDO1), or expression of ligands such as programmed death-ligand 1 (PD-L1), directly impact T-cell function by inhibiting their activation and proliferation, or by inducing apoptosis (Vesely et al. 2011). Moreover, tumor cells recruit and modulate regulatory T-cells (Tregs) and myeloid-derived suppressor cells (MDSCs), the two major immunosuppressive leukocyte populations (Gabrilovich and Nagaraj 2009; Facciabene et al. 2012). Tregs produce IL-10, TGF-β, and express T-cell co-inhibitory molecules like PD-L1 and cytotoxic T-lymphocyte-associated protein 4 (CTLA-4) (Terabe and Berzofsky 2004; Facciabene et al. 2012). MDSCs, which comprise a heterogeneous group of myeloid cells, also inhibit lymphocyte function by several mechanisms. They produce TGF-β and IL-10, deprive the TME of arginine or cysteine, needed by T-cells to proliferate (Gabrilovich and Nagaraj 2009), and produce arginase and inducible nitric oxide synthase (iNOS) that inhibit T-cell function (Bronte and Zanovello 2005; Rodriguez and Ochoa 2008).

Importantly, as the understanding of the cancer immunoediting process improves, therapeutic strategies that target molecular players from each of the three phases are being developed. More specifically, substantial work has been invested into developing immunotherapies that aim to increase the quality and quantity of immune effector cells and/or eliminate the tumor-induced immunosuppression. These include, for example, vaccines that elicit strong and specific immune responses against tumor antigens (Thomas and Prendergast 2016; Sahin and Tureci 2018). Additionally, approaches involving the adoptive transfer of *in vitro* expanded or genetically engineered tumor-specific lymphocytes (such as chimeric antigen receptor (CAR) T-cell products) are currently being investigated and have shown promising outcomes in high-grade B-cell malignancies (Dudley et al. 2002; Rosenberg et al. 2011; Labanieh et al. 2018; Majzner and Mackall 2019). Last, methodologies that inhibit or eliminate the molecular or cellular mediators of cancer-induced immunosuppression are being developed, including the antibody-based blockade of immune-checkpoint receptors like

programmed cell death 1 (PD-1)/PD-1 ligand (PD-L1) and CTLA-4, or the targeting and depletion of Tregs. (Leach et al. 1996; Iwai et al. 2002; Hodi et al. 2010; Topalian et al. 2012; Sharma and Allison 2015).

1.1.3 T-cell exhaustion in cancer

During acute infection, antigen-presenting cells (APCs) exhibit pathogen-derived antigen peptides through the MHC type I complex, which binds to the T-cell receptor (TCR) of naïve $CD8^+$ T-cells. Upon selective recognition of the MHC-antigen complex together with co-stimulatory signals, T-cells get activated, clonally expand, and differentiate into effector cells. They express cytotoxic molecules, like perforin and granzymes, and secrete cytokines like IFNγ and TNFα to ultimately kill target cells. Once the antigen is cleared, most effector $CD8^+$ T-cells undergo apoptosis, and only a small fraction differentiates into memory cells. Memory $CD8^+$ T-cells persist in the absence of antigens and can rapidly expand and exert effector functions in response to antigen re-exposure (Wherry and Ahmed 2004; Williams and Bevan 2007) (Figure 2).

In contrast, during chronic viral infection and cancer, where the immune response fails and antigen exposure persists, effector T-cells become ‘exhausted’, a dysfunctional state that renders them uncapable of eradicating the infection or tumor. The acquisition of such phenotype is considered an evolutionarily conserved adaptation to chronic antigen presence and TCR stimulation (Blank et al. 2019). In other words, it represents a compromise between the need of the organism to resolve the tumor or infection and the amount of inflammation-induced damage that it can tolerate (Speiser et al. 2014). Exhausted T-cells (T_{EX}) are characterized by a reduced capacity to secrete cytokines and effector molecules, and express higher levels of inhibitory receptors, including PD-1, CTLA-4, T-cell immunoglobulin and mucin-domain containing-3 (TIM-3), lymphocyte-activation gene 3 (LAG3), and T-cell immunoreceptor with Ig and ITIM domains (TIGIT) (Wherry 2011). Recently, high levels of the ectoenzyme ectonucleoside triphosphate diphosphohydrolase-1 (CD39) that converts extracellular ATP and ADP into AMP have been reported in tumor-reactive T_{EX} cells (Gupta et al. 2015; Simoni et al. 2018). Besides, these hyporesponsive cells are distinct from anergic and senescent T-cells, with an aberrant transcriptional program, a dysregulated metabolism, and a unique epigenetic landscape (Wherry et al. 2007; Alfei and Zehn 2017; McLane et al. 2019) (Figure 2). Chronic TCR stimulation is the main driver of T-cell exhaustion, as evidenced by the role of TCR signaling-driven transcription factors in upregulating the expression of inhibitory receptors, and at the same time maintaining the long-term survival of T_{EX} cells. This includes TFs like the nuclear factor of activated T-cells 1 (NFATC1), interferon regulatory factor 4 (IRF4), basic leucine zipper ATF-like transcription factor (BATF), nuclear receptor subfamily

4 group (NR4A), and thymocyte selection associated high mobility group box (TOX) (Martinez et al. 2015; Man et al. 2017; Chen et al. 2019; Khan et al. 2019; Yao et al. 2019).

Besides, soluble mediators have been shown to promote exhaustion, including IL-10 and TGF-β (Li et al. 2006; Brooks et al. 2008; Tinoco et al. 2009; Ni et al. 2015) (Figure 2). To date, T_{EX} cells have been described in tumor mouse models and in numerous cancer entities, including melanoma, chronic myeloid leukemia, non-small cell carcinoma, colorectal cancer, ovarian cancer, Hodgkin lymphoma, and chronic lymphocytic leukemia (Mumprecht et al. 2009; Matsuzaki et al. 2010; Zhang et al. 2010; Baitsch et al. 2011; Riches et al. 2013; Schietinger et al. 2016; Zhang et al. 2018b).

Single-cell RNA sequencing and mass cytometry analyses have recently shown that T_{EX} cells represent a heterogeneous population with a gradual degree of dysfunction (van der Leun et al. 2020). Moreover, a subset of PD-1^+ precursor cells with self-renewal capacity that gives rise to the terminally differentiated T_{EX} population has been identified in mouse models of chronic viral infection and cancer (Paley et al. 2012; Im et al. 2016; Utzschneider et al. 2016; Siddiqui et al. 2019) (Figure 2). These progenitors of exhausted cells are characterized by lower levels of PD-1, depend on the transcription factor T-cell factor 7 (TCF7), and express slam family member 6 (SLAMF6), as well as C-X-C chemokine receptor type 5 (CXCR5) (Im et al. 2016; Utzschneider et al. 2016; Brummelman et al. 2018; Miller et al. 2019; Siddiqui et al. 2019). Aside from the expression of such TFs, their gene expression profile is similar to that of $CD8^+$ memory precursor cells, $CD4^+$ follicular helper T-cells (T_{FH}), and hematopoietic stem cells (Wu et al. 2016b; Hashimoto et al. 2018). They can additionally be distinguished from the terminally exhausted subset based on the expression of the transcription factors Eomesodermin (EOMES) and T-box transcription factor 21 (or also known as TBET): precursor cells are PD-1^{int} $TBET^{hi}$, whereas terminally differentiated T_{EX} are PD-1^{hi} $EOMES^{hi}$ (Paley et al. 2012). Evidence of their progenitor potential comes from experiments showing that, upon adoptive transfer into virus-infected or tumor-bearing mice, these cells can proliferate and generate terminally differentiated T_{EX} cells. Instead, the latter only expand to a limited extent and retain the same PD-1^{hi} terminally differentiated phenotype (Im et al. 2016; Utzschneider et al. 2016; Wu et al. 2016b; Sade-Feldman et al. 2018; Kurtulus et al. 2019; Siddiqui et al. 2019). Crucially, mouse experiments showed that precursor cells are necessary for the response upon PD-1 blockade (Im et al. 2016; Utzschneider et al. 2016; Kurtulus et al. 2019; Miller et al. 2019). While αPD-1 therapy does not alter the distinct epigenomic state of T_{EX} cells and, thus, only restores their effector function transiently, it induces the proliferation and differentiation of precursor cells into terminally differentiated T_{EX} cells (Pauken et al. 2016; Miller et al. 2019).

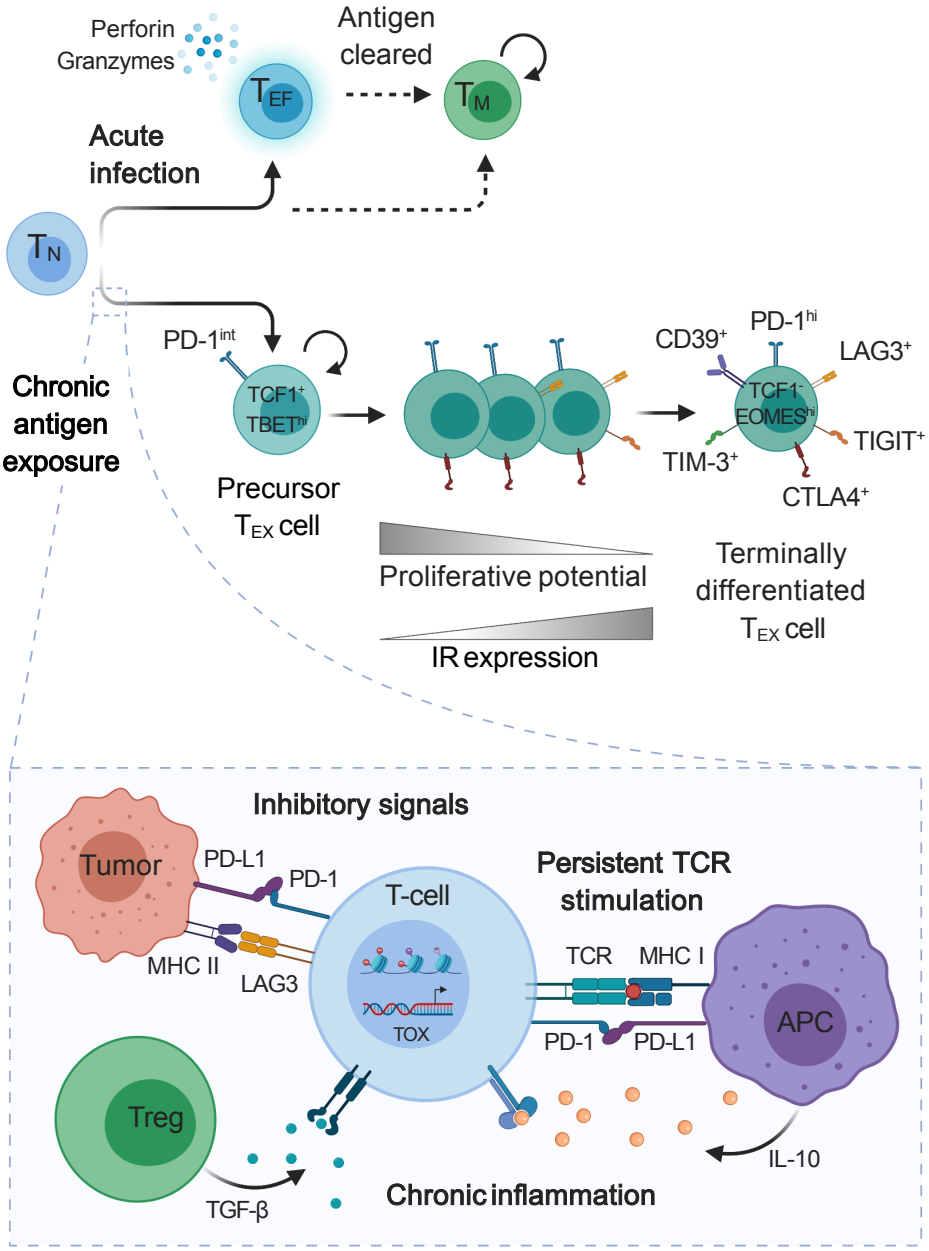

Figure 2: Development of CD8$^+$ T-cell exhaustion. During initial viral infection, naïve CD8$^+$ T-cells become activated upon antigen recognition, proliferate and differentiate into effector T-cells to kill infected target cells. Once the pathogenic agent is cleared, effector T-cells undergo apoptosis and only a small population of memory T-cells (T_M) persists (top). In case of chronic viral infection or cancer, effector T-cells gradually acquire an exhausted phenotype with reduced proliferation and effector function, and increased expression of inhibitory receptors (IRs). Within the heterogeneous population of exhausted cells, precursor cells (PD-1^{int} TCF1$^+$ TBET^{hi}) have self-renewal capacity and give rise to terminally differentiated T_{EX} cells (PD-1^{hi} TCF1$^-$ EOMES^{hi}) (middle). Described factors involved in the induction of an exhaustion phenotype are a persistent antigen presentation by APCs and subsequent TCR stimulation. Besides, inhibitory receptors provide negative signals to T-cells, preventing a normal T-cell effector response. Additionally, immunoregulatory cells, APCs and tumor cells contribute to a persistent state of inflammation by secreting inhibitory cytokines (like IL-10 or TGF-β) that further contribute to exhaustion. Altogether these signals contribute to the distinct transcriptional and epigenetic state of T_{EX} cells, driven by transcription factors such as TOX. IR = inhibitory receptor. Figure created with BioRender.com.

Even though the altered pathways and the molecular mechanisms leading to T-cell exhaustion are not completely understood, the knowledge acquired up until today has unveiled many potential opportunities for therapeutic interventions. For example, the combination of checkpoint inhibitors with agents targeting other co-inhibitory molecules (like LAG3, TIGIT, or CD39), soluble factors, or epigenetic programs represents a promising approach for improving immunotherapy outcomes (Jin et al. 2010; Johnston et al. 2014; Zhang et al. 2014; Chauvin et al. 2015). Finally, current efforts focus on elucidating how the re-invigoration of T-cell responses upon checkpoint blockade can be improved and prolonged to achieve a complete eradication of tumor cells in cancer patients (Hashimoto et al. 2018; Blank et al. 2019).

1.1.4 $CD4^+$ type 1 regulatory T-cells (T_R1) and their role in cancer

$CD4^+$ T-cells comprise several subsets of cells with distinct phenotypes and functions. Generally, they can be divided into conventional $CD4^+$ T-cells and regulatory cells (Tregs) expressing forkhead box protein P3 (FOXP3). Conventional $CD4^+$ T-cells are also referred to as $CD4^+$ T helper (T_H) cells and assist in the polarization and activation of other immune cells by establishing direct ligand-receptor interactions as well as releasing cytokines (Zhu et al. 2010)). Depending on the cytokines they produce and the expression pattern of their surface molecules, activated T_H cells can be differentiated into T_H1, T_H2 and T_H17, each having a distinct impact on the cellular and humoral immune response (Zhu et al. 2010). Instead, Tregs are specialized to suppress the immune response, in order to restore tissue homeostasis and maintain self-tolerance (Romano et al. 2019).

In addition to Tregs, $CD4^+$ type 1 regulatory T-cells (T_R1) have been identified as another suppressive T-cell type. These T_R1 cells were first described more than thirty years ago by Groux et al. as an IL-10-producing $CD4^+$ T-cell subset that suppressed antigen-specific T-cell responses but was FOXP3-negative (Groux et al. 1997). Aside from IL-10, T_R1 cells express the surface markers PD-1, LAG3, and CD49b, yet they represent a heterogeneous population and the expression of any of these markers is not exclusive to these cells (Akdis et al. 2004; Gagliani et al. 2013; Okamura et al. 2015; Roncarolo et al. 2018). T_R1 cells are induced by IL-10 receptor signaling and TCR activation, but the molecular mechanisms underlying their development are not completely understood, and only recently, B lymphocyte-induced maturation protein 1 (*BLIMP1*), c-MAF, aryl hydrocarbon receptor (AHR), and EOMES TFs have been shown to promote a T_R1 cell phenotype (Quintana et al. 2008; Pot et al. 2009; Heinemann et al. 2014; Zhang et al. 2017; Roncarolo et al. 2018). T_R1 cells induce immune suppression through several mechanisms. These include the secretion of cytokines such as IL-10 and TGF-β (de Waal Malefyt et al. 1991; Levings et al. 2001; Gregori et al. 2010; Roncarolo et al. 2014), as well as the expression of PD-1 and CTLA-4, which inhibits the function of both T-cells and APCs (Akdis et al. 2004; Okamura et al. 2015; Facciotti et al.

2016). Besides, they disrupt T-cell metabolism by CD39 and CD73 expression, and directly kill APCs via secretion of granzyme B (GZMB) and perforin 1 (PRF1), thus preventing the latter to promote T-cell activation (Tree et al. 2010; Magnani et al. 2011).

Notably, high frequencies of T_R1 cells have been described in some tumor entities such as head and neck squamous cell carcinoma, liver cancer, and metastatic melanoma (Bergmann et al. 2008; Pedroza-Gonzalez et al. 2015; Yan et al. 2017). Moreover, a highly suppressive function of these cells was observed in Hodgkin's lymphoma, head and neck squamous cell carcinoma, and hepatocellular carcinoma (Dennis et al. 2013; Roncarolo et al. 2018). However, the limited available data on their presence and function in cancer emphasizes the need for additional studies to help address the question whether T_R1 cells play a similar role in other malignancies such as leukemia.

1.2 Chronic Lymphocytic Leukemia (CLL)

1.2.1 Epidemiology, diagnosis and clinical staging

Chronic lymphocytic leukemia (CLL) is one of the most prevalent leukemias in western countries, with an estimated age-adjusted incidence rate of 4.6 newly diagnosed cases per year per 100,000 people in the US (Howlader N 2017). It affects mostly elderly people, with a median age of 72 at diagnosis, and higher prevalence in males than females (male/ female ratio of 1.7:1) (Howlader N 2017).

According to the 2008 World Health Organization criteria, CLL is diagnosed by lymphocytosis with more than 5,000 B lymphocytes per microliter in peripheral blood (PB) (Swerdlow et al. 2016). The leukemia cells are characteristically small and phenotypically mature when inspected in blood smears, and flow cytometric or immunohistochemical analyses distinguish them from other types of lymphoma by the co-expression of CD19, CD20, CD23, and the T-cell antigen CD5 (Kipps et al. 2017; Hallek et al. 2018). Patients with CLL can also present symptoms of autoimmune cytopenia, develop lymphadenopathy, hepatomegaly and splenomegaly (Nabhan and Rosen 2014). The majority of patients, however, are asymptomatic at the time of diagnosis, and the clinical course is highly variable, ranging from remaining symptom-free for decades, to rapidly developing symptoms or high-risk disease that requires treatment (Kipps et al. 2017).

Disease staging is performed according to the Rai (0, I/II, and III/IV) and Binet (A, B and C) systems (Rai et al. 1975; Binet et al. 1981). Both of them classify patients into low, intermediate, and high risk according to similar clinical features including lymphocytosis, lymphadenopathy, anemia and thrombocytopenia (Rai et al. 1975; Binet et al. 1981). The Rai staging system is more commonly used in the US, whereas the Binet classification is regularly applied in Europe (Kipps et al. 2017). While the two staging systems help to stratify patients, additional biomarkers are routinely measured to provide valuable prognostic information

(Hallek et al. 2018; Parikh 2018). Factors associated with poorer outcome include expression of zeta chain of T-cell receptor associated protein kinase 70 (ZAP-70), CD38, and CD49d by leukemia cells (Damle et al. 1999; Orchard et al. 2004; Rassenti et al. 2004; Shanafelt et al. 2008), cytogenetic lesions (further discussed in the Section 1.2.3), as well as elevated levels of soluble β_2-microglobulin and thymidine kinase in serum (Hallek et al. 1996; Pflug et al. 2014). Patients are also stratified based on the degree of somatic mutations in the immunoglobulin (Ig) heavy chain variable gene (*IGHV*) expressed by the CLL cells (Damle et al. 1999; Hamblin et al. 1999). Patients with mutated *IGHV*, which is defined as a greater than 2% difference from the germline sequence, have a higher median overall survival than those with unmutated *IGHV* (Damle et al. 1999; Hamblin et al. 1999). These two groups of patients also harbor differences in the underlying tumor genetic lesions, the degree of clonal evolution, epigenetic changes, and active signaling pathways present in the leukemia cells, as well as in the kind of interactions established within the tumor microenvironment (Allsup et al. 2005; Herve et al. 2005; Fabbri and Dalla-Favera 2016; Ten Hacken and Burger 2016). In fact, these profound divergences between *IGHV*-unmutated and -mutated patients have been suggested to relate to a different cell of origin of the leukemia (Fabbri and Dalla-Favera 2016).

1.2.2 The cellular origin of CLL

1.2.2.1 Normal B-cell development

B lymphocyte development and maturation is a tightly regulated, multistep process. It is initiated in the bone marrow (BM), where hematopoietic stem cells (HSCs) give rise to common lymphoid progenitor cells, that in turn differentiate into B-cell or T-cell lineages (De Obaldia and Bhandoola 2015; Melchers 2015). In a specific niche that influences the process, pro-B-cells transition to pre-B-cells by undergoing a stepwise recombination of immunoglobulin variable region genes, prior to the assembly of the complete B-cell receptor (BCR) genetic locus (Brack et al. 1978; Schatz et al. 1989; Melchers 2015). After this, each B-cell expresses a unique BCR, and those showing high affinity against self-antigens (which is estimated to be 75 % of B-cells (Wardemann et al. 2003)) undergo additional rounds of receptor editing, or, upon failure, are eliminated by apoptosis induction (LeBien 2000; Cambier et al. 2007). Immature B-cells leave the BM and migrate to the B-cell follicles within the secondary lymphoid organs (SLOs), i.e. LNs and spleen. Upon antigen encounter, B-cells get activated and engage in an intricate cross-talk with surrounding cells forming the germinal centers (GCs), which results in their expansion, diversification, and differentiation to express high-affinity BCRs (Victora and Nussenzweig 2012; Pieper et al. 2013). More specifically, B-cells enter the dark zone of the GCs and experience rapid proliferation and somatic hypermutation, the process in which point mutations are introduced in the *IGHV* and the immunoglobulin light chain V region (*IGLV*) genes to increase the immunoglobulin repertoire diversity (Methot and Di Noia 2017).

In the light zone, those B-cells expressing BCRs with the highest antigen affinity are positively selected, expand, and may undergo class switch recombination, replacing IgM and IgD with IgA, IgG, or IgE (Methot and Di Noia 2017). Ultimately, B-cells differentiate into either memory B-cells, which can rapidly respond to microbial antigens upon re-encounter, or long-lived antibody-secreting plasma cells (Shapiro-Shelef and Calame 2005; Klein and Dalla-Favera 2008).

The majority of B-cells that reside in SLOs, including follicular B-cells (also named B-2), and marginal zone B-cells, originate from the above-described developmental process, and are central to adaptive immune responses (Wang et al. 2020). A third type of B-cells, instead, is part of the innate immune system, and derives from progenitor cells found in the fetal liver (Baumgarth 2017; Wang et al. 2020). These so-called B-1 cells, which are $CD5^+$, are mostly present in the peritoneal and pleural cavities, and constitute a major source of antibodies, produced without the 'help' from T-cells. Of note, even though transitional and mature $CD5^+$ B-cells have been identified in human PB, these cells have predominantly been described in mice, and their origin and role in humans is poorly understood (Baumgarth 2017).

1.2.2.2 The putative cell of origin of CLL

The exact B-cell phenotype from which CLL cells originate remains controversial (Forconi et al. 2010; Chiorazzi and Ferrarini 2011). Some of the genetic and epigenetic lesions leading to CLL development may already occur in hematopoietic stem cells (HSCs), as evidenced by several studies (Fabbri and Dalla-Favera 2016) (Figure 3). For example, HSCs from CLL patients engrafted in immunodeficient mice generate clonal B-cells, and are frequently $CD5^+$ and $CD23^+$, similarly to CLL cells (Kikushige et al. 2011). Besides, common mutations present in CLL cells have been found in multipotent progenitor cells from CLL patients, and clonal hematopoiesis has been linked to an increased risk of developing CLL (Damm et al. 2014; Genovese et al. 2014; Jaiswal et al. 2014). The characteristic expression of CD5 on CLL cells led to the conception, for decades, that CLL cells derive from the B-1 lineage (Stall et al. 1988; Caligaris-Cappio 1996). In addition, $CD5^+$ B-1 cells of neonatal origin give rise to a CLL-like disease with restricted BCRs and up-regulated *c-Myc* expression in aged mice (Hayakawa et al. 2016). However, several studies have demonstrated that CLL cells have transcriptional and phenotypic characteristics that are incompatible with a B-1 lineage. Klein et al. and others showed that the gene expression profile of CLL cells is largely homogeneous – irrespective of the *IGHV* mutation status – and similar to that of antigen-experienced $CD27^+$ memory B-cells (Klein et al. 2001; Rosenwald et al. 2001; Seifert et al. 2012). Moreover, subsets of circulating $CD27^+$ memory-like B-cells with mutated and unmutated *IGHV* genes have been described (Klein et al. 1998). Collectively, these results support the idea that *IGHV*-mutated CLL derives from antigen-experienced, T-cell dependent, post-GC memory B-cells that have undergone

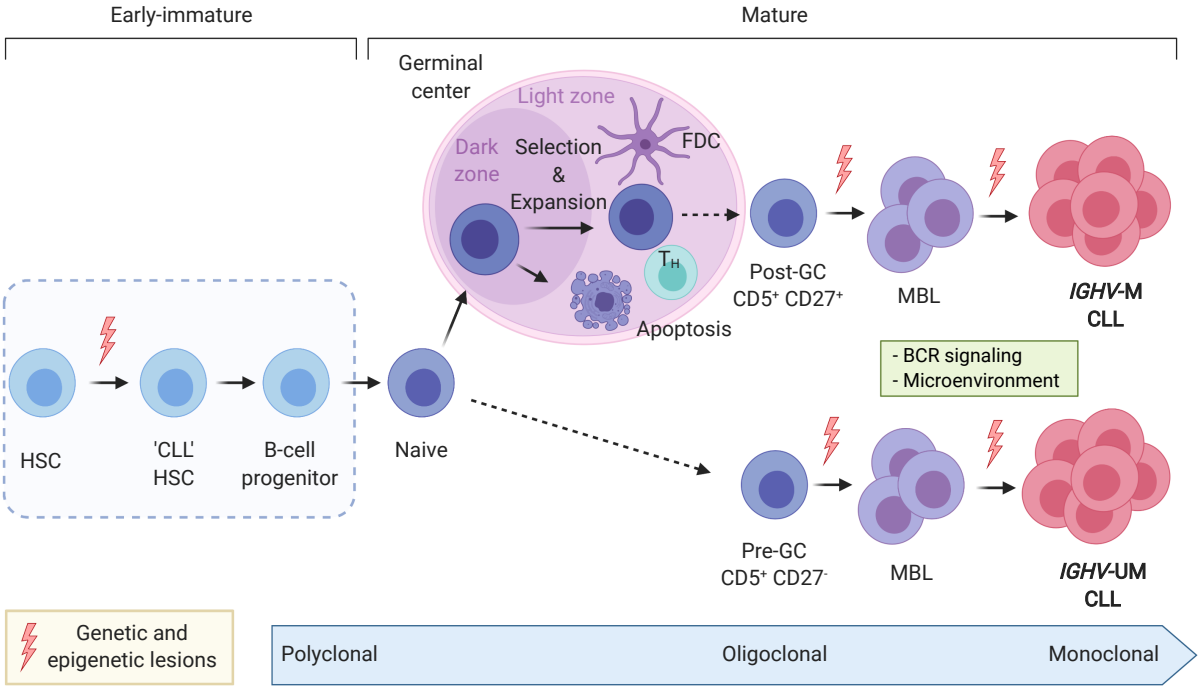

Figure 3: The putative cellular origin of CLL cells. CLL transformation may start at HSC stage, were first genetic and epigenetic changes occur. *IGHV*-unmutated (*IGHV*-UM) CLL cells may arise from naïve pre-GC $CD5^+$ $CD27^-$ B-cells, while mutated-*IGHV* (*IGHV*-M) CLL cells are likely to originate from $CD5^+$ $CD27^+$ post-GC B-cells. In addition to genetic and epigenetic aberrations, BCR stimulation and signals from the microenvironment contribute to the generation of the MBL precursor state, prior to CLL transformation. HSC = hematopoietic stem cell, GC = germinal center, T_H = $CD4^+$ helper T-cell, FDC = follicular dendritic cell, MBL = monoclonal B-cell lymphocytosis. Figure modified from Fabbri and Dalla-Favera 2016 using BioRender.com.

somatic hypermutation, while *IGHV*-unmutated CLL cells originate from conventional naïve B-cells that have not entered the GCs (Fabbri and Dalla-Favera 2016) (Figure 3). In agreement with this hypothesis, epigenomic analysis of CLL cells revealed that DNA methylation patterns of *IGHV*-unmutated leukemia cells resemble those of $CD5^+$ naïve B-cells, whereas *IGHV*-mutated cells appear more similar to memory B-cells (Kulis et al. 2012). More recently, work from Oakes et al. elegantly showed that DNA methylation patterns of CLL cells resemble those of normal B-cells with different degree of maturation, thus indicating that leukemia cells likely derive from a continuum of B-cell developmental stages (Oakes et al. 2016).

The current model of leukemogenesis supports a multistep process where genetic and/or epigenetic alterations, subsequent antigen-driven clonal selection and expansion, as well as microenvironmental signals give rise to monoclonal B-cell lymphocytosis (MBL), the CLL precursor state, and ultimately CLL (Strati and Shanafelt 2015). The fact that both CLL subtypes harbor a highly restricted and biased BCR repertoire indicates that a strong antigen-driven selective pressure plays a significant role in malignant transformation (Vardi et al. 2014; Stamatopoulos et al. 2017). Approximately one third of CLL patients can be classified into groups based on shared motifs within the heavy chain complementarity-determining region 3

(CDR3, also referred to as stereotyped BCR). Such grouping also reflects similar epigenetic, genetic and functional characteristics of the disease, with patients in each group showing a similar course and outcome (Ghiotto et al. 2004; Tobin et al. 2004; Stamatopoulos et al. 2007; Vardi et al. 2014; Stamatopoulos et al. 2017). *IGHV*-unmutated CLL cells frequently express BCRs with low-affinity and poly-reactivity or self-reactivity, whereas *IGHV*-mutated ones tend to have oligo-reactive or mono-reactive BCRs with high affinity to unknown but likely exogenous antigens (Herve et al. 2005; Chu et al. 2008; Binder et al. 2010; Ten Hacken and Burger 2016).

1.2.3 Genetic alterations in CLL

The advent of whole-exome and whole-genome sequencing has tremendously helped to unravel the genetic landscape of CLL. Notably, CLL patients carry a wide range of genetic variability, and unlike other tumor entities, no single main oncogenic driver has been identified (Puente et al. 2011; Quesada et al. 2011; Landau et al. 2015; Puente et al. 2015). Instead, genetic and epigenetic alterations, including chromosomal aberrations, somatic mutations, epigenetic modifications, as well as changes in miRNA expression, contribute to CLL pathogenesis and determine the clinical course of the disease (Kipps et al. 2017). Nevertheless, compared to most of other solid tumors and hematological malignancies, CLL displays a low mutational burden, with a slightly higher number of somatic mutations in *IGHV*-mutated versus -unmutated patients (Puente et al. 2011; Lawrence et al. 2013; Landau et al. 2015).

Cytogenetic alterations can be detected in 80 % of CLL patients, and because their presence impacts CLL development, a hierarchical model for patient classification based on chromosomal abnormalities has been proposed to identify patients with higher risk of disease progression and poor survival (Dohner et al. 2000). The four most common chromosomal alterations are deletions on chromosomes 13 (del(13q)), 11 (del(11q)), and 17 (del(17p)), as well as trisomy 12 (Dohner et al. 2000; Zenz et al. 2010; Fabbri and Dalla-Favera 2016). Deletion 13q14.3 is the most frequent genetic lesion, present in > 50 % of patients, and is associated with a favorable prognosis (Dohner et al. 2000; Dal Bo et al. 2011; Ouillette et al. 2011). The deleted region contains the *DLEU2-mir-15a/16-1* cluster, which controls the expression of negative regulators of apoptosis, as well as proteins involved in cell cycle progression (Calin et al. 2008; Klein et al. 2010). Del(17p), can be found in 7 % of patients, and it involves the inactivation of the tumor suppressor gene *TP53* (Wattel et al. 1994; Dohner et al. 1995; Dohner et al. 2000; Landau et al. 2015). Del(11q) is present in 18 % of CLL patients, and is frequently associated with alterations in the ataxia telangiectasia mutated (*ATM*) gene, which is part of the DNA repair machinery (Schaffner et al. 1999; Dohner et al. 2000; Stankovic and Skowronska 2014). Both *TP53* and *ATM* losses are associated with genomic instability,

resistance to chemotherapy and overall poor prognosis (Dohner et al. 2000; Austen et al. 2007; Stankovic and Skowronska 2014). Last, trisomy 12 is found in approximately 15 % of patients with CLL, and even though it is linked with a higher risk of progressing into the more aggressive lymphoma Richter syndrome, or with the development of secondary tumors, the exact mechanisms that link this chromosomal abnormality to CLL pathogenesis remain unclear (Chigrinova et al. 2013; Fabbri et al. 2013; Strati et al. 2015).

Somatic mutations present in CLL cells have been found to affect genes involved in multiple cellular processes. These include genes related to the DNA damage response (for example *TP53* and *ATM*), RNA processing (for example splicing factor 3B subunit 1 (*SF3B1*), and exportin 1 (*XPO1*)), and chromatin modification (like histone H1.4 (*HIST1H1E*), chromodomain helicase DNA binding protein 2 (*CHD2*) and zinc finger MYM-type containing 3 (*ZMYM3*)). Notch signaling (including the notch receptor 1 (*NOTCH1*) gene itself), B-cell activity pathways, and pathways related to an inflammatory response (like myeloid differentiation primary response 88 (*MYD88*)) can be affected as well (Quesada et al. 2011; Wang et al. 2011; Quesada et al. 2012; Landau et al. 2013; Landau et al. 2015; Mansouri et al. 2015; Puente et al. 2015). Mutations in some of these genes, such as *NOTCH1* and *SF3B1*, are of substantial prognostic value and allow for a better stratification of patients (Baliakas et al. 2015; Rossi et al. 2015). Besides, driver mutations like *SF3B1* and *TP53* have been shown to be present in tumor subclones that expand in CLL patients after treatment, and serve as a predictive factor for disease progression (Landau et al. 2013).

Although the majority of cases develop sporadically, some genetic factors are involved in familial predisposition for CLL, as first-degree relatives of CLL patients have an 8.5-fold higher risk to develop the disease (Cerhan and Slager 2015). Using genome-wide association studies, more than 40 genetic loci have been linked to CLL susceptibility (Di Bernardo et al. 2008; Crowther-Swanepoel et al. 2010; Slager et al. 2012; Berndt et al. 2013; Speedy et al. 2014). Despite a modest impact of each individual locus on disease development, a large number of risk alleles leads to higher CLL susceptibility (Crowther-Swanepoel et al. 2010). The majority of CLL-associated single nucleotide polymorphisms (SNPs) are located in areas of open chromatin, but, interestingly, only few are found within or next to genes whose function might impact disease development, and thus their role in CLL pathogenesis remains poorly understood (Speedy et al. 2014).

1.2.4 Current and emerging therapies for CLL

Treatment for CLL is usually not applied in patients who have an asymptomatic, early stage disease, as it has been shown that overall survival in indolent cases does not improve after treatment (Dighiero et al. 1998). These patients are monitored and only treated when evidence

of disease progression or symptoms appear (Hallek et al. 2018). Despite multiple treatment options being available, CLL remains incurable (Burger 2020). Exceptionally, allogeneic stem cell transplantation is considered a curative strategy, but its application is restricted to patients of younger age and limited by donor availability, plus complications like graft-versus-host disease and immunosuppression often occur (Gribben et al. 2005; Dreger et al. 2010). For decades, standard treatments for CLL were based on alkylating agents (including chlorambucil, bendamustine and cyclophosphamide) and purine analogue chemotherapies (fluradabine, pentostatin and cladribine) (Nabhan and Rosen 2014; Parikh 2018). Notably, the introduction of monoclonal antibodies targeting the CD20 antigen expressed on the surface of B-cells (like rituximab and obinutuzumab) has strongly impacted CLL management (Stilgenbauer et al. 2009). Combining the latter with chemotherapeutics – an approach called chemoimmunotherapy – has significantly improved both overall survival and progression-free survival (PFS), and is the current standard first-line therapy (Parikh 2018).

Importantly, research from the last 10 years has underscored the importance of the BCR signaling pathway in CLL pathogenesis (Herishanu et al. 2011; Stevenson et al. 2011; Le Roy et al. 2012; Burger and Chiorazzi 2013; Ferrer and Montserrat 2018). BCR engagement leads to cell survival and proliferation signals in healthy B-cells as well as CLL cells and, consequently, the use of small molecule inhibitors of BCR-downstream kinases has led to a clinical success (Kipps et al. 2017; Sharma and Rai 2019; Yosifov et al. 2019). For example, treatment with the Bruton's tyrosine kinase (BTK) inhibitor ibrutinib, or the phosphatidylinositol-3 kinase delta (PI3Kδ) inhibitor idelalisib has been approved in the United States and Europe for treatment of patients with relapsed CLL, as it improves PFS as well as overall survival in these patients (Byrd et al. 2014; Furman et al. 2014). In addition, ibrutinib is currently the first treatment option for patients carrying *TP53* mutations and del(17p). Interestingly, treatment with these inhibitors results in significant LN and spleen shrinkage, together with a transiently increased lymphocytosis, likely due to a mobilization of CLL cells from the secondary lymphoid organs to the periphery (Ponader et al. 2012; Woyach et al. 2014; Chen et al. 2016). Besides BCR signaling inhibitors, selective B-cell lymphoma 2 (*BCL-2*) inhibitors are showing promising results for relapsed or refractory patients. In fact, the small molecule inhibitor venetoclax has been approved for second-line treatment of relapsed or refractory CLL patients with del(17p) (Parikh 2018).

Finally, based on the emerging success of immunotherapeutic strategies in several solid and hematological cancers (Fesnak et al. 2016; Ribas and Wolchok 2018), cellular immunotherapies and immune checkpoint inhibitors are currently being tested in clinical trials (NCT03331198, NCT02329847, NCT02332980, NCT02362035). For example, the use of genetically modified T-cells expressing a CAR targeting CD19 on B-cells induced durable remission in several pilot studies with relapsed/refractory CLL patients, but its efficacy was

modest when compared to that in patients with acute lymphoblastic leukemia (Porter et al. 2015; Turtle et al. 2017). As results with single-agent treatment using a blocking antibody against PD-1 led to disappointing results in CLL (Ding et al. 2017), ongoing investigations focus on the combination of immune checkpoint blockade (ICB) and kinase inhibitors (NCT02329847, NCT02332980, NCT02362035).

1.2.5 The Eμ-TCL1 mouse model of CLL

Several murine models reproducing common CLL genetic lesions have been developed, including mouse lines with a deletion of chromosome 14qC3, which corresponds to human del(13q), or of the *IRF4* gene. Other mouse lines overexpress genes that are altered in CLL, like T-cell leukemia/lymphoma 1a (*TCL1*), tumor necrosis factor superfamily member 13 (*TNFSF13*), and *BCL-2,* or harbor a *SF3B1* mutation and *ATM* deletion (Bichi et al. 2002; Stein et al. 2002; Zapata et al. 2004; Klein et al. 2010; Lia et al. 2012; Shukla et al. 2013; Yin et al. 2019). To date, the Eμ-TCL1 model is the most widely used mouse model to investigate CLL (Simonetti et al. 2014; Bresin et al. 2016). Bichi et al. established this mouse line by exogenously placing the human *TCL1* gene under the control of the Ig heavy chain promoter (Bichi et al. 2002). Practically 100 % of the transgenic mice start to show $CD5^+$ B-cell proliferation at 2 months of age, and these cells can be detected in spleen at 3-5 months of age, and in BM at 5-8 months of age (Bichi et al. 2002). At the age of 13-18 months, mice become manifestly ill, with splenomegaly, lymphadenopathy and elevated $CD5^+$ B-cell counts in PB, BM and SLOs (Bichi et al. 2002). The malignant B-cells show unmutated *IGHV* genes and a stereotyped BCR, suggesting that the model mimics the more aggressive form of human CLL (Yan et al. 2006). Indeed, the highest levels of *TCL1* expression are found in *IGHV*-unmutated patients, and *TCL1* expression correlates with ZAP-70 expression, as well as with the presence of del(11q) (Herling et al. 2006; Pekarsky et al. 2006). Functionally, the *TCL1* gene acts as an oncogene by transporting AKT serine/threonine kinase 1 (*AKT1*) into the nucleus and by enhancing its enzymatic activity, which leads to both apoptosis resistance and enhanced proliferation (Russo et al. 1989; Mok et al. 1999; Pekarsky et al. 2000; Noguchi et al. 2007). It also increases nuclear factor kappa light chain enhancer of (NF-κB) activity, thus supporting CLL cell survival and proliferation (Pekarsky et al. 2008; Gaudio et al. 2012). Besides, higher levels of *TCL1* expression and co-recruitment of TCL1-AKT to the BCR membrane complex in CLL cells correlate with BCR signaling intensity (Herling et al. 2009). Of note, the long latency of the disease in the mice suggests that the *TCL1* overexpression likely serves as an initial trigger, and additional genetic lesions and microenvironmental factors may be required for a complete malignant transformation (Simonetti et al. 2014).

To overcome this latency and the high heterogeneity in tumor onset in the transgenic mouse line, adoptive transfer (AT) of Eμ-TCL1 leukemic cells into wild-type (WT) C57BL/6 mice is

commonly performed. Such approach represents a reproducible and more homogeneous system where mice develop a CLL-like disease within few weeks or months (Hofbauer et al. 2011; McClanahan et al. 2015b; Hanna et al. 2019).

The use of the Eμ-TCL1 mouse model has significantly advanced the understanding of the molecular and cellular pathomechanisms of CLL. For example, the role of the BCR signaling or the Toll-like receptor signaling, as well as the importance of continuous autoantigen stimulation in CLL development were examined with the use of this model system (Holler et al. 2009; Bertilaccio et al. 2011; Nganga et al. 2013; Woyach et al. 2014). Likewise, because it is fully immunocompetent, it recapitulates the tumor microenvironment and has been successfully used to understand the cross-talk between leukemic cells and the surrounding cells (Kern et al. 2004; Gorgun et al. 2009; Scielzo et al. 2010; Troeger et al. 2012), as well as for preclinical studies of novel therapies (McClanahan et al. 2015a; Wierz et al. 2018; Hanna et al. 2020).

1.3 The tumor microenvironment in CLL

1.3.1 The complex interplay between CLL cells and their microenvironment

Normal B-cells are programmed to interact with their microenvironment during the processes of differentiation, antigen presentation, maturation, and antibody secretion, in order to execute a well-coordinated and tightly regulated immune response against infection (Herishanu et al. 2013). It is thus unsurprising that CLL cells retain the ability to communicate with their microenvironment, even though the normal compartmentalization and regulation of the immune response is altered. In fact, CLL cells are highly reliant on the interactions with the microenvironment for their survival and proliferation, especially in BM and secondary lymphoid structures. Such strong dependency is evidenced by the fact that *in vitro* cultured CLL cells rapidly undergo apoptosis, whereas their survival is significantly extended when co-cultured with non-malignant cells such as monocyte-derived nurse-like cells (NLCs) or mesenchymal bone marrow stromal cells (BMSCs) (Burger et al. 2000; Deaglio and Malavasi 2009). Besides, proliferation of CLL cells in patients is restricted to the pseudofollicles of secondary lymphoid organs, where tight interactions with the surrounding cells that shape the transcriptomic profile of CLL cells occur (Messmer et al. 2005; Herishanu et al. 2011). More specifically, CLL cells residing in the LNs overexpress genes related to BCR signaling as well as genes downstream of the NF-κB and NFAT pathways compared to PB and BM CLL cells (Herishanu et al. 2011).

Multiple cell types constitute the CLL TME, including mesenchymal-stromal cells, endothelial cells, fibroblasts, neutrophils, monocytes, macrophages, dendritic cells, T-cells and NK cells. Through adhesion molecules, ligand-receptor interactions and soluble factors, these

cells establish a crosstalk with CLL cells, the complexity of which remains incompletely defined (Burger 2011; Kipps et al. 2017). The main cellular and molecular components of the CLL microenvironment are summarized in Figure 4.

The majority of studies investigating the role of stromal cells in CLL have been performed using BMSCs. These cells provide attachment and growth factors in *in vitro* co-cultures with CLL cells via the CXCR4-CXCL12 axis, and protect CLL cells from spontaneous and drug-induced apoptosis (Panayiotidis et al. 1996; Lagneaux et al. 1998; Burger et al. 1999; Kurtova et al. 2009). Other cytokines, chemokines, proangiogenic factors, and extracellular matrix components secreted by mesenchymal cells promote CLL cell migration and survival. These include integrins β1 and β2, vascular cell adhesion molecule 1 (VCAM1), VEGF, and MMP9 (Lagneaux et al. 1998; de la Fuente et al. 2002; Ringshausen et al. 2004; Redondo-Munoz et al. 2006; Gehrke et al. 2011). Importantly, the interaction between CLL cells and stromal cells results in the activation of both cell types and induces the release of C-C motif chemokine ligand (CCL) 3 (CCL3) and CCL4 by CLL cells for the recruitment of other leukocytes like T-cells (Burger et al. 2009; Ding et al. 2009).

Endothelial and follicular dendritic cells (FDCs) play a similarly important role in homing CLL cells and providing protection from apoptosis (Badoux et al. 2011; Cols et al. 2012; Maffei et al. 2012). Activation and proliferation of malignant cells occur upon binding to integrins as well as B-cell activating factor (BAFF) and a proliferation-inducing ligand (APRIL) expressed by microvascular endothelial cells (Cols et al. 2012).

Burger et al. first described a critical involvement of monocytes in supporting CLL with the observation that PB monocytes co-cultured with CLL cells differentiate into ‘nurse-like cells’ that prolong leukemic cell survival (Burger et al. 2000). This *in vitro* model system has been extensively used to examine the mechanisms by which monocytes and macrophages support leukemia cells. For example, NLCs attract and enhance CLL cell survival via secretion of chemokines CXCL12 and CXCL13, as well as through BAFF and APRIL expression (Burger et al. 2000; Nishio et al. 2005; Burkle et al. 2007). Additional supporting interactions include the binding of CD38 – the expression of which in CLL cells is associated with poor prognosis – with CD31, and of semaphorin CD100 to Plexin B1 (Granziero et al. 2003; Deaglio et al. 2005). Besides, CLL cells contribute to an inflammatory microenvironment by secreting exosomes that induce monocytes to secrete CCL2 (Haderk et al. 2017), which in turn, recruits more monocytes, and CD14, which improves CLL cell survival *in vitro* (Seiffert et al. 2010; Schulz et al. 2011). Of note, NLCs exhibit a gene expression profile similar to TAMs, which have been found in spleen and LNs of CLL patients (Tsukada et al. 2002; Burkle et al. 2007). Moreover, monocytes isolated from PB of CLL patients show a skewed phenotype from classical inflammatory $CD14^{+}$ $CD16^{-}$ to patrolling $CD14^{low}$ $CD16^{+}$ with a deregulation of genes involved in inflammation and phagocytosis (Maffei et al. 2013). Murine experiments have

recently confirmed the pro-tumorigenic role of myeloid cells: their depletion using clodronate liposomes led to a significantly improved control of CLL development, as well as a partial

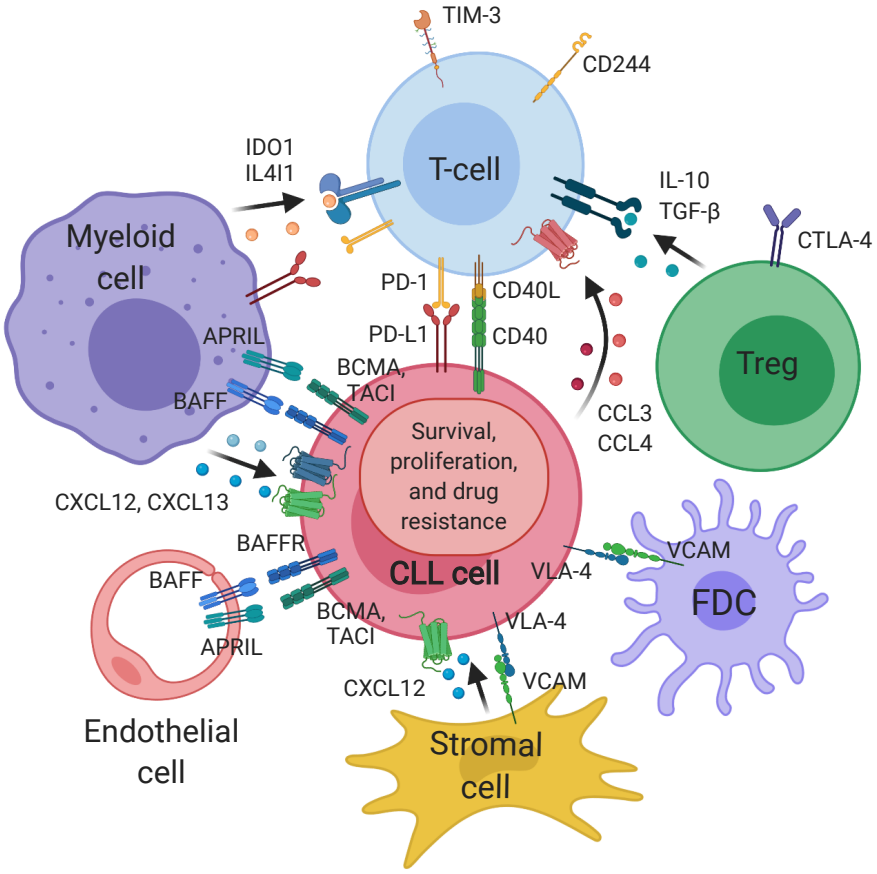

Figure 4: Cellular and molecular components of the CLL tumor microenvironment (TME). CLL cells receive pro-survival, proliferation and drug resistance-inducing signals from multiple cells present in their microenvironment. CLL cells are recruited to the LNs via CXCL12 and CXCL13 secreted by stromal and myeloid cells. In SLOs, myeloid cells and endothelial cells support CLL cell survival and proliferation via cytokines including BAFF and APRIL. FDCs, stromal cells and T-cells further contribute in supporting CLL cells by expression of VCAM1 and CD40L, respectively. CLL cells in turn, secrete CCL3 and CCL4 to recruit leukocytes. In addition, CLL cells promote an immunosuppressive TME by expressing PD-L1, and inducing Treg differentiation. Tres, in turn, express CTLA-4 and secrete IL-10 and TGF-β. Myeloid cells contribute to the inhibition of T-cell function by PD-L1 expression and IDO1 secretion. CLL T-cells exhibit an exhausted phenotype, with elevated expression of inhibitory receptors including PD-1, TIM-3 and CD244. PD-1 = programmed cell death protein 1, PD-L1 = PD-1 ligand, CTLA-4 = cytotoxic T-lymphocyte-associated protein 4, Tim-3 = T-cell Immunoglobulin and mucin-domain containing-3, CD40L = CD40 ligand, IL4I1 = interleukin 4 induced gene 1, IL-10 = interleukin 10, TGFβ = transforming growth factor β, IDO1 = indoleamine 2,3-dioxygenase, Treg = regulatory T-cell, FDC = follicular dendritic cell, CCL3, CCL4 = chemokine ligand 3 and 4, CXCL12 and 13 = C-X-C motif chemokine 12 and 13, BAFF = B-cell activating factor, BAFFR = BAFF receptor, APRIL = a protein-inducing ligand, BCMA = B-cell maturation antigen, TACI = transmembrane activator and CAML interactor, VCAM1 = vascular cell adhesion protein 1, VLA-4 = Integrin α4β1. This figure includes a schematic representation of the main components of the CLL TME. A complete description of the interactions identified thus far has been reviewed by ten Hacken and Burger (Ten Hacken and Burger 2016). Figure created using BioRender.com.

restoration of systemic inflammation (Galletti et al. 2016; Hanna et al. 2016).

CLL cells modify their microenvironment to evade immune surveillance via multiple mechanisms. They produce IL-10 and TGF-β, and express high levels of PD-L1 that directly affect T-cell function. (Lotz et al. 1994; Fayad et al. 2001; Ramsay et al. 2012; Brusa et al. 2013). Treg cell numbers are increased in PB and LNs of CLL patients, and have been shown to be correlated with tumor load and higher Binet and Rai stages (Beyer et al. 2005; Giannopoulos et al. 2008; D'Arena et al. 2011; Biancotto et al. 2012; Palma et al. 2017). These suppressor cells also express higher levels of CTLA-4, and produce increased amounts of IL-10 and TGF-β compared to control Tregs (Beyer et al. 2005; Motta et al. 2005; Biancotto et al. 2012). Further contributing to an immunosuppressive microenvironment, myeloid cells exhibit increased expression of IDO1, interleukin 4 induced gene 1 (IL4I1), as well as PD-L1, which help suppress T-cell function and induce Treg differentiation *in vitro* (Giannoni et al. 2014; Jitschin et al. 2014; Sadik et al. 2020). Last, circulating DCs from CLL patients are reported to harbor an immature phenotype and are unable to stimulate an effective T-cell response (Orsini et al. 2003).

1.3.2 The role of T-cells in the CLL microenvironment

The role of T-cells in CLL remains one of the most debated subjects in CLL research. Both $CD4^+$ and $CD8^+$ T-cell numbers are increased in PB of CLL patients, and a higher proportion of these cells exhibit an antigen-experienced effector or memory phenotype in contrast to healthy donor T-cells (Catovsky et al. 1974; Totterman et al. 1989; Christopoulos et al. 2011; Palma et al. 2017; Elston et al. 2020; Roessner et al. 2020b). However, it is unclear whether these cells are expanded because of tumor recognition, antigen-independent inflammatory signals, or infection-derived antigens, which are more prevalent in CLL patients (Burger 2011).

$CD4^+$ T-cells isolated form CLL patients display a higher expression of the activation markers CD160 and human leukocyte antigen (HLA)-DR, as well as the proliferation marker KI-67, but also express higher levels of the inhibitory receptors PD-1 and TIGIT (Riches et al. 2013; Catakovic et al. 2017; Palma et al. 2017; Elston et al. 2020). Both T_H1 and T_H2 T-cell subsets have been reported to be predominant in PB of CLL patients (Podhorecka et al. 2002; Gorgun et al. 2005; Buggins et al. 2008; Roessner et al. 2020b). Additionally, cytokines secreted by either T_H1 cells (IL-2, IFNγ, and TNFα) or T_H2 cells (IL-4) have been shown to improve CLL cell survival and proliferation in *in* vitro cultures (Foa et al. 1990; Dancescu et al. 1992; Buschle et al. 1993; Trentin et al. 1996; de Totero et al. 1999; Monserrat et al. 2014). However, these reports investigated T-cells isolated from PB, and thus provide limited information about the phenotype and role of $CD4^+$ T-cells residing in the LNs, where interactions with CLL cells occur. In lymphoid tissues, one of the most abundant T-cell subsets are $CD4^+$ T follicular helper cells (T_{FH}), which express $CXCR5^+$ as well as inducible T-cell

costimulatory (ICOS), and support B-cell differentiation via CD40L- CD40 and ICOS- ICOS ligand (ICOSL) binding (King et al. 2008). In fact, CD40 signaling in CLL cells induces their survival and proliferation via PI3K/AKT and NF-κB pathways (Fluckiger et al. 1992; Romano et al. 1998; Furman et al. 2000; Cuni et al. 2004; Os et al. 2013). Similarly, the T_{FH} cytokine IL-21 promotes CLL cell proliferation *in vitro*, altogether suggesting that these cells provide crucial support to CLL cell survival (Ahearne et al. 2013; Pascutti et al. 2013). Mouse experiments aimed at deciphering the influence of $CD4^+$ T-cells on CLL progression have reported contradictory results: autologous $CD4^+$ T-cells were necessary for CLL cell proliferation in patient-derived xenograft (PDX) mouse models (Os et al. 2013), whereas an anti-tumoral effect by these cells was described using PDX as well as the Eμ-TCL1 mouse models (Bagnara et al. 2011; Kocher et al. 2016). More recently, the depletion of *TBET*-expressing T_H1 $CD4^+$ T-cells in TCL1 mice was shown to have no effect in leukemia progression (Roessner et al. 2020b). Of note, no data about the presence, phenotype or function of T_R1 cells in CLL has been reported to date. Additional functional analyses are thus required to elucidate the role of $CD4^+$ T-cell subsets in CLL.

Evidence for an anti-tumoral effect by $CD8^+$ T-cells comes from a described spontaneous regression of the disease in some patients, in addition to the identification of mutations resulting in neo-antigens that potentially induce a $CD8^+$ T-cell response (Del Giudice et al. 2009; Rajasagi et al. 2014). Besides, *in vivo* studies using the TCL1 AT mouse model showed that CLL progresses significantly faster in the absence of $CD8^+$ T-cells (Hanna et al. 2019). As reported in other tumor entities, however, $CD8^+$ T-cells from PB of CLL patients exhibit an activation-induced exhaustion phenotype, with increased expression of activation markers as well as inhibitory receptors, including human leukocyte antigen -DR isotype (HLA-DR), CD69, PD-1, CD244, TIM-3 and CTLA-4, and an altered transcriptional and epigenetic state (Totterman et al. 1989; Gorgun et al. 2005; Motta et al. 2005; Nunes et al. 2012; Brusa et al. 2013; Riches et al. 2013; Wu et al. 2016a; Taghiloo et al. 2017; Hanna et al. 2019; Elston et al. 2020). Moreover, T-cells from CLL patients are unable to form effective immunological synapses due to cytoskeleton aberrations, and further show defects in proliferation and cytotoxicity (Gorgun et al. 2005; Ramsay et al. 2008; Riches et al. 2013). Nevertheless, as in $CD4^+$ T-cell-centered studies, most research has focused on PB $CD8^+$ T-cells, and very limited data on their phenotype in LNs exists. Importantly, Hanna et al. recently reported that $CD8^+$ T-cell exhaustion is more pronounced in SLOs compared to PB, with higher levels of PD-1 and reduced production of GZMB and TNFα after *in vitro* stimulation (Hanna et al. 2019). In a similar manner, exhausted T-cells are enriched in spleen compared to blood of TCL1 AT mice (Hanna et al. 2019). With the aim to assess the effect of immune check point blockade in CLL, several studies have used this mouse model and observed encouraging results. For example, anti-PD-L1, as well as dual anti-PD-1 and anti-LAG3 treatment in the mice reinvigorated $CD8^+$

T-cell function and improved CLL control (McClanahan et al. 2015a; Wierz et al. 2018). However, as previously mentioned, the respective treatment in CLL patients has so far been ineffective (Ding et al. 2017), hence highlighting the need for a better understanding of the T-cell compartment in CLL patients.

2 Aims of the thesis

Even though the recent development of novel targeted agents and combinatorial strategies have substantially improved therapeutic effectiveness in CLL, it is still considered an incurable disease. Drug resistance remains highly prevalent, and thus highlights the need for the creation of innovative methods to treat patients with CLL. Because CLL cells strongly rely on signals form their microenvironment to survive and proliferate, understanding the interplay between leukemia cells and bystander cells could be central to identify new treatment approaches targeting these interactions. However, whether T-cells exert pro- or anti-tumoral effects within the CLL microenvironment remains under debate. Besides, the phenotype of these cells in the secondary lymphoid organs, where the interactions with tumor cells occur, has been poorly studied hitherto.

2.1 Characterization of the T-cell compartment in CLL

In order to address these open questions, the central aim of this work was to characterize the phenotype of T-cells isolated from CLL patients at a new level of resolution using single-cell technologies. For this purpose, $CD8^+$ T-cells from CLL lymph nodes, peripheral blood and bone marrow, together with lymph nodes of individuals without cancer were immunophenotyped using mass cytometry. Additionally, to evaluate the transcriptomic and clonal profile of nodal T-cells at the single-cell level, the 10x Genomics platform was used. At the same time, this approach enabled the study of the specific interactions established between T-cell subsets and CLL cells.

Currently, the Eμ-TCL1 mouse model represents the most suitable tool for the *in vivo* investigation of the precise role of immune cell subsets in the context of CLL. Thus, in addition to the abovementioned analyses, the transcriptomes of individual T-cells isolated form splenocytes of leukemia-bearing mice were analyzed to assess their resemblance with LNs from CLL patients.

2.2 Exploring the role of the transcription factor EOMES in $CD8^+$ T-cells in CLL

EOMES is a known master regulator of T-cell differentiation and function, and has recently been linked to T-cell exhaustion. Hence, another goal of the present study was to investigate the role of EOMES in T-cell function in the context of CLL. To this end, EOMES expression patterns in human and murine T-cell subsets were investigated using single-cell transcriptome

and mass cytometry analyses, and its functional role was assessed *in vivo* using the TCL1 mouse model.

2.3 Defining the role of T_R1 cells in CLL

While an immunosuppressive role of T_R1 $CD4^+$ T-cells has been described in several tumor entities, their existence and function in CLL has not been explored thus far. The aim of the present work was therefore to investigate the presence and phenotype of T_R1 cells in CLL patients using mass cytometry and transcriptome single-cell data. Besides, the TCL1 mouse model was employed to investigate the molecular mediators regulating T_R1 cell function and to elucidate their contribution in CLL development.

3 Materials and Methods

3.1 Materials

3.1.1 Human samples

Lymph node (LN), peripheral blood (PB), and bone marrow (BM) samples from CLL patients, and reactive lymph node (rLN) samples from heathy controls were obtained after informed consent and according to the guidelines of the Hospital Clínic Ethics Committee, the Ethics Committee of the University of Heidelberg, and the Declaration of Helsinki. Patients with CLL were diagnosed following the World Health Organization (WHO) classification criteria (Swerdlow 2017). All clinical information of the patients analyzed in this work is provided in Table 1, Table S12, and Table S13.

Table 1: Clinical data of CLL patients and healthy controls.

Patient ID	Tissue	Diagnosis	Sex	Age at sampling	Age at diagnosis	*TP53* status	*IGHV* status	TL (%)	Treatment status	Binet	Rai	TFS (months)	OS (months)
BC1	LN	CLL ACC	M	72	70	-	M	92	Untreated	B	I	26.3	74.9
BC1	PB	CLL ACC	M	72	70	-	M	41.80	Untreated	B	I	26.3	74.9
BC10	LN	CLL TR	F	61	59	0	U	64.80	Treated	A	III	22.3	28.2
BC11	BM	CLL	M	53	52	0	U	70	Treated	A	I	6.5	121.7
BC12	LN	CLL	M	77	77	0	U	53.94	Untreated	B	I	-	-
BC12	PB	CLL	M	77	77	0	U	67.76	Untreated	B	I	-	-
BC13	LN	CLL	M	72	67	0	U	53.28	Treated	A	0	52.2	-
BC13	PB	CLL	M	72	67	0	U	75.60	Treated	A	0	52.2	-
BC14	LN	CLL	M	72	60	0	U	91	Treated	A	0	122.4	-
BC14	PB	CLL	M	72	60	0	U	94	Treated	A	0	122.4	-
BC15	LN	CLL	F	58	56	0	U	70.56	Treated	A	0	19.6	140.5
BC15	LN	CLL	F	65	56	0	U	78.40	Treated	A	0	19.6	140.5
BC15	PB	CLL	F	65	56	0	U	69	Treated	A	0	19.60	140.47
BC2	LN	CLL ACC	M	70	69	0	U	88	Untreated	B	I	2.9	-
BC3	LN	CLL	F	58	57	0	U	79.20	Untreated	B	I	-	-
BC3	BM	CLL	F	58	57	0	U	83.42	Untreated	B	I	-	-
BC4	LN	CLL	M	56	53	NA	M	76.26	Treated	A	0	39.3	-
BC5	LN	CLL	F	47	46	0	M	32.80	Untreated	A	I	-	-
BC5	LN	CLL	F	46	46	0	M	64.17	Untreated	A	I	-	-
BC5	PB	CLL	F	46	46	0	M	45.10	Untreated	-	-	-	-
BC6	LN	CLL ACC	M	84	62	-	-	68	Treated	A	0	69	282.4
BC7	LN	CLL	M	43	43	0	M	83.30	Untreated	A	I	-	-

BC8	LN	CLL	M	75	73	0	U	59.40	Treated	A	I	0.0	51.2
BC8	PB	CLL	M	76	73	0	U	60	Treated	A	I	0.0	51.2
BC9	LN	CLL	M	54	53	0	U	86	Treated	A	III	14.9	56.4
BC9	PB	CLL	M	54	53	0	U	84	Treated	A	III	14.9	56.4
BC9	BM	CLL	M	54	53	0	U	94	Treated	A	III	14.9	56.4
HD1	LN	CLL	M	72	56	0	M	95	Pretreated	A	III	8.1	-
HD10	LN	CLL	M	71	71	0	M	89	Untreated	B	III	-	-
HD11	LN	CLL	M	70	62	1	-	88	Treated	A	IV	19.3	-
HD2	LN	CLL	M	78	78	0	M	77.2	Untreated	B	I	-	-
HD3	LN	CLL	M	69	69	0	M	75	Untreated	B	I	5.0	-
HD4	LN	CLL	M	79	79	0	M	88.6	Untreated	B	I	1.0	-
HD5	LN	CLL	M	72	71	0	U	88.9	Untreated	B	I	14.7	-
HD6	LN	CLL	M	76	75	0	M	78.6	Untreated	A	I	6.5	-
HD7	LN	CLL	M	53	53	0	U	91.4	Untreated	C	III	0.3	-
HD8	LN	CLL	M	72	71	0	M	NA	Untreated	A	III	16.4	39.7
HD9	LN	CLL	M	75	76	-	-	84.3	Untreated	-	-	-	-
rLN1	LN	rLN	M	-									
rLN10	LN	rLN	F	52									
rLN11	LN	rLN	F	34									
rLN12	LN	rLN	M	30									
rLN13	LN	rLN	M	59									
rLN2	LN	rLN	M	32									
rLN3	LN	rLN	M	50									
rLN4	LN	rLN	F	39									
rLN5	LN	rLN	M	20									
rLN6	LN	rLN	M	49									
rLN7	LN	rLN	M	18									
rLN8	LN	rLN	M	33									
rLN9	LN	rLN	M	20									

Note: TL = tumor load, TFS = treatment-free survival, OS = overall survival, LN = lymph node, PB = peripheral blood, BM = bone marrow, CLL = chronic lymphocytic leukemia, CLL ACC = accelerated CLL, CLL TR = CLL with Hodgkin transformed cells, rLN = reactive LN, M = male, F = female, - = not available.

3.1.2 Mouse lines

Mice used in this work were obtained from the central animal facility of the German Cancer Research Center (DKFZ, Heidelberg), kindly provided by external research groups, or purchased from Janvier Labs (Saint-Berthevin) or Jackson laboratories (Bar Harbor). A list of

the specific mouse strains used, including their respective background and supplier, is provided in Table 2. Mice were kept under specific pathogen-free conditions in the animal facility of DKFZ. Experimental and control groups were sex- and age-matched in all studies performed. Mice were euthanized with carbon dioxide (CO_2) overdose or cervical dislocation. All animal experiments were conducted in accordance with the governmental regulations and authorized by the local authorities under the G-25/16, G-98/16 and G-53/15 and G-36/14 experimental projects.

Table 2: Mouse lines used in this work.

Short name	Full name	Background	Supplier
Eomes$^{-/-}$	Lck-cre x Eomes$^{fl/fl}$ x Foxp3-IRES-mRFP (FIR) x Il10-GFP (tiger) (Wan and Flavell 2005)	129Sv/C57BL/6 J	Dr. Ana Izcue[1]
Eomes$^{+/+}$	Eomesfl/fl x FIR x tiger (WT) (Wan and Flavell 2005)	CD45.2-C57BL/6 J	Dr. Ana Izcue[1]
Eμ-TCL1	B6.Cg-Tg(Igh-V186.2-TCL1A)3Cro 75 (Bichi et al. 2002)	CD45.2-C57BL/6 N	Dr. Carlo Croce[2]
Eμ-TCL1	B6.Cg-Tg(Igh-V186.2-TCL1A)3Cro 75 (Bichi et al. 2002)	CD45.2-C57BL/6 J	Dr. Carlo Croce[2]
Il10rb$^{-/-}$	STOCK-Il10rbtm1Agt (Spencer et al. 1998)	CD45.2-C57BL/6 J	Jackson laboratories[3]
Il10 reporter (Fir x tiger)	B6-Foxp3tm1Flv Il10tm1Flv / Plich (Kamanaka et al. 2006)	CD45.2-C57BL/6 J	Dr. Ana Izcue[1]
Rag2$^{-/-}$	B6.129S(Cg)-Rag2tm1Fwa/FwaOrl 314 (Shinkai et al. 1992)	CD45.2-C57BL/6 J	DKFZ central animal facility
WT C57BL/6 J	NA	CD45.2-C57BL/6 J	Janvier Labs[4]
WT C57BL/6 N	NA	CD45.2-C57BL/6 N	Janvier Labs[4]

Note: NA = Not Available. [1] = Max-Planck Institute of Immunology and Epigenetics, Freiburg, [2] = Ohio State University, Columbus, [3] = Bar Harbor, [4] = Saint-Berthevin.

3.1.3 Antibodies

Table 3: Mass cytometry antibodies.

Antibody	Isotope	Clone	Reference	Supplier	Staining
2B4 (CD244)	113In*#	C1.7	329502	Biolegend	Surface
CD127/IL-7Ra	149Sm	A019D5	314901B	Fluidigm	Surface

CD134/OX40	158Gd	ACT35	315801B	Fluidigm	Surface
CD137/4-1BB	173Yb	4B4-1	317301B	Fluidigm	Surface
CD152/CTLA-4	170Er	14D3	317000B	Fluidigm	Surface
CD185/CXCR5	171Yb	51505	317100B	Fluidigm	Surface
CD19	139La*#	HIB19	302202	Biolegend	Surface
CD197/CCR7	167Er*	G043H7	353202	Biolegend	Surface
CD223/LAG3	165Ho	11C3C65	316503B	Fluidigm	Surface
CD25	169Tm	2A3	316900B	Fluidigm	Surface
CD27	155Gd	L128	315500B	Fluidigm	Surface
CD278/ICOS	148Nd	C398.4A	314801B	Fluidigm	Surface
CD279/PD-1	174Yb	EH12.2H7	317402B	Fluidigm	Surface
CD3	141Pr*	UCHT1	300402	Biolegend	Surface
CD357/GITR	159Tb	621	315902B	Fluidigm	Surface
CD38	144Nd	HIT2	314401B	Fluidigm	Surface
CD39	160Gd	A1	316000B	Fluidigm	Surface
CD4	145Nd*	RPA-T4	300502	Biolegend	Surface
CD44	166Er	BJ18	316600B	Fluidigm	Surface
CD45	89Y	HI30	308900B	Fluidigm	Surface
CD45RA	143Nd	H100	314300B	Fluidigm	Surface
CD45RO	164Dy	UCHL1	316400B	Fluidigm	Surface
CD47	209Bi	CC2C6	320900B	Fluidigm	Surface
CD56/NCAM	176Yb	NCAM16.2	317600B	Fluidigm	Surface
CD7	147Sm	CD7-6B7	314700B	Fluidigm	Surface
CD73	168Er	AD2	316801B	Fluidigm	Surface
CD8a	146Nd*	RPA-T8	301002	Biolegend	Surface
CD95/FAS	152Sm	DX2	315201B	Fluidigm	Surface
Cisplatin viability	195Pt		201064	Fluidigm	
DNA content	191/193Ir		201192	Fluidigm	
EOMES	175Lu*	WD1928	14-4877-82	ebioscience	Intracellular
FOXP3	162Dy	259D/C7	3162024A	Fluidigm	Intracellular
Granzyme K	142Nd*	GM26E7	370502	Biolegend	Intracellular

HELIOS	156Gd*	22F6	137202	Biolegend	Intracellular
HLA-DR	151Eu	G46-6	3151023B	Fluidigm	Surface
KI-67	172Yb	B56	3172024B	Fluidigm	Intracellular
KLRG1	115In*#	SA231A2	367702	Biolegend	Surface
TBET	161Dy	4B10	3161014B	Fluidigm	Intracellular
TCF7	163Dy*	7F11A10	655202	Biolegend	Intracellular
TIGIT	153Eu	MBSA43	3153019B	Fluidigm	Surface
TIM-3	154Sm	F38-2E2	3154010B	Fluidigm	Surface
TOX	150Nd*	TXRX10	14-6502-82	ebioscience	Intracellular

Note: * = Isotopes conjugated *in-house* to respective purified monoclonal IgG antibodies in the Department of Oncology in the Luxembourg Institute of Health (LIH, Luxembourg). # = Isotopes were purchased from Trace Sciences International (113In) or Sigma (115In, 139, LA).

Table 4: Flow cytometry antibodies.

Marker	Fluorochrome	Species reactivity	Clone	Supplier	Reference
CD107A	PE	Mouse	1D4B	eBioscience	12-1071-83
CD11B	eFluor® 450	Mouse	M1/70	eBioscience	48-0112-82
CD11B	PerCP-Cy5.5	Mouse	M1/70	eBioscience	45-0112-82
CD127	PE	Mouse	A7R34	Biozol Diagnostica	BLD-135010
CD127	PE-Dazzle	Mouse	A7R34	Biozol Diagnostica	BLD-135032
CD127	BV605	Mouse	A7R34	Biozol Diagnostica	BLD-135041
CD127	PE-Cy7	Mouse	A7R34	Biolegend	25-1371-82
CD127	APC	Mouse	A7R34	Biozol Diagnostica	BLD-135012
CD19	FITC	Mouse	1D3	eBioscience	11-0193-86
CD19	PE-Dazzle	Mouse	6D5	Biolegend	115554
CD19	AF700	Mouse	1D3	eBioscience	56-0193-82
CD19	PE-Cy7	Mouse	1D3	eBioscience	25-0193-81
CD19	PE	Mouse	1D3	eBioscience	12-0193-83
CD19	FITC	Human	HIB19	Biolegend	302206

CD244	APC	Mouse	eBio244F4	eBioscience	17-2441-82
CD3	V450	Mouse	500A2	BD Bioscience	560801
CD3	APC	Mouse	145-2C11	Biolegend	100321
CD3	PE	Human	HIT3a	BD Bioscience	555340
CD3E	BV605	Mouse	145-2C11	Biolegend	BLD-100351
CD3E	FITC	Mouse	145-2C11	Biolegend	100306
CD4	eFluor®450	Mouse	GK1.5	eBioscience	48-0041-82
CD4	BV605	Mouse	RM4-5	Biolegend	BLD-100548
CD4	PerCP-Cy5.5	Mouse	RM4-4	Biolegend	116012
CD4	APC-Cy7	Mouse	RM4-5	Biolegend	100526
CD4	APC	Mouse	RM4-4	Biozol Diagnostica	BLD-100516
CD44	AF700	Mouse	IM7	eBioscience	56-0441-82
CD44	PerCP-Cy5.5	Human/ Mouse	IM7	Biozol Diagnostica	BLD-103032
CD44	FITC	Human/ Mouse	IM7	eBioscience	11-0441-85
CD45	PerCP-Cy5.5	Mouse	30-F11	Biolegend	BLD-103132
CD45	BV711	Mouse	30-F11	Biolegend	103147
CD45	AF700	Mouse	30-F11	Biolegend	103128
CD5	APC	Mouse	53-7.3	Biolegend	100626
CD5	BV605	Mouse	53-7.3	BD Bioscience	563194
CD5	PE	Mouse	53-7.3	eBioscience	12-0051-81
CD5	APC	Human	UCHT2	Biolegend	300612
CD69	PE-Dazzle	Mouse	H1.2F3	Biolegend	BLD-104536
CD8A	APC-Cy7	Mouse	53-6.7	Biolegend	100714
CD8A	BV605	Mouse	53-6.7	Biolegend	100744
CX3CR1	PE-Dazzle	Mouse	SA011F11	Biolegend	149014
EOMES	PE	Mouse	Dan11mag	eBioscience	12-4875-82
EOMES	PerCP-eFluor710	Human/ Mouse	Dan11mag	eBioscience	46-4875-80

FOXP3	PeCy7	Mouse	FJK-16s	eBioscience	25-5773-80
FOXP3	AF700	Mouse	FJK-16s	eBioscience	56-5773-82
GZMB	V450	Mouse	NGZB	eBioscience	48-8898-82
GZMB	FITC	Mouse	NGZB	eBioscience	11-8898-80
IFNG	PerCP-Cy5.5	Mouse	XMG1.2	eBioscience	45-7311-82
IL-2	APC	Mouse	JES6-5H4	Biolegend	503810
IL-2	PE-Cy7	Mouse	JES6-5H4	eBioscience	25-7021-82
KI-67	FITC	Mouse	SolA15	eBioscience	11-5698-82
KI-67	PE	Mouse	MIB-1	Biozol Diagnostica	652404
LAG3	PE	Mouse	eBioC9B7W	eBioscience	12-2231-82
NK1.1	FITC	Mouse	PK135	Biolegend	108706
PD-1	PE-Cy7	Mouse	RPM1-30	Biolegend	109110
PD-1	APC	Mouse	RPM1-30	Biolegend	109112
PD-1	PE-Dazzle	Mouse	RPM1-30	Biolegend	109116
PD-1	PE	Mouse	RPM1-30	Biolegend	169104
TNF	eFluor® 450	Mouse	MP6-XT22	eBioscience	48-7321-82

3.1.4 Chemicals and reagents

Table 5: Chemicals and reagents used in this work.

Name	Experiment/ Purpose	Supplier	Reference
10 % Tween 20	scRNA sequencing	Biomol GmbH, Hamburg	E108
2-Mercaptoethanol (55 mM)	Cell culture	Thermo Fisher Scientific, Waltham	21985-023
4’,6-diamidino-2-phenylindole (DAPI)	Flow cytometry staining	Sigma-Aldrich, Steinheim	D9542-1MG
Agencourt® AMPure® XP, 60 mL	scRNA sequencing	Beckman Coulter, Brea	A63881
Cotrim K-ratiopharm 240 mg	Mouse experiments	Ratiopharm, Ulm	3788230
Dimethylsulfoxid (DMSO)	Freezing medium	Sigma-Aldrich, Steinheim	41639
DirectPCR Lysis Reagent (Mouse Tail) 50 mL	PCR	Viagen Biotech, Los Angeles	101-T

Dulbecco's Modified Eagle's Medium (DMEM)	Cell culture	Sigma-Aldrich, Steinheim	D6046
Dulbecco's Phosphate Buffered Saline (PBS)	Misc.	Sigma-Aldrich, Steinheim	D8537
DynabeadsTM MyOneTM SILANE	scRNA sequencing	10x Genomics, Pleasanton	PN-2000048
eBioscience 1-Step Fix/Lyse Solution	Flow cytometry staining	Thermo Fisher Scientific, Waltham	00-5333-57
eBioscience Cell Stimulation Cocktail (500X)	T-cell stimulation	Thermo Fisher Scientific, Waltham	00-4970-93
eBioscience Fixable Viability Dye eFluor 506	Flow cytometry staining	Thermo Fisher Scientific, Waltham	65-0866-14
eBioscience Protein Transport Inhibitor Cocktail	T-cell stimulation	Thermo Fisher Scientific, Waltham	00-4980-93
Ethanol	Misc.	Fisher Scientific GmbH, Schwerte	10342652
Ethidium Bromide Solution (1 %)	PCR	Carl Roth, Karlsruhe	2218
Fetal Bovine Serum (FBS)	Misc.	Sigma-Aldrich, Steinheim	F7524
GeneRuler 1 kb Plus DNA Ladder	PCR	Fisher Scientific Oy, Vantaa	11581625
Gibco HEPES (1 M)	Cell culture	Thermo Fisher Scientific, Waltham	15630056
Gibco L-Glutamine (200 mM)	Cell culture	Thermo Fisher Scientific, Waltham	25030024
Gibco MEM Non-Essential Amino Acids Solution (100X)	Cell culture	Thermo Fisher Scientific, Waltham	11140035
Gibco Penicillin/Streptomycin (10,000 U/mL)	Cell culture	Thermo Fisher Scientific, Waltham	15140122
Glycerol (50 %), Sterile Solution	scRNA sequencing	BioVision BV, Milpitas	B1012-100
High Sensitivity D1000 Reagents	scRNA sequencing	Agilent Technologies, Santa Clara	5067-5585
High Sensitivity D5000 Reagents	scRNA sequencing	Agilent Technologies, Santa Clara, USA	5067-5593
Invitrogen 123count eBeads Counting Beads	Flow Cytometry Staining	Thermo Fisher Scientific, Waltham	01-1234-42
Normal Rat Serum	Cell isolation	Jackson ImmunoResearch Laboratories, West Grove	012-000-120

Prima Amp Hot Start Master Mix	PCR	Steinbenner Laborsysteme, Wisenbach	SL-9714-10ml
Proteinase K	PCR	Thermo Fisher Scientific, Waltham	11826724
RNase free water	Misc.	Ambion, Carlsbad	AM9937
RPMI 1640	Cell culture	Sigma-Aldrich, Steinheim	R8758
Sodium Pyruvate (100 mM)	Cell culture	Thermo Fisher Scientific, Waltham	11360039

Note: Misc. = Miscellaneous, U = Units.

3.1.5 Buffers and solutions

Table 6: Buffers and solutions used in this work.

Buffer	Experiment/ Purpose	Composition/ Supplier	Catalog #
eBioscience Foxp3 / Transcription Factor Staining Buffer Set	Flow Cytometry Staining	Thermo Fisher Scientific, Waltham	00-5523-00
eBioscience IC Fixation Buffer	Flow Cytometry Staining	Thermo Fisher Scientific, Waltham	00-8222-49
eBioscience Permeabilization Buffer (10X)	Flow Cytometry Staining	Thermo Fisher Scientific, Waltham	00-8333-56
FACS buffer	Flow Cytometry Staining	PBS + 2% FBS	NA
Freezing Media	Cryopreservation	90% FBS + 10% DMSO	NA
MACS Buffer	Cell isolation	Miltenyi Biotec, Bergisch Gladbach	130-091-221
Qiagen Buffer EB	scRNA sequencing	Qiagen, Hilden	19086
RBC Lysis Buffer (10X)	Cell isolation	Biolegend, San Diego	420301

Note: NA = Not Applicable.

3.1.6 Kits

Table 7: Commercial kits used in this work.

Name	Experiment/ Purpose	Supplier	Reference
CD90.2 MicroBeads, Mouse	Cell isolation	Miltenyi Biotec, Bergisch Gladbach	130-121-278
Chromium™ i7 Multiplex Kit, 96 rxns	scRNA sequencing	10x Genomics, Pleasanton	120262
Chromium™ Single Cell 3'/5' Library Construction Kit, 16 rxns	scRNA sequencing	10x Genomics, Pleasanton	PN-1000020
Chromium™ Single Cell 3' Library & Gel Bead Kit v2, 4 rxns	scRNA sequencing	10x Genomics, Pleasanton	PN-120267
Chromium™ Single Cell 5' Library & Gel Bead Kit, 4 rxns	scRNA sequencing	10x Genomics, Pleasanton	PN-1000014
Chromium™ Single Cell A Chip Kit, 16 rxns	scRNA sequencing	10x Genomics, Pleasanton	PN-1000009
Chromium™ Single Cell V(D)J Enrichment Kit, Human T Cell, 96 rxns	scRNA sequencing	10x Genomics, Pleasanton	PN-1000005
Chromium™ Single Cell V(D)J Enrichment Kit, Mouse T Cell, 96 rxns	scRNA sequencing	10x Genomics, Pleasanton	PN-1000071
QIAamp DNA Micro Kit (50)	DNA isolation	Qiagen, Hilden	56304
QIAquick PCR Purification Kit	PCR product purification	Qiagen, Hilden	28104
EasySep Mouse CD4+ T cell isolation kit	Cell isolation	Stemcell Technologies, Vancouver	19852
EasySep Mouse CD8+ T cell isolation kit	Cell isolation	Stemcell Technologies, Vancouver	19853
Easysep Mouse Pan-B Cell Isolation Kit	Cell isolation	Stemcell Technologies, Vancouver	19844
Qubit dsDNA HS Assay Kit	scRNA sequencing	Thermo Fisher Scientific, Waltham	Q32854

Note: Rxn = reaction.

3.1.7 Consumables

Table 8: Consumables used in this work.

Name	Experiment/ Purpose	Supplier	Reference
96-Well U Bottom Plate	Miscellaneous	Techno Plastic Products (TPP), Trasadingen	TPP92197
Cell Culture Dish 100/20 mm	Miscellaneous	Greiner Bio-one, Frickenhausen	664160
Conical Tubes (15 mL, 50 mL)	Miscellaneous	Techno Plastic Products (TPP), Trasadingen	91014, 91054
Corning Plastic Serological Pipettes (5mL, 10 mL, 25 mL, 50 mL)	Miscellaneous	Corning, New York	CLS4487, CLS4488, CLS4489, CLS4490
Corning® Costar® Reagent Reservoirs (50 mL)	Flow Cytometry Staining	Corning, New York	CLS4870-5EA
Cryo.s, 2 mL	Cryopreservation	Greiner bio-one, Frickenhausen	TPP91014, TPP91050
DNA LoBind Tubes, DNA LoBind, 1,5 mL	scRNAseq/ Cell sorting	Eppendorf, Hamburg	22431021
Eppendorf Safe-Lock Microcentrifuge Tubes (1.5 mL, 2 mL, 5mL)	Miscellaneous	Eppendorf, Hamburg	22363204
Falcon Polystrene Round Bottom Tubes (5 mL)	Flow Cytometry Staining	Corning, New York	352052
Falcon® 70 µm Cell Strainer	Tissue dissociation	Corning, New York	352350
Fine Dosage Syringes, Injekt®-F Solo	Cell injection	VWR International, Radnor	720-2561
GentleMACS™ C Tubes	Tissue dissociation	Miltenyi Biotec, Bergisch Gladbach	130-093-237
High Sensitivity D1000 ScreenTape	scRNA sequencing	Agilent Technologies, Santa Clara	5067-5584
High Sensitivity D5000 ScreenTape	scRNA sequencing	Agilent Technologies, Santa Clara	5067-5592
LS columns	Cell isolation	Miltenyi Biotec, Bergisch Gladbach	130-042-401

MiniCollect® K2E K2EDTA	Blood collection	Greiner Bio-one, Frickenhausen	450532
Mr. Frosty™ Freezing Container	Cryopreservation	Nunc, Rosklide	5100-0001
NEOJECT® Hypodermic Needles (23G, 25G and 27G)	Cell injection	Dispomed Witt, Gelnhausen	10025, 10089, 10127
Pipette Tips (10 µL, 20 µL, 100 µL, 200 µL, 1000 µL)	Miscellaneous	Steinbenner Laborsysteme, Wisenbach	TP50010, TP50020, TP50100, TP50200, TP51250
Vi-CELL™ XR	Cell counting	Beckman Coulter, Brea	383721

3.1.8 Equipment and devices

Table 9: Equipment and devices used in this work.

Name	Experiment/ Purpose	Supplier
10x Magnetic Separator	scRNA sequencing	10x Genomics, Pleasanton
10x Vortex Adapter	scRNA sequencing	10x Genomics, Pleasanton
4200 TapeStation	scRNA sequencing	Agilent Technologies, Santa Clara
Accu-jet® pro Pipette Controller	Misc.	BrandTech, Essex
BD FACSAria™ II	Cell sorting	BD (Becton, Dickinson & Company), Franklin Lakes
BD FACSArisa Fusion	Cell sorting	BD (Becton, Dickinson & Company), Franklin Lakes
BD FACSCanto II	Flow Cytometry Staining	BD (Becton, Dickinson & Company), Franklin Lakes
BD LSR II	Flow Cytometry Staining	BD (Becton, Dickinson & Company), Franklin Lakes
BD LSRFortessa™	Flow Cytometry Staining	BD (Becton, Dickinson & Company), Franklin Lakes
C1000 Touch™ Thermal Cycler	scRNA sequencing	Bio-Rad Laboratories, Hercules
Cell Culture Safety Cabinet, Herasafe KS	Cell culture	Thermo Fisher Scientific, Waltham
Centrifuge 5810 R	Miscellaneous	Eppendorf, Hamburg
Centrifuge Heraeus Fresco 17	Miscellaneous	Thermo Fisher Scientific, Waltham

Chromium Next GEM Secondary Holder	scRNA sequencing	10x Genomics, Pleasanton
Chromium Single Cell Controller Instrument	scRNA sequencing	10x Genomics, Pleasanton
Easysep Magnet	Cell isolation	Stemcell Technologies, Vancouver
Eppendorf ThermoMixer C	scRNA sequencing	Eppendorf, Hamburg, Germany
FastGene Mini Centrifuge	scRNA sequencing	Nippon Genetics, Düren
Gammacell 40 Exactor	Mouse irradiation	Best Theratronics, Ottawa
GentleMACS Dissociator	Tissue dissociation	Miltenyi Biotec, Bergisch Gladbach
Heracell 150i Incubator	Cell culture	Thermo Fisher Scientific, Waltham
Heracell 240i Incubator	Cell culture	Thermo Fisher Scientific, Waltham
MACS Magnet Stand	Cell isolation	Miltenyi Biotec, Bergisch Gladbach
MasterCycler EP Gradient S	PCR	Eppendorf, Hamburg
PIPETMAN L Multichannel P8x200L, 20-200 µL	Miscellaneous	Gilson, Middleton
Pipettes (2 µL, 20 µL, 100 µL, 200 µL, 1000 µL)	Miscellaneous	Gilson, Middleton
QuadroMACS Separator	Cell isolation	Miltenyi Biotec, Bergisch Gladbach
Qubit 4.0 Fluorometer	scRNA sequencing	Thermo Fisher Scientific, Waltham
Scissors Surgical 11,5 cm Curved ST/ST	Tissue extraction	DKFZ Lagermaterial, Heidelberg
Tweezers Anatomical 10,5 cm Straight	Tissue extraction	DKFZ Lagermaterial, Heidelberg
Tweezers Surgical 10,5 cm Curved	Tissue extraction	DKFZ Lagermaterial, Heidelberg
UV-Gel Documentation System	PCR	BioRad, Hercules
Vi-CELL XR 2.03	Cell counting	Beckman Coulter Inc.,Brea
Vortex Mixer Neolab 7-2020	Miscellaneous	neoLab Migge, Heidelberg
Water Bath Julabo SW-20C	Miscellaneous	Julabo, Seelbach

3.1.9 Software

Table 10: Software used in this work.

Name	Experiment/Purpose	Source	Version
Affinity Designer	Figure creation	Serif Ltd, West Bridgford	1.8.2.620
BD FACSDiva™	Flow cytometry data acquisition	BD (Becton, Dickinson & Company), Franklin Lakec	3149011B
CyTOF® Software	Mass cytometry data acquisition	Fluidigm Corporation, South San Francisco	6.7.1014
EndNote™ X9	Bibliography management	Thomson Reuters, Carlsbad	19.3.1.13758
FlowJo	Flow cytometry analysis	BD (Becton, Dickinson & Company), Franklin Lakes	X 10.0.7
GraphPad Prism	Statistical analysis, graph creation	GraphPad Software, San Diesgo	5.04/7
Microsoft Excel	Miscellaneous	Microsoft, Redmond	2016
Microsoft PowerPoint	Miscellaneous	Microsoft, Redmond	2016
Microsoft Word	Miscellaneous	Microsoft, Redmond	2016
Mosaic Vivarium (DKFZ production)	Mouse colonies management	Virtual Chemistry, San Jose	2018-1201-2020-0430a-Risky
R	Bioinformatic analyses	The R Foundation	3.5

3.2 Methods

3.2.1 Human tissue processing and conservation

LN samples obtained in the Hospital Clínic (Barcelona) were processed as follows: one half of the resected LN underwent routine histopathological and flow cytometry immunological evaluation. The other half was homogenized using a 70 µm cell strainer (Falcon, 352350) to obtain a single-cell suspension, which was resuspended in Roswell Park Memorial Institute (RPMI 1640, Sigma-Aldrich, R8758) medium containing 10 % dimethyl sulfoxide (DMSO, Sigma-Aldrich, D4540) and 60 % heat-inactivated fetal bovine serum (FBS; Thermo Fisher Scientific, F7524). Single-cell suspensions of peripheral blood (PB) and bone marrow (BM) were obtained via Ficoll-Paque sedimentation (GE-Healthcare, GE17-1440-02) and cryopreserved as described above. Lymph nodes collected at the University of Heidelberg (Heidelberg) were minced and suspended in RPMI 1640 medium (Sigma-Aldrich, R8758) supplemented with 10 % FBS (Thermo Fisher Scientific, F7524), 2 mM L-Glutamine (Thermo Fisher Scientific, 25030024), and penicillin and streptomycin (P/S, Thermo Fisher Scientific,

15140122) at a final concentration of 100 U/mL and 100 µg/mL, respectively. Cells were next filtered through a 40 µm strainer (Sigma-Aldrich, CLS431750), washed once with phosphate-buffered saline (PBS, Thermo Fisher Scientific, 10010023), and resuspended in RPMI 1640 medium (Sigma-Aldrich, R8758) supplemented with 20 % FBS (Thermo Fisher Scientific, F7524) and 10 % DMSO (SERVA Electrophoresis GmbH, 20385.01). All samples were cryopreserved in liquid nitrogen until further analysis.

3.2.2 Tumor models

3.2.2.1 Transgenic Eµ-TCL1 mice

Eµ-TCL1 (TCL1) transgenic mice were bred in the central animal facility of the German Cancer Research Center (DKFZ, Heidelberg). The mouse line was maintained by crossing heterozygous TCL1 with wild-type (WT) C57BL/6 littermates, resulting in an approximately 1:1 ratio of WT and heterozygous TCL1 mice. Two colonies of TCL1 mice were bred separately in order to maintain the N and J C57BL/6 substrains. The respective substrain background was confirmed via SNP analysis of tissue DNA using the Genome Scanning Service from The Jackson Laboratory (Bar Harbor). TCL1 mice were closely monitored for signs of illness, and leukemia development was confirmed by palpable splenomegaly and detection of $CD5^+$ $CD19^+$ leukemia cells in PB at an age of 10 to 15 months. Mice were sacrificed when reaching a specified time point or moribund state, and spleens were collected, processed and cryopreserved as described in Section 3.2.2.5.

Mice genotyping was performed using tail tissue DNA. Briefly, tissue was enzymatically digested by incubation in DirectPCR Lysis Reagent (Viagen Biotech, 101-T) containing Proteinase K (20 mg/mL, Thermo Fisher Scientific, 11826724) at 56 °C overnight followed by an incubation at 80 °C for 45 min the next day. PCR master mix was then prepared by adding 1:20 of lysate and 0.5 mM of forward (5-GCCGAGTGCCCGACACTC-3) and reverse (5-CATCTGGCAGCAGCTCGA-3) primers to 1X Prima Amp Hot Start Master Mix (Steinbenner Laborsysteme, SL-9714-10ml). The PCR reaction was performed in a MasterCycler EP Gradient S (Eppendorf) with the following settings:

Step	Temperature	Time (hh:mm:ss)
1	95 °C	00:02:00
2	95 °C	00:00:10
3	59 °C	00:00:10
4	72 °C	00:00:25
5	Go to Step 2, x34 (35 cycles)	
6	72 °C	00:03:00

Samples were run on a 1 % (w/v) agarose gel, stained with ethidium bromide (Carl Roth, 2218), and imaged using a UV-Gel documentation system (BioRad).

3.2.2.2 TCL1 Adoptive Transfer

TCL1 mice with tumor loads of more than 85 % were used for a first round of adoptive transfer (AT) of leukemia cells into C57BL/6 wild type (WT) recipients. In short, single-cell suspensions of TCL1 splenocytes were prepared and 1-1.5 x10^7 cells were injected into the tail vein (i.v.) or the peritoneal cavity (i.p.) of 8-12 weeks-old WT female mice. These transplanted mice reached end-stage disease between 3 and 5 months. One-time expanded leukemia cells were next used for the actual AT experiments in which WT, *Rag2*$^{-/-}$, *Il10* reporter (Fir x Tiger), or bone marrow chimeric mice were injected. The specific procedure used for adoptive transfer in *Rag2*$^{-/-}$ and bone marrow chimeric mice is detailed in Sections 3.2.2.3 and 3.2.2.4 respectively. The AT experiments in WT mice were conducted as follows: splenocytes from TCL1 AT mice were thawed, washed, and enriched for leukemic B-cells by using the EasySep™ Mouse Pan-B Cell Isolation Kit (Stemcell Technologies, 19844) according to manufacturer's instructions. Specifically, single-cell suspensions were resuspended in MACS buffer (Miltenyi Biotec, 130-091-221) at a concentration of 1 x10^8 cells/mL, and 50 µL/mL Normal Rat Serum (Jackson ImmunoResearch Laboratories, 012-000-120) was added prior to incubation with 50 µL/mL antibody Isolation Cocktail (Stemcell Technologies, 19844) for 5 min at room temperature. Next, 50 µL/mL RapidSpheres™ were added following a 2.5 min incubation step at room temperature. Sample-containing tubes were subsequently placed into an Easysep Magnet (Stemcell Technologies) and magnetic-based cell separation was allowed by incubation for 2.5 min at room temperature. B-cells were recovered by pouring the non-bound cell suspension into a new collection tube. Finally, cells were counted using a Vi-CELL XR 2.03 cell counter (Beckman Coulter Inc.) and resuspended to a concentration of 1 x10^8 cells/mL in PBS in order to intravenously inject 1 x10^7 cells. Tumor growth in injected mice was monitored by flow cytometry staining of $CD5^+$ $CD19^+$ cells from PB every two weeks. Importantly, all adoptive transplantations were performed with animals of the same J or N substrain for donor and recipient mice, to avoid allograft rejection (Ozturk et al. 2019). TCL1 AT experiments in WT and Fir x Tiger mice were conducted in collaboration with Dr. Philipp Rößner and Dr. Bola Hanna from the Department of Molecular Genetics in the German Cancer Research Center (DKFZ), Heidelberg.

3.2.2.3 Adoptive T-cell and tumor transfer into *Rag2* KO mice

Adoptive transfer of T-cells and TCL1 AT tumor cells into *Rag2*$^{-/-}$ mice was performed over two sequential days. On day 1, *Eomes*$^{-/-}$, *Il10rb*$^{-/-}$ and their respective WT control mice *Eomes*$^{+/+}$ and C57BL/6 J, were sacrificed and spleens were collected and processed as detailed in

Section 3.2.2.5 for obtaining single-cell suspensions. Next, $CD4^+$ or $CD8^+$ T-cells were isolated using the EasySep Mouse $CD4^+$ T-cell isolation kit or the EasySep Mouse $CD8^+$ T-cell isolation kit (both from Stemcell Technologies, 19852 and 19853) respectively, applying the manufacturer's instructions. In brief, cells were resuspended at a concentration of 2 $x10^8$ cells/mL in MACS Buffer (Miltenyi Biotec, 130-091-221) and 50 µL/mL Normal Rat Serum (Jackson ImmunoResearch Laboratories, 012-000-120) was added. Cells were next incubated for 10 min at room temperature with 50 µL/mL antibody Isolation Cocktail before 125 µL/mL RapidSpheres™ were added to the mix and incubated for 10 min at room temperature. Lastly, cells were placed into the Easysep Magnet (Stemcell Technologies) for 2.5 min at room temperature, and unbound T-cells were collected in new tubes. Finally, cells were counted, resuspended in PBS, and 1 $x10^6$ cells were intravenously injected. T-cells were isolated from 2-3 mice and pooled together for injection. On day 2, frozen splenocytes from TCL1 AT were retrieved and T-cell depleted using CD90.2 beads (CD90.2 MicroBeads, 130-121-278) following the provider's recommendations. First, thawed cells were washed by centrifugation at 300 g for 5 min and resuspended in PBS. Next, cells were resuspended in ice-cold MACS buffer (90 µL per 1 $x10^7$ cells) and incubated with CD90.2 beads (10 µL per 1 $x10^7$ cells) for 15 min at 4 °C. Excess beads were removed by addition of MACS buffer and centrifugation at 300 g for 5 min before adjusting cell concentration to 0.5 $x10^8$ cells/mL. Thereafter, the cell suspension was applied onto a magnetic LS column (Miltenyi Biotec, 130-042-401) located in a QuadroMACS Separator (Miltenyi Biotec) and the run-through solution containing non-T-cells was collected in a new tube. Finally, cells were counted, adjusted to a concentration of 5 $x10^7$ cells/mL and 100 µL of cell suspension were injected intravenously in 6-8 weeks old *Rag2*$^{-/-}$ female mice. The purity of both T-cells and tumor cells was typically above 90 %, as assessed by fluorescence-activated cell sorting (FACS) immunostaining. Tumor and T-cell expansion in *Rag2*$^{-/-}$ mice was measured weekly by submandibular blood withdrawal and subsequent whole-blood FACS staining, as detailed in Section 3.2.3.3. Mice were closely monitored for disease symptoms and were sacrificed at the study endpoint, 4-5 weeks after AT, by increasing CO_2 concentration. Spleen and inguinal LNs were dissected and processed as described in Section 3.2.2.5.

3.2.2.4 Generation of *Eomes* bone marrow chimeric mice

Rag2$^{-/-}$ mice, which lack mature T- and B-cells (Shinkai et al. 1992), were used as recipient for the generation of BM chimera, as it was previously observed that irradiation does not entirely deplete T-cells in host C57BL/6 mice, resulting in incomplete chimerism in the T-cell compartment of C57BL/6 chimera (data not shown, inhouse observation). Mice were subjected to whole-body irradiation in a Gammacell 40 Exactor (Best Theratronics) receiving two doses of 550 Rad at two time points 3 h apart. The following day, lethally irradiated *Rag2*$^{-/-}$ mice were

reconstituted with BM cells from *Eomes*$^{-/-}$ or *Eomes*$^{+/+}$ mice. BM cell suspensions were prepared as follows: *Eomes*$^{-/-}$ and *Eomes*$^{+/+}$ mice were sacrificed, their femurs and tibias were dissected, and BM cells were flashed out by injection of PBS + 2 % FBS into the bone marrow with a 25 G needle. For removal of cell clumps and generation of single-cell suspensions, cells were filtered through a 70 µm cell strainer (Corning, 352350), and subsequently washed once by centrifuging at 300 g for 5 min and resuspending in PBS + 2 % FBS. Next, mature T-cells were depleted by incubation with CD90.2 beads (CD90.2 MicroBeads, Miltenyi Biotec, 130-121-278) and subsequent column-based magnetic cell isolation strictly applying manufacturer's instructions. Cells were washed with PBS and centrifuged at 300 g for 5 min prior to incubation with CD90.2 beads (10 µL per 1 x10^7 cells) in MACS buffer (90 µL per 1 x10^7 cells, Miltenyi Biotec, 130-091-221) for 15 min at 4 °C. After a washing step, cells were resuspended at a concentration of 0.5 x10^8 cells/mL in MACS buffer and applied to a LS column placed in a QuadroMACS Separator (Miltenyi Biotec). Non-labeled cells flowing through the column were collected, centrifuged and resuspended in PBS to adjust the concentration at 2.5 x10^7 cells/mL. Finally, 200 µL of the cell suspension were intravenously injected into *Rag2*$^{-/-}$ mice. After BM transplantation, mice were provided for 3 weeks with soft food and water containing 400 mg/mL antibiotic Cotrim K (contains Trimethoprim and sulfamethoxazole, Ratiopharm, 3788230) to prevent infections. Four weeks later, complete BM reconstitution was evaluated by FACS immunostaining of major immune cell types present in peripheral blood (as assessed by CD3, CD19, CD4, CD8, CD11b, CX3CR1, and CD45). Once complete chimerism was achieved, i.e. 6 weeks after BM injection, leukemia cells were retrieved from frozen TCL1 AT splenocytes and depleted of T-cells using CD90.2 beads (CD90.2 MicroBeads, Miltenyi Biotec, 130-121-278) as detailed above. The resulting cell suspension was adjusted to a concentration of 5 x10^7 cell/mL and 100 µL were i.p. transferred to mice. Tumor growth was monitored every second week by peripheral blood immunostaining, as explained in Section 3.2.3.3. At the experimental endpoint, mice were sacrificed by increasing CO_2 concentration and spleens were dissected to be processed (see Section 3.2.2.5) and immunostained for FACS analysis (see 3.2.3.3).

3.2.2.5 Mouse organ collection and processing

PB was obtained via submandibular vein or cardiac puncture, collected in ethylenediaminetetraacetic acid (EDTA)-coated tubes (Greiner Bio-one, 450532) and stained for FACS analysis as described in Section 3.2.3.3.

Dissected inguinal LNs were dissociated using a 70 µm Falcon Cell strainer (Corning, 352350) and single cells were collected in tubes with PBS supplemented with 2 % FBS. Cells were counted and centrifuged for 5 min at 300 g in order to be subsequently resuspended in

PBS containing 2 % FBS at a concentration of 3 x10^7 viable cells/mL for immunostainings (see Section 3.2.3.1).

Spleens were collected in Gentle MACS tubes C (Miltenyi Biotec, 130-093-237) with RPMI medium (Sigma-Aldrich, R8758) supplemented with 10 % FBS and 1 % P/S and single-cell suspensions were generated with a gentleMACS tissue dissociator (Miltenyi Biotec). Erythrocytes were lysed by incubation with red blood cell (RBC) Lysis Buffer (Biolegend, 420301) for 5 min at room temperature. The reaction was stopped by addition of PBS and cells were centrifuged at 300 g for 5 min. For removal of clumps, cells resuspended in ice-cold PBS were filtered through a 70 µm cell strainer (Corning, 352350). After counting, the cell concentration was adjusted according to the subsequent use: for immunostainings to 3 x10^7 cells/mL in FACS buffer (PBS + 2 % FBS) (see Sections 3.2.3.1 and 3.2.3.2), or for cryopreservation in liquid nitrogen to 1 x10^8 cells/mL in freezing media (90 % FBS + 10 % DMSO).

3.2.3 Flow Cytometry analysis

3.2.3.1 Cell surface staining

Single-cell suspensions were immunostained with antibodies against cell surface proteins (Table 4) in FACS buffer containing 0.1 % fixable viability dye (Thermo Fisher Scientific, 65-0866-14) for 30 min at 4 °C. Cells were subsequently washed twice by centrifuging at 300 g for 5 min and resuspending in FACS buffer. When direct analysis was not possible, cells were fixed with IC fixation buffer (Thermo Fisher Scientific, 00-8222-49) for 30 min at room temperature, washed twice with FACS buffer, and stored in FACS buffer at 4 °C in dark conditions until being analyzed by flow cytometry.

3.2.3.2 Staining of intracellular proteins and transcription factors

For transcription factor or intracellular cytokine staining, cell surface-stained cells were fixed for 30 min at room temperature with Foxp3 fixation/permeabilization buffer (Thermo Fisher Scientific, 00-5523-00). After a washing step with FACS buffer, cells were permeabilized for 30 min at room temperature with 1X permeabilization buffer (Thermo Fisher Scientific, 00-8333-56). Intracellular staining with antibodies against transcription factors or cytokines (Table 4) was performed in 1X permeabilization buffer for 30 min at room temperature. Excess antibodies were washed twice with 1X permeabilization buffer and cells were resuspended in 1X permeabilization buffer and stored at 4°C in dark conditions until they were analyzed by flow cytometry.

3.2.3.3 Whole-blood staining

In order to analyze peripheral blood of mice by FACS immunostaining, 25 µL of blood were stained with antibodies against cell surface proteins (Table 4) for 30 min at 4 °C. Blood was then incubated with 2 mL of 1X 1-Step Fix/Lyse Solution (Thermo Fisher Scientific, 00-5333-57) for 15 min at room temperature in dark conditions for erythrocytes lysis and cell fixation. Cells were spun down at 600 g, and the pellet was resuspended in 150 µL of PBS. To obtain absolute cell numbers, 25 µL of 123count eBeads™ (Thermo Fisher Scientific, 01-1234-42) were added to the samples right before flow cytometric measurement. Absolute cell numbers in PB were calculated using the following formula:

$$absolute\ count\ (cells/\mu L) = \left(\frac{cell\ count \times bead\ volume}{bead\ count \times cell\ volume}\right) \times bead\ concentration$$

3.2.3.4 Cell sorting

Single-cell suspensions from LNs of CLL patients were retrieved by partially thawing vials of cryopreserved cells in order to preserve unused cells. Single-cell suspensions from TCL1 AT splenocytes were prepared as detailed in Section 3.2.2.5. Samples were stained for cell surface proteins for 30 min. After two washing steps with PBS, cells were resuspended in PBS + 5 % FBS containing 0.2 µg/mL 4',6-diamidino-2-phenylindole (DAPI) prior cell sorting. The gating strategy for $CD3^+$ T-cell and CLL cell sorting is depicted in Figure 5. Cells were sorted in PBS + 2 % FBS using a BD FACSAria™ II or BD FACSArisa Fusion (both from BD

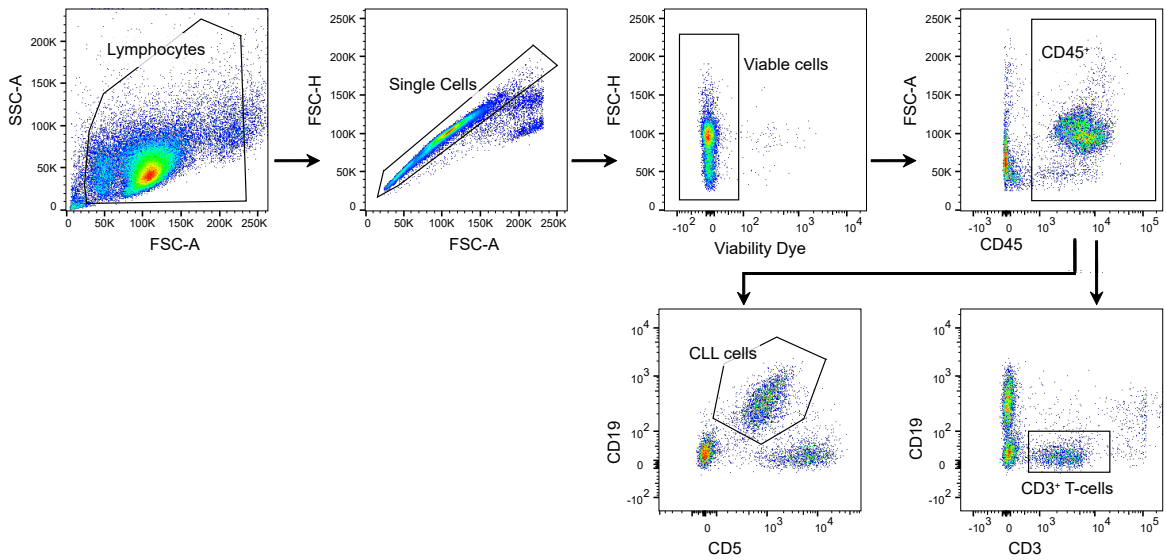

Figure 5: Gating strategy for FACS sorting of CLL cells and $CD3^+$ T-cells from human LN and murine spleen. Cell debris (identified by SSC-A vs. FSC-A) and doublets (identified by FSC-H vs. FSC-A) were first excluded followed by selection of viable cells (cells negative for viability dye). Leukocytes were then selected ($CD45^+$) and CLL cells were identified as $CD5^+$ $CD19^+$, and T-cells as $CD3^+$ $CD19^-$.

Biosciences) cell sorter with FACSDiva Software (BD Biosciences). The purity of cells after sorting was above 95 %.

3.2.3.5 Data acquisition and analysis

Cell fluorescence was assessed using a BD LSRFortessa™ or a FACS Canto II (both from BD Biosciences) flow cytometer, and data was analyzed using FlowJo X 10.0.7 software (FlowJo). In each experiment, single fluorochrome stainings were used to compensate for spectral overlap, which was corrected both before sample acquisition and when analyzing the data with FlowJo. Fluorescence minus one (FMO) controls were employed for proper gating of positive cell populations. FMO-normalized Mean Fluorescence Intensity (nMFI) for unimodal distributions or percentage of positive cells for bimodal distributions were determined for populations of interest. The standard gating strategy for analysis of CLL cells and T-cells is depicted in Figure 6.

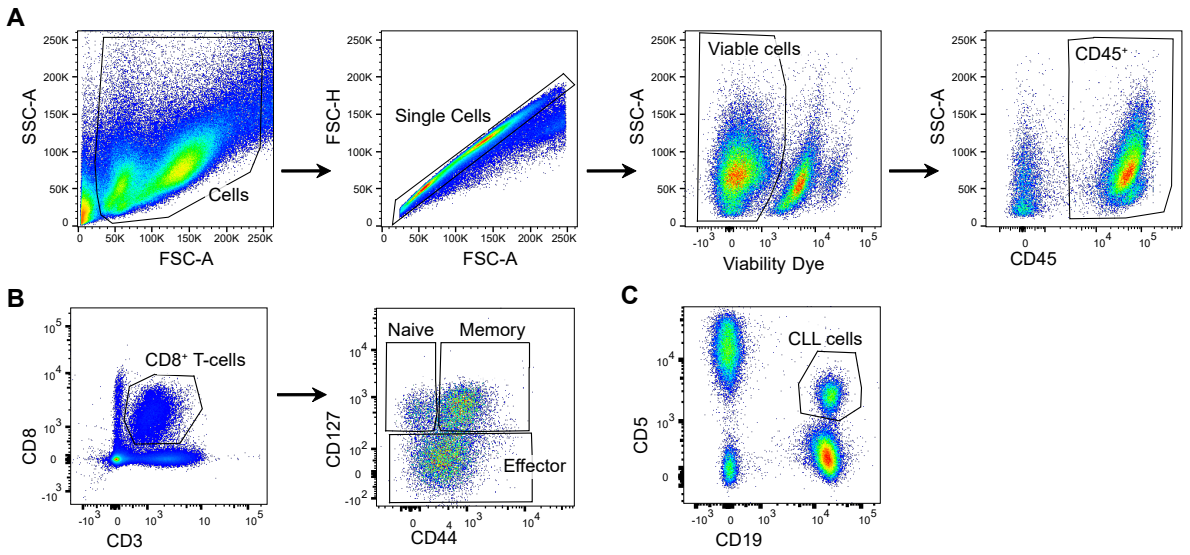

Figure 6: Gating strategy for T-cell subsets and tumor identification from murine spleen. **(A)** Gating of leukocytes was performed by exclusion of cell debris (identified by SSC-A vs. FSC-A) and doublets (identified by FSC-H vs. FSC-A), selection of live cells (cells negative for viability dye) and selection of $CD45^+$ cells (SSC-A vs. $CD45^+$). **(B)** T-cell gating was performed on leukocytes and based on $CD3^+$ $CD8^+$ for $CD8^+$ T-cells as exemplified, or $CD3^+$ $CD4^+$ for $CD4^+$ T-cells. Naïve ($CD127^+$ $CD44^-$), memory ($CD127^+$ $CD44^+$) and effector ($CD127^-$ $CD44^+$) cell subsets were identified as well. **(C)** CLL cells were gated as $CD5^+$ $CD19^+$ cells after leukocyte selection.

3.2.4 Ex vivo T-cell functional assays

Single-cell suspensions of mouse splenocytes were resuspended in DMEM medium (Sigma-Aldrich, D6046) supplemented with 10 % FBS (Sigma-Aldrich, F7524), 100 µg/mL P/S (Thermo Fisher Scientific, 15140122), 2mM L-glutamine (Thermo Fisher Scientific, 25030024), 10 mM Hydroxyetyl-Piperazineethane-Solfonic Acid (HEPES, Thermo Fisher Scientific,

15630056), 55 µM ß-mercaptoethanol (Thermo Fisher Scientific, 21985-023), 1 mM sodium pyruvate (Thermo Fisher Scientific, 11360039) and 100 µM non-essential amino acids (Thermo Fisher Scientific, 11140035), at a concentration of $3x10^7$ cells/mL. Cells were seeded in 96-well plates and cultured with cell stimulation cocktail (Thermo Fisher Scientific, 00-4970-93) and protein transport inhibitor cocktail (Thermo Fisher Scientific, 00-4980-93) for 6 h at 37°C and 5 % CO_2. CD107a antibody (Thermo Fisher Scientific, 12-1071-83) was added to the culture for assessment of degranulation capacity. Next, cells were washed twice with FACS buffer and immunostained for cell surface and intracellular proteins as described in Section 3.2.3.2.

3.2.5 Identification of chromatin states and RNA-seq tracks of the *EOMES* locus

Chromatin immunoprecipitation sequencing (ChIP-seq) data from antibodies detecting histone modifications H3K4me, H3K4me1m, H3K27ac, H3K36me3, H3K27me3, and H3K9me3 was downloaded from the Blueprint Epigenome Consortium (The BLUEPRINT Consortium 2016, www.blueprint-epigenome.eu) for the following cell types: $CD8^+$ memory T-cells, $CD8^+$ T-cells, $CD4^+$ memory T-cells, $CD4^+$ T-cells, NK cells, naïve B-cells, germinal center (GC) B-cells, memory B-cells, plasma cells, mature neutrophils, eosinophils and monocytes. Chromatin state assignment was performed using the chromHMM pipeline (Ernst and Kellis 2012; Beekman et al. 2018), and all profiles were corrected using their corresponding input. Each chromatin state was assigned for a 200 bp window. In addition, .bigWig tracks from the above-mentioned cell subtypes were downloaded from the Blueprint Epigenome Consortium, and aligned to the GRCh38 genome using unique mappings. The chromatin state assignments and RNA-seq alignments were performed by Dr. Vicente Chapaprieta from the Institut d'Investigacions Biomèdiques August Pi I Sunyer (IDIBAPS, Barcelona).

3.2.6 Mass Cytometry by Time of Flight (CyTOF) analysis

Sample preparation, data acquisition and initial data processing described in 3.2.6.1, 3.2.6.2, and 3.2.6.3 were performed by Dr. Marina Wierz from the Department of Oncology in the Luxembourg Institute of Health (LIH, Luxembourg) as part of a cooperation project.

3.2.6.1 CyTOF panel and metal labeling of antibodies

A panel of 42 heavy metal-labeled antibodies for detection of both surface and intracellular proteins was adopted from Bengsch et al. and modified based on literature research in order to characterize diverse T-cell phenotypes (Bengsch et al. 2018). The complete list of proteins detected and the heavy metal-conjugated antibodies used are listed in Table 3. Where no heavy metal-conjugated antibodies were commercially available, coupling of heavy metal to

respective antibodies was performed using the Maxpar® X8 Multimetal Labeling kit (Fluidigm, 201300) following the manufacturer's instructions.

3.2.6.2 Sample preparation

Frozen cell suspensions were thawed and washed prior to incubation in 15 mL of pre-heated RPMI 1640 (Sigma-Aldrich, R8758) containing 10 % FBS (Sigma-Aldrich, F7524) in a roller incubator for 30 min at room temperature. Cells were filtered through a 100 µm cell strainer (CellTrics, 04-004-2328) to remove dead cells. Next, B-cell depletion was performed using human CD19 microbead (Miltenyi Biotec, 130-050-301) labeling according to the manufacturer's protocol. In brief, cells were incubated with CD19 Microbeads for 15 min at 4 °C, washed, resuspended in MACS buffer (Miltenyi, 130-091-221) and loaded onto MACS® LS Columns (Miltenyi Biotec, 130-042-401) placed in a MidiMACS^{TM} Separator (Miltenyi Biotec). Finally, the flow-through fraction containing unlabeled CD19$^-$ cells was collected, washed in MACS buffer, filtered through a 70 µm cell MACS SMartStrainer (Miltenyi Bitec, 130-098-462), and counted prior to mass cytometry processing.

3.2.6.3 Cell staining and CyTOF sample acquisition

CD19-depleted single-cell suspensions were stained as previously described (Wierz et al. 2018). Briefly, cells were stained with 5 µM cisplatin (Cell-ID Cisplatin, Fluidigm, 201064) for 5 min in order to label dead cells. Cells were then washed with PBS + 0.5 % FBS and centrifuged at 500 g for 10 min. Cell surface staining was performed by adding the antibody-cocktail and incubating for 30 min at room temperature. After a washing step, cells were fixed with Fixation/Permeabilization buffer (Thermo Fisher Scientific, 88-8824-00) following the manufacturer's instructions. Intracellular staining was performed by incubating the antibody-cocktail for 30 min at room temperature. After a washing step, cells were stained with cell-ID Intercalator-Ir (Fluidigm, 201192A) in fixation and permeabilization solution, followed by another two washing steps with PBS and ddH_2O, respectively. Prior to acquisition, cells were resuspended at a concentration of 5 x 10^5 cells/mL in ddH_2O with 1:10 calibration beads (EQ Four Element Calibration Beads, Fluidigm, 201078). Samples were analyzed at a flow rate of 0.03 mL/min with the Helios mass cytometer (Fluidigm) at the National Cytometry Platform (NCP) of the Luxembourg Institute of Health (LIH, Luxembourg). Initial data processing and quality control were performed by the NCP, where flow cytometry standard (FCS) files were normalized with EQ beads using the HELIOS instrument acquisition software (Fluidigm, version 6.7.1014).

As a first analysis step, samples were pre-gated as follows: gates were placed on cells (Beads vs. Ir191), singlets (Ir193 vs. Ir191) and live cells (Pt195$^-$). Next, non-B immune cells (CD19$^-$ CD45$^+$) and CD3$^+$ T-cells (CD3$^+$ NCAM$^-$) were selected, and finally, either CD4$^+$ or

$CD8^+$ ($CD4^+$ vs. $CD8^+$) cells were gated and exported as .fcs files. $CD4^+$ and $CD8^+$ cells were further analyzed in close collaboration with Dr. Yashna Paul. The present study focuses on the analysis of $CD8^+$ T-cells, whereas a detailed investigation of the $CD4^+$ T-cell dataset can be found elsewhere (Paul 2020).

3.2.6.4 Mass cytometry data processing and sample clustering

All raw data .fcs files together with their metadata files containing sample ID and staining information were merged into a flowSet object using flowCore package (Hahne et al. 2009). Signal intensities for each marker were arcsinh-transformed using a co-factor of 5 (default) (Bruggner et al. 2014). Sample quality was assessed based on library size per sample and an analysis of cell counts, with the later ranging from 333 to 1.57 x 10^5 cells. Multi-dimension scaling (MDS) plotting using median arcsinh-transformed marker expression for all cells in each sample was used for sample clustering analysis. Data processing and analysis was performed by Dr. Yashna Paul from the Molecular Genetics Division (B060) in the German Cancer Research Center (DKFZ, Heidelberg).

3.2.6.5 Mass cytometry single-cell clustering

Cytometry data analysis tools (CATALYST, (Chevrier et al. 2018)) R package containing FlowSOM (Van Gassen et al. 2015) and ConsensusClusterPlus (Wilkerson and Hayes 2010) metaclustering methods was used for cell cluster identification using all cells from all samples. Clustering was performed using arcsinh-transformed expression of 32 markers, i.e., excluding the markers that were utilized for cell population gating. The maximum number of clusters allowed to be evaluated was set to maxK = 14, after biological relevance of obtained clusters was assessed, and $k < 14$ and $k > 14$ were verified to be underfitting or overfitting, respectively. Cell clustering was visualized using a t-distributed stochastic neighbor embedding (t-SNE) algorithm, displaying 1 x10^3 random cells from each sample in order to reduce computation time. The robustness of this approach was evaluated by repeatedly plotting an increasing number of randomly picked cells from each sample, with a range of 200 to 1,000 cells, and evaluating the similarity of the 14 subpopulations recognized in the respective t-SNE plots. Bioinformatic data analysis was performed in collaboration with Dr. Yashna Paul. For cell subset annotation, combined expression of lineage markers as well as unique expression of activation and exhaustion-related markers was considered.

3.2.6.6 Correlation of cluster proportions with clinical data

The clinical data summarized in Table 1 was correlated with the cluster abundance for every CLL patient sample. Briefly, the following clinical parameters were categorized into the following balanced sets: sex (female/ male), *IGHV* mutation status (mutated/ unmutated), Binet

stage (A/ B, C), Rai stage (0, I/ II, III, IV), time to first treatment (> 16.4 months/ <16.4 months), and treatment status (treated/ untreated). Next, the enrichment or depletion of clusters in each condition was calculated using a Mann-Whitney U test. Additionally, the parameters age, % of tumor cells, and time to first treatment were correlated with cluster abundances using Pearson correlations.

3.2.7 Single-cell transcriptome analyses

3.2.7.1 Single-cell RNA sequencing of $CD3^+$ T-cells from lymph nodes of CLL patients

Three CLL LN samples were processed for single-cell RNA sequencing. $CD3^+$ T-cells and CLL cells from these samples were sorted as described in Section 3.2.3.4, and single-cell transcriptomes were generated using the Chromium Next GEM Single Cell V(D)J Reagent Kits v1.1 (10x Genomics, PN-1000167, PN-1000020, PN-1000005, PN-1000127, PN-1000213) following the manufacturer's protocol. Briefly, for a target cell recovery of 5,000 cells, the concentration of T-cells was adjusted to 1 $x10^3$ cells/µL and tumor cells were added at a ratio of 1:20. Cells were then loaded into the Single Cell A Chip (Chromium™ Single Cell A Chip Kit, 10x Genomics, PN-1000009) together with Reverse Transcription (RT) Master Mix (10x Genomics, PN-1000011). Gel beads (10x Genomics, PN-1000010) and partitioning oil (10x Genomics, PN-1000009) were subsequently loaded into respective wells of the chip, before placing it into the Chromium Controller (10x Genomics). In the Chromium Controller, nanoliter scale Gel Beads-in-emulsion (GEMs) are generated, each containing a single cell. Inside the GEM, the cell is lysed and its polyadenylated transcripts bind the barcoded bead. Such barcodes consist of a unique 10 nucleotide sequence named unique molecular identifier (UMI), which are later used during the data analysis process to link each transcript to its respective cell.

Next, GEMs were retrieved from the chip, placed in PCR tubes, and reverse transcription of poly-adenylated mRNA was performed in a thermal cycler (Bio-Rad Laboratories) with the following protocol:

Step	Temperature	Time (hh:mm:ss)
1	53 °C	00:45:00
2	85 °C	00:05:00
3	4 °C	Hold

GEMs were subsequently broken by addition of Recovery Agent (10x Genomics, PN-1000009), and pooled cDNA was purified from GEM-RT reaction mixture as follows: Dynabeads Cleanup Mix (10x Genomics, PN-2000048) were added, and a 10x Magnetic Separator (10x Genomics) was used to pool beads for removal of supernatant containing GEM-RT reagents. After washing with 80 % ethanol, Elution Solution I (10x Genomics, PN-

1000011) was added for recovery of 5' Gene Expression (GEX) cDNA. Full length GEX cDNA was subsequently amplified by adding cDNA Amplification Mix (10x Genomics, PN-1000011) and incubated in a thermal cycler following the protocol below.

Step	Temperature	Time (hh:mm:ss)
1	98 °C	00:00:45
2	98 °C	00:00:20
3	67 °C	00:00:30
4	72 °C	00:01:00
5	Go to Step 2, 13x (14 cycles)	
6	72 °C	00:01:00
7	4 °C	Hold

Amplified GEX cDNA was purified using Agencourt AMPure beads (Beckman Coulter, A63881) and 80 % ethanol in a 10x Magnetic Separator (10x Genomics, PN-230003) before proceeding to quality control (QC) and quantification in a 4200 TapeStation (Agilent Technologies). Next, 2 µL cDNA were transferred to new tubes for target enrichment of V(D)J segments via PCR amplification using CDR3 region-specific primers (10x Genomics, PN-1000005). In brief, Target Enrichment 1 Reaction Mix (10x Genomics, PN-1000011 and 1000005) was added and samples were incubated in a thermal cycler with the following protocol:

Step	Temperature	Time (hh:mm:ss)
1	98 °C	00:00:45
2	98 °C	00:00:20
3	67 °C	00:00:30
4	72 °C	00:01:00
5	Go to Step 2, 9x (10 cycles)	
6	72 °C	00:01:00
7	4 °C	Hold

Amplified V(D)J-enriched cDNA was then cleaned using Agencourt AMPure beads and 80 % ethanol in a 10x Magnetic Separator prior to the addition of Target Enrichment 2 Reaction Mix (10x Genomics, PN-1000011 and 1000005) and incubating in a thermal cycler using the protocol listed as above. Enriched cDNA was cleaned, and size selected using Agencourt AMPure beads and 80 % ethanol in a 10x Magnetic Separator prior to QC and quantification in a 4200 TapeStation (Agilent Technologies). Library preparation from 50 ng of V(D)J-enriched cDNA was performed by adding Fragmentation Mix (10x Genomics, PN-1000011) to the samples and placing them into a thermal cycler with the following settings:

Step	Temperature	Time (hh:mm:ss)
Fragmentation	32 °C	00:02:00
End Repair & A-tailing	65 °C	00:30:00
Hold	4 °C	Hold

Subsequently, Adaptor Ligation Mix (10x Genomics, PN-1000011) was added and samples were further incubated as detailed:

Step	Temperature	Time (hh:mm:ss)
1	20 °C	00:15:00
2	4 °C	Hold

Reaction reagents were removed using Agencourt AMPure beads and 80 % ethanol in a 10x Magnetic Separator, and Sample Index PCR Mix (10x Genomics, PN-1000011 and PN-120262) was added prior to incubation in a thermal cycler with the following settings:

Step	Temperature	Time (hh:mm:ss)
1	98 °C	00:00:45
2	98 °C	00:00:20
3	54 °C	00:00:30
4	72 °C	00:00:20
5	Go to Step 2, 8x (9 cycles)	
6	72 °C	00:01:00
7	4 °C	Hold

The library was cleaned up with Agencourt AMPure beads and 80 % ethanol in a 10x Magnetic Separator, and final QC and quantification were performed before sequencing.

For library construction of GEX cDNA, Fragmentation Mix was added to 50 ng of sample, and the resulting mixture was incubated in a thermal cycler as follows:

Step	Temperature	Time (hh:mm:ss)
Fragmentation	32 °C	00:05:00
End Repair & A-tailing	65 °C	00:30:00
Hold	4 °C	Hold

Samples were next size-selected using Agencourt AMPure beads and 80 % ethanol in a 10x Magnetic Separator, prior to addition of Adaptor Ligation Mix and incubation in a thermal cycler with the following settings:

Step	Temperature	Time (hh:mm:ss)
1	20 °C	00:15:00
2	4 °C	Hold

A cleaning step using Agencourt AMPure beads and 80 % ethanol in a 10x Magnetic Separator was performed before adding Sample Index PCR Mix and incubating in a thermal cycler with the following settings:

Step	Temperature	Time (hh:mm:ss)
1	98 °C	00:00:45
2	98 °C	00:00:20
3	54 °C	00:00:30
4	72 °C	00:00:20
5	Go to Step 2, 15x (16 cycles)	
6	72 °C	00:01:00
7	4 °C	Hold

Constructed libraries were purified by using Agencourt AMPure beads and 80 % ethanol in a 10x Magnetic Separator, and QC was performed before sequencing.

GEX libraries were sequenced on a HiSeq 4000 machine (Illumina) using a Paired-End (26 + 74 bp) setup or on a NovaSeq 6000 (Illumina) with a Paired-End (28+94 bp) S1 setup, and V(D)J-enriched libraries were sequenced on a NextSeq 550 (Illumina) using a Paired-End (150 bp) configuration at the High Throughput Sequencing Unit of the Genomics and Proteomics Core Facility at the German Cancer Research Center (DKFZ, Heidelberg).

3.2.7.2 Single-cell RNA sequencing of $CD3^+$ T-cells from splenocytes of TCL1 AT mouse model

Two TCL1 AT mouse spleen samples were processed for single-cell RNA sequencing. Mice were euthanized and dissected spleens were processed as described in Section 3.2.2.5. Samples were subsequently FACS-sorted as described in Section 3.2.3.4. Sorted $CD3^+$ T-cells were resuspended to a concentration of 1 $x10^3$ cells/mL and tumor cells were added at a ratio of 1:20. Single-cell transcriptomes were generated using the Chromium Single Cell V(D)J Reagent Kits (10X Genomics, PN-1000014, PN-1000020, PN-1000071, PN-1000009 and PN-120262) following the manufacturer's instructions. The utilized protocol is detailed in Section 3.2.7.1 with a minor modification: Target Enrichment 1 Reaction Mix and Target Enrichment 2 Reaction Mix (both from 10x Genomics, PN-1000011) contained mouse-specific primers for V(D)J region amplification (10x Genomics, PN-1000071). GEX libraries were sequenced on a NovaSeq 6000 machine (Illumina) with a Paired-End (28+94 bp) S1 setup, and V(D)J-enriched libraries were sequenced on a NextSeq 550 (Illumina) using a Paired-End (150 bp) setup at

the High Throughput Sequencing Unit of the Genomics and Proteomics Core Facility at the German Cancer Research Center (DKFZ, Heidelberg).

3.2.7.3 Data processing, dimensional reduction, cell cluster visualization and identification of differentially expressed genes

Raw reads in .fastq format were aligned to the GRCh38 human reference genome or mm10 mouse reference genome using the Cell Ranger pipeline (10x Genomics). Sparse count matrices for each sample were generated as output files, as well as a quality control report, including the estimated number of cells sequenced, mean reads per cell, median genes per cell, and Q30 quality score.

For data normalization, scaling and dimensionality reduction and cell clustering, the Seurat v3 toolkit (Butler et al. 2018; Stuart et al. 2019) in R3.5 (The R Fundation, version 3.5) was used. First, cells with low-quality data were removed based on the number of genes expressed and mitochondrial gene content. Specifically, cells with < 200 genes and cells with > 3,000 genes, which were considered doublets, as well as cells with > 10 % mitochondrial genes were removed. In addition, genes present in < 2 cells were excluded for downstream analysis. Hereafter, datasets of the same species (i.e. the three human datasets and the two mouse datasets) were merged, and data was transformed and normalized utilizing SCTransform() function. Per default the 3,000 most variable genes from each sample were identified and considered for canonical correlation analysis (CCA) using the RunCCA() function, and merged data sets were integrated into a new dimensional reduction space. The 3,000 most variable genes were next selected for principal component (PC) analysis via RunPCA() function. Between 15 – 18 PCs were considered for further cell clustering. Using the FindNeighbors() function, a shared nearest neighbor graph (SNN) was created, and a hierarchical clustering using Louvain algorithm was generated with the FindClusters() function, with the resolution parameter set to 0.6. Non-linear dimensional reduction using t-SNE was performed in order to visualize the datasets. Finally, FindMarkers() and FindAllMarkers() functions using the non-parametric Wilcoxon rank sum test identified differentially expressed genes for each cluster, with an adjusted (Bonferroni correction) p-value of 0.05 set for considering significance. Bioinformatic processing and analysis of the data was performed by Dr. Yashna Paul.

3.2.7.4 Computational separation of $CD3^+$ T-cells into $CD8^+$ and $CD4^+$ cells

In addition to analysis and cell clustering of total $CD3^+$ T-cells, computational separation of $CD8^+$ and $CD4^+$ T-cells was carried out in order to perform a re-clustering and identify further cell subsets. For the human CLL LN dataset, cell splitting was performed selecting *CD8A*- and *CD4*-expressing clusters. For splitting $CD8^+$ and $CD4^+$ cells present in the same cluster, the Seurat function CellSelector() was used. The TCL1 AT mouse dataset comprised multiple

clusters containing both $CD4^+$ and $CD8^+$ cells, which required cell separation based on a calculation of pairwise distances between gene counts and centroids of the 3,000 most variable genes between $CD4^+$ and $CD8^+$ specific clusters. Bioinformatic cell separation was performed by Dr. Yashna Paul.

3.2.7.5 V(D)J T-cell analysis

V(D)J transcripts from single cells were aligned and counted using the Cell Ranger pipeline, which also generated a quality control report providing the approximate number of cells analyzed, mean read pairs per cell, a number of cells with a productive V-J spanning pair, as well as a Q30 quality score. In addition, an output file containing TCR α- and β-chain CDR3 nucleotide sequences and a cell barcode for all single cells was generated. Only productive rearrangements were evaluated, and 3 or more cells containing the same α- and β-chain CDR3 consensus nucleotide sequences were considered cell clones. Because both V(D)J transcripts and gene expression data contained common cell barcode IDs, the Seurat workflow allowed the mapping of the TCR information into the single-cell t-SNEs. Bioinformatic pipelines for this analysis were implemented by Dr. Yashna Paul.

The VDJdb browser (Bagaev et al. 2020) was used in order to identify CDR3 regions from the V(D)J single-cell dataset whose antigen-specificity has been reported. Both TCR α- and β-chain CDR3 amino acid sequences of the 10 most abundant clones from each sample were used for the literature analysis aimed at identifying previously described binding epitopes.

3.2.7.6 Intercellular communication analysis by CellPhoneDB

The CellPhoneDB pipeline (Vento-Tormo et al. 2018; Efremova et al. 2020) was used in order to determine intercellular communications between the identified clusters. A count matrix file containing gene expression values for each cell, and a count meta file with cell type annotations were used as input, while only considering those genes, for which at least 10 % of cells expressed it. The number of statistical iterations was set to 10, and a p-value < 0.05 was considered significant when determining whether a given interaction is cell-type-specific. The bioinformatic pipeline for CellPhoneDB analysis was implemented in collaboration with Dr. Murat Iskar from the Molecular Genetics Division (B060) at the German Cancer Research Center (DKFZ, Heidelberg).

3.2.8 Correlation between $CD8^+$ T-cells clusters from single-cell RNA sequencing and mass cytometry

For correlating the $CD8^+$ T-cells clusters identified with both single-cell RNA-seq and mass cytometry experiments, only the genes and proteins common in both datasets were considered. Next, the average profiles per cluster were calculated and these values were

mean-centered in comparison to all clusters defined for each of the datasets. The Pearson correlation coefficient was next calculated for each pair of mass cytometry versus single-cell RNA-seq clusters to identify the most similar between the two datasets. The bioinformatic pipeline for subset correlation was programmed by Dr. Murat Iskar from the Molecular Genetics Division (B060) at the German Cancer Research Center (DKFZ, Heidelberg).

3.2.9 Statistical analysis

The Mann-Whitney U test was used to investigate significant differences between two groups, while one-way analysis of variance (ANOVA) was used to determine differences between more than two groups. Pearson correlation was applied to examine linear correlation between cluster proportions per patient and clinical information. All these tests were calculated using GraphPad Prism (GraphPad Software). The statistical test used in each case is indicated in the corresponding figure legend. A confidence interval of 95 % (p-value of < 0.05) was considered for rejection of the null hypothesis.

4 Results

4.1 Dissecting the CD8⁺ T-cell compartment of CLL using mass cytometry and single-cell RNA-seq analyses

Single-cell technologies are increasingly being used to decipher the complexity of the tumor microenvironment of numerous cancers (Tirosh et al. 2016; Zheng et al. 2017; Azizi et al. 2018; Guo et al. 2018). The use of such methodologies has revealed a considerable heterogeneity of T-cell phenotypes within and between patients (Chevrier et al. 2017; Li et al. 2019; Wagner et al. 2019), the understanding of which is crucial to better predict therapy response. In order to comprehensively characterize the T-cell compartment associated with CLL, a large-scale and high-dimensional analysis of T-cells from CLL patients as well as healthy controls (HC) was conducted using both single-cell immunophenotype and transcriptome analyses. Specifically, CLL lymph nodes (LNs) together with paired peripheral blood (PB) and bone marrow (BM) samples, as well as reactive LNs (rLNs) from HC were investigated using mass cytometry with a panel of 42 antibodies. Additionally, single-cell RNA-seq analyses of T-cells from 3 CLL LN samples enabled the simultaneous study of their transcriptome and complete TCR sequences. The use of this approach facilitated the identification of diverse CLL T-cell subtypes with a distinct clonal expansion state, their association with clinical characteristics, and their potential cross-talk with tumor cells (Figure 7). This project was conducted in close collaboration with Dr. Yashna Paul, who focused her work on the description of the CD4⁺ T-cells analyzed (Paul 2020). The present work concentrates on the examination of CD8⁺ T-cells, and results obtained are explained in detail in the succeeding sections 4.2 and 4.3.

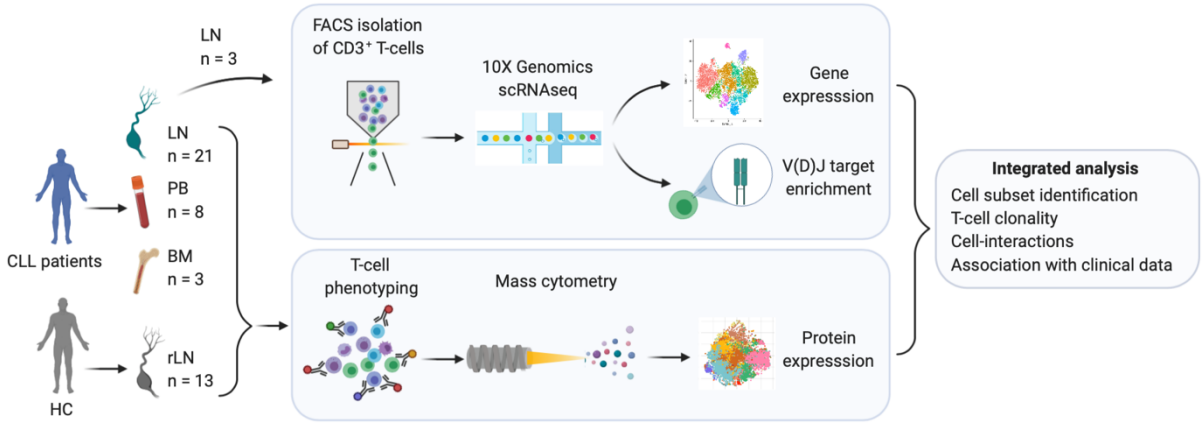

Figure 7: Overview of the experimental design to characterize the T-cell compartment in CLL. Workflow detailing the processing and number of samples analyzed by single-cell RNA-seq and mass cytometry (CyTOF) techniques. The precise methodology used for data acquisition and analysis is described in Sections 3.2.6 and 3.2.7. HC = healthy controls, LN = lymph node, rLN = reactive lymph node, PB = peripheral blood, BM = bone marrow.

4.2 Global CD8$^+$ T-cell profiling of CLL and control tissues by mass cytometry

Phenotypic alterations in the T-cell compartment in CLL patients have been extensively reported in PB samples (Totterman et al. 1989; Riches et al. 2013; Palma et al. 2017), but corresponding analyses are missing for LN tissue, despite the fact that it represents the main location of tumor-T-cell interactions (Burger 2011; Herishanu et al. 2011). To generate a complete characterization of the CD8$^+$ T-cell landscape in CLL, 48 samples from CLL LNs, PB, BM, as well as rLN of individuals without cancer were investigated using time of flight mass spectrometry (CyTOF) with a panel of 42 antibodies. Sample processing and data acquisition was performed in collaboration with Dr. Marina Wierz, from Luxembourg Institute of Health (LIH), Luxembroug, while data processing and analysis was performed in collaboration with Dr. Yashna Paul from the German Research Center (DKFZ), Heidelberg. The analysis yielded approximately 1.35 x10^6 CD8$^+$ T-cells, with a median of 1.11 x10^4 cells per sample. Using the t-SNE algorithm for dimensional reduction (Maaten and Hinton 2008), cells were classified into 14 clusters which were annotated based on the differential expression of the detected markers (Figure 8A and B). The expression of CD45RA, CD45RO and C-C chemokine receptor type (CCR) 7 (CCR7) was measured for general T-cell classification, which resulted into 1 naïve (T_N, CD45RA$^+$, CD45RO$^-$, CCR7$^+$), 1 central memory (T_{CM}, CD45RA$^-$, CD45RO$^+$, CCR7$^+$), 6 effector memory (T_{EM}, CD45RA$^-$, CD45RO$^+$, CCR7$^-$), and 2 effector (T_{EF}, CD45RA$^+$, CD45RO$^-$, CCR7$^-$) subsets. In addition, 3 CD4$^+$ CD8$^+$ double positive (DP) and 1 KI-67$^+$ proliferating (Prolif.) clusters were identified. DP_2 and PD_3 subsets constituted less than 1 % of cells in all samples except for two samples, and were therefore not further examined. A more detailed analysis of the expression of several markers comprising co-stimulatory (CD244, ICOS, CD27, KLRG1, and OX-40) and inhibitory receptors (PD-1, TIGIT and CTLA-4), ectoenzymes (CD73, CD39 and CD38), transcription factors (TCF7, TOX, HELIOS, TBET and EOMES) and the cytokine GZMK, allowed the identification of several cell subsets, which were hierarchically clustered in three subgroups (Figure 8B).

The first group comprised the two effector subsets, T_{EF1} and T_{EF2}, and the effector memory subset T_{EM3}. These were characterized by a moderate expression of TIGIT, KLRG1 and a high expression of the transcription factor TBET. In addition, T_{EF1} had higher expression levels of GZMK and CD27, while T_{EF2} presented greater expression of both TBET and HELIOS TFs (Figure 8B).

The second group was comprised of subsets with a distinctive high expression of IL7R, CCR7 and TCF7, and no expression of activation or exhaustion markers, as expected for naïve and central memory cells (Gattinoni et al. 2017). Notably, two effector memory subsets presented a similar expression pattern but with significant differences between each other.

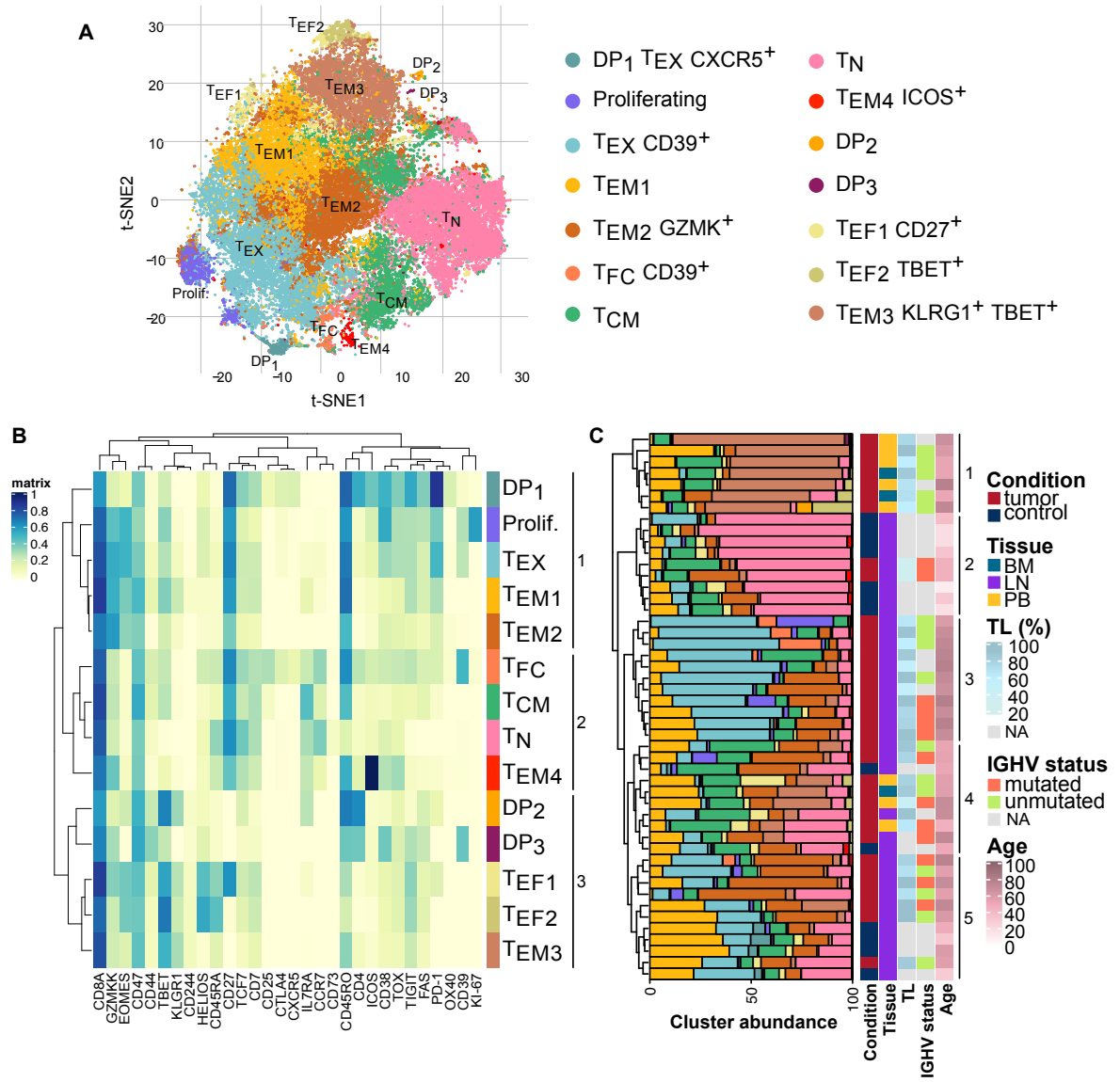

Figure 8: CD8⁺ T-cell landscape of CLL patients. (A) t-SNE plot of the 14 clusters identified with all analyzed samples. 1 x10^3 cells of each sample are depicted. **(B)** Heatmap showing median (arcsinh-transformed) protein expression of the 30 markers considered (columns) for each cluster (rows) identified. Both markers and clusters were grouped based on hierarchical clustering (with Pearson correlation and complete linkage). The three groups of clusters are indicated. **(C)** Hierarchical clustering (with Pearson correlation and complete linkage) of samples based on the CD8⁺ T-cell subset abundances in each sample. The five groups of samples identified are indicated. Cell subsets are color-coded as defined in (A). Row annotations (left) indicate sample condition (tumor or control), tissue of origin (BM, bone marrow, LN, lymph node, and PB, peripheral blood), tumor load (TL), *IGHV* mutation status (mutated or unmutated), and age (years). NA = not available.

While T_{EM4} contained cells with specifically high levels of ICOS and some GZMK expression, the other cluster was characterized by the expression of CD25, CTLA-4, as well as CXCR5, and was subsequently defined as a subset of follicular CD8⁺ cells (T_{FC}) (Yu and Ye 2018). Interestingly, T_{FC} cells exhibited intermediate expression of both inhibitory and co-stimulatory receptors, as well as naïve-related markers like TCF7, CCR7 and IL7R (Figure 8B).

The third group was characterized by clusters with an intermediate to high expression of exhaustion markers including PD-1, TIGIT, CD39, CD38, FAS, TOX and EOMES. More specifically, T_{EM1} and T_{EM2} GZMK$^+$ clusters presented moderate levels for these proteins and higher expression of GZMK, resembling a pre-dysfunctional effector memory population that expresses GZMK as well as intermediate levels of inhibitory molecules. The third cluster was defined as exhausted (T_{EX}) based on the higher expression of PD-1, TIGIT, and CD39 (McLane et al. 2019). Of note, proliferating cells had a very similar phenotype to T_{EX} cells, suggesting they could constitute a dividing subset of these cells. Intriguingly, DP_1 cells expressed the highest levels of exhaustion markers (i.e. PD-1, FAS; TIGIT, TOX, and CD38), as well as markers of follicular cells, like CXCR5 and CTLA-4 (Figure 8B).

To investigate the heterogeneity of T-cell immunophenotypes across samples, frequencies of the identified T-cell subsets were determined for each individual sample and a hierarchical clustering based on compositional similarity was performed. As shown in Figure 8C, in addition to a high inter-sample heterogeneity, five distinct groups were identified: one first group containing a high proportion of T_{EM3} KLRG1$^+$ TBET$^+$ cells, comprised PB and BM samples; a second group of samples, which presented high amounts of naïve cells, was mainly composed of HC LN samples; a third group with elevated percentages of T_{EX} cells contained only CLL LN samples; and the fourth and fifth groups, harbored no enrichment of a specific cell subset, organ or sample condition (Figure 8C). The definition of the five groups was not related to any clinical condition such as tumor load or *IGHV* mutation status. Instead, samples of younger age appeared to be enriched in group 2, suggesting that age might influence the CD8$^+$ T-cell phenotype present in LNs (Figure 8C). The effect of age in sample composition is further discussed in Section 4.2.3.

Taken together, these results provide a global picture of the CD8$^+$ T-cell landscape present in CLL patients, composed of subsets ranging from undifferentiated naïve cells, to central memory, effector, and effector memory cells with a diverse degree of activation and exhaustion. Besides, sample clustering based on subset frequencies revealed noticeable differences between tissues, as well as CLL samples compared to HC.

4.2.1 T-cells in CLL LNs exhibit a distinct immunophenotype compared to PB and BM tissues

The immunophenotypic analysis of the CD8$^+$ T-cell compartment revealed a tissue-related grouping of samples (Figure 8C), indicating that tissue cues significantly determine T-cell composition. In line with this, a higher presence of T-cells with an exhausted phenotype in LNs compared to PB has recently been suggested (Hanna et al. 2019). However, additional studies exhaustively analyzing the phenotypical differences between these two tissues are lacking, and the T-cell composition in CLL BM have not been characterized thus far. Therefore, for a comprehensive assessment of CD8$^+$ T-cell phenotypic differences among the three tissues,

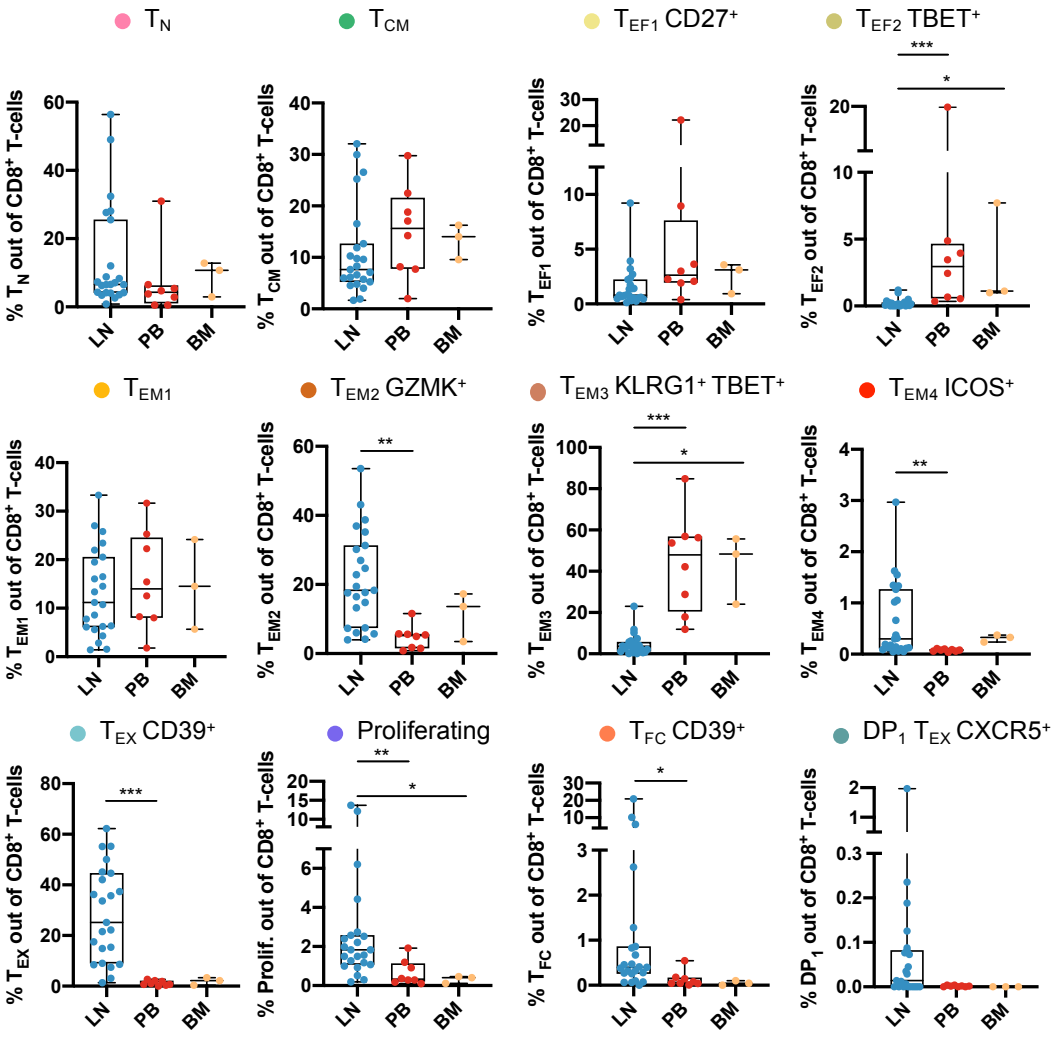

Figure 9: T-cells from LNs have a distinct phenotype compared to PB and BM. Percentage of cells belonging to a given cluster out of total CD8$^+$ T-cells for each sample were compared between LN (n = 21), PB (n = 8) and BM (n = 3) samples (*p<0.05, **<0.01, ***<0.001, Kruskal-Wallis test with multiple comparisons).

cluster frequencies between LN, PB and BM samples from CLL patients were compared (Figure 9). Notably, T_N, T_{CM}, T_{EF1} CD27$^+$, T_{EM1}, and DP_1 T_{EX} CXCR5$^+$ cell subsets were present in similar frequencies in the different tissues (Figure 9). Instead, PB and BM samples, which did not significantly differ between each other, showed an enrichment of T_{EF2} TBET$^+$ and T_{EM3} KLRG1$^+$ TBET$^+$ in contrast to LN samples. Interestingly, CLL LNs exhibited higher proportions of T_{EM2} GZMK$^+$, T_{EX} CD39$^+$ and proliferating cells, indicating an enhanced activated and exhausted phenotype of CD8$^+$ T-cells in this tissue. Moreover, T_{EM4} ICOS$^+$ and T_{FC} CD39$^+$ subsets were also enriched in LNs (Figure 9).

In addition to defining tissue-related differences, an intra-patient correlation for the identified T-cell subsets was determined, by comparing the frequencies of cell subsets in PB and LN samples (Figure 10). A significant positive correlation was identified for T_N, T_{CM} and T_{EM1} subsets, clusters with high frequencies in both tissues. In contrast, percentages of the other

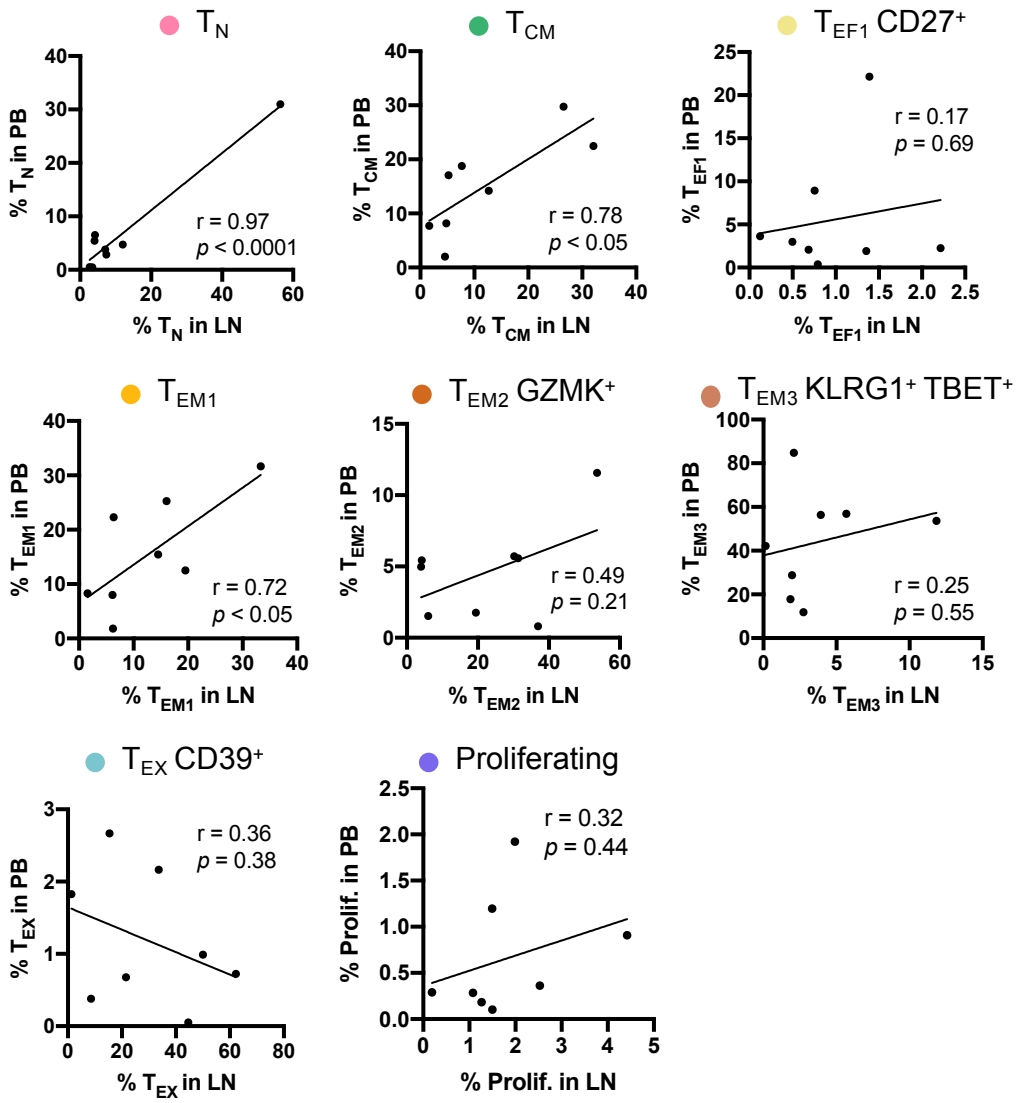

Figure 10: T-cell subset abundances in PB do not completely correlate with those in LN samples. Cluster abundances were correlated (Pearson correlation) using paired LN (x-axis) and PB (y-axis) samples from CLL patients (n = 8). Pearson correlation coefficient and p-values (*p*) are depicted correspondingly.

effector and effector memory subtypes and importantly, of T_{EX} and proliferating cells present in LN tissue, did not correlate with their frequencies in PB (Figure 10), underscoring a differential compartmentalization for certain cell subsets, including exhausted T-cells.

Overall, these results confirm that $CD8^+$ T-cell phenotype differences exist between PB and LNs, and provide a first account of the similarities of $CD8^+$ T-cell distribution in PB and BM of CLL patients. In addition, they underscore the limited correlation between LNs and PB and indicate the accumulation of exhausted T-cells in CLL LNs rather than in PB and BM.

4.2.2 CD8⁺ T-cells from CLL and HC LNs are phenotypically distinct

In order to identify the CLL-specific T-cell phenotypical changes, the comparison of CLL LNs with non-malignant LNs is essential. However, such comparison has not previously been performed. Consequently, the CD8⁺ T-cell composition of CLL LNs was compared to that of rLN samples. As shown in Figure 5, non-malignant LNs were composed of a significantly higher frequency of T_N, with an average frequency of 40.59 % per sample, in contrast to 11.35 % in CLL LNs. T_{EF1} cells, as well as DP_1 cells, despite being overall less abundant in the LNs, were also found significantly enriched in control samples, with the latter being almost absent in CLL samples (Figure 11). Importantly, CLL LNs were significantly enriched in T_{EX}, with an average frequency of 30.49 % in comparison to 11.33 % in control samples. Besides, T_{EM3} KLRG1⁺ TBET⁺ and proliferating cells were also found in greater frequencies in CLL LNs (Figure 11).

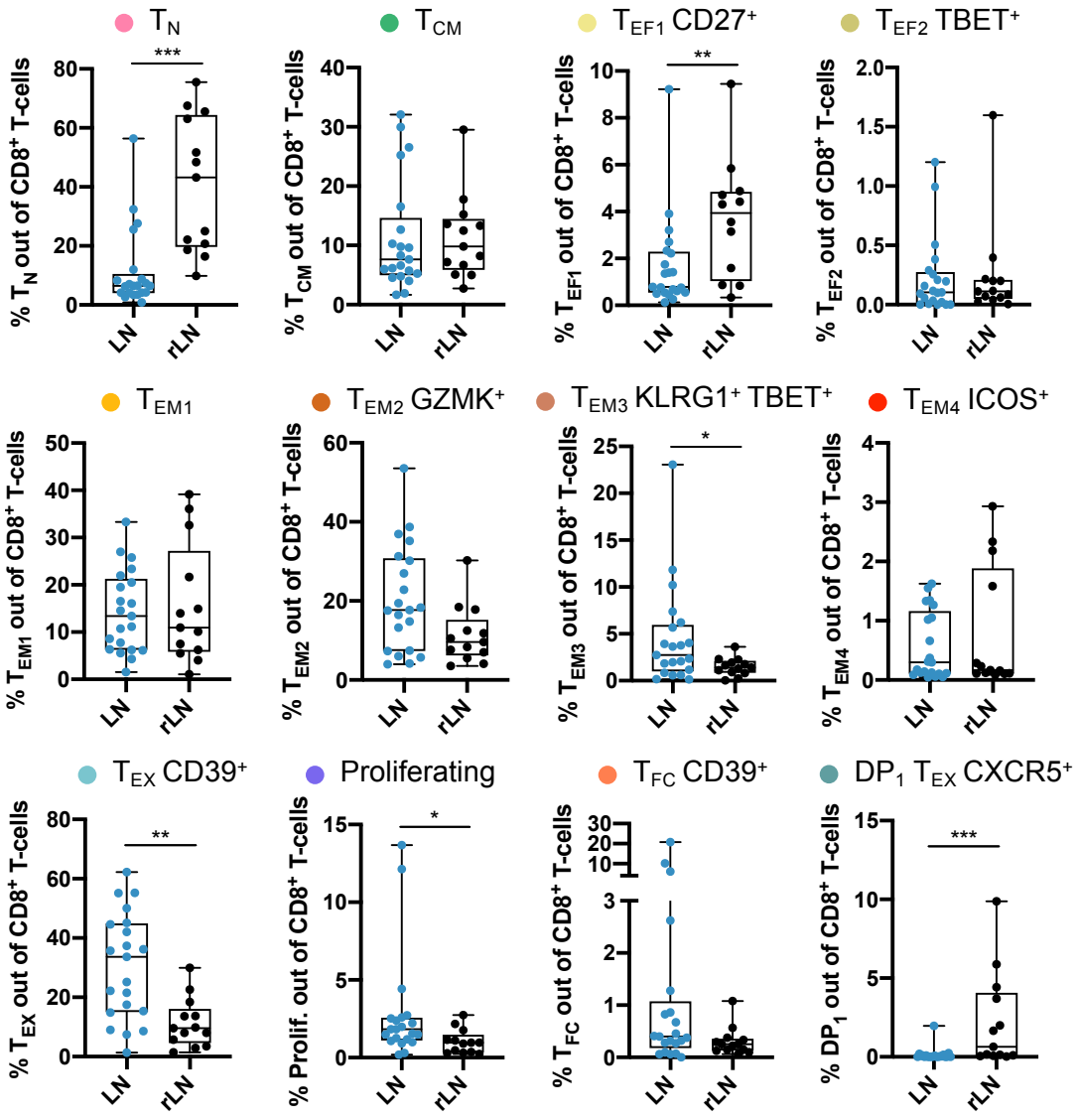

Figure 11: T-cells from CLL LNs have a distinct phenotype compared to HC LNs. Abundance of cells of a given cluster out of total CD8⁺ T-cells for each sample in CLL LNs (n = 21) compared to rLNs (n = 13) (*p<0.05, **<0.01, ***<0.001, Mann-Whitney U test).

Collectively, these results illustrate the CD8$^+$ T-cell phenotypic similarities between LNs from CLL patients and HCs, but at the same time provide evidence for the existence of CLL-specific effector and exhausted CD8$^+$ T-cell states.

4.2.3 Clinical associations with CD8$^+$ T-cell distribution in CLL LNs

Previous studies have identified a CD8$^+$ T-cell effector memory phenotype in CLL blood samples that is related to a progressive disease (Palma et al. 2017; Gonnord et al. 2019). To ascertain the relationship between the identified CD8$^+$ T-cell subsets with disease outcome in the studied cohort, cell subset frequencies in LN samples were correlated with the clinical parameters Binet and Rai staging, tumor load, *IGHV* mutation status, treatment-free survival, and overall survival. Similar to previous studies (Novak et al. 2015; Gonnord et al. 2019), no correlation between cell subtype percentage and Binet and Rai stage, treatment-free survival or overall survival data were identified (data not shown). On the other hand, T_{EM1} cell frequencies were positively associated with tumor load (Figure 12A). This was in line with a negative correlation between naïve T-cell percentages and tumor load (Figure 12B), thus indicating an increase of antigen-experienced T-cells in CLL LNs accompanying tumor growth.

Mutational status of the *IGHV* gene in CLL cells has been shown to have a minor impact on expression of immune checkpoint and activation markers in T-cells isolated from peripheral blood mononuclear cells (PBMCs) of CLL patients (Palma et al. 2017). Intriguingly, levels of T_{EM4} ICOS$^+$ cells were significantly decreased in *IGHV*-unmutated compared to mutated samples (Figure 12C), which provides evidence for an impact of the *IGHV* mutational status in CLL cells on shaping the nodal TME.

The average age of the studied CLL patient cohort is significantly higher than that of controls (Figure 13A), which represents a confounding factor for the identification of changes in T-cell phenotypes. In order to determine the contribution of this factor to the cell subset distribution, age of patients and HCs at sampling was correlated with cell cluster abundances. While CLL

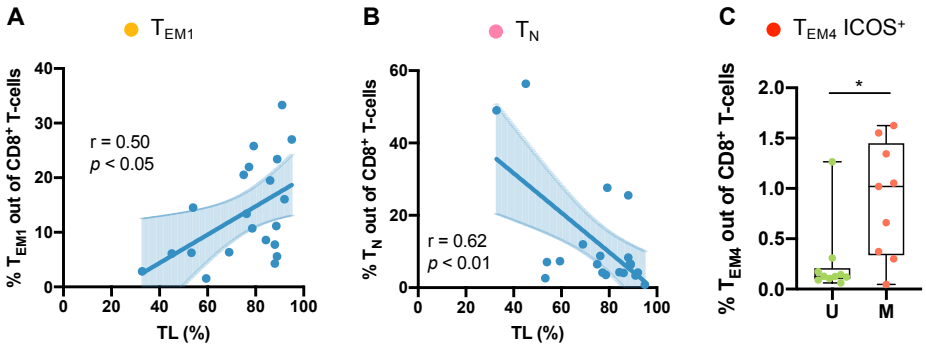

Figure 12: Relationship between CD8$^+$ landscape and clinical outcomes. (A-B) Pearson correlation of **(A)** naïve and **(B)** T_{EM1} subset abundances with tumor load (in %) in CLL LN samples (n = 21). **(C)** Boxplot showing T_{EM4} ICOS$^+$ subset abundances in LNs of *IGHV* unmutated (n = 9) versus mutated CLL patients (n = 10) (*p<0.05, Mann-Whitney U test). U = *IGHV* unmutated, M = *IGHV* mutated, TL = tumor load.

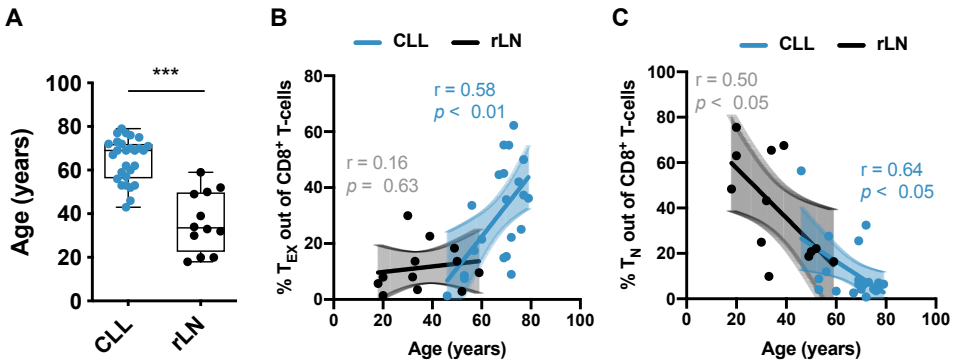

Figure 13: Average age differences between CLL patients and HCs have a limited effect as confounding factor. (A) Age of CLL patient (n = 21) and HC (n = 13) samples at sampling (***p<0.001, Mann-Whitney U test). **(B-C)** Pearson correlation plot of percentage of **(B)** T_{EX} and **(C)** T_N cell subsets (y axis) with age (x axis) for CLL and HC control samples.

samples of older age patients showed increased percentages of T_{EX} cells, this association was not present in control samples (Figure 13B). In addition, proportions of T_N cells negatively correlated with age in both control and CLL samples (Figure 13C), in accordance with the previously described shrinkage of the naïve T-cell compartment during aging (Goronzy et al. 2015).

In summary, these data underscore the limited impact of the T-cell compartment on the clinical outcome of CLL patients. Besides, they confirm the existence of an effector memory population that expands in response to tumor growth, and reveal a previously unrecognized difference in the abundance of $CD8^+$ T_{EM4} $ICOS^+$ cells between *IGHV*-mutated and -unmutated CLL patients. The age of the sample donors as a confounding factor, in addition, is shown to have a minor impact in T-cell subset differences between CLL patients and HCs.

4.3 Single-cell transcriptome profiling of nodal T-cells from CLL patients

4.3.1 Characterization of the T-cell transcriptome from CLL LNs

Single-cell transcriptome studies of intratumoral T-cells enable an unbiased examination of the vast heterogeneity of T-cell states found both within and between cancer patients (Zheng et al. 2017; Azizi et al. 2018; Li et al. 2019). Transcriptional profiling of T-cells from three CLL LNs was performed in order to characterize their distinct T-cell subsets and their clonal diversity. $CD3^+$ T-cells and CLL cells of CLL LNs were FACS-sorted and subjected to single-cell RNA-seq using the 10x Genomics platform. Data processing and analysis was conducted in collaboration with Dr. Yashna Paul from the German Research Center (DKFZ), Heidelberg. After QC filtering (see Section 3.2.7.3), approximately 6.6 $x10^3$ $CD3^+$ T-cells, with an average of 131,234 reads per cell and a median of 1,447 genes per cell, were further analyzed. The t-

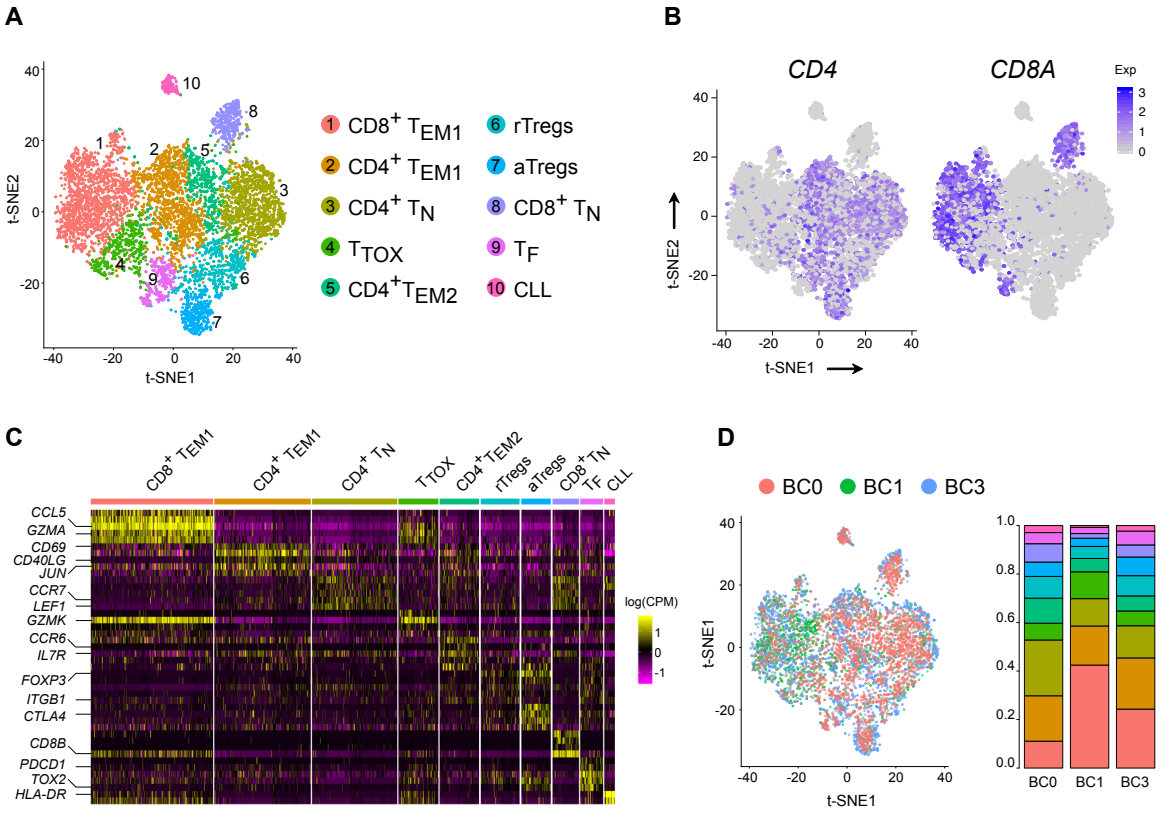

Figure 14: Transcriptional profiling of nodal T-cells from CLL patients. (A) t-SNE plot of CD3$^+$ T-cells and CLL cells color-coded according to the clusters identified **(B)** Gene expression (UMI) counts) of *CD4* and *CD8A* genes in all cells. Exp = UMIs. **(C)** Heatmap depicting the top most differentially expressed genes for each cluster. Each column represents a single cell and each row a single gene, with the annotation of 1-2 marker genes per cluster. Clusters are ordered based on their size. Expression is shown as logarithm of counts per million reads (log CPM). **(D)** t-SNE plot depicting sample distribution (left) and cell subset abundances in each sample (right). Colors correspond to those shown in (A). BC0, BC1, BC3 = sample IDs.

SNE algorithm was used for dimensional reduction and unbiased cell clustering yielding the formation of 10 subsets based on their gene expression profiles (Figure 14A). These clusters were comprised of 5 CD4$^+$ T-cell clusters, 2 CD8$^+$ T-cell clusters, 2 clusters which contained both, CD4$^+$ and CD8$^+$ T-cells, and one cluster of spiked-in CLL cells (Figure 14A-B). More specifically, both CD4$^+$ and CD8$^+$ naïve cells were identified based on the expression of marker genes such as *CCR7*, lymphoid enhancer-binding factor 1 (*LEF1*), selectin L (*SELL*) and transcription factor 7 (*TCF7*) (Figure 14C) (Gattinoni et al. 2017). Subsets identified as effector memory CD8$^+$ (CD8$^+$ T_{EM1}) and cytotoxic T-cells (T_{TOX}), were characterized by a similarly high expression of effector molecules like granzymes (*GZMA*, *GZMK*, *GZMH*), with CD8$^+$ T_{EM} expressing slightly higher levels of cytokines like *CCL4*, *CCL5*, *IFNG* and *PRF1* (Figure 14C). In contrast, CD4$^+$ T_{EM1} cells showed higher expression of TFs related to T-cell activation (*FOS*, *JUN*, *FOSB*) (Yukawa et al. 2020), and activation-related genes (*CD69*, *ICOS*, *CD40L*) (Azizi et al. 2018). A second CD4$^+$ T_{EM2} subset expressed genes related to cytokine signaling such

as *CCR6*, *IL7R*, and lymphotoxin β (*LTB*) (O'Shea and Murray 2008; Lee and Korner 2019; Piao et al. 2019). Tregs were identified based on the expression of *FOXP3*, *CTLA4* and IL2RA, and further subdivided into resting Treg (rTregs), and active Treg (aTregs) cells. While the former subgroup was characterized by a higher expression of naïve-related genes, the later expressed higher levels of inhibitory receptors (*TIGIT*, *ICOS*) and genes involved in the TNFRSF- NF-κB-pathway (*TNFRSF4*, *TNFRSF1B*, *BIRC3*) (Zemmour et al. 2018; Miragaia et al. 2019) (Figure 14C). In addition, a cell subset with a gene signature characteristic of $CD4^+$ T_{FH} was identified, overexpressing both inhibitory receptors, including *PDCD1* and *TIGIT*, and genes like *TOX2* and *CD200* (Crotty 2011; Dorfman and Shahsafaei 2011; Roider et al. 2020). Surprisingly, however, it included both $CD4^+$ and $CD8^+$ T-cells (Figure 14B). Finally, CLL cells were easily recognizable by the expression of multiple immunoglobulin genes (such as *IGKV3-20* and *IGKC*), genes encoding the HMC (*HLA-DR*, *HLA-DRB1*, *CD74*), and the BCR complexes (*CD79A*, *CD79B*) (Figure 14C). As previously observed in the analysis of mass cytometry data, a substantial heterogeneity existed between the three patients analyzed, with one sample containing significantly more $CD8^+$ T_{EM1} cells than the other two (Figure 14D).

The above analysis provides a general overview of the T-cell subsets present in the LNs of CLL patients, but delivers limited information on the different $CD8^+$ T-cell states. Hence, to gain further insight into $CD8^+$ T-cell heterogeneity, $CD4^-$ $CD8^+$ T-cells were clustered separately. As shown in Figure 15A, 8 transcriptionally distinct $CD8^+$ T-cell clusters could be identified based on differentially expressed marker genes. Subsets of naïve cells were identified as in the previous analysis. Interestingly, $CD8^+$ follicular T-cells (T_{FC}) showed the most discrete phenotype, with a high expression of inhibitory receptors, a moderate expression of naïve-related genes, and no expression of effector molecules, like granzymes or cytokines (Yu and Ye 2018) (Figure 15B). From the previously identified $CD8^+$ T_{EM} cell cluster, 5 new subsets emerged: a T_{CM} subset was classified based on the moderate expression of naïve-associated genes, and the low expression of effector molecules. In addition, a T_{EM} subset with strong expression of heat-shock proteins (e.g. *HSP90AA1*, *HSPA1A*) was identified (Figure 15B). Of note, a very small set of cells (11 cells, representing the 0.48 % of total cells), which expressed high levels of mitochondrial genes (e.g. *MT1F*, *MT1X*), and only slightly exceeded the threshold for the exclusion of low-quality cells, was considered a technical artifact and therefore excluded from further analyses. Finally, and as the previous analysis suggested, the

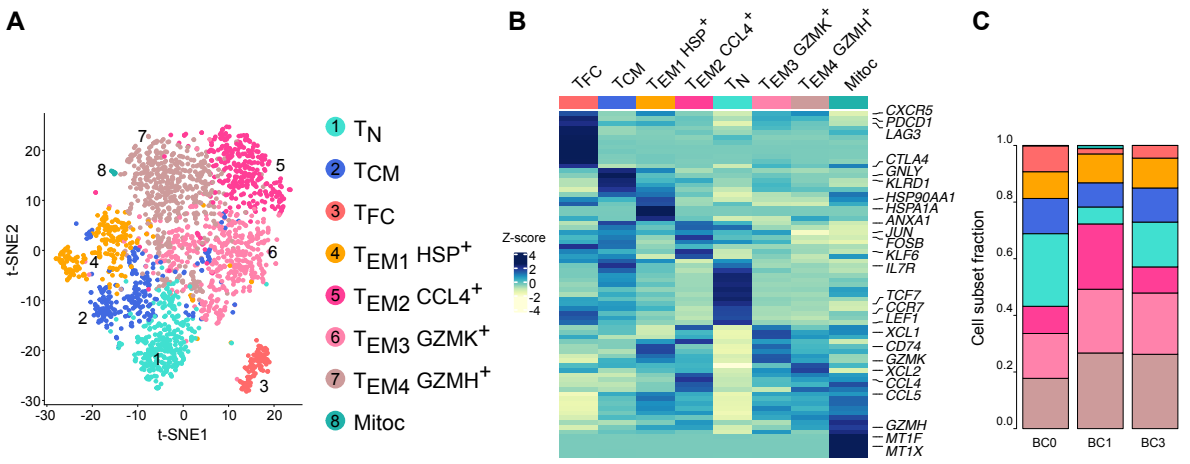

Figure 15: Characterization of CD8$^+$ T-cells from CLL LNs. (A) t-SNE map clustering CD8$^+$ T-cells form 3 CLL LNs. Each dot represents a single cell, colored according to cluster identity. **(B)** Heatmap displaying enrichment (Z-score) of most differentially expressed genes in each cluster (color-coded as in (A)). Marker genes per cluster are noted (right). **(C)** Cell subset frequencies for each sample. Colors correspond to clusters as annotated in (A). BC0, BC1 and BC3 = sample IDs.

differences between the 3 remaining T_{EM} subsets were subtle, and only small gene expression differences separated these clusters. Specifically, T_{EM2} CCL4$^+$ expressed slightly higher levels of *CCL4* and annexin A1 (*ANXA1*), and the AP-1 TF subunits *JUN* and *FOS*; T_{EM3} GZMK$^+$ expressed increased levels of *GZMK*, *KLRG1*, and C-X-C motif chemokine ligand 1 (*XCL1*), as well as slightly higher levels of *PDCD1* and *LAG3*; and T_{EM4} GZMH$^+$ showed a higher expression of *GZMH* and X-C motif chemokine ligand 2 (*XCL2*) (Figure 15B). Interestingly, the higher percentage of CD8$^+$ T_{EM} cells previously recognized in the BC1 sample corresponded to a specifically increased frequency of T_{EM2} CCL4$^+$, rather than a general higher percentage of the different T_{EM} subsets (Figure 15C).

Altogether, the single-cell transcriptome analysis of T-cells from CLL LNs provides an unbiased account of CLL-associated T-cell phenotypes. Similar to the mass cytometry analysis, single-cell RNA-seq identifies subsets of CD8$^+$ T_N, T_{CM}, T_{FC} and T_{EM}, but at the same time, it underscores the high degree of similarity between the CD8$^+$ T_{EM} cell subsets and the distinct transcriptional profile of the T_{FC} cells.

4.3.2 Integration of the mass cytometry and single-cell RNA sequencing data reveals general cell subset overlap

Using both single-cell RNA-seq and mass cytometry analyses identified CD8$^+$ T-cell subsets with distinct phenotypes, thus raising the question, whether the same populations exist at the transcriptome and proteome level respectively. To answer this question, the CD8$^+$ T-cell profile of all clusters identified at the transcriptome and proteome level were integrated (see Methods, Section 3.2.8). As shown in Figure 16A, general cell subsets (i.e. T_N, T_{CM}, T_{FC}, and T_{EM}) found

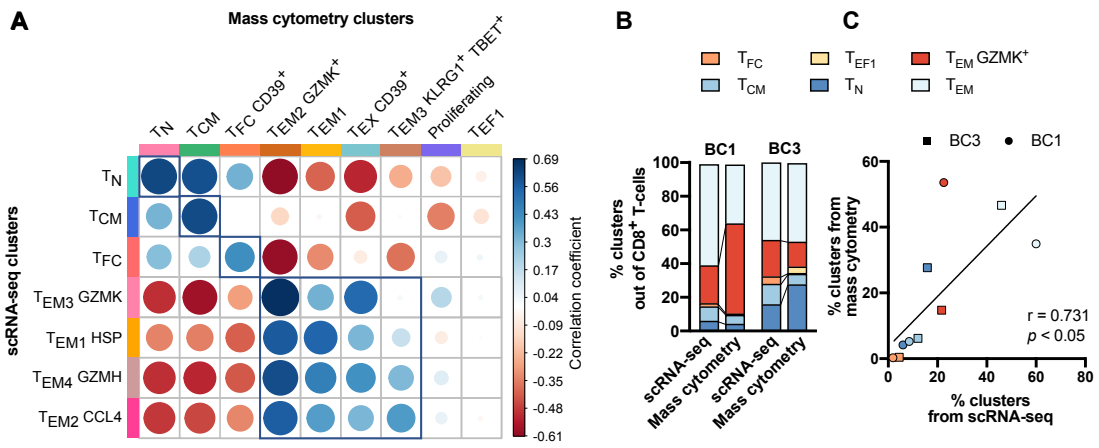

Figure 16: Correspondence of mass cytometry clusters with single-cell RNA-seq clusters. (A) Heatmap showing Pearson correlation between each pair of clusters identified with single-cell RNA-seq and mass cytometry. Average profile values for each cluster were calculated and mean-centered in comparison to the rest of the clusters from the dataset. Clusters of > 1 % in BC1 and BC3 samples are depicted from the mass cytometry dataset. Color scale and dot size depict correlation coefficient. **(B)** Cell subset distribution of the major cell subsets T_{FC}, T_{CM}, T_{EF}, T_N, T_{EM} (including T_{EM1}, T_{EM2}, T_{EM3} and T_{EX}) and T_{EM} GZMK$^+$ in samples BC1 and BC3 present in both single-cell RNA-seq and mass cytometry datasets. **(C)** Pearson correlation of major cell subset percentages determined with mass cytometry and single-cell RNA-seq as grouped in (B) for samples BC1 and BC3.

in both datasets positively correlated. Because only a limited number of marker genes differentiating T_{EM} subsets in the single-cell RNA-seq dataset were present in the mass cytometry dataset, no one-to-one equivalent T_{EM} cluster could be assigned (Figure 16A). In addition, proliferating and effector cells, which were only defined using mass cytometry analysis, did not correlate with any single-cell RNA-seq cluster. Importantly, cell subset frequencies were comparable between the two methodologies (Figure 16B), and significantly correlated with each other in the two LN samples present in both datasets (Figure 16C).

Overall, the above analysis validates that mass cytometry and single-cell RNA-seq analyses capture similar CD8$^+$ T-cell subsets, underscoring their robustness and discarding the possibility of a detection bias towards any specific cell subset (i.e. naïve, effector memory, central memory, effector, and follicular) by the techniques.

4.3.3 T-cell clonality in CLL is associated with an effector memory CD8$^+$ T-cell phenotype

The reconstruction of T-cell receptor (TCR) sequences at the single-cell level and overlap with their transcriptional profiles allows the identification of clonal diversity within identified T-cell subsets. With this approach, an enrichment of clonally-expanded cells with cytotoxic and dysfunctional phenotypes has been reported in several tumors (Guo et al. 2018; Zhang et al. 2018b; Li et al. 2019; Yost et al. 2019). To assess the degree of clonality in the analyzed CLL LN samples, T-cells with both transcriptome and productive TCR sequence information were

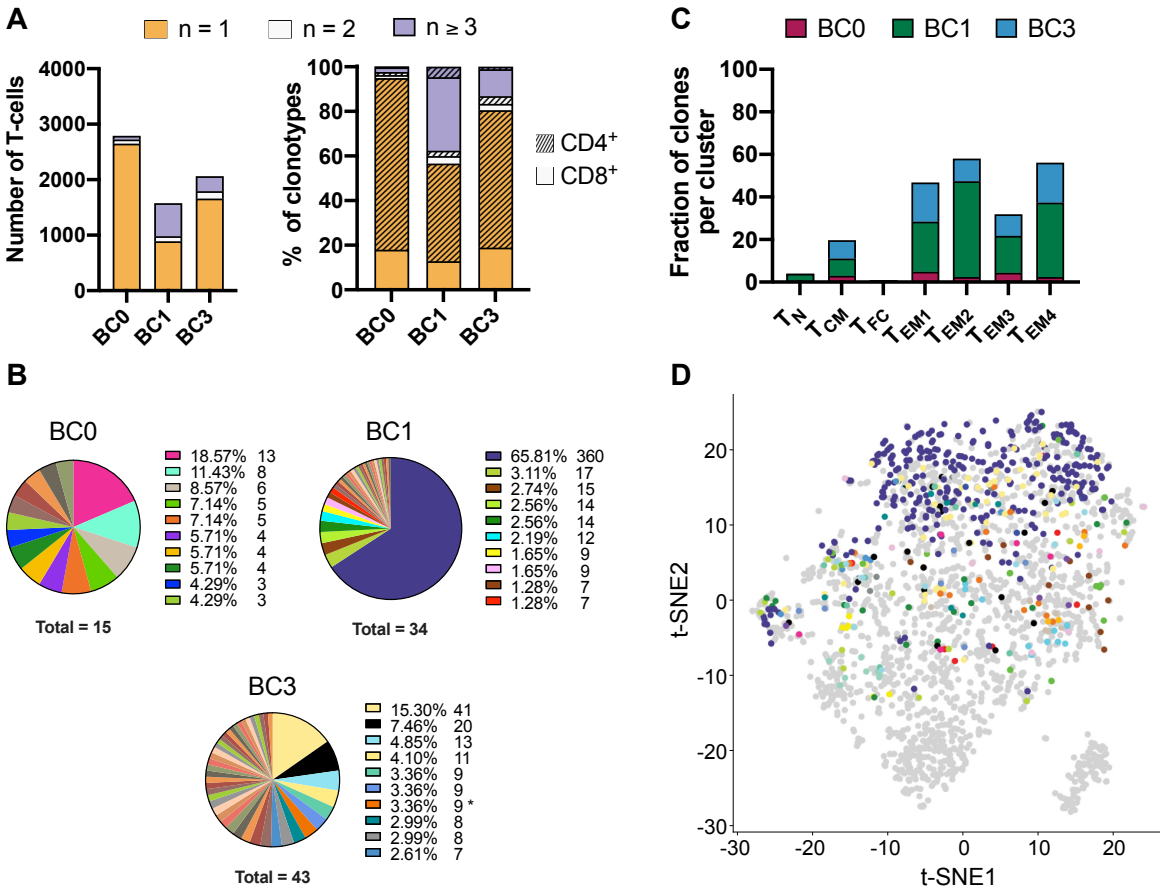

Figure 17: Clonal expansion is restricted to T_{EM} $CD8^+$ T-cells. (A) Number of total $CD3^+$ T-cells belonging to clonotypes with 1, 2, or 3 and more cells with the same TCR sequence in each sample. Left: absolute numbers, right: percentage out of total cells. The distinction between $CD4^+$ and $CD8^+$ T-cells is made in the left graph. **(B)** T-cell conal composition in the 3 CLL LNs samples. Percentages and cell numbers are given for the 10 most abundant clones. The total number of expanded clones is shown below the chart. * marks BST2-recognizing TCR. **(C)** Percentage of expanded clones per $CD8^+$ T-cell cluster. The contribution from each of the three samples is color-coded. **(D)** t-SNE plot of $CD8^+$ T-cells from the 10 most expanded clones (color-coded, n = 885). Cells with no shared TCR are depicted in grey. BC0, BC1 and BC3 = sample IDs.

classified based on the distribution of identical paired α and β chains shared between one, two, or three and more cells (Figure 17A). A diverse degree of clonal expansion (i.e. an identical TCR present in at least three cells) was observed in the three samples, being 2.44, 13.20 or 37.66 % of total cells (Figure 17A), with no shared TCR clones amongst them. Besides, clonal diversity differed greatly between patients, with little clonal expansion in the BC0 sample, a strongly dominating clone in BC1, and a wider repertoire of smaller clones in the BC3 sample (Figure 17B). Since $CD4^+$ T-cells showed negligible clonal enrichment, and because a significant proportion of $CD8^+$ T-cells were clonally expanded (Figure 17A), the clonal composition across $CD8^+$ T-cell subsets was examined. Interestingly, considerable percentage (between 31.82 and 58.04 %) of cells from the 4 T_{EM} clusters were constituted by clones, in contrast to the little clonal expansion found in the T_N, T_{CM} and T_{FC} cell subsets (Figure

17C and D). Importantly, expanded clones were not restricted to a specific cluster, but distributed between several subsets, with T_{EM2} $CCL4^+$ and T_{EM4} $GZMH^+$ sharing most of them (Figure 17C).

In order to identify TCR clones recognizing known epitopes, CDR3 amino acid sequences for the 10 most abundant clones in each sample were compared against the VDJdb database including CDR3 regions known or likely to react against reported epitopes (Bagaev et al. 2020). TCR sequences described to recognize the pp65 gene epitope from cytomegalovirus (CMV) were found in the BC0 and BC1 samples, including the latter's most abundant clone (Table 11). In addition, matrix protein 1 (M1) from Influenza virus and mRNA export factor ICP29 (BMLF1) from Epstein-Barr-Virus (EBV) were found in BC0 and BC1, respectively (Table 11). Available clinical data of these samples indicated no CMV positivity at time of sampling but at earlier stages of disease (Table S13), suggesting a persistence of viral-reacting T-cells over time. Intriguingly, sample BC3 contained a TCR described to recognize the bone marrow stromal cell antigen 2 (BST2) protein, mostly present in the T_{EM3} $GZMK^+$ cluster. This transmembrane protein, originally described to regulate B-cell development (Goto et al. 1994; Ishikawa et al. 1995), has been reported to be overexpressed in CLL (Gong et al. 2015) and several other malignancies, including lung and breast cancer (Wang et al. 2009; Mahauad-Fernandez et al. 2014), as well as multiple myeloma, where it has been suggested as a therapeutic target (Ozaki et al. 1997; Tai et al. 2012). The presence of a putative T-cell clone binding to a CLL-overexpressed protein thus constitutes further evidence of the existence of CLL-reactive T-cells with a pre-exhausted phenotype.

Table 11: List of known and putative epitope-reactive TCRs.

	Clone ID	Fraction (%, AC)	CDR3	V	J	Epitope	Gene	Sp
BC0	CL9	4.29 (3)	TRA: CASYNTDKLIF	TRAV38-2/DV8	TRAJ34	GILGFVFTL	M1	Influenza
			TRB: CASSLALNYGYTF					
	CL7	4.29 (3)	TRA: CAALRDDKIIF	TRAV12-2	TRAJ30	NLVPMVATV	pp65	CMV
			TRB: CASSFGSYNEQFF					
	CL11	4.29 (3)	TRA: CAVRTSGYSTLTF	TRAV21	TRAJ11	NLVPMVATV	pp65	CMV
			TRB: CASCPGQGNTGELFF					
BC1	CL1	65.81 (360)	TRA: CAASFSGTYKYIF	TRAV29/DV5	TRAJ40	NLVPMVATV	pp65	CMV
			TRB: CASSPSPGGVEKLFF					
	CL8	2.19 (12)	TRB: CASSQSPGGTQYF	TRBV14	TRBJ2-5	GLCTLVAML	BMLF1	EBV
			TRA: CALSEGDSGNTPLVF					
	CL10	1.65 (9)	TRA: CAGASNTGKLIF	TRAV27	TRAJ37	NLVPMVATV	pp65	CMV
			TRB: CASSLAQGSGANVLTF					
BC3	CL8	3.36 (9)	TRA: CAVSLSNFGNEKLTF	TRAV12-2	TRAJ48	LLLGIGILV	BST2	Homo S.
			TRB: CASSYGDRGSNQPQHF					

Note: AC = absolute number of cells, Sp = species, TRA = T-cell receptor α chain, TRB = T-cell receptor β chain.

Altogether, this data reveals a broad TCR repertoire from CLL LNs, which illustrates a heterogeneous clonal diversity between patients as well as a phenotypically diverse clonal expansion restricted to $CD8^+$ T_{EM} cells. In addition, the distinction of specific TCR sequences recognizing previously described epitopes underscores an anti-viral, and potentially anti-tumoral reactivity.

4.3.4 Decoding the interactome between CLL cells and T-cells in the CLL LN niche

Tumor-associated changes in the CLL TME are considered to benefit CLL cells, as they largely depend on their interactions with neighboring cells for receiving proliferation and survival signals in the SLOs (Burger 2011). Hence, to predict the cell-cell interactions occurring in the CLL LNs, CellPhoneDB, a computational tool for the identification of cell subset-specific expression of ligand and receptor pairs in the transcriptome (Vento-Tormo et al. 2018), was used (see Methods Section 3.2.7.6). Interestingly, the highest number of interactions were predicted between CLL cells and T_{TOX}, T_{FC}, and $CD8^+$ T_{EM1} cells (Figure 18A), subsets that also generally established a higher number of interactions with any given subset. The other clusters, in contrast, and specially $CD4^+$ T_N and rTregs, interacted comparably less with any cell subpopulation (Figure 18A).

To gain insight into the CLL-T-cell interactome, the specific interactions between CLL cells and all the T-cell subsets were investigated. On the one hand, well-known pro-survival and proliferation signals for CLL cells, such as CD40- CD40L, IL2 secretion, and TRAIL- TRAILR1 (Secchiero et al. 2005; Decker et al. 2010; Pascutti et al. 2013), were found between CLL cells and $CD4^+$ T subsets, as well as T_F cells (Figure 18B). CLL cells additionally interacted with Tregs through the expression of the adhesion molecule L-selectin. Moreover, as a result of their activated and effector state, $CD8^+$ T_{EM1} and T_{TOX} cells specifically secreted TNFα and IFNγ, the receptors of which were expressed by CLL cells. On the other hand, other interactions reported to induce CLL programmed cell death, including binding of signal regulatory protein gamma (SIRPG) to CD47 (Martinez-Torres et al. 2015) or inhibition thereof by leukocyte associated Ig like receptor 1 (LAIR1) to leukocyte Ig like receptor B4 (LILRB4) (Zurli et al. 2017), were observed between CLL cells and $CD4^+$ T-cells, T_{TOX}, and T_{FC} cells (Figure 18B). Interestingly, CD52 glycoprotein, which is therapeutically targeted with alemtuzumab, was found to interact with sialic acid binding Ig like lectin 10 (SIGLEC10) not only among CLL cells, but also in several T-cell subsets and specially $CD4^+$ T_{EM2} cells.

Furthermore, the crosstalk between CLL cells and T-cells was not unidirectional, as T-cells also received signals from leukemia cells, the effect of which has not been investigated in CLL. In short, signals were mediated by CD28- CD86 interaction, and CD44 binding to L-galectin 9

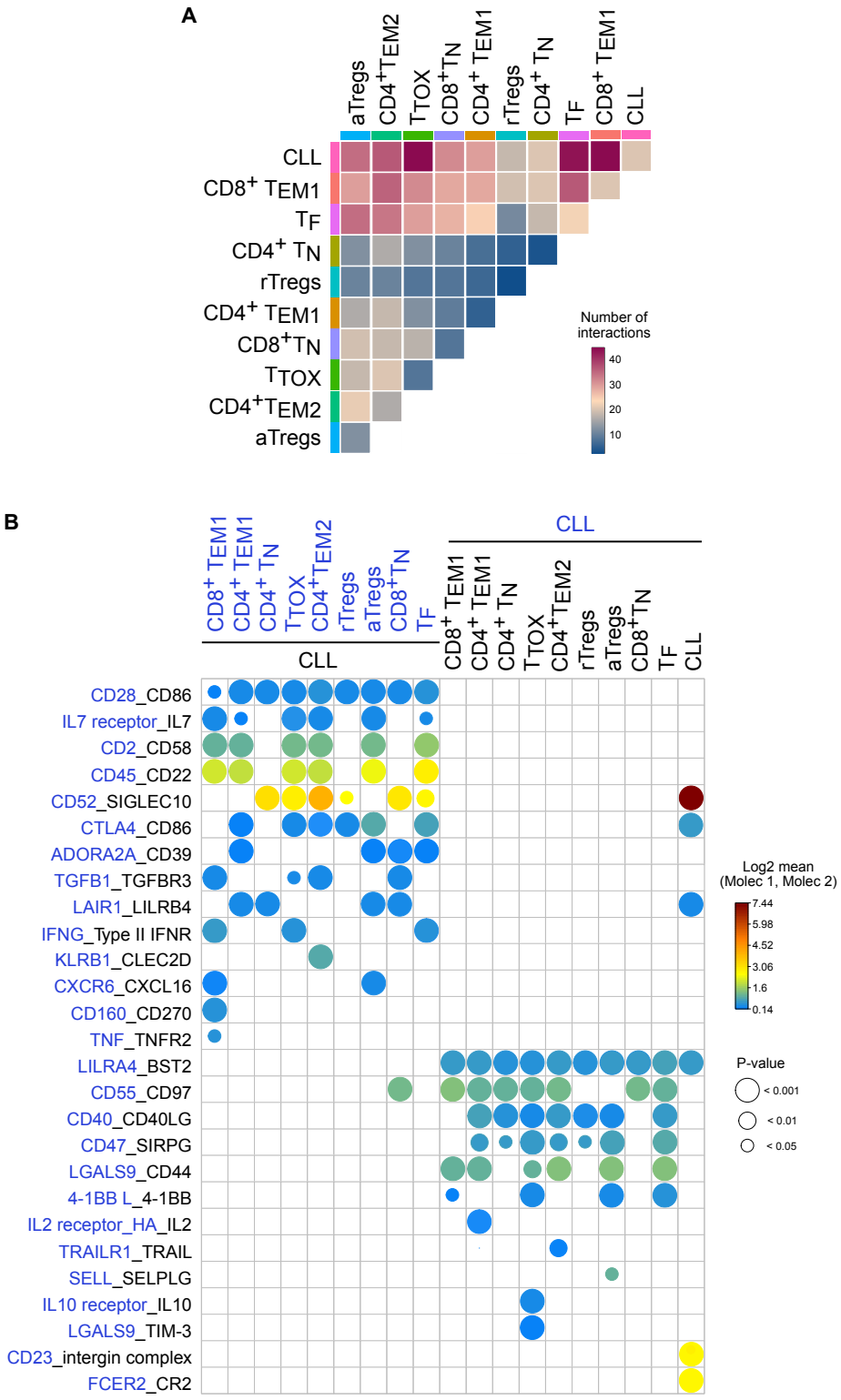

Figure 18: Decoding the crosstalk between CLL cells and T-cells in the LN niche. (A) Heatmap depicting the number of predicted interactions between cell clusters identified by single-cell RNA-seq. **(B)** Significant curated ligand-receptor interactions between CLL and T-cell subsets depicted as a dot plot. Dot color represents log2 mean of the combined expression of ligand and receptor pair. Dot sizes represent p-values, which were determined using a permutation test. Gene names were substituted by protein names for CD45 (*PTPRC*), CD39 (*ENTPD1*), CD270 (*TNFRSF14*), TNFR2 (*TNFRSF1B*), CD97 (*ADRGE5*), 4-1BB ligand (*TNFSF9*), 4-1BB (*TNFRSF9*), TRAILR1 (*TNFRSF10A*), TRAIL (*TNFSF10*), TIM-3 (*HAVCR2*), CD23 (*FCER2*) and the integrin complex (aXb2).

(LGALS9) in activated cells. In addition, $CD8^+$ T_{EM1}, T_{TOX}, aTregs and T_{FC} cells interacted with CLL cells via 4-1BB- 4-1BB ligand, and CD160 in case of $CD8^+$ T_{EM1} cells. Specific recruitment of $CD8^+$ T_{EM1} and aTreg cells by CLL cells might result from CXCL16- CXCR6 interaction. In contrast, T-cells also received coinhibitory signals via LAIR1, and specifically via TIM-3 for T_{TOX} cells. Of note, the T-cell inhibitory signals expected from the interactions PD-1- PD-L1 and TIGIT- PVR were not found amongst the significant CLL cell-type specific interactions, but were present in the list of detected interactions in the dataset, indicating a more ubiquitous expression of the ligands also in the T-cells.

Overall, these results reveal a complex cellular network of interactions, where T-cells and leukemic cells establish a cross-talk consisting of both positive and negative signals, contributing to an impaired anti-tumor T-cell response, and altered normal immune function in CLL patients.

4.4 Single-cell RNA-seq-based T-cell profiling of the TCL1 AT mouse model

4.4.1 Characterization of the transcriptome of T-cells from TCL1 AT spleen

The TCL1 AT mouse model represents a valuable tool for studying CLL pathomechanisms (Hamblin 2010). To gain insight into the T-cell heterogeneity of the TCL1 AT mouse and validate its resemblance to human CLL T-cells, splenic T-cells from 2 TCL1 AT mice with a TL of approximately 92 % were analyzed. More specifically, $CD3^+$ T-cells were FACS-sorted and subjected to single-cell RNA-seq using 10x Genomics. Data processing and analysis was performed in collaboration with Dr. Yashna Paul from the German Research Center (DKFZ, Heidelberg). After QC filtering, a total of 8.5 $x10^3$ T-cells, with an average of 77,268 reads per cell and a median of 1,861 genes per cell, were considered for clustering and cell subset investigation. Thirteen clusters were identified based on to their differential gene expression (Figure 19A), which comprised $CD4^+$ and $CD8^+$ T-cells, CLL cells, and myeloid cells. The latter population, which expressed no *Cd3*, *Cd4*, *Cd8a*, or *Cd19*, but expressed multiple genes related to innate cells, including the Fc fragment of IgE receptor Ig (*Fcer1g*), lysozyme C-2 (*Lyz2*), and colony stimulating factor 1 receptor (*Csf1r*), was likely a result of a lower purity of the cell sorting prior the single-cell RNA-seq. Only few of the T-cell clusters could be unequivocally subdivided into $CD4^+$ or $CD8^+$ T-cells (Figure 19A), since most of them contained both T-cell types. Even though $CD4^+$ and $CD8^+$ T-cells did not overlap in the t-SNE clustering, due to the strong exclusive expression of *Cd4* and *Cd8a* (Figure 19B), such grouping indicates that the two T-cell types share highly similar transcriptomic phenotypes.

Subsequently, the 11 T-cell clusters were characterized according to their transcriptome profile. The overexpression of naïve marker genes, including *Ccr7* and *Lef1*, identified 4 clusters of T_N cells, with one exclusively containing $CD8^+$ T-cells, another $CD4^+$, and two small

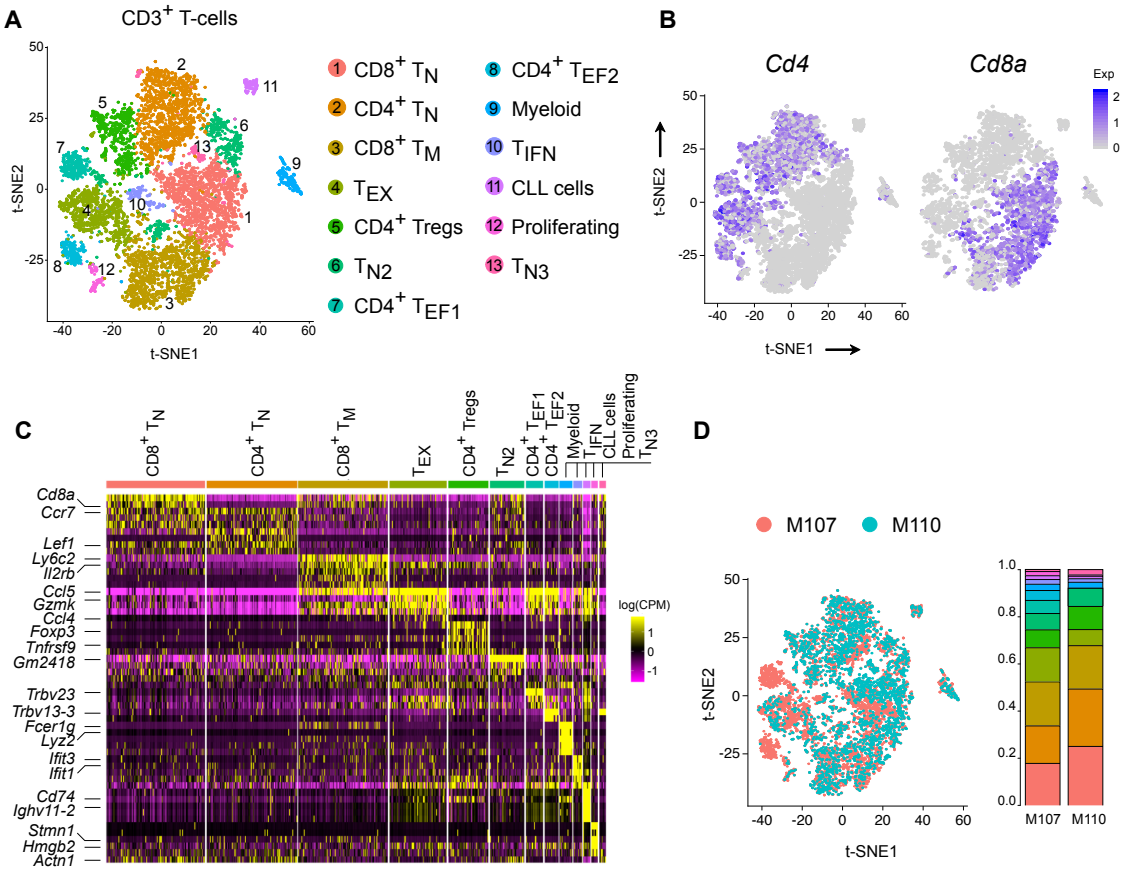

Figure 19: Transcriptome profiling of T-cells from TCL1 AT mice. (A) t-SNE plot of CD3$^+$ T-cells and CLL cells. The 13 clusters identified are depicted with distinctive colors. **(B)** Gene expression (UMI counts) of *Cd4* and *Cd8a* genes in all cells. **(C)** Heatmap showing 2-5 most differentially expressed genes between the identified clusters. Each column denotes a cell and each row a gene. Between 1 and 2 marker genes are annotated per cluster. Expression is represented as logarithm counts per million reads (log CPM). **(D)** t-SNE plot depicting the cell distribution according to the mouse of origin (left) and cluster fractions in each sample (right), with colors as in (A). M107 and M110 = sample IDs.

clusters including both (T_{N2-3}) (Figure 19C). CD8$^+$ memory T-cells (T_M) were determined based on the expression of *Cd7*, interleukin-2 receptor subunit beta (*Il2rb*) and lymphocyte antigen 6c2 (*Ly6c2*) (Aandahl et al. 2003; Istaces et al. 2019), and the lower expression of both naïve and effector-related genes in relation to other clusters. In addition, CD4$^+$ Treg cells were recognized by the expression of *Foxp3* and tumor necrosis factor receptor superfamily member 4 (*Tnfrsf4*). Importantly, an exhausted T-cell subset (T_{EX}), which contained mostly CD4$^+$ T-cells, but also CD8$^+$ cells, was recognized based on the elevated expression of inhibitory receptors like *Tigit*, *Lag3*, and *Pdcd1*, as well as several effector molecules, including chemokine ligand 5 (*Ccl5*) and *Gzmk* (Figure 19C). Moreover, two other CD4$^+$ effector (T_{EF1-2}) subsets were remarkably similar to T_{EX} cells at the transcriptomic level, but specifically expressed T-cell receptor α and β genes (i.e. *Trbv23* together with *Trav6-3*, and *Trbv13-3* with *Trav19* respectively), suggesting they represent expanded T-cell clones (Figure 19C). Intriguingly, a small cluster including both CD4$^+$ and CD8$^+$ cells, with a very distinct

transcriptional signature was also identified. This subset expressed genes related to type I interferon response, including interferon induced protein with tetratricopeptide repeats 1 and 3 (*Ifit1*, *Ifit3*), signal transducer and activator of transcription 1 (*Stat1*), and interferon regulatory factor 7 (*Irf7*). Besides, the top 50 differentially expressed genes of this cluster showed an enrichment for the gene ontology (GO) biological process term 'type I interferon signaling pathway' (GO:0060337, adjusted p-value = 7.15 $x10^{-18}$) defining this cluster as T_{IFN} cells. Finally, cells with high levels of cell-cycle associated genes, like stathmin (*Stmn1*), high mobility group box 2 (*Hmgb2*), and marker of proliferation KI-67 (*Mki67*), were denoted as proliferating cells. These cells also expressed effector molecules like *Gzmk* and granzyme B (*Gzmb)*, indicating an on-going proliferation of effector cells.

It is worth noting, that even though the two mice analyzed (M107 and M110) were injected with the same TCL1 tumor clone and presented comparable tumor load at time of sampling (both with >90 % CLL cells out of $CD45^+$ cells in spleen), their T-cell response appeared to be remarkably different: on the one hand, M107 seemed to have an overall stronger T-cell reaction, as all cells from T_{EF1-2} and most of T_{EX} cluster originate from this mouse (Figure 19D). In contrast, more than 50 % of cells in M110 were naïve cells, and the abundance of T_{EX}, or proliferating cells was comparably lower in this sample (Figure 19D). This observation reveals a previously unrecognized high heterogeneous inter-sample T-cell response, regardless of the transplanted TCL1 tumor clone.

Taken together, this data provides a comprehensive account of the T-cell phenotypes acquired upon leukemia development in the TCL1 AT mouse model of CLL.

4.4.2 Limited clonal expansion of $CD8^+$ T-cells from TCL1 AT mouse splenocytes

The existence of a clonally expanded $CD8^+$ T-cell population in blood of CLL patients as well as in spleens of TCL1 AT mice has been reported by previous studies (Serrano et al. 1997; Vardi et al. 2017; Blanco et al. 2018; Hanna et al. 2019). To confirm these results, as well as to compare the T-cell clonality profile of the TCL1 AT mouse model to the one of LNs from CLL patients identified in this work, selective enrichment and single-cell RNA-seq of the TCR region was performed.

Several interesting observations were made upon inspection of the clonal distribution in the murine samples. First, a clearly distinct clonal expansion pattern occurred in the two samples analyzed (Figure 20A-B), in line with the previously recognized dissimilar cluster distribution between the two mice. In M107, out of all T-cells, approximately 20 % represented clonal cells (Figure 20A), with two dominant clones constituting 50 % of the expanded cells (Figure 20B). In contrast, only a 4 % of cells were clonally expanded in M110 (Figure 20A), characterized by small and non-dominant clones (Figure 20B). Second, and surprisingly, clonal cells were

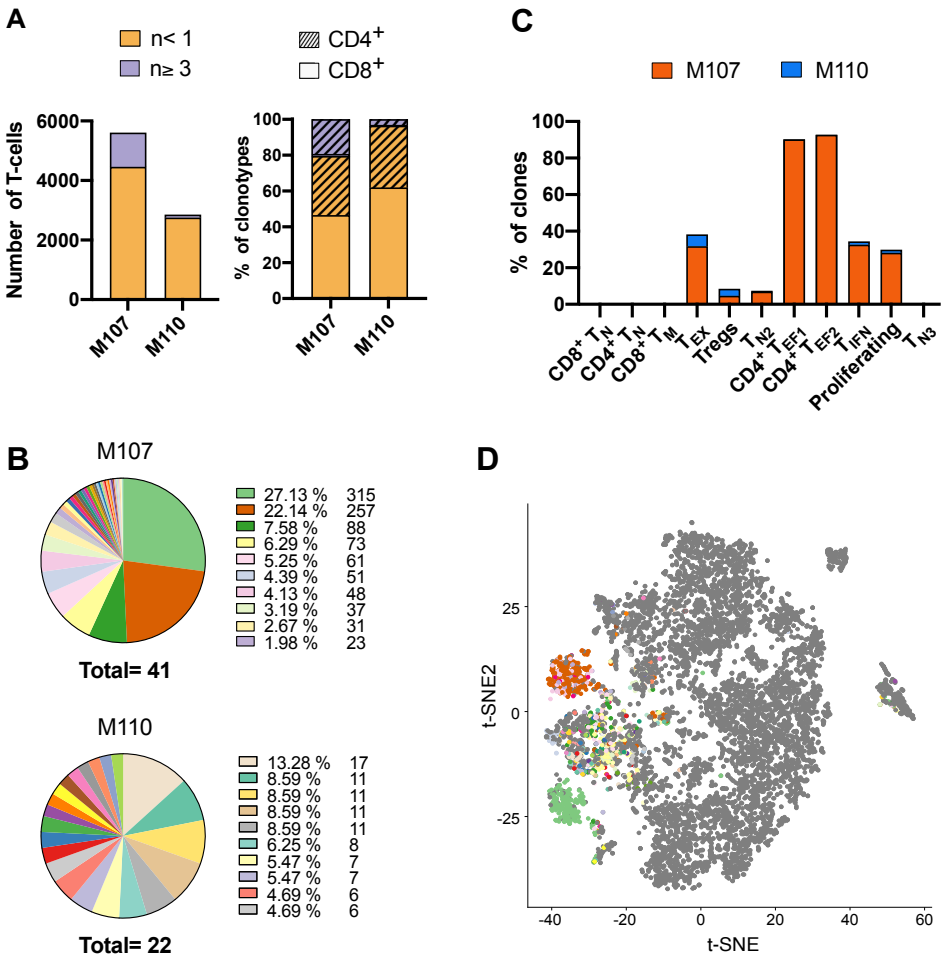

Figure 20: Clonal expansion in the TCL1 AT mouse model occurs in the CD4⁺ T-cell compartment. (A) Total number of non-expanded (n < 3) or clonally expanded (n ≥ 3) CD3⁺ T-cells (left), and percentage out of total cells (right) in each mouse sample. Distinction between CD4⁺ and CD8⁺ T-cells is made in the left graph. **(B)** Clonal composition of mouse samples M107 and M110. Fractions and numbers of cells for the 10 most abundant clones are given next to the plots. The total number of clones is annotated below the chart **(C)** Percentage of cells associated with a clone out of total cells per cluster. Sample contribution is color-coded. **(D)** t-SNE plot of CD3⁺ T-cells, CLL and myeloid cells from M107 and M110 samples with all T-cell expanded clones colored distinctively. Cells with no shared TCR are colored in grey.

mostly CD4⁺ T-cells (Figure 20A), as opposed to the dominant CD8⁺ T-cell clonal expansion occurring in human CLL LN samples (see Section 4.3.3, Figure 17). Last, clonal T-cell expansion was confined to several cell subsets: CD4⁺ T_{EF1} and T_{EF2} exclusively contained clonal cells, and the CD4⁺ and CD8⁺-containing T_{EX} cluster likewise comprised numerous clones (Figure 20C-D). In addition, the T_{IFN} cluster and proliferating cells, followed by Treg and T_{N2} cells, also contained some clonally expanded cells, suggesting that a tumor T-cell response involves a reaction of multiple T-cell phenotypes in the TCL1 AT mice.

In sum, a heterogeneous and of predominantly CD4⁺ T-cells clonal expansion was ascertained in the TCL1 AT mouse model, an observation that is clearly distinct from the

human situation, and which underscores the complex, variable, and tumor-dependent immune response to leukemia growth.

4.4.3 Interactions between CLL cells and the T-cell compartment in the TCL1 AT mouse model

In order to investigate the cellular crosstalk between CLL cells and the T-cell subsets characterized in the murine samples, the CellPhoneDB approach was used, akin to the human analysis. Notably, CLL cells established the highest number of interactions, especially with T_{IFN}, $CD8^+$ T_M, Tregs and myeloid cells. Besides, myeloid cells and activated T-cell subsets showed a higher amount of interactions in comparison to naïve subsets (Figure 21A).

Additionally, by examining the specific intercellular network between CLL cells and their microenvironment, known pro-leukemic signals were identified (Figure 21B). As an example, CLL cells appeared to receive survival signals via the interactions of CD40- CD40L provided by $CD4^+$ T-cell subsets, SELL- SELPLG by T_{EX} and $CD4^+$ $T_{EF1\text{-}2}$, and CD80- CD274 by Tregs, T_{IFN}, and myeloid cells (Figure 21B). Other interactions that have been shown to promote a homing environment to CLL cells included CD74 (Binsky et al. 2007), as well as several integrin complexes and semaphorins (i.e. SEMA4D and SEMA7A) (Ten Hacken and Burger 2016), the ligands of which were mainly expressed by myeloid cells. Interestingly, and as observed in the human samples, CLL cells expressed the receptors for the pro-inflammatory molecules IFNγ, TNFα, and CCL5, produced by the activated T-cell subsets, namely $CD4^+$ $T_{EF1\text{-}2}$, T_{IFN}, T_{EX}, and proliferating cells. Instead, signals that have been reported to inhibit CLL cell proliferation, like CD47- SIRPG or TGF-β secretion (Lagneaux et al. 1998; Martinez-Torres et al. 2015), were expressed by $CD8^+$ T_N, $CD8^+$ T_M, T_{N2}, T_{IFN}, myeloid, and proliferating cells. Of note, CD52 was expressed by both CLL cells and activated T-cell subsets, comparably to LNs of CLL patients (Figure 21B).

On the other hand, T-cells – specifically T_{EX}, $CD4^+$ $T_{EF1\text{-}2}$ and proliferating cells – were predicted to receive a variety of signals from CLL cells, including co-stimulatory ones via sialophorin (SPN) and integrin subunit alpha L (ITGAL) binding to intercellular adhesion molecule 1 (ICAM1) (Figure 21B). However, these subsets were also exposed to many other inhibitory signals, such as CD39- ADORA2A, PD-1 binding to both PD-L1 and PD-L2, and binding of lymphotoxin α (*LTA*) to TNFR1 and TNFR2 (Figure 21B).

Overall, this data shows a complex intercellular relationship between TCL1 leukemic cells and their microenvironment, which was similarly identified in the human samples used in this work. Thus, it proves that the mouse model largely recapitulates the pathogenic situation taking place in CLL patients.

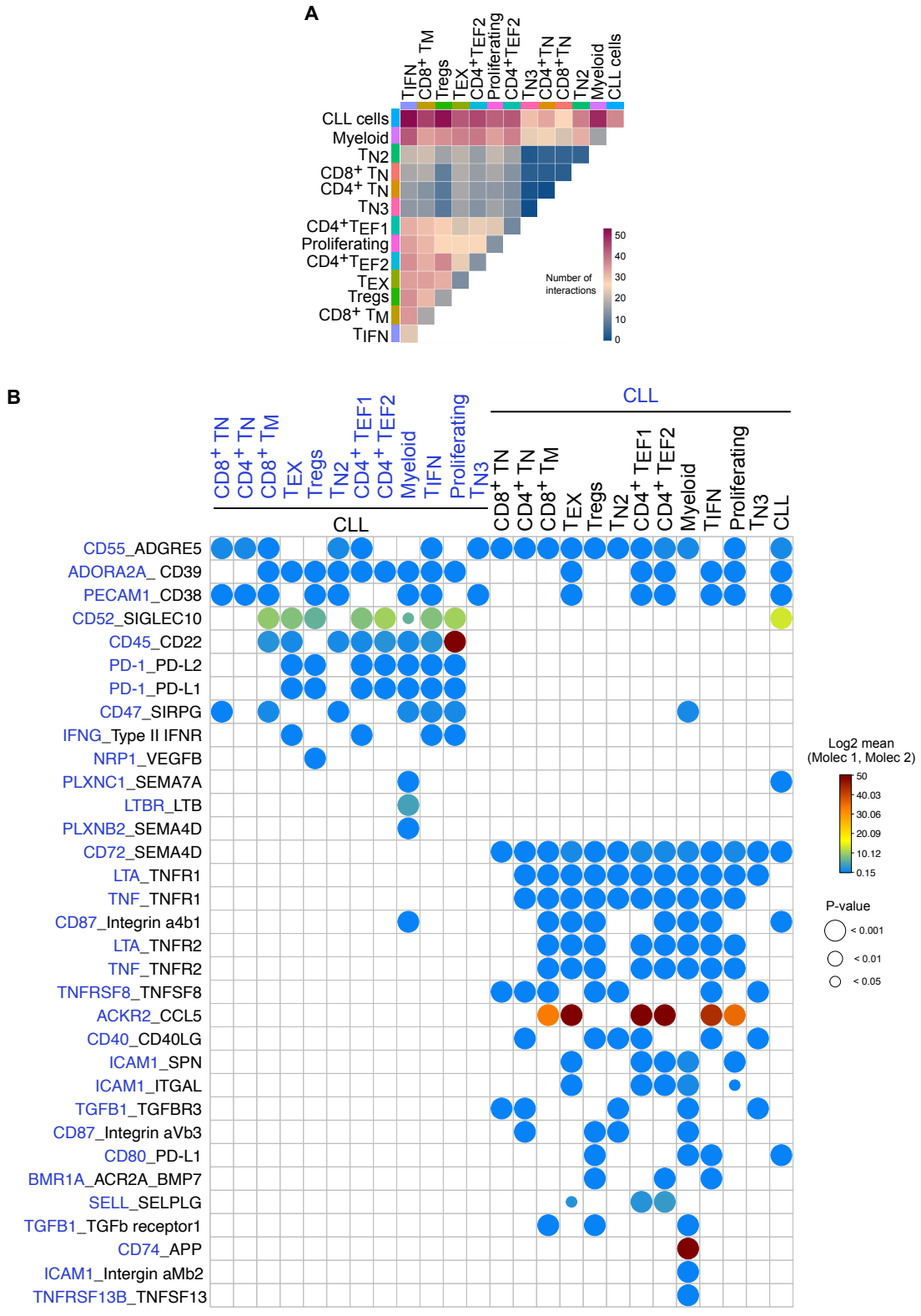

Figure 21: Interactions between CLL cells and their microenvironment in the TCL1 AT mouse model resemble those in the human system. (A) Heatmap showing the number of predicted interactions between cell subsets. **(B)** Plot depicting significant curated ligand-receptor interactions between CLL cells and all cell subsets. Dot color indicates combined log2 mean expression of ligand and receptor. Size of the dots represents the p-value, calculated by permutation test. Gene names were substituted for the respective protein names for CD39 (*ENTPD1*), CD45 (*PTPRC*), PD-1 (*PDCD1*), PD-L1 (*CD274*), PD-L2 (*PDCD1LG2*), TNFR1 (*TNFRSF1A*), TNFR2 (*TNFRSF1B*), TACI (*TNFRSF13B*) and APRIL (*TNFSF13*).

4.5 EOMES is necessary for anti-tumor activity of $CD8^+$ T-cells in CLL

4.5.1 *EOMES* expression in T-cells is associated with accessible chromatin

Whole genome association studies have shown that a single-nucleotide polymorphism (SNP) located 13 kb 5' upstream of the *EOMES* gene (rs9880772) is associated with a significantly increased risk to develop CLL (Berndt et al. 2016; Speedy et al. 2019). To identify cell types with a euchromatic state at the *EOMES* locus that could hence be functionally affected by the SNP, chromatin status as well as RNA expression of the *EOMES* gene were investigated in mature hematopoietic cells. This was performed in collaboration with Dr. Vicente Chapaprieta, from the Institut d'Investigacions Biomèdiques August Pi i Sunyer, Barcelona. More precisely, chromatin states resulting from the presence of the six histone marks H3K4me3, H3K4me1m, H3K27ac, H3K36me3, H3K27me3, or H3K9me3, together with RNA-seq data included in the reference epigenomes produced by the Blueprint project (The BLUEPRINT Consortium 2016), were examined. Open chromatin and active promoters, as well as RNA transcripts at the EOMES locus were mostly detected in NK-cells and T-cells, with memory $CD8^+$ T-cells and NK cells presenting the highest RNA expression (Figure 22A). In contrast, a heterochromatic state and no *EOMES* expression were observed in B-cells at different maturation states. Next, *EOMES* mRNA expression in cell subsets from the 3 CLL LNs analyzed by single-cell RNA-seq was examined. In agreement with the previous observations, *EOMES* expression was highest in $CD8^+$ T_{EM1}, but was also present in $CD4^+$ T_{EM1}, T_{TOX} and T_F cell subsets. Notably, no expression was detected in CLL cells (Figure 22B).

EOMES is a TF that regulates T-cell effector function (Intlekofer et al. 2008; Banerjee et al. 2010; Pipkin et al. 2010) and has been associated with T-cell exhaustion in chronic infections and cancer (Li et al. 2018; Weulersse et al. 2020). To assess its role in CLL, the previously investigated mass cytometry data of CLL LNs was used to profile EOMES expression in $CD8^+$ T-cells. The single-cell analyses showed that EOMES protein was mostly expressed in effector (T_{EF1} and T_{EF2}), effector memory (T_{EM1}, and T_{EM2}), proliferating, and exhausted T_{EX} cells, with the latter two showing the highest levels (Figure 22C, D). Intriguingly, T_{EM3} and T_{EM4} cells did express substantially less EOMES (Figure 22C), suggesting the existence of an alternative mechanism for memory differentiation and/or persistence. Notably, median EOMES protein expression was significantly higher in LNs of CLL samples in contrast to HC samples (Figure 22E), likely as a reflection of the earlier reported higher frequencies of T_{EX}, T_{EF1}, and proliferating subsets (Figure 11D).

Collectively, these data suggest that T-cells, but not CLL cells harbor open chromatin at the *EOMES* locus, thus enabling *EOMES* expression. Besides, EOMES protein levels are highest in CLL-derived exhausted $CD8^+$ T-cells.

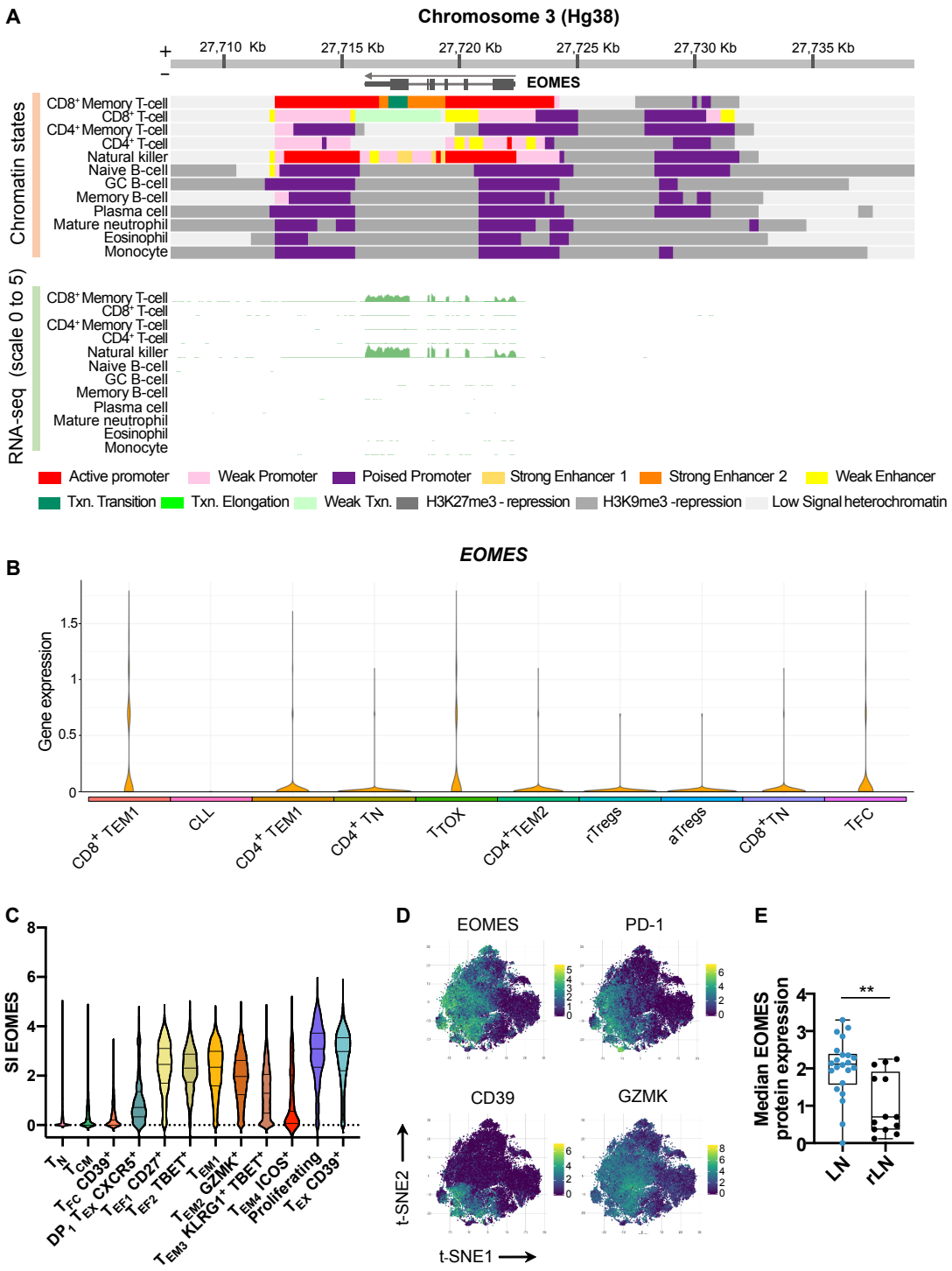

Figure 22: *EOMES* chromatin and transcriptomic status in hematopoietic cells. (A) Chromatin state at the *EOMES* locus derived from the integration of H3K4me3, H3K4me1 H3K27ac, H3K36me3, H3K27me3 and H3K9me3 histone marks in hematopoietic cells of healthy individuals (n = 3, upper panel), together with RNA-seq signal from the reference epigenomes generated in the Blueprint project database (n = 3, scale = log2 RPKM) (lower panel). Data was generated in collaboration with Dr. Vicente Chapaprieta, from the Institut d'Investigacions Biomèdiques August Pi i Sunyer, Barcelona **(B)** Violin plot depicting *EOMES* gene expression (UMI counts) in single-cell clusters identified in LNs from 3 CLL patients. **(C)** Violin plot showing EOMES signal intensity (SI) in clusters defined with mass cytometry analyses. **(D)** t-SNE plot depicting protein levels of EOMES, PD-1, CD39 and GZMK in CD8+ T-cells measured by mass cytometry. **(E)** Median EOMES protein levels in CLL (n = 21) compared to rLN (n= 13) samples (**p<0.01, Mann-Whitney U test).

4.5.2 EOMES$^+$ CD8$^+$ T-cells accumulate in the Eμ-TCL1 mouse model and exhibit an exhausted phenotype

To further characterize the role of EOMES in CLL, its expression was investigated in both the Eμ-TCL1 and the TCL1 AT mouse models of CLL. Importantly, *Eomes* transcripts in the single-cell transcriptome dataset of TCL1 AT mice were restricted to effector and memory T-cells, but absent in CLL and myeloid cells (Figure 23A). Besides, they were most abundant in T_{EX} cells co-expressing *Pdcd1* and *Lag3* genes, as observed in human T-cells.

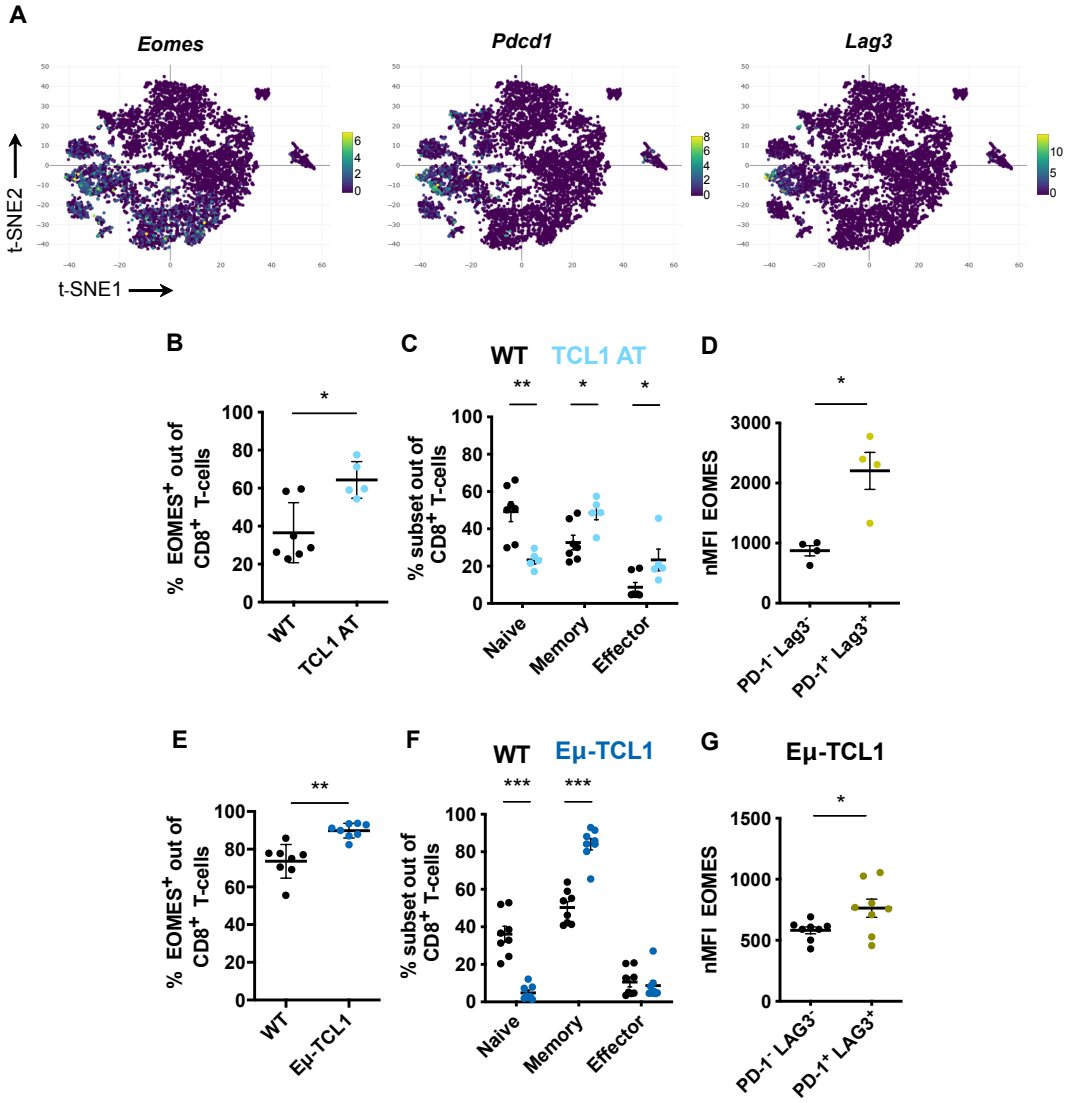

Figure 23: EOMES$^+$ CD8$^+$ T-cells accumulate in the TCL1 mouse models. (A) Gene expression (UMI counts) of *Eomes*, *Pdcd1* and *Lag3* in single-cell data from TCL1 AT mice. **(B)** Fraction of EOMES$^+$ cells out of CD8$^+$ T-cells in TCL1 AT (n = 5) and respective control mice (n = 7). **(C)** Percentage of naïve, memory and effector cells in WT compared to TCL1 AT mice. **(D)** Normalized fluorescence intensity (nMFI) of EOMES in effector and memory PD-1$^-$ LAG3$^-$ and PD-1$^+$ LAG3$^+$ CD8$^+$ T-cells form TCL1 AT mice (n = 4). **(E)** Fraction of EOMES$^+$ out of CD8$^+$ T-cells in age- and sex- matched Eμ-TCL1 (n= 8) and WT mice (n = 8). **(F)** Percentage of naïve, memory and effector cells in WT and Eμ-TCL1 mice. **(G)** EOMES nMFI values in PD-1$^-$ LAG3$^-$ and respective double positive effector and memory CD8$^+$ T-cells in Eμ-TCL1 mice. Mean and SEM are depicted, and single dots represent each mouse analyzed (*p<0.05, **<0.01, ***>0.001, Mann-Whitney U test).

At the protein level, flow cytometry analyses revealed an increase of EOMES$^+$ CD8$^+$ T-cells in TCL1 AT compared to age- and sex-matched WT mice (Figure 23B), likely as a result of the known T-cell skewing towards antigen-experienced effector and memory T-cells (Figure 23C) (McClanahan et al. 2015b; Hanna et al. 2019). EOMES levels in exhausted T-cells were next examined in tumor-bearing mice. In concordance with the transcriptomic data, PD-1$^+$ LAG3$^+$ effector and memory CD8$^+$ T-cells exhibited higher EOMES levels in comparison with their double-negative counterparts (Figure 23D). Lastly, similar results were detected in the transgenic Eμ-TCL1 mice (Figure 23E-F), which, as a consequence of their disease onset at advanced age, exhibited an overall higher percentage of EOMES$^+$ cells. Moreover, EOMES levels were likewise significantly increased in exhausted PD-1$^+$ LAG3$^+$ T-cells compared to non-exhausted memory and effector cells in these mice (Figure 23G).

Taken together, these results illustrate that both the Eμ-TCL1 and the TCL1 AT mouse models recapitulate the accumulation of EOMES$^+$ CD8$^+$ T-cells in the TME of CLL patients, and its higher expression in exhausted T-cells.

4.5.3 *Eomes*-deficient CD8$^+$ T-cells fail to expand and control CLL development in the TCL1 AT mouse model

Following the previous observations, the question arises whether EOMES has an effect on CLL-tumor control via regulation of T-cell function. To investigate the role of EOMES in T-cell-mediated control of CLL, *Eomes* knock-out (*Eomes*$^{-/-}$) BM chimera were generated using *Rag2*$^{-/-}$ mice, which fail to produce mature T- and B-cells (Shinkai et al. 1992). Next, mice were adoptively transferred with Eμ-TCL1 leukemic cells, and tumor load as well as T-cell phenotype

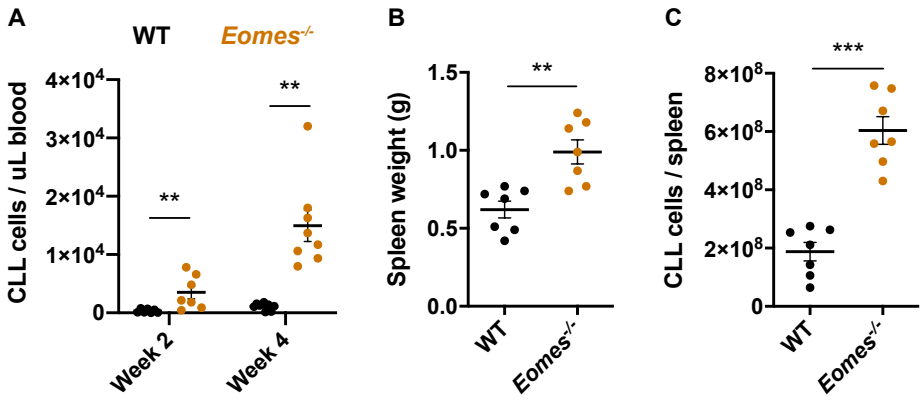

Figure 24: *Eomes*-deficiency in the TME of TCL1 AT mice leads to impaired tumor control. *Rag2*$^{-/-}$ mice were irradiated and subsequently injected with either WT or *Eomes*$^{-/-}$ BM cells. Next day, mice were injected with leukemia cells from TCL1 mice. **(A)** Absolute counts of CD5$^+$ CD19$^+$ CLL cells in peripheral blood 2 and 4 weeks after tumor injection in *Eomes*$^{-/-}$ BM chimera (n = 7) and WT BM chimera mice (n = 8) as determined by flow cytometry. **(B)** Spleen weight and **(C)** absolute counts of CLL cells in spleen at experimental endpoint (4 weeks after tumor injection). Horizontal and vertical bars display mean and SEM respectively. Each dot symbolizes one mouse (**p<0.01, ***<0.001, Mann-Whitney U test).

were examined by flow cytometry. Surprisingly, tumors developed faster in mice with an *Eomes*-deficient hematopoietic system compared to WT BM chimeric *Rag2*$^{-/-}$ mice, as measured in PB over time (Figure 24A). In accordance with this, *Eomes*$^{-/-}$ mice also presented a higher tumor burden in spleen at the experimental end-point 4 weeks later, with both increased spleen weight (Figure 24B) and CLL numbers per spleen (Figure 24C).

This enhanced tumor growth in *Eomes* BM-deficient mice was accompanied by diminished CD8$^+$ T-cell numbers in spleen (Figure 25A) and a reduced percentage of KI-67$^+$ CD8$^+$ T-cells (Figure 25B), hinting at an impaired tumor control due to a lack of expansion of these cells. However, CD8$^+$ T-cells did not differ in their phenotype, as similar proportions of naïve, memory

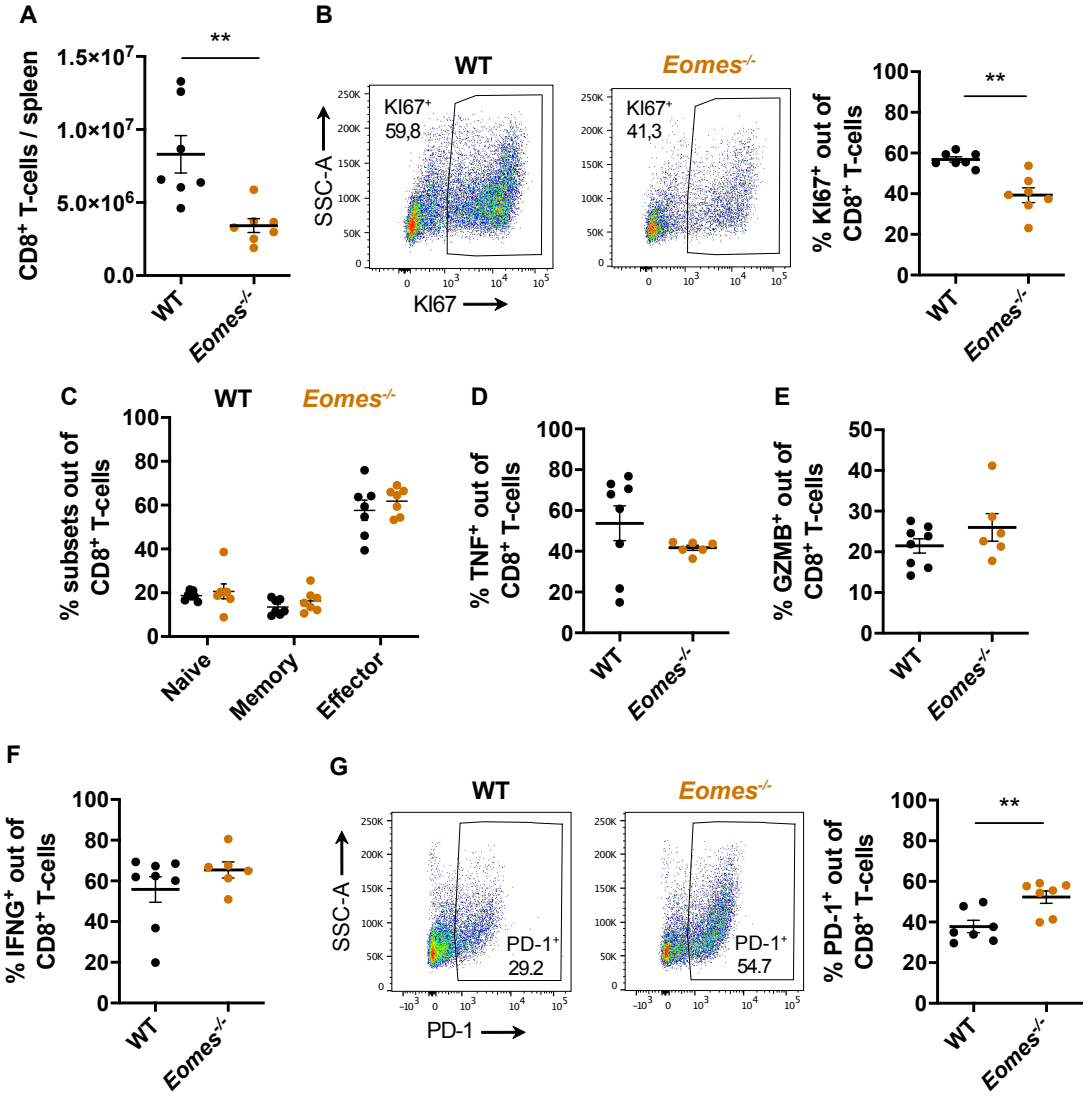

Figure 25: CD8$^+$ T-cells from *Eomes*$^{-/-}$ BM chimeric mice fail to expand upon leukemic cell transplantation. (A) Absolute counts of CD8$^+$ T-cell per spleen in WT versus *Eomes*-deficient BM chimeric *Rag2*$^{-/-}$ mice. **(B)** Representative histograms and percentages of KI-67$^+$ cells among CD8$^+$ T-cells in spleen. **(C)** Percentage naïve, memory and effector subsets out of total CD8$^+$ T-cells. **(D)** Representative histogram and precentages of PD-1$^+$ CD8$^+$ T-cells. **(E)** Frequencies of TNFα^+, **(F)** GZMB$^+$, and **(G)** IFNγ^+ cells among CD8$^+$ T-cells after *ex vivo* stimulation with PMA and ionomycin for 6 hours. Graphs show mean ± SEM, with each dot representing one mouse (**p>0.01, ***>0.001, Mann-Whitney U test).

and effector T-cells were identified (Figure 25C). Besides, comparable frequencies of cells expressed the effector molecules GZMB, TNFα and IFNγ after *ex vivo* stimulation with phorbol myristate acetate (PMA) and ionomycin (Figure 25D-F). Intriguingly, the lack of EOMES was associated with a higher frequency of $CD8^+$ T-cells expressing PD-1 (Figure 25G). These results indicate that lack of $CD8^+$ T-cell expansion is involved in the impaired tumor control of *Eomes*-deficient mice.

To corroborate these observations and exclude the implication of other cells in the microenvironment, such as $CD4^+$ T-cells, *Eomes*$^{-/-}$ or WT $CD8^+$ T-cells were injected in *Rag2*$^{-/-}$ mice. The following day, these mice were injected with TCL1 leukemic cells, and tumor development was monitored. Similar to the *Eomes*$^{-/-}$ BM chimera, leukemia development occurred significantly faster in mice that had received *Eomes*$^{-/-}$ $CD8^+$ T-cells compared to mice injected with WT $CD8^+$ T-cells. This was determined based on absolute numbers of CLL cells in PB over time (Figure 26A), as well as by an increased spleen weight and tumor content in this organ at experimental end-point, 4 weeks after tumor cell injection (Figure 26B-C).

Likewise, $CD8^+$ T-cells lacking EOMES expanded significantly less in leukemic *Rag2*$^{-/-}$ mice than their WT counterparts, as they were present in lower numbers in spleen (Figure 27A). The frequency of naïve, memory and effector subsets remained unchanged (Figure 27B), as well as the proportion of cells expressing the effector molecules TNFα, GZMB and IFNγ after *ex vivo* stimulation with PMA and Ionomycin (Figure 27C-E).

In summary, these observations reveal an essential role of EOMES for $CD8^+$ T-cell expansion and maintenance in mice that develop CLL-like disease, which results in an impaired tumor control.

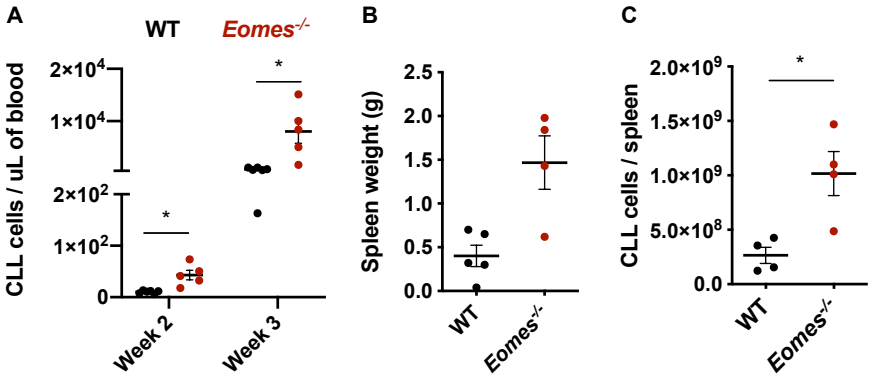

Figure 26: Leukemia development is enhanced in *Rag2*$^{-/-}$ mice transplanted with *Eomes*$^{-/-}$ $CD8^+$ T-cells. WT or *Eomes*$^{-/-}$ $CD8^+$ T-cells were injected into *Rarg2*$^{-/-}$ mice prior leukemia cell transplantation. **(A)** Absolute numbers of $CD5^+$ $CD19^+$ CLL cells in PB 2 and 3 weeks after tumor injection of *Rag2*$^{-/-}$ mice injected with *Eomes*$^{-/-}$ (n = 5) or WT (n = 5) $CD8^+$ T-cells as measured by flow cytometry. **(B)** Spleen weight of injected mice at experimental end-point. **(C)** Absolute counts of CLL cells in spleen. Graphs display mean ± SEM, and each dot represents one mouse (*p>0.05, Mann-Whitney U test).

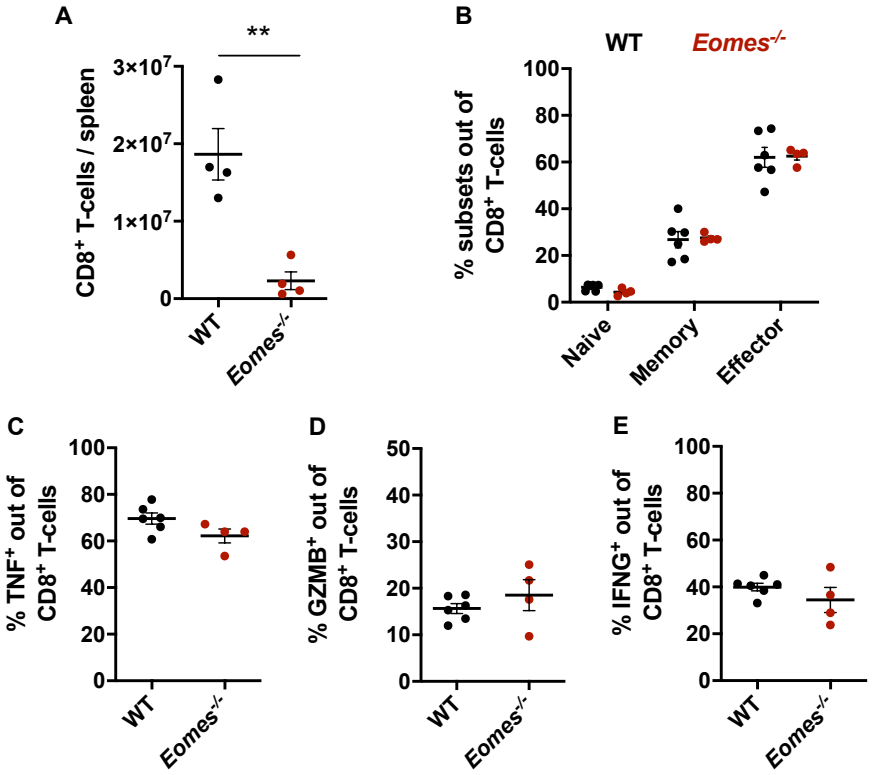

Figure 27: *Eomes*$^{-/-}$ CD8$^+$ T-cells fail to expand upon CLL cell transplantation into *Rag2*$^{-/-}$ mice. (A) CD8$^+$ T-cells numbers per spleen in mice injected with *Eomes*$^{-/-}$ or WT CD8$^+$ T-cells. **(B)** Pecentage of naïve, memory and effector CD8$^+$ T-cells. **(C-E)** Frequency of **(C)** TNFα^+, **(D)** GZMB$^+$, and **(E)** IFNγ^+ CD8$^+$ T-cells after *ex vivo* stimulation with PMA and Ionomycin for 6 hours. Graphs display mean ± SEM and each dot represents one mouse (*p>0.05, **>0.01, Mann-Whitney U test).

4.6 The anti-tumor activity of CD4$^+$ T regulatory type 1 cells is controlled by EOMES and IL-10

4.6.1 CLL LNs exhibit increased numbers of EOMES$^+$ PD-1$^+$ T$_R$1-like CD4$^+$ T-cells

EOMES has been described to regulate the development of CD4$^+$ type 1 regulatory T-cells (T$_R$1) (Zhang et al. 2017; Gruarin et al. 2019). These cells characteristically produce IL-10, GZMK and IFNγ (Gruarin et al. 2019; Mazzoni et al. 2019), express several inhibitory receptors such as PD-1, TIGIT, CD39 and LAG3, and have immunosuppressive functions (Roncarolo et al. 2018). However, their role in tumor development remains elusive and completely undefined in CLL. Hence, the presence of CD4$^+$ T$_R$1 was investigated in CLL patients. First, examination of CD4$^+$ T-cells from CLL LNs analyzed by single-cell RNA-seq identified 9 clusters, which included naïve, Tregs, memory, and effector memory T-cells (Figure 28A). Interestingly, a cluster of cells differentially expressed *PDCD1*, *TIGIT* and several granzymes, including *GZMK* (Figure 28B).

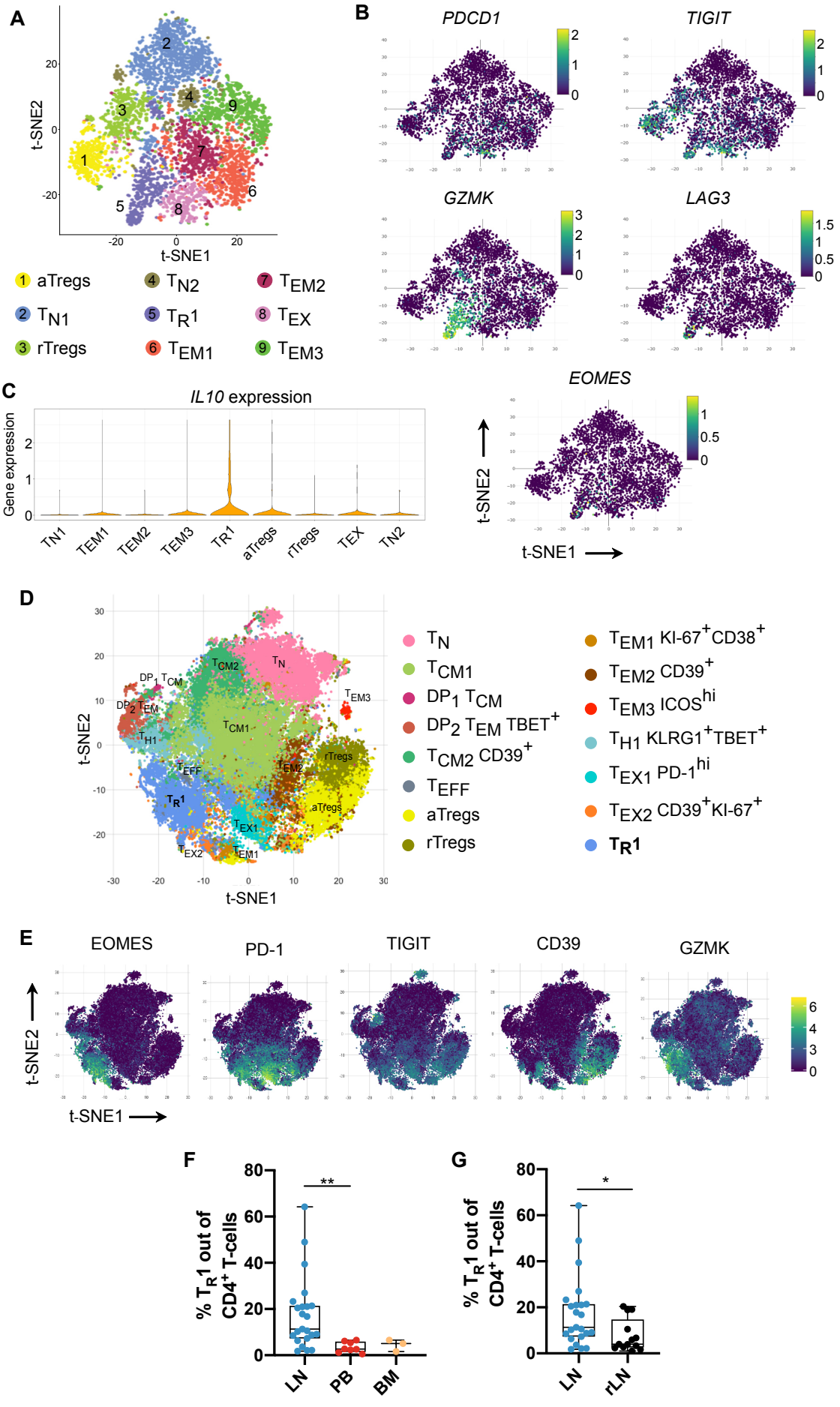
A
t-SNE2
t-SNE1
1 aTregs
2 TN1
3 rTregs
4 TN2
5 TR1
6 TEM1
7 TEM2
8 TEX
9 TEM3
B
PDCD1
TIGIT
GZMK
LAG3
C
IL10 expression
Gene expression
TN1
TEM1
TEM2
TEM3
TR1
aTregs
rTregs
TEX
TN2
EOMES
D
TN
TCM1
DP1 TCM
DP2 TEM TBET+
TCM2 CD39+
TEFF
aTregs
rTregs
TEM1 KI-67+CD38+
TEM2 CD39+
TEM3 ICOShi
TH1 KLRG1+TBET+
TEX1 PD-1hi
TEX2 CD39+KI-67+
TR1
E
EOMES
PD-1
TIGIT
CD39
GZMK
F
% TR1 out of CD4+ T-cells
LN
PB
BM
G
% TR1 out of CD4+ T-cells
LN
rLN

Figure 28: EOMES$^+$ PD-1$^+$ T_R1-like cells accumulate in CLL LNs. (A) t-SNE plot of CD4$^+$ T-cells analyzed by single-cell RNA-seq. Identified clusters are distinguished with different colors. **(B)** RNA expression of *EOMES*, *PDCD1*, *TIGIT*, *LAG3* and *GZMK* in CD4$^+$ T-cells. **(C)** Violin plots depicting *IL10* RNA expression in the CD4$^+$ T-cell clusters **(D)** t-SNE plot of 1 x10^3 CD4$^+$ T-cells analyzed by mass cytometry displaying the 15 identified clusters classified according to differential protein expression. Clusters are given with different colors. **(E)** Protein expression of EOMES, PD-1, TIGIT, CD39 and GZMK in CD4$^+$ T-cells. **(F)** Frequency of T_R1 cells in LN (n = 22), PB (n = 8) and BM (n = 3) of CLL patients. **(G)** Frequency of T_R1 cells in LN (n = 21), compared to HC (n = 13) (*p<0.05, **<0.01, Mann-Whitney U test). A complete characterization of the CD4$^+$ T-cell compartment has been described elsewhere (Paul 2020).

In addition, these cells expressed *EOMES*, *LAG3* and *IL10* genes (Figure 28B-C), thus highly resembling T_R1 cells. Next, and further confirming the presence of T_R1 cells in CLL LNs, a subset of effector memory CD4$^+$ T-cells co-expressing EOMES$^+$ PD-1$^+$ was identified with mass cytometry analyses of CD4$^+$ T-cells (Figure 28D-E). This subset also expressed other inhibitory receptors like TIGIT and CD39, and produced GZMK (Figure 28E). Last, the distribution of T_R1 cells in the different tissues, as well as sample condition – i.e. CLL versus control samples – was inspected. Intriguingly, a significantly higher frequency of T_R1-like cells was found in LNs compared to PB and BM (Figure 28F), underscoring an implication of these cells in the CLL TME niche. Moreover, T_R1 cells were significantly enriched in CLL LNs compared to healthy controls (Figure 28G).

Altogether, these results confirm the accumulation of T_R1 cells in the LNs of CLL patients, and thus suggest the possibility of a pathological involvement of this cell subset in CLL.

4.6.2 T_R1 cells accumulate in the Eμ-TCL1 mouse model

To further investigate the role of T_R1 cells in CLL, their presence was analyzed in the Eμ-TCL1 and TCL1 AT mouse models of CLL. For this purpose, splenocytes from end-stage diseased mice were isolated, stained, and analyzed by flow cytometry. In both models, a significantly higher fraction of EOMES$^+$ PD-1$^+$ T_R1-like cells was measured in the leukemia-bearing mice compared to their respective age- and sex-matched WT controls (Figure 29A). Interestingly, the frequency of T_R1 cells was higher in aged Eμ-TCL1 mice compared to the younger TCL1 AT mice, in line with a previously described accumulation of EOMES$^+$ CD4$^+$ T-cells with age (Lupar et al. 2015). Additionally, the majority of T_R1 cells in TCL1 AT mice expressed LAG3 (Figure 29B), further corroborating their T_R1 phenotype (Gagliani et al. 2013). Next, the *Il-10* reporter mice Fir x Tiger were used to investigate IL-10 production upon leukemia development. Interestingly, an accumulation of FOXP3$^-$ IL-10-producing CD4$^+$ T-cells co-expressing PD-1 was detected in all leukemic mice while being completely absent in unchallenged controls (Figure 29C), thus indicating a CLL-specific increase of IL-10-producing T_R1 cells.

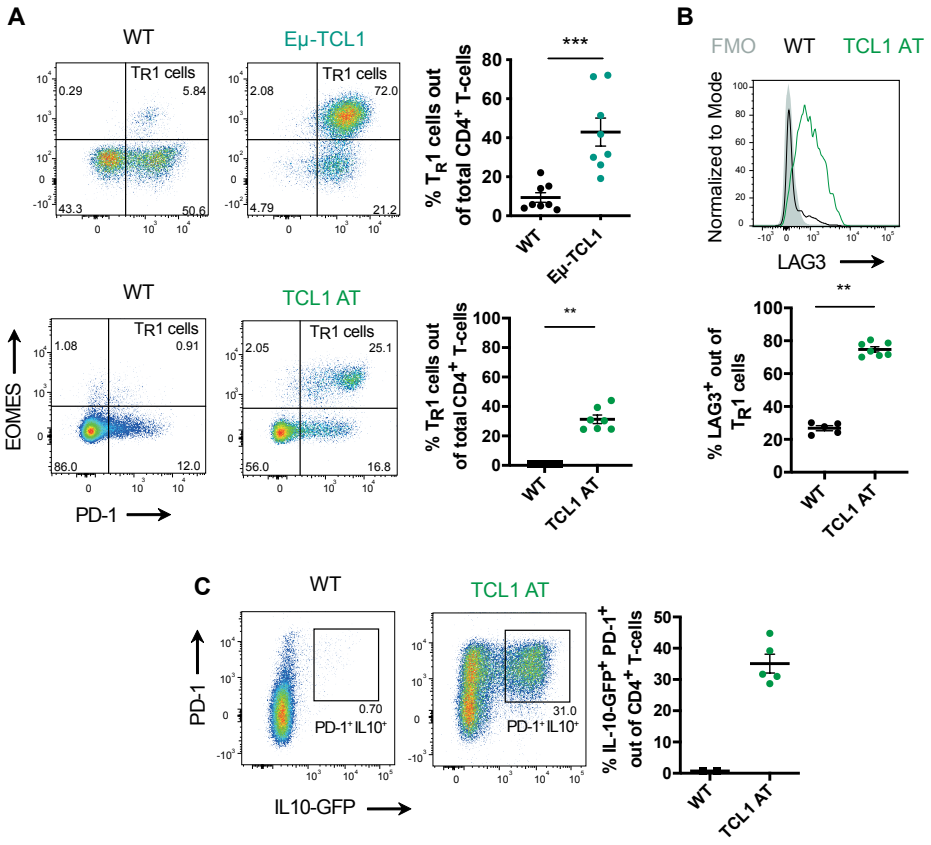

Figure 29: IL-10 producing T_R1 cells expand in TCL1 leukemic mice. (A) Representative dot plots (left and center panels) as well as proportion (right graph) of T_R1 (EOMES$^+$ PD-1$^+$) cells among CD4$^+$ T-cells in Eμ-TCL1 (n = 8) (upper row) and TCL1 AT (n = 7) (lower row) mice including respective WT controls (n = 8, n = 5, respectively). **(B)** Representative histogram (upper panel) and proportion of LAG3$^+$ among T_R1 cells in WT (n = 5) and TCL1 AT mice (n = 7) (lower graph). **(C)** Representative dot plots (left and center panels) and percentage of IL-10-GFP$^+$ PD-1$^+$ cells out of FOXP3$^-$ CD4$^+$ T-cells in WT (n = 2) and TCL1 AT FIR x Tiger mice (n = 5) (right panel) (**p<0.01, ***<0.001, Man-Whitney test). Data was generated in collaboration with Dr. Philipp Rößner and Dr. Bola Hanna from the Department of Molecular Genetics at the German Cancer Research Center (DKFZ), Heidelberg.

In summary, this data thus shows that IL-10 producing T_R1 cells accumulate upon leukemia development in the Eμ-TCL1 and TCL1 AT mouse models of CLL.

4.6.3 EOMES is essential for T_R1-mediated tumor control in TCL1 AT mice

Even though numerous reports describe an accumulation of T_R1 cells in several types of cancers, including Hodgkin's lymphoma, head and neck squamous cell carcinoma, and colorectal cancer, the role of T_R1 cells in the tumor microenvironment remains under debate (Bergmann et al. 2008; Dennis et al. 2013; Scurr et al. 2014). In order to investigate the impact of T_R1 cells on leukemia progression, the conditional *Eomes*$^{-/-}$ mice were used, as EOMES has an essential role for the development of functional T_R1 cells (Zhang et al. 2017; Gruarin et al. 2019). For this purpose, *Rag2*$^{-/-}$ mice were transplanted with CD4$^+$ T-cells isolated from

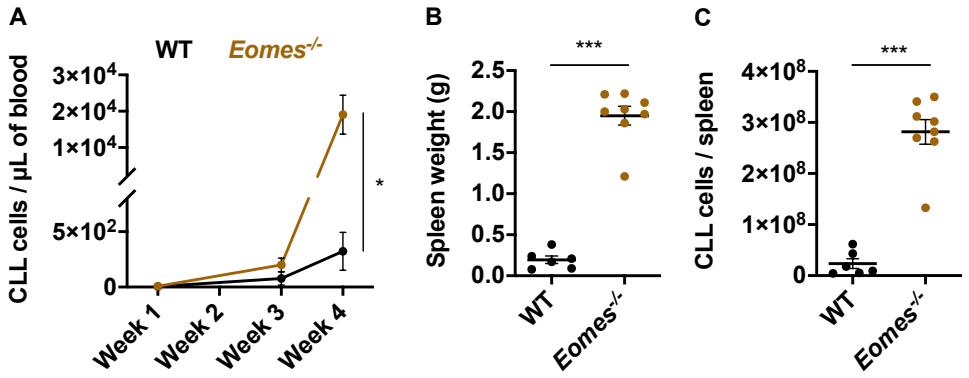

Figure 30: Leukemia growth is enhanced in *Rag2*$^{-/-}$ mice transplanted with *Eomes*$^{-/-}$ CD4^{+} T-cells. *Rag2*$^{-/-}$ mice were transplanted with *Eomes*$^{-/-}$ or WT CD4^{+} T-cells prior injection of leukemia cells the following day. **(A)** Leukemic CD5^{+} CD19^{+} cell count in peripheral blood of *Rag2*$^{-/-}$ mice injected with WT (n = 6) or *Eomes*$^{-/-}$ (n = 8) CD4^{+} T-cells as measured by flow cytometry over time. **(B)** Spleen weight of mice at experimental end-point. **(C)** Absolute CLL cell counts per spleen at experimental end-point. Graphs show mean ± SEM and each dot represents one mouse (*p>0.05, ***>0.001, Mann-Whitney U test).

spleens of either *Eomes*$^{-/-}$ or *Eomes*$^{+/+}$ *Il10*-GFP reporter mice, prior to adoptive transfer of TCL1 leukemia cells. Surprisingly, significantly higher amounts of CLL cells were measured in PB of mice injected with *Eomes*$^{-/-}$ CD4^{+} T-cells compared to those injected with WT CD4^{+} T-cells (Figure 30A). In line with this, mice injected with *Eomes*-deficient CD4^{+} T-cells showed higher spleen weight (Figure 30B) and tumor load in this organ (Figure 30C).

Monitoring the expansion and phenotype of the transplanted CD4^{+} T-cells revealed a higher amount of *Eomes*$^{-/-}$ CD4^{+} T-cells compared to WT cells in PB of leukemic mice over time (Figure 31A). However, *Eomes*$^{-/-}$ CD4^{+} T-cell absolute counts per spleen (Figure 31B), as well as counts per CLL cell (Figure 31C) were significantly lower when measured at the experimental end-point. Accordingly, a lower fraction of *Eomes*-deficient T-cells proliferated in the spleen, as measured by KI-67 staining (Figure 31D), further indicating that EOMES is associated with T_R1 expansion in CLL. Moreover, lack of EOMES resulted in an inferior fraction of CD4^{+} T-cells expressing the T_R1 marker proteins LAG3 (Figure 31E), and IL10 (Figure 31F), as well as IFNγ (Figure 31G), CD107A, and GZMB (Figure 31H) molecules, involved in effector function.

Collectively, these data highlight an essential role of EOMES for the control of CLL progression in mice as a result of its involvement in T_R1 expansion and cytotoxic function.

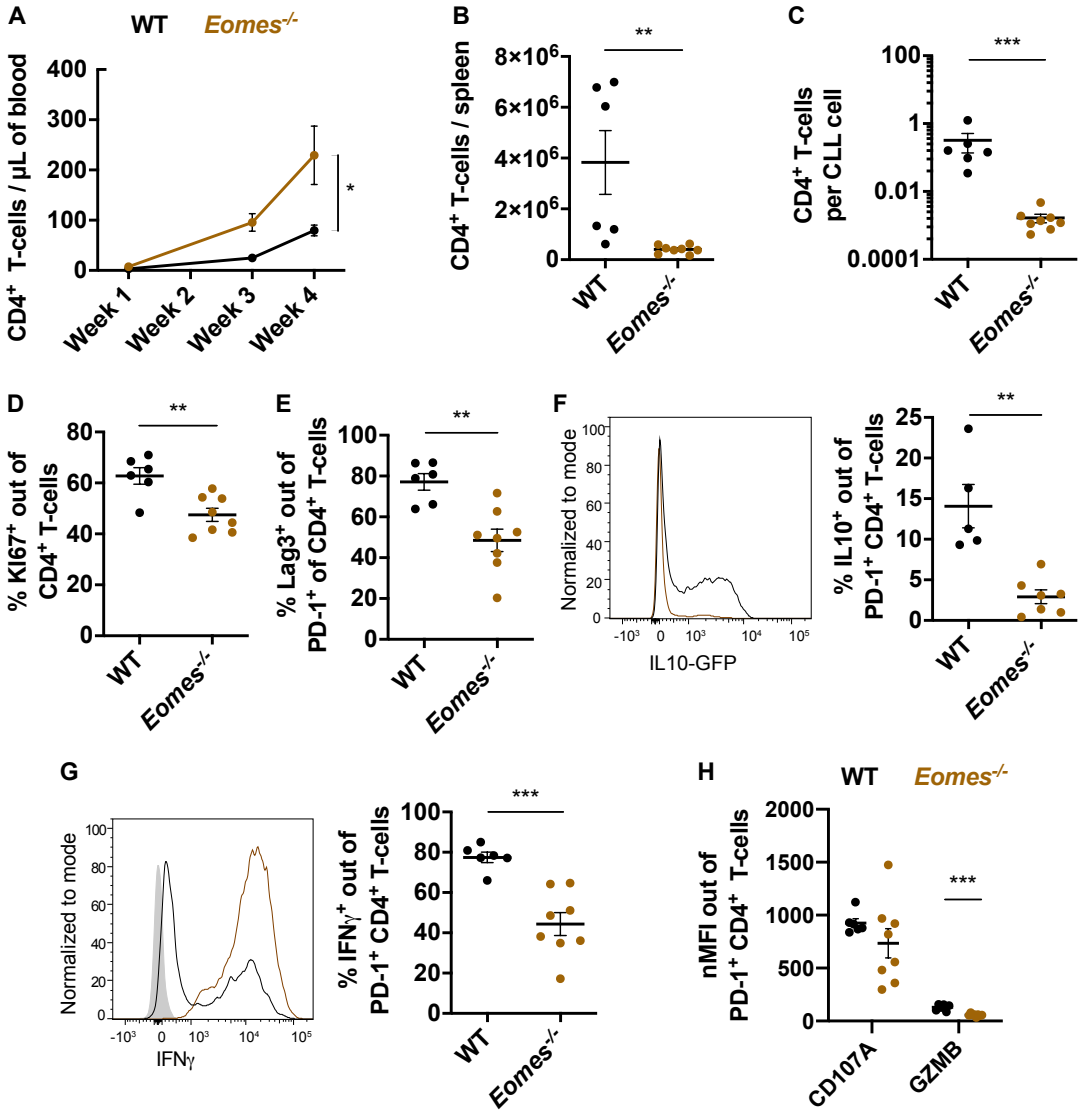

Figure 31: EOMES is necessary for T_R1-mediated tumor control in TCL1 AT mice. (A) Absolute numbers of $CD5^+$ $CD19^+$ CLL cells in PB of *Rag2*$^{-/-}$ mice injected with *Eomes*$^{-/-}$ or WT $CD4^+$ T-cells over time. **(B)** $CD4^+$ T-cell counts per spleen as well as **(C)** per CLL cell at experimental end-point (4 weeks after leukemia injection). **(D)** Fraction of $KI\text{-}67^+$ among $CD4^+$ cells. **(E)** Percentage of $LAG3^+$ cells among $PD\text{-}1^+$ $CD4^+$ T-cells. **(F)** Representative histogram (left panel) and quantification (right graph) of the percentage of IL10-GFP expressing $PD1^+$ $CD4^+$ T-cells. **(G)** Representative histogram (left) and fraction of $IFN\gamma^+$ cells among PD-1 $CD4^+$ T-cells, as well as **(H)** nMFI of CD107A and GZMB among PD-1 $CD4^+$ T-cells after *ex vivo* stimulation with PMA and Ionomycin. Graphs display mean ± SEM and each dot represents one mouse (***p*>0.01, ***>0.001, Mann-Whitney U test).

4.6.4 IL10 receptor is essential for the tumor-control function of T_R1

IL-10 receptor (IL10R) signaling has been shown to be essential for T_R1 function (Brockmann et al. 2017). To investigate the role of IL10R-mediated signaling in T_R1 cells and its impact in CLL control, either *Il10rb*$^{-/-}$ or *Il10rb*$^{+/+}$ $CD4^+$ T-cells were injected into *Rag2*$^{-/-}$ mice prior to TCL1 adoptive transfer. Interestingly, mice injected with *Il10rb*-deficient $CD4^+$ T-cells presented higher CLL counts in PB over time (Figure 32A), as well as at the experimental end-

point in spleen (Figure 32B-C), indicating that *Il10rb*$^{-/-}$ CD4^{+} T-cells control tumor growth less efficiently than their WT counterparts.

To further assess the contribution of CD4^{+} T-cells in the observed decrease of tumor control, T-cell expansion was monitored over time in PB. CD4^{+} T-cell counts were increased in mice injected with *Il10rb*$^{-/-}$ CD4^{+} T-cells compared to those injected with WT CD4^{+} T-cells three and four weeks after tumor transplantation (Figure 33A). A similar trend was observed in spleen at the experimental end point (Figure 33B), possibly due to the bigger spleen size (Figure 32B), as the number of CD4^{+} T-cells per CLL cell was reduced in these mice (Figure 33C). In addition, no significant difference in proliferation of CD4^{+} T-cells was found between the two groups (Figure 33D). Since the proportion of T_R1 cells was significantly higher in mice that had received *Il10rb*-deficient CD4^{+} T-cells (Figure 33E), the effect of IL10R signaling on T_R1 phenotype and effector function was subsequently analyzed. Clustering of FOXP3^{-} CD4^{+} T-cells based on the expression of KI-67, LAG3, PD-1 and EOMES as measured by flow cytometry, revealed phenotypic differences between the EOMES^{+} PD-1^{+} T_R1-like cells of *Il10rb*$^{-/-}$ origin and the WT T_R1 cells (Figure 33F), likely driven by a higher expression of PD-1 (Figure 33G). Moreover, a reduced cytotoxic function of *Il10rb*$^{-/-}$ EOMES^{+} PD-1^{+} CD4^{+} T-cells compared to WT T_R1 cells was identified, as measured by IFNγ, CD107A and GZMB expression upon *ex vivo* stimulation (Figure 33H, I).

Altogether, these results underscore that EOMES is indispensable for the accumulation of tumor-reactive T_R1 cells, whose function, in turn, depends on IL10R signaling for limiting CLL progression.

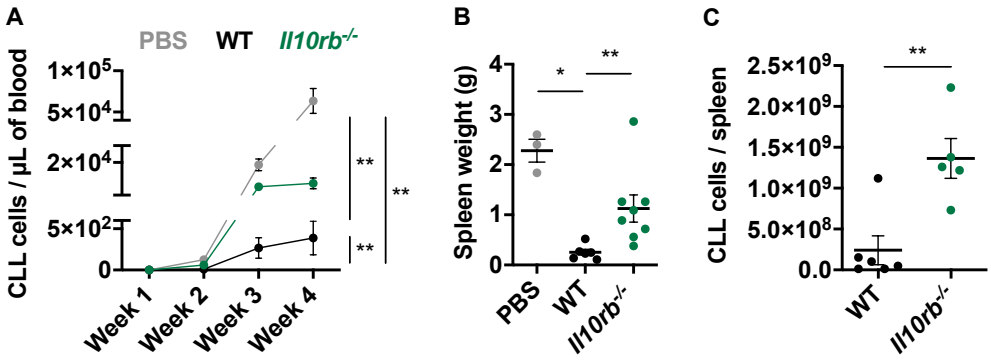

Figure 32: CLL progression is enhanced in *Rag2*$^{-/-}$ mice injected with *Il10rb*$^{-/-}$ CD4^{+} T-cells. *Rag2*$^{-/-}$ mice were injected with WT or *Il10rb*$^{-/-}$ CD4^{+} T-cells or PBS and transplanted with TCL1 leukemia cells the following day. **(A)** CD5^{+} CD19^{+} CLL cell counts over time in PB of *Rag2*$^{-/-}$ mice injected with *Il10rb*$^{-/-}$, WT CD4^{+} T-cells or PBS. **(B)** Spleen weight and **(C)** CLL cell counts in this organ at experimental end-point (4 weeks after leukemia injection). Mean ± SEM is shown, and each dot represents one mouse (*p>0.05, **>0.01, Mann-Whitney U test).

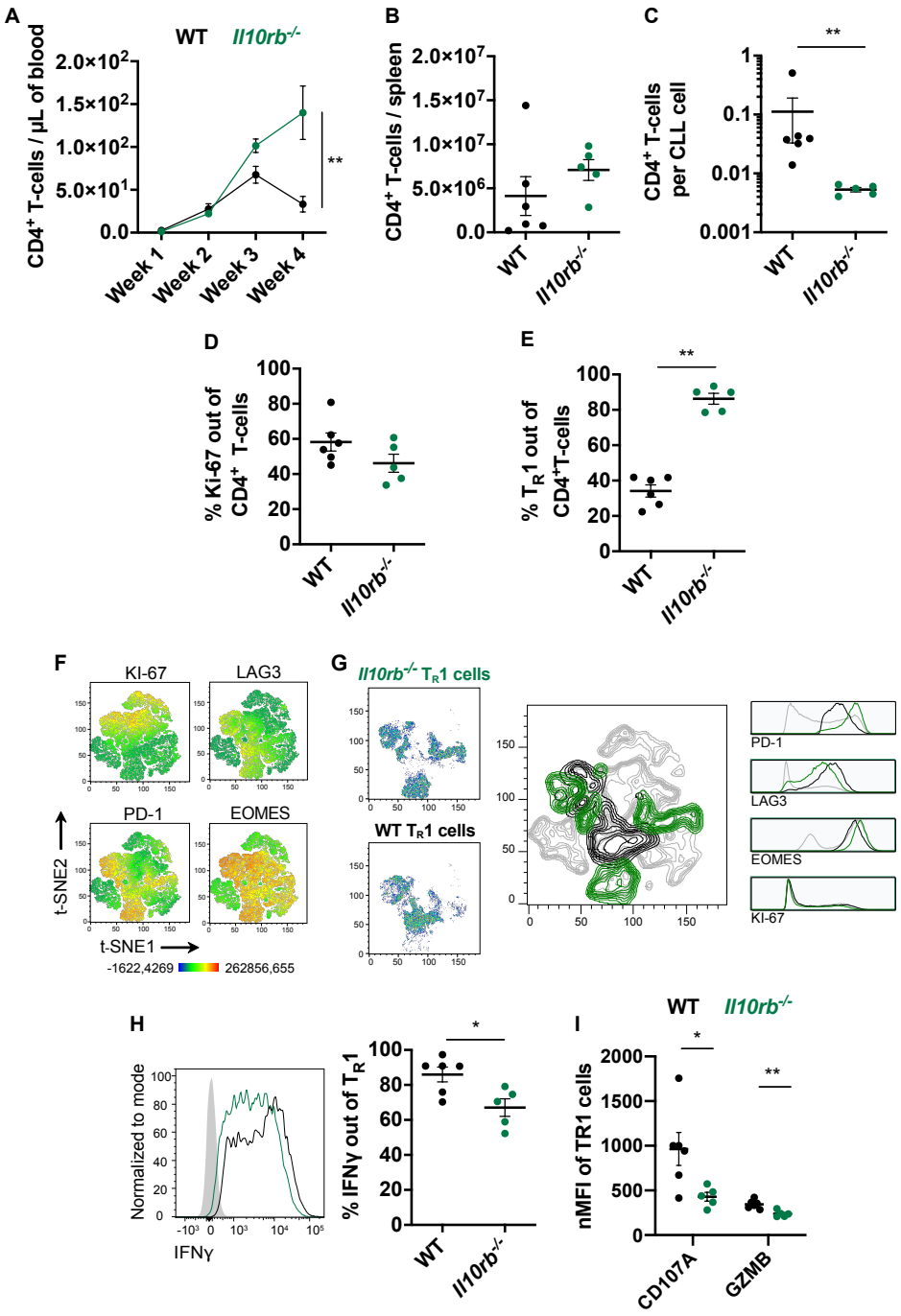

Figure 33: IL10R signaling is essential for T_R1-mediated control of CLL in *Rag2*$^{-/-}$ mice. **(A)** CD4$^+$ T-cell counts over time in PB of *Rag2*$^{-/-}$ mice transplanted with either *Il10rb*$^{-/-}$ (n = 6) or WT (n = 5) CD4$^+$ T-cells. **(B-C)** CD4$^+$ T-cell numbers **(B)** per spleen and **(C)** per CLL cell at experimental end-point (4 weeks after leukemia transplantation). **(D)** Percentage of KI-67$^+$ cells out of CD4$^+$ T-cells. **(E)** Fraction of T_R1 cells out of CD4$^+$ T-cells. **(F)** A t-SNE plot with concatenated WT and *Il10rb*$^{-/-}$ CD4$^+$ T-cells based on the expression of KI-67, LAG3, PD-1 and EOMES was generated. Marker expression for clustered CD4$^+$ T-cells is shown. **(G)** Distribution of *Il10rb*$^{-/-}$ (top left) and WT (bottom left) T_R1 (EOMES$^+$ PD-1$^+$) cells in the t-SNE plot, and highlighted in green and black, over the rest of CD4$^+$ T-cells, in grey (middle plot). Histograms of marker expression in T_R1 cells are shown (right panels). **(H)** Representative histogram (left panel) and percentage (right graph) of IFNγ-expressing T_R1 cells, as well as **(I)** CD107A and GZMB$^+$ cells after *ex vivo* stimulation with PMA and Ionomycin. Mean ± SEM is displayed in all graphs, and each dot represents one mouse (*p<0.05, **<0.01, Mann-Whitney U test).

5 Discussion

Knowledge of CLL-associated changes in the T-cell compartment has rapidly evolved over the last few decades. Even though it is currently clear that CLL development elicits an accumulation of both $CD4^+$ and $CD8^+$ antigen-experienced T-cells (Totterman et al. 1989; Brusa et al. 2013; Hanna et al. 2019), it remains uncertain whether they support CLL-cell survival and proliferation, or instead, control disease progression. In addition, discouraging results obtained in clinical trials using immune checkpoint inhibitors and CAR-T-cell treatments (Porter et al. 2015; Ding et al. 2017) highlight the need for a deeper understanding of the distinct T-cell phenotypes associated with CLL. Finally, further investigation of the T-cells residing in the secondary lymphoid organs, where interactions between leukemic cells and their microenvironment occur, is especially necessary.

To address these unresolved questions, the present work aimed at characterizing the distribution, phenotype, and function of T-cells from CLL patients using single-cell transcriptome and mass cytometry analyses. These data were complemented with studies using the TCL1 mouse model, in order to resolve the role of specific T-cell subsets in CLL.

This work constitutes the first study to examine CLL T-cells at the single-cell level, thereby unraveling the distinct T-cell subsets present in CLL and their differential compartmentalization in lymphoid tissues. Besides, it identifies an EOMES-dependent tumor-control function for both $CD8^+$ T-cells and $CD4^+$ T_R1 cells.

5.1 Single-cell analyses identify the CLL lymph node as a distinct niche where exhausted $CD8^+$ T-cells accumulate

Single-cell technologies have provided valuable insight into T-cell heterogeneity and function in cancer, with the aim to improve immunotherapeutic interventions. While mass cytometry analyses permit an unsupervised clustering of a substantial number of cells based on their protein expression, it requires the *a priori* selection of a limited number of markers, restricting the investigation of cell phenotypes. Conversely, single-cell RNA-seq is a completely unbiased approach, but is currently limited by its high cost, and the reported modest correlation between mRNA transcripts and protein levels (Maier et al. 2009; Schwanhausser et al. 2011). The combinatorial use of both technologies in this work thus allowed a sophisticated and multilevel analysis, while limiting the individual shortcomings of the two techniques. Importantly, the integration of the two methods confirmed that they identify equivalent cell subsets in comparable frequencies, which validates the analyses performed using either approach.

On the one hand, the mass cytometry analyses performed herein allowed to go beyond the investigation of the canonical T_N, T_{CM}, T_{EF} and T_{EM} $CD8^+$ T-cell subsets, as typically done with flow cytometry, and shed light into the degree of heterogeneity present within these cell subtypes. More specifically, two subsets of T_{EF} cells, as well as six T_{EM} subsets were defined, each exhibiting a distinct immunophenotype. In addition, a subset of $CD8^+$ T_{FC} cells, with intermediate levels of both exhaustion and naïve markers was newly identified in CLL LNs. Similar $CXCR5^+$ $CD8^+$ T-cells have been characterized in tonsils, or LN samples from patients with follicular lymphoma, diffuse large B-cell lymphoma, and Hodgkin lymphoma (Tang et al. 2017; Le et al. 2018; Chu et al. 2019); but also as tumor-infiltrating lymphocytes in several solid tumor entities, such as lung, colorectal, and pancreatic cancers (Bai et al. 2017; Brummelman et al. 2018; E et al. 2018). In these contexts, $CD8^+$ T_{FC} cells exert an anti-tumor function via cytokine secretion and direct tumor-cell killing (Bai et al. 2017; Tang et al. 2017; Brummelman et al. 2018; E et al. 2018). Besides, these $CXCR5^+$ $CD8^+$ T-cells harbor stem-like features and have been suggested to be equivalent to the precursor exhausted $TCF7^+$ $PD\text{-}1^{int}$ $CD8^+$ T-cells identified in chronically infected mice (Brummelman et al. 2018). In the present work, however, the absence of effector molecules at the single-cell transcriptome and protein level failed to provide any evidence that the described $CD8^+$ T_{FC} cells kill CLL cells. Instead, the gene expression profile and the cell-cell interaction analyses suggested that they might have functions similar to germinal center-residing $CD4^+$ T_{FH} cells, which promote maturation and proliferation of B-cells via CD40 ligation (Grewal and Flavell 1998; Gaspal et al. 2006; Vinuesa et al. 2016). At the same time, neither the immunophenotypic nor the transcriptomic characteristics of these $CD8^+$ T_{FC} cells provided any indication that they constitute a precursor state of exhausted T-cells.

Intriguingly, the present work described a subset of T-cells that are both $CD4^+$ and $CD8^+$ double positive (DP cells), and express high levels of PD-1 and other exhaustion-related markers. DP cells have been detected in samples of healthy LNs, breast cancer, melanoma, Hodgkin lymphoma, and colorectal cancer (Rahemtullah et al. 2006; Desfrancois et al. 2009; Desfrancois et al. 2010; Sarrabayrouse et al. 2011; Overgaard et al. 2015), but an exhausted-like state as the one herein recognized has not been previously described in these cells.

Finally, the identification of a T_{EM} cluster with an exhaustion phenotype is of particular relevance, given the implication of exhausted T-cells for the success of immunotherapies (Im et al. 2016; Utzschneider et al. 2016; Miller et al. 2019; Siddiqui et al. 2019). Exhausted T-cells are commonly defined by an increased expression of inhibitory receptors and a reduced cytotoxicity (Wherry 2011). The present work does not provide a direct functional assessment of the identified T_{EX} cells, and thus whether they retain effector capabilities remains unclear. Nevertheless, the elevated protein expression of the inhibitory receptors PD-1 and TIGIT, as well as the exhaustion markers CD39, EOMES, and TOX, and the reduced levels of GZMK,

highly resemble the phenotype of T_{EX} cells defined in several tumor entities (Chevrier et al. 2017; Lavin et al. 2017; Bengsch et al. 2018). Interestingly, T_{EM1} and T_{EM2} GZMK$^+$ subsets, which showed intermediate levels of the exhaustion markers and higher GZMK expression, likely correspond to an intermediate functional state, as previously described by inferred developmental trajectories in single-cell studies in melanoma, liver cancer, breast cancer, and non-small-cell lung cancer (Zheng et al. 2017; Guo et al. 2018; Li et al. 2019; Wagner et al. 2019). The application of similar methods to ascertain cell differentiation dynamics would be useful to confirm the relation of T_{EM1} and T_{EM2} GZMK$^+$ subsets with T_{EX} cells.

On the other hand, single-cell RNA-seq analyses of T-cells from CLL LNs determined cell subsets based on their differential gene expression. In general, the transcriptome profile of the identified cell clusters strongly resembled that of subsets described in numerous studies investigating T-cell heterogeneity in various tumor types, where similar marker genes denoted T_N, cytotoxic T-cells, Tregs, follicular T-cells, as well as CD8$^+$ and CD4$^+$ T_{EM} cells (Tirosh et al. 2016; Chung et al. 2017; Puram et al. 2017; Li et al. 2019; Aoki et al. 2020; Kim et al. 2020; Roider et al. 2020). The presence of similar phenotypes therefore suggests that a largely analogous T-cell response is elicited upon tumor growth in solid and hematopoietic cancers (van der Leun et al. 2020).

However, clustering of all cells including CLL cells and both CD4$^+$ and CD8$^+$ T-cells delivered limited information on the different CD8$^+$ T-cell subsets. Thus, further CD8$^+$ T-cell-specific clustering allowed to inspect the transcriptomic differences between these cells. Specifically, CD8$^+$ T_{EM} cells could be divided in several subsets, which differed in the expression of several genes related to cytotoxic function, including granzymes and chemokines, as well as heat-shock proteins. Although a cluster of cells expressing heat-shock proteins has been described in melanoma (Sade-Feldman et al. 2018), an interpretation of its biological relevance should be taken with caution, since heat-shock and stress response gene expression changes could originate from technical artifacts linked to sample preparation (O'Flanagan et al. 2019). Independently of this, differential protein levels of granzymes and other cytokines have been reported in CD8$^+$ T-cells from PB upon antigen recognition (Sandberg et al. 2001; Bade et al. 2005), indicating the existence of CD8$^+$ T-cell subsets with distinct cytotoxic properties. Interestingly, the observation that individual TCR clones were shared by the T_{EM2} CCL4$^+$ and T_{EM4} GZMH$^+$ subsets suggests that these cells are not completely independent of each other, but might constitute cell state transitions. Indeed, the existence of such relationship between T-cell subsets sharing the same TCR sequences has been further supported with trajectory analyses on CD8$^+$ T-cells from non-small-cell lung cancer (Guo et al. 2018). The identification of T_{EM3} GZMK$^+$ cells may, in turn, represent further evidence for the presence of the above-mentioned pre-dysfunctional population in CLL.

Notably, no T_{EM} subset overexpressed inhibitory receptors or other exhaustion-related markers, hampering the definition of a T_{EX} subset. This observation differs from numerous single-cell RNA-seq studies of infiltrating T-cells in solid tumors, in which a subset of T-cells displaying features of exhaustion was described (Tirosh et al. 2016; Zheng et al. 2017; Sade-Feldman et al. 2018; Li et al. 2019). The lack of a specific T_{EX} subset in the present work might be explained by the lower number of cells and samples analyzed, which could have hindered the identification of small cell populations, especially if their phenotype is highly similar to other subsets, like T_{EM3} $GZMK^+$ cells.

In addition to immunophenotyping the $CD8^+$ T-cells from PB, BM and LNs of CLL patients, the analysis of the cell subset distribution revealed significant differences between the three compartments, underlining the effect of the tissue environment on the diversity of T-cell states. PB samples contained increased frequencies of T_{EF2} $TBET^+$ and T_{EM3} $KLRG1^+$ $TBET^+$ subsets, in line with a reported expansion of TBET-expressing effector $CD8^+$ T-cells in blood versus LNs of CLL patients (Riches et al. 2013; de Weerdt et al. 2019; Hanna et al. 2019). Intriguingly, BM tissue composition resembled that of PB rather than LN. This observation together with the previously described lower CLL cell proliferation rate in this tissue suggests that BM is not a central location for leukemia development and interactions between malignant B-cells and their TME (van Gent et al. 2008; Herndon et al. 2017). Nevertheless, a contamination of T-cells from PB during biopsy acquisition, which would mask the real BM composition, cannot be excluded, and thus future experiments should validate these observations.

Interestingly, the unique presence of several T-cell subsets in LNs defined this tissue as a distinct niche. On the one hand, $CD8^+$ T_{FC} and T_{EM4} $ICOS^+$ were found in higher percentages in LNs, in accordance with their physiological function in the formation and maintenance of GCs in SLOs (Crotty 2011; Wikenheiser and Stumhofer 2016). On the other hand, earlier studies have described an enrichment of T_{EM} cells in LN compared to PB of CLL patients, as well as an increased percentage of PD-1-expressing cells (de Weerdt et al. 2019; Hanna et al. 2019). Importantly, the results of the present work confirm and further expand on these observations, reporting higher frequencies of T_{EM2} $GZMK^+$, T_{EX}, and proliferating cells in LNs. Given the increased interactions occurring between CLL cells and their surrounding cells in LNs compared to PB (Herishanu et al. 2011; Pasikowska et al. 2016; Herndon et al. 2017), it is tempting to speculate that the LN niche facilitates chronic TCR stimulation by constant antigen exposure and persistence of inflammatory signals, thereby contributing to T-cell exhaustion (Wherry 2011). Overall, the divergence between the two tissues, and specially the accumulation of T_{EX} cells in LNs, which is poorly reflected in PB, highlights that biomarkers based on blood T-cells might not accurately reflect the LN T-cell composition. Thus, further

evaluation of T-cell phenotypic characteristics particularly in this tissue is needed in order to better understand the functional role of the diverse T-cell subsets in leukemia progression.

Finally, one fascinating observation was made upon association of $CD8^+$ T-cell subset frequencies with clinical factors: different percentages of $CD8^+$ T_{EM4} $ICOS^+$ cells were found between *IGHV*-mutated and unmutated patients. Importantly, an analogous $CD4^+$ T_{EM} $ICOS^+$ population identified upon $CD4^+$ T-cell investigation, was likewise enriched in *IGHV*-mutated compared to unmutated CLL patients (data not shown, described by Paul, 2020), suggesting that ICOS expression in T-cells is linked to *IGHV* mutational status in CLL. ICOS is a member of the immunoglobulin family of co-receptor molecules that is rapidly induced upon TCR activation (Hutloff et al. 1999; Yoshinaga et al. 1999; McAdam et al. 2000) and has been described to play a co-stimulatory function in T-cell adaptive immunity (Arimura et al. 2002). In addition, it has also been linked with the generation of class-switched antibodies and germinal center reaction when binding to ICOSL in APCs (Yoshinaga et al. 2000; Hu et al. 2011). Given the aforementioned function, it is tempting to speculate that the distinctive presence of ICOS-expressing T-cells in *IGHV*-mutated and unmutated cases might be linked to the proposed different cellular origin of CLL cells (Seifert et al. 2012). Accordingly, post-GC *IGHV*-mutated CLL cells might promote the accumulation of $ICOS^+$ T-cells, whereas pre-GC *IGHV*-unmutated ones would not. Future studies should focus on understanding the role of $ICOS^+$ T-cells in the TME niche in CLL, including additional experimental validation of these results with a larger patient cohort.

5.2 CLL elicits a tumor-specific $CD8^+$ T-cell response

It has been extensively described that increased numbers of antigen-experienced $CD8^+$ T-cells are found in patients with CLL in comparison to healthy individuals (Nunes et al. 2012; Brusa et al. 2013; Gothert et al. 2013; Riches et al. 2013; Palma et al. 2017). However, the question whether these cells are bystanders that accumulate as a consequence of tumor-related microenvironmental changes, or whether they recognize and react against CLL cells is still under debate. In addition, because SLOs are also the site of effector T-cell accumulation during infections, leukemia-associated alterations can be masked by co-occurring immune responses against pathogens. Infections are, in fact, especially prevalent in CLL patients, in which leukemia-induced immunosuppression often leads to reactivation of EBV or CMV infections (Riches and Gribben 2013; Forconi and Moss 2015; Garcia-Barchino et al. 2018). Partly addressing this question, studies have reported an association between $CD8^+$ T-cell numbers and tumor load (Catovsky et al. 1974; Totterman et al. 1989; Hanna et al. 2019), and the $CD8^+$ T-cell per CLL-cell ratio has been linked to improved overall survival of CLL patients (Gonzalez-Rodriguez et al. 2010). In addition, Kowalewski et al. identified CLL-specific

antigens and demonstrated that a T-cell immune recognition of tumor cells occurred only in patients and not in healthy controls, and that the patients displaying such immune responses had, in turn, a survival benefit (Kowalewski et al. 2015). With these observations, the hypothesis that $CD8^+$ T-cells react against malignant cells has been increasingly gaining attention. However, most of these studies have only investigated cells isolated from PB, and have not compared T-cell phenotypes between CLL and tumor-free LN samples. The present work provides four novel layers of evidence that further support a leukemia-directed T-cell immune response.

First, changes in subset frequencies distinguished CLL LNs from rLNs of cancer-free donors, emphasizing the existence of specific CLL-associated changes in the T-cell compartment. More precisely, the decreased percentage of T_N cells in CLL LNs largely contributed to the separation of CLL from control samples. In addition, one of the central findings of this work is that exhausted T-cells accumulate in CLL LNs compared to healthy controls, as observed by the increased frequency of T_{EX} $CD39^+$ and proliferating cells, together with a tendency of higher T_{EM2} $GZMK^+$ numbers in patient samples. This observation would not only support the idea of the accumulation of tumor-reactive T-cells but also confirm the existence of a dysfunctional T-cell subset induced by CLL cells. In fact, CD39 has recently been described to be present on tumor antigen-specific T-cells but absent on virus-specific ones across several tumor entities, suggesting CD39 as a surrogate marker for exhausted, tumor-reactive T-cells (Canale et al. 2018; Duhen et al. 2018; Simoni et al. 2018).

Second, the association of T-cell phenotypes with the clinical parameters of patients revealed that T_{EM1} subset frequencies in LNs positively correlated with TL, while at the same time, the number of T_N cells decreased with higher TL percentages. These correlations suggest that with increasing leukemia cell amounts, higher numbers of T_N cells get activated upon antigen recognition and acquire a T_{EM} phenotype. Similar associations have been described in blood of CLL patients (Palma et al. 2017; Hanna et al. 2019), which indicates that the on-going anti-tumor reactivity from the LNs is partly reflected in the periphery.

This idea is supported by the third layer of evidence: the investigation of TCR sequences at the single-cell level showed that clonally expanded T-cells predominantly consisted of $CD8^+$ T_{EM} cells. In line with this, an increased T-cell oligoclonality in the blood of CLL patients compared to healthy controls has previously been reported based on bulk RNA-seq of the TCR beta chain (Serrano et al. 1997; Vardi et al. 2017; Blanco et al. 2018). Even though T-cell clonality alone cannot be used as a proxy for tumor-reactivity, as evidenced by the presence of virus-specific TCRs, the identification of a T-cell clone recognizing the CLL-overexpressed BST2 protein in this study further reinforces these findings (Gong et al. 2015; Bagaev et al. 2020).

Fourth, the use of the TCL1 AT mouse model showed that lack of $CD8^+$ T-cell expansion due to a lack of EOMES led to a significantly enhanced leukemia development, underlining that $CD8^+$ T-cells exert some control of CLL growth. The available evidence for the role of EOMES in regulating $CD8^+$ T-cell activation and exhaustion is further discussed in Section 5.5.

Altogether, the results obtained in this study indicate that the accumulation of $CD8^+$ T_{EM} cells in CLL does not result from unspecific stimulatory cues present in the CLL microenvironment, but occurs as a consequence of an antigen-specific recognition of leukemia cells.

Following the consideration of the enrichment of T_{EX} as well as the correlation of T_{EM} cells with tumor load in CLL LNs, the questions arise whether a developmental relationship between antigen-experienced T_{EM} and T_{EX} cells exists, and which factors underlay T-cell exhaustion in CLL. As discussed earlier, the investigation of state differentiation trajectories using single-cell data as well as *in vivo* validation would help resolve the former. Because frequencies of T_{EX} cells were not directly associated with TL, additional factors to tumor antigen load likely determine the differentiation and accumulation of T_{EX} cells. Similar to what has been described in chronic viral infections, secreted factors like IL-10, TGF-β, and type I IFNs (Brooks et al. 2006; Ejrnaes et al. 2006; Tinoco et al. 2009; Teijaro et al. 2013; Wilson et al. 2013), or the TCR stimulation strength (Blattman et al. 2009; Martinez-Usatorre et al. 2018), might also regulate T-cell exhaustion in CLL. In addition, whether the accumulation of T_{EX} cells has a clinical impact remains to be elucidated. Even though no direct correlation between T_{EX} cells and clinical outcome could be established in this work, an implication of these cells in disease development should not be excluded. Along this line, studies with larger patient cohorts have found higher levels of $PD\text{-}1^+$ antigen-experienced T-cells in blood of progressive CLL patients (Palma et al. 2017), and patients with a more advanced disease stage presented increased levels of terminally differentiated $CD8^+$ T-cells (Brusa et al. 2013). Because tumor-reactive T_{EX} cells are promising targets for immunotherapy, follow-up experiments with larger patient cohorts should elucidate the origin and functional role of T_{EX} cells in LNs of CLL patients. Ultimately, a better understanding of the transcriptomic and functional characteristics of tumor-reactive T-cells will significantly aid in improving existing and novel immunotherapy approaches for CLL.

Finally, it is important to underline that there are some limitations to the results obtained using single-cell analyses in this work. First, the comparison performed between CLL and healthy control groups bears a sample collection bias. On the one hand, even though rLN are classified as tumor-free, dissections of these tissues are performed in case of persistent LN enlargement, which might occur due to an acute inflammation (Slack 2016; Tzankov and

Dirnhofer 2018). Such condition likely impacts the T-cell subset composition and therefore these samples do not accurately represent a LN of a healthy individual. As an example, the increased percentages of T_{EF1} $CD27^+$ an DP_1 T_{EX} $CXCR5^+$ in rLNs in comparison to CLL LNs may be a consequence of an on-going immune response (Hendriks et al. 2000; Kitchen et al. 2004; Nascimbeni et al. 2004). Consequently, some additional CLL-induced changes which also occur during acute infections could remain undetected. On the other hand, LN biopsies from CLL patients are not routinely performed, but only obtained to examine cases with lymphadenopathy, or when the progression into a lymphoma is suspected. Therefore, the phenotypical characterization herein identified might only represent a fraction of CLL patients whit enlarged LNs.

Second, a significant difference in the average age between HC and CLL samples exists in the studied cohort, representing a confounding factor in the comparison of these two groups. Although a contribution of age in all subset frequency differences cannot be completely excluded, the association between these two factors suggests that only the differences observed in T_{EX} and T_N subsets might be directly influenced by age. Shrinkage of the naïve T-cell compartment as a consequence of aging has been widely described (Goronzy et al. 2015), making it difficult to distinguish between the contributions of disease state and age. Instead, T_{EX} cell percentages do not increase along with age in HC donors, and CLL patients of older age display a wide range of T_{EX} percentages, which suggests that leukemia development might determine, in part, the accumulation of these cells. A future analysis of the T-cell phenotype differences between CLL LNs and HC avoiding an age bias should therefore confirm the reported observations.

Third, even though single-cell technologies are becoming standard laboratory methodologies, technical as well as analysis-related challenges may still affect the quality of the generated data. In general, factors that influence data quality in single-cell studies include the cell isolation procedure, the number of cells analyzed, the transcript capture efficiency, the doublet cell rate, and the sequencing depth (Lahnemann et al. 2020). At the computational level, regardless of the technology used, bioinformatic processing, including dimensionality reduction and cell clustering, requires the selection of various parameters (e.g. clustering resolution) which may also impact the results and the interpretation of the data. As only vague guidelines for these metrics exist to date, the range of results that can be obtained remains excessive (Kiselev et al. 2019). In the present work, an optimized experimental processing of the samples and a sequencing coverage saturation minimized technical noise. However, the analysis of only three samples via single-cell RNA-seq likely limited both the identification of all existing T-cell states in CLL patients and the significance of the described clusters. At the same time, the relatively small number of cells examined likely prevented the discovery of minor T-cell subpopulations present in the CLL LNs (Szabo et al. 2019; Le et al. 2020).

Regarding the mass cytometry dataset, even though it provided a good general impression of the CLL-associated T-cell changes, its small sample size restricted the statistical power of the downstream analyses. With respect to the bioinformatic analyses, despite following various approaches to define the true dimensionality and number of clusters for the two datasets (Butler et al. 2018; Stuart et al. 2019), the determined number of cell subsets likely does not represent the biological ground truth. Ultimately, whether the herein described subsets precisely reflect existing T-cell types – with the definition of a cell type being an interesting question by itself – will require the generation of larger single-cell datasets and additional functional assays.

5.3 The cellular crosstalk between CLL cells and T-cells in the LN niche is composed of both stimulatory and inhibitory signals

CLL cells essentially depend on their microenvironment in the SLOs for receiving pro-survival and proliferation signals from neighboring cells (Burger 2011). Through microenvironmental interactions, LN-resident CLL cells upregulate gene sets of the NF-κB pathway, resulting in increased anti-apoptotic signaling (Herishanu et al. 2011) and protection from chemotherapeutical agents (Vogler et al. 2009). Upon these observations, there has been an intense effort to characterize the interactions responsible for the transcriptional changes in CLL cells, in order to modulate them and thus achieve the complete eradication of malignant cells. However, up until now, most studies used bulk transcriptomic approaches, as well as *in vitro* co-culturing systems, utilizing cells isolated form PB (Burger et al. 2000; Vogler et al. 2009; Herishanu et al. 2011; Pascutti et al. 2013). Under these conditions, the complexity of the microenvironmental connections is likely underestimated, and the contribution from specific cells residing in the LNs cannot be recognized. Hence, single-cell transcriptome analyses represent a valuable tool for assessing the cross-talk between CLL cells and T-cell subsets, where not only the signals regulating leukemia cell growth, but also those modulating T-cell function can be identified.

The data obtained in this work provide a first account of the specific cellular interactions that are likely established between T-cells and CLL cells in the LNs. As normal B-cells depend on signals from follicular helper T-cells in germinal centers (Qi 2016; Vinuesa et al. 2016), CLL cells similarly benefit from these interactions, including the above-mentioned pro-survival signals from CD40- CD40L binding (Kitada et al. 1999; Pascutti et al. 2013). Crucially, the performed single-cell analyses elucidated that all $CD4^+$ subsets, aside of T_{FH} cells, provide pro-survival signals to CLL cells by expressing CD40L. Furthermore, these subsets appeared to establish additional interactions with CLL cells, such as CD28 binding to CD86, IL-2 secretion, as well as TRAILR binding to TRAIL, the signaling of which have been shown to stimulate leukemia cells (Suvas et al. 2002; Secchiero et al. 2005; Rau et al. 2009; Decker et al. 2010).

Tregs additionally interacted with CLL cells via SELL- SELPLG, which has been reported to promote malignant B-cell adhesion (Csanaky et al. 1994). Importantly, $CD8^+$ T_{EM} and T_{TOX} cells expressed CD28, and secreted TNFα and INFγ, while CLL cells expressed the respective receptors for these molecules. With this finding, the idea of $CD8^+$ T-cells exerting only an anti-tumoral function is confronted by the fact that these interactions have been shown to promote survival and proliferation on CLL cells (Buschle et al. 1993; Reittie et al. 1996). Simultaneously, the cell subsets inducing CLL cell survival and proliferation could provide apoptotic signals via LAIR1-LILRB4 and SIRPG- CD47 interactions, a mechanism suggested to be involved in restraining tumor growth in long-term non-progressing patients (Martinez-Torres et al. 2015; Zurli et al. 2017).

In addition to the identification of the signals affecting CLL cells, this analysis was able to describe the mechanisms by which CLL cells modulate their microenvironment, evading immune surveillance by inhibitory signal induction on T-cells. For example, CLL cells interacted with $CD4^+$ T_{EM} via LILRB4- LAIR1, and with T_{TOX} cells by galectin-9 binding to TIM-3, the signaling of which have been shown to inhibit T-cell effector function (Meyaard et al. 1997; Das et al. 2017).

Altogether, these observations illustrate the existence of an intricate network of stimulatory and inhibitory signals established between T-cells and CLL cells. The single-cell component of this approach, in addition, helps to discriminate at cell-subset level the specificity of these interactions, and underscores the difficulties of classifying T-cells as strictly pro- or anti-tumoral. A significant limitation of the present analysis, however, is that the ligands and receptors expressed in a general or cell subset-unspecific manner were not further investigated, but could still significantly impact the signalome of leukemic cells and surrounding T-cells. Moreover, it remains unclear whether the interactions that were identified play a determinant role in disease progression. Future work should thus focus on analyzing the complete CLL interactome, including interactions established between all cell subsets present in the tissue, and should compare the cross-talk established between cells in LNs from CLL patients to that found in healthy lymph nodes. Such approach would undoubtedly facilitate the identification of signals that are specific to or increased during leukemia development. The use of imaging-based spatial single-cell technologies at the protein level (Giesen et al. 2014) would for example prove the specificity as well as relevance of the identified interactions, which could ultimately be tested experimentally in mouse models. The knowledge acquired with these studies could be central for the identification of new therapeutic targets for CLL and significantly improve the response to existing therapies.

5.4 The suitability and limitations of the TCL1 AT mouse model of CLL

Since its generation almost 20 years ago (Bichi et al. 2002), the Eμ-TCL1 mouse model has contributed substantially to the characterization of CLL pathogenic mechanisms as well as the development and testing of novel therapeutic approaches (Bresin et al. 2016). Notably, previous research reported evidence that the fully immunocompetent mouse line and the adoptive transfer model recapitulate the complex TME in the different organs and thus represent a valuable tool for investigating the leukemia-associated niche. For example, with the aim of comparing the tumor-induced T-cell defects between the Eμ-TCL1 mouse model and CLL patients, Gorgun et al. using bulk RNA microarrays observed that the gene-expression patterns in splenic $CD4^+$ and $CD8^+$ T-cells of leukemic mice highly resembled those from respective cells in PB of CLL patients (Gorgun et al. 2009). Succeeding efforts by other groups identified in the murine model a marked T-cell subset skewing from naïve to antigen experienced cells, and a CLL-induced exhausted phenotype, analogous to human CLL (Hofbauer et al. 2011; Gassner et al. 2015; McClanahan et al. 2015a; McClanahan et al. 2015b; Wierz et al. 2018; Hanna et al. 2019). Adding to this knowledge, the results obtained in this work describe at the single-cell level the acquired phenotypes of splenic T-cells from end-stage diseased TCL1 AT mice, thereby detailing the similarities and disparities between the mouse model and CLL patients. Importantly, clustering of murine T-cells based on their transcriptomic profile identified an overall T-cell phenotype comparable to LN-derived T-cells from CLL patients: murine T-cells were constituted by a high percentage of naïve cells, and subsets of effector and memory cells, as well as Tregs. Conversely, cell subsets containing $CD4^+$ and $CD8^+$ T-cells in a proliferating and exhausted state were exclusively identified in the murine samples. In line with the above-mentioned reports, the presence of these cells in the murine model provide further evidence for the existence of these cells in CLL.

Additionally, the identification of a subset of T-cells with a distinct transcriptomic profile induced by IFN type I signaling is intriguing and poses several fascinating questions about their origin and role in the CLL TME. A similar type I IFN-driven $CD4^+$ T-cell population has been identified in single-cell studies of different tumors and of allergy, in both human and mouse, suggesting that these cells can be generally induced by tissue inflammation (Magen et al. 2019; Szabo et al. 2019; Tibbitt et al. 2019). On the one hand, Szabo et al. proposed that type I IFN-responding cells represent a TCR-induced early activation state of $CD4^+$ T-cells prior to initiation of proliferation (Szabo et al. 2019). Instead, another study found these cells to be at the end of the inferred differentiation path (Magen et al. 2019), thus leaving the question of their origin unanswered. Regarding their function, type I IFN signaling has been linked to cancer immunosurveillance by increasing *PRF1* and *GZMB* gene expression, and promoting cell survival of cytotoxic T lymphocytes (Curtsinger et al. 2005; Guillot et al. 2005;

Ilander et al. 2014). Despite this, IFNα administration to pre-treated CLL patients did not have any effect on progression-free survival or $CD4^+$ T-cell counts (O'Brien et al. 1995). Additional studies will be therefore necessary to confirm the presence of this subset in patients and to assess its role in CLL.

In contrast, follicular T-cells including both $CD8^+$ T_{FC} and $CD4^+$ T_{FH}, which were readily distinguished in LNs of CLL patients with a very distinct transcriptomic profile, were not detected in spleen of TCL1 AT mice. The fact that these cells were not recognized in murine samples might be due to the low number of cells and samples analyzed, and thus additional samples should be examined to exclude this possibility. Additionally, $CD4^+$ T_{FH} cells and $CD8^+$ $CXCR5^+$ cells have previously been detected in LNs and spleen of mice (Im et al. 2016; Miles et al. 2016; Yu and Ye 2018; Magen et al. 2019), and therefore, a complete absence of these cells in the spleen of TCL1 mice seems unlikely. Because research of $CD8^+$ T_{FC} cells is scarce in CLL patients, and given their described role in anti-tumor immunity in other cancers, the identification and subsequent characterization of these cells in mouse will be of great importance for determining their pro- or anti-tumor role in CLL.

Further contributing to the hypothesis of a tumor-specific T-cell reaction in CLL, an enrichment of clonally expanded $CD4^+$ and $CD8^+$ T-cells has previously been observed in TCL1 mice (Hofbauer et al. 2011; Hanna et al. 2019), similar to what was described for patients (Vardi et al. 2017; Blanco et al. 2018). For $CD8^+$ T-cells, this enrichment was shown to be specific to effector cells (Hanna et al. 2019). In line with this, the evaluation of T-cell clonality based on the single-cell data obtained herein revealed that the clonal expansion of murine $CD8^+$ T-cells is restricted to T_{EX} cells. Strikingly, however, the complete picture of the clonal status of all T-cell subtypes in the TCL1 AT mouse model underscored that clonally expanded T-cells were predominantly $CD4^+$ T-cells, in sharp contrast to human LNs, where $CD8^+$ T-cells represented the clonally expanded fraction. While this observation should be taken with caution, as it is based on the analysis of only two murine samples, such a disparity raises important questions about the suitability of the mouse model to precisely recapitulate the T-cell immune response of CLL patients. Hence, it will be crucial to validate these observations with the analysis of additional samples.

Interestingly, T-cell expansion clearly occurred to a greater extent in one of the analyzed mouse samples versus the other, despite the fact that both mice were transplanted with CLL cells from the same donor mouse and had a similar tumor load at time of sampling. This disparate response could derive from the heterogeneous CLL clone dynamics occurring in the mouse model (Zaborsky et al. 2019), with some tumor clones eliciting a stronger immune reaction compared to others (McGranahan et al. 2016).

Last, and most importantly, the cellular interactions found in the CLL TME of the TCL1 AT mouse model largely resembled those of the CLL LNs. Both CLL-supportive and inhibitory signals were found to be present in the respective murine subsets, mainly $CD4^+$ T-cells, but also T_{IFN}, T_{EX}, and $CD8^+$ T_M cells. In addition, inhibitory signals for T-cells, including CD39-ADORA2A and PD-1- PD-L1 and PD-L2, could be observed in the mouse data set, which is in line with a previously described improvement of leukemia immune control when blocking these interactions (McClanahan et al. 2015a; Arruga et al. 2020).

The additional presence of myeloid cells highlights the role of these cells in providing support to CLL cells, as they expressed multiple signals including ligands that bind to integrins and semaphorins in CLL cells, which have been shown to promote proliferation and survival of malignant B-cells (Vincent et al. 1996; Granziero et al. 2003; Deaglio et al. 2005). At the same time, these cells also aggravate T-cell inhibition by expressing PD-L1 and ADORA2A (data not shown, (Hanna et al. 2016). Given these observations, it would be interesting to examine the interactome of the complete CLL TME in order to identify the most prominent interactions promoting both leukemia cell survival and T-cell exhaustion.

Overall, the analysis performed here underlines that the T-cell distribution and phenotype in the TCL1 mouse model largely recapitulates the pathogenic situation in CLL patients, and thus represents an effective tool for the study of the functional role of T-cells in CLL progression.

5.5 EOMES is necessary for $CD8^+$ T-cell expansion and control of CLL development

As previously mentioned, CLL has a strong component of heritability, with an approximately 8.5-fold increased risk for first-degree relatives of CLL patients (Goldin et al. 2009). Among numerous genetic alterations, genome-wide association studies have identified several SNPs increasing susceptibility to CLL (Berndt et al. 2013; Berndt et al. 2016). One of these, rs9880772, is located in close proximity to the *EOMES* gene and, based on their H3K27ac profiles, appears to be in a heterochromatic region in CLL cells (Speedy et al. 2019). The examination of the chromatin state based on six histone modifications (H3K4me3, H3K4me1, H3K27ac, H3K36me3, H3K27me3, and H3K9me3) of several B-cell subsets in this work corroborated this observation. Adding further evidence, both bulk RNA and single-cell RNA-seq identified no *EOMES* transcript in B-cell subsets and CLL cells, respectively. Altogether, these observations point towards the exciting possibility that the abovementioned *EOMES* SNP might be related to CLL pathogenesis through its expression in cells from the TME rather than in the neoplastic cell itself. In other words, the *EOMES* SNP could lead to an inferior capacity of microenvironmental cells to control malignant B-cells. Following this idea, the rs9880772 genotype was obtained for 14 LN samples analyzed by mass cytometry. However,

risk allele frequency was too low (1 out of 14) to statistically assess the relationship with EOMES protein levels (See Supplementary Section 6.1). Of note, the odds-ratio of this SNP is only 1.17 (Berndt et al. 2013), and accordingly, a dramatic effect on *EOMES* expression or function cannot be expected. Ultimately, the exact effect of rs9880772 in *EOMES* remains unanswered, and would need to be assessed in a sufficiently large cohort of CLL patients.

Confirming that *EOMES* is expressed in cells of the tumor microenvironment, memory $CD8^+$ T-cell, as well as NK cells, exhibited open chromatin at the *EOMES* locus, and correspondingly, expression of the gene. Importantly, the single-cell RNA sequencing analysis of CLL LNs showed that *EOMES* is expressed in $CD8^+$ T_{EM1} cells but also in the $CD4^+$ T_{EM1}, T_{TOX}, and T_F cells, the identification of which would have otherwise been missed with the bulk microarray data. Hence, a SNP-driven effect on CLL control through all these cells is possible. While the role of EOMES in $CD8^+$ and $CD4^+$ T-cells has been investigated in the present work, its function in NK cells in the CLL context has not been addressed. Given that EOMES regulates NK cell proliferation and effector function (Gordon et al. 2012; Daussy et al. 2014; Zhang et al. 2018a), the *EOMES* SNP is likely to also affect these cells, and thus this question should be addressed in future studies.

EOMES regulates the transcriptional program that promotes $CD8^+$ T-cell effector cytolytic differentiation, and maintains memory T-cell homeostasis by regulating *IL-2RB* expression (Intlekofer et al. 2008; Cruz-Guilloty et al. 2009; Banerjee et al. 2010; Pipkin et al. 2010). Besides, its expression has been reported highest in exhausted T-cells in several tumors, including colorectal cancer, melanoma, non-small cell lung cancer and acute myeloid leukemia (O'Brien et al. 1995; Sade-Feldman et al. 2018; Zhang et al. 2018b; Jia et al. 2019; Li et al. 2019). Accordingly, EOMES protein levels were detected in all T_{EF}, T_{EM} subsets in mass cytometry analyses and its expression was highest in T_{EX} and proliferating cells. Thus, the higher EOMES levels in CLL LN samples compared to rLN are unsurprising, given the significantly higher frequency of T_{EX} and proliferating cells in CLL patients. In addition, these results were mirrored in the Eμ-TCL1 and TCL1 AT mouse models, where leukemic mice showed higher frequencies of $EOMES^+$ $CD8^+$ T-cells compared to WT mice. Such difference is a result of a disease-driven T-cell skewing towards effector and memory T-cells. Notably, the discrepancy in subset frequencies and consequently EOMES levels between the two mouse models can likely be explained by the dynamics of the disease development. Eμ-TCL1 mice develop a CLL-like disease over the duration of one year and thus pronounced T_M changes may result from acquired memory to some tumor clones (Landau et al. 2013). Conversely, a more acute immune reaction against CLL cells might be present in the TCL1 AT model. Importantly, higher expression of EOMES in exhausted T-cells was demonstrated with both single-cell RNA-seq and flow cytometric analyses in both mouse models, in agreement with the expression pattern observed in human T-cells.

Crucially, the presented data show that EOMES-deficiency leads to an impaired $CD8^+$ T-cell proliferation and, consequently, to faster CLL development, providing evidence for a $CD8^+$ T-cell-mediated control of CLL. These results are in agreement with a previous study showing that constitutive expression of EOMES enhances $CD8^+$ T-cell expansion and survival, thereby improving tumor control in a mouse model of lymphoma (Furusawa et al. 2018). Instead, no significant impact of EOMES on the differentiation or functional capacity of $CD8^+$ T-cells was observed in the TCL1 AT mice, diverging from the described involvement of EOMES in regulating the expression of effector molecules such as perforin, granzyme B and IFNγ, as well as memory formation (Intlekofer et al. 2008; Cruz-Guilloty et al. 2009; Banerjee et al. 2010; Pipkin et al. 2010). It is important to keep in mind, however, that EOMES plays distinct roles under acute and chronic inflammatory conditions. On the one hand, the above-mentioned function in promoting the expression of effector genes is explained under an acute immune response to viral infection. On the other hand, EOMES has been suggested to induce a specific distinct set of genes associated with T-cell exhaustion in chronic viral infection (Doering et al. 2012). In this context, depletion of EOMES in CMV-reacting $CD8^+$ T-cells leads to a decreased exhaustion phenotype, including lower expression of PD-1, and increased levels of TNFα^+ IFNγ^+ cells (Paley et al. 2012). In cancer, Li et al. reported that tumor-infiltrating lymphocytes lacking *Eomes* fail to expand and produce effector molecules, but also express lower levels of the inhibitory receptors PD-1 and TIM-3 (Li et al. 2018). Further complicating the situation, this disparity might partly be due to the overlapping function of EOMES with the phylogenetically-related TF TBET (encoded by *TBX21*), which has been described to induce expression of effector molecules during acute infections in a similar manner as EOMES (Intlekofer et al. 2005; Intlekofer et al. 2008), but does not induce an exhausted phenotype under chronic viral infections (Kao et al. 2011). Hence, the interplay of several factors likely masks the specific role of EOMES in controlling T-cell effector function and exhaustion in the CLL mouse model. Additional studies will be necessary to elucidate the specific conditions under which this TF contributes to the acquisition of a cytotoxic or dysfunctional state of $CD8^+$ T-cells. For example, the employment of single-cell ATAC-seq and ChIP-seq techniques will significantly aid in unraveling the gene regulatory network of EOMES at every T-cell differentiation state (Grosselin et al. 2019; Satpathy et al. 2019).

5.6 T_R1 cells control CLL progression and are regulated by EOMES and IL10R signaling

As discussed above, the single-cell RNA-seq analyses performed in this work revealed that *EOMES* is expressed in $CD4^+$ T-cell subsets, thus indicating that these cells could also be functionally affected by the rs9880772 SNP. In fact, EOMES promotes the development of $CD4^+$ T_R1 cells (Zhang et al. 2017; Gruarin et al. 2019), a cell subset with potent

immunosuppressive properties (Roncarolo et al. 1988; Bacchetta et al. 1994; Groux et al. 1997). In a collaborative effort with Dr. Yashna Paul, the characterization of the $CD4^+$ T-cell compartment in both single-cell RNA-seq and mass cytometry data sets of CLL LNs identified a subset resembling T_R1 cells (Paul 2020). Since the use of different terminology to describe this cell population has often generated confusion, Roncarolo et al. proposed four criteria to be considered for defining T_R1 cells. These four criteria are (1) the production of IL-10, (2), a suppressive function, (3) expression of inhibitory receptors, including PD-1 and LAG3, and (4) the absence of FOXP3 expression (Roncarolo et al. 2018). In agreement with these characteristics, the identified $CD4^+$ $EOMES^+$ cells expressed the inhibitory receptors PD-1, LAG3, CD39, and TIGIT, and the cytokine IL-10, but no FOXP3. Furthermore, one of the described immunosuppressive mechanisms of T_R1 cells involves the secretion of granzymes and perforin 1, and subsequent killing of APCs (Tree et al. 2010; Magnani et al. 2011). Crucially, these effector molecules were also present in the T_R1 cell subset, thus fulfilling all four criteria for their classification as T_R1.

Importantly, T_R1 cells were more abundant in LNs of CLL patients rather than PB or BM, where they are likely to interact with CLL cells and contribute to disease progression or control. In addition, their frequencies were increased in CLL LNs in comparison to rLNs from non-cancer individuals, indicating that leukemia induces the accumulation of these cells. This was further evidenced by the examination of the TCL1 mouse model, in which increased frequencies of T_R1 cells were observed upon leukemia development in both Eμ-TCL1 and TCL1 AT models. Notably, T_R1 expansion was accompanied with a higher IL-10 expression by these cells in TCL1 AT mice compared to non-leukemic mice, confirming their immunosuppressive phenotype. Moreover, work performed by Dr. Ekaterina Lupar and Dr. Ana Izcue from the Max-Planck Institute (Freiburg), showed that the transcriptional profile of the identified $EOMES^+$ T_R1-like murine cells overlaps with that of human T_R1 cells (data not shown, (Roessner et al. 2020a)).

In cooperation with the TF BLIMP1, EOMES transcriptionally activates IL-10, represses T-helper lineage differentiation (Neumann et al. 2014), and similarly to $CD8^+$ T-cells, induces the expression of effector molecules (Zhang et al. 2017). The adoptive transfer of *Eomes*$^{-/-}$ $CD4^+$ T-cells together with CLL cells in *Rag2*$^{-/-}$ mice confirmed that EOMES is indispensable for T_R1 differentiation, as $CD4^+$ T-cells expanded significantly less and produced lower levels of IL-10, as well as effector molecules. Of note, several integrins were found among EOMES-regulated genes (Roessner et al. 2020a), which might influence cell migration and homing, and consequently, be responsible for the increased numbers of *Eomes*$^{-/-}$ $CD4^+$ T-cells in PB of the leukemic mice. Surprisingly, the lack of T_R1 cells led to an enhanced CLL development, indicating that these cells control leukemia growth. Since IL-10 has been shown to be essential for maintaining the function and IL-10 production of T_R1 cells (Brockmann et al. 2017), IL-10R

signaling was investigated to further understand the regulation of these cells. Interestingly, *Il10rb*$^{-/-}$ CD4^{+} T-cells proliferated similarly to WT CD4^{+} T-cells, but *Il10rb*$^{-/-}$ T_R1 cells displayed higher expression of PD-1 along with reduced levels of cytotoxic molecules, indicating an enhanced exhaustion phenotype. These results might seem inconsistent with the commonly described immunosuppressive role of IL-10 (Brooks et al. 2006; Ni et al. 2015), but several studies have reported that IL-10 signaling through STAT3 prevents dysfunction in CD8^{+} T-cells (Naing et al. 2016; Gorby et al. 2020), Hanna et al. unpublished work). Thus, a similar mechanism could be active in CD4^{+} T-cells. Furthermore, *Il10rb*-deficient CD4^{+} T-cells showed a reduced control of CLL development, suggesting that IL-10-mediated signaling in T_R1 cells is necessary for their effector activity and CLL control.

The herein reported anti-leukemic role of T_R1 cells might appear to be in contradiction with the reported function of T_R1 cells in several tumor entities, where they have been shown to exert immunosuppression and thereby facilitate tumor growth (Bergmann et al. 2008; Dennis et al. 2013; Pedroza-Gonzalez et al. 2015; Yan et al. 2017; Song et al. 2018). It is crucial to consider, however, that the same regulatory mechanisms might lead to a different outcome in the CLL context, where the leukemic cells themselves are APCs (Hall et al. 2005; Mayr et al. 2006; Os et al. 2013), and therefore, subjected to the immunosuppressive effect of T_R1 cells. In other words, while in solid tumors the killing of APCs by T_R1 cells might imply a negative regulatory effect for tumor immune control, in this context, it could lead to the killing of CLL cells and thereby a better outcome.

The role of CD4^{+} T-cells in CLL, in fact, remains under intense debate. Numerous *in vitro* studies based on the co-culturing of autologous CD4^{+} T-cells and CLL cells describe a reduced apoptosis or enhanced CLL cell proliferation induced by CD4^{+} T-cell-derived cues, including IFNγ, IL-4 or CD40L (Buschle et al. 1993; Os et al. 2013; Pascutti et al. 2013; Bhattacharya et al. 2015). The striking discrepancy from the results reported herein can be explained by the fact that these studies used CD4^{+} T-cells isolated from PB, where, as observed in this work, T_R1 cells might be present in very low frequencies. On the contrary, *in vivo* studies using the TCL1 AT model, which captures the complex CLL immune microenvironment, reported either a faster or no difference in CLL development in the absence of CD4^{+} T-cells (Kocher et al. 2016; Hanna et al. 2019; Roessner et al. 2020b). As discussed above, a direct anti-tumor role of T_R1 cells in CLL seems plausible. Nevertheless, the lack of CD8^{+} T-cells in *Rag2*$^{-/-}$ mice made it impossible to assess the effect of T_R1 cells on CD8^{+} T-cells, and hence, the assumption that increased T_R1 cell numbers would lead to a better tumor control should be taken with caution. In fact, given the suppressive characteristics of T_R1 cells, a scenario where the negative impact on tumor-reactive CD8^{+} T-cells would compensate or even overturn the direct anti-tumor role of T_R1 cells should be considered. Besides, total CD4^{+} T-cells from spleens of either WT, *Eomes*$^{-/-}$ or *Il10rb*$^{-/-}$ mice were injected into recipient mice, which implies that other

$CD4^+$ T-cell subsets, apart from T_R1 cells, might have expanded and thus impacted on tumor growth. For example, TBET-expressing T_H1 cells have been shown to accumulate in the TCL1 mouse model (Roessner et al. 2020b). These cells produce increasing levels of IFNγ along with disease progression (Roessner et al. 2020b), which have been shown to promote CLL cell survival and proliferation (Buschle et al. 1993). Although the data obtained in this work represent a good starting point for the characterization of T_R1 cells in CLL, additional studies using a fully immunocompetent mouse model and nodal samples from CLL patients will be necessary to fully elucidate their relevance in this disease.

5.7 A novel layer for uncovering the pathological role of T-cells in CLL

Collectively, the results obtained in this work comprehensively characterize the heterogeneous T-cell compartment of CLL patients, and significantly contribute to our understanding of the disease's complex microenvironment. Based on the integration of several single-cell approaches and the use of the TCL1 mouse model, they describe the distinct phenotypic T-cell states acquired under pathogenic conditions, identify previously unrecognized, novel populations, and decipher the role of $CD8^+$ T_{EM} and T_R1 T-cells in controlling CLL progression. While requiring additional experimental validation, these cellular and mechanistic insights represent a pivotal starting point for future studies evaluating the contribution of the microenvironmental niche to leukemia control or/and development. At the same time, these results raise a number of fascinating conceptual and translational questions, the answers to which will help to significantly improve the therapeutic options for CLL patients, and perhaps, other B-cell malignancies.

Single-cell technologies have provided the crucial ability to ascertain the degree of heterogeneity present within $CD8^+$ and $CD4^+$ T-cells, and importantly, delineate the potential contribution of each subset to the milieu of the CLL LN. One of the subsequent questions, for example, is how the T-cell compartment is shaped upon tumor development. Even though CLL is a typically indolent disease, characterized by long periods of observation without treatment, progression eventually occurs (Hallek et al. 2018). Thus, longitudinal sample analysis from individual patients will be central to recognize molecular and cellular patterns determining the course of leukemia development.

A similar question in relation to treatment-induced changes in the CLL microenvironment should be also addressed. Earlier studies reporting immune alterations under ibrutinib or idelalisib treatment indicate that the balance or interactions between cell subsets are likely affected under these treatments (Dubovsky et al. 2013; Dong et al. 2014; Furman et al. 2014; Lampson et al. 2016; Niemann et al. 2016). Because some kinase inhibitors were reported to negatively affect T-cell survival and function (Dong et al. 2014; Hofland et al. 2019), the impact

of these novel inhibitors on individual immune cell subsets should be assessed. Along this line, Rendeiro et al. profiled for the first time the temporal dynamics of immune cells from CLL patients under ibrutinib treatment with a multi-omics approach (Rendeiro et al. 2020). Analyzing single-cell RNA-seq data generated from PBMCs of 4 patients at several time-points over the course of 8 months of treatment, they describe a downregulation of genes related to T-cell activation and an acquired quiescence-like gene signature in $CD8^+$, and to a lesser extent, $CD4^+$ T-cells upon treatment. Following a similar approach with a larger patient cohort would allow linking the phenotypical T-cell alterations to leukemic cell subclonal heterogeneity and treatment outcome.

The evidence for an enrichment of a $CD8^+$ T_{EX} $CD39^+$ population along with a potential pre-dysfunctional axis in CLL LNs raises several key questions. First, owing to the expression of inhibitory receptors including PD-1, CD39, and TIGIT, this subset might be a promising target for immune checkpoint blockade therapy. In this context, a pre-clinical study using the TCL1 AT mouse model reported an improved leukemia control as well as a restored T-cell cytotoxic phenotype under anti-PD-L1 therapy (McClanahan et al. 2015a). However, as previously mentioned, single anti-PD-1 therapy in CLL patients has led to unsatisfactory results, with only some patients with Richter transformation showing response to treatment (Ding et al. 2017). Hence, research efforts currently focus on identifying combination therapies of several immune checkpoints, or with small molecule inhibitors already in use in CLL. In murine experiments, combined PD-1 and LAG3 blockade, as well as treatment with ibrutinib and αPD-1/PD-L1, reduced tumor burden more efficiently than monotherapy (Wierz et al. 2018; Hanna et al. 2020). Besides, several clinical trials combining immune checkpoint blockade with kinase inhibitors are being conducted (NCT02329847, NCT02332980, NCT02362035, NCT02420912, NCT03514017, NCT03153203 and NCT03283137), and first results point towards a response rate of 61 % (Younes et al. 2019), indicating that targeting immune checkpoints in combinations with other therapies might significantly improve the clinical outcome of CLL patients.

Targeting of CD39 in CLL has increasingly gained attention, as it is expressed in both CLL cells and T-cells, with the abundance of the latter correlating with disease severity (Pulte et al. 2011; Perry et al. 2012). Despite having minor effects on leukemia development, the fact that CD39 receptor (ADORA2A) blockade in TCL1 AT mice has been shown to restore T-cell responses and repolarize monocytes to M1-like phenotype represents an encouraging strategy for combination-based therapeutic approaches (Arruga et al. 2020).

The effect of antibody-based blocking of TIGIT has not been investigated in CLL, yet its immunosuppressive role makes it a promising novel target for immunotherapy. In pre-clinical studies, blockade of both TIGIT and PD-L1 in in the murine CT26 tumor model resulted in

reestablishment of T-cell function and complete tumor rejection (Johnston et al. 2014). Similar effects on improving T-cell cytotoxicity were described upon *ex vivo* combined blockade of TIGIT and PD-1 in tumor-infiltrating lymphocytes from melanoma patients (Chauvin et al. 2015), and several clinical trials in solid or metastatic tumors are being conducted (NCT04047862, NCT03563716, NCT03628677 and NCT02913313). Importantly, αTIGIT treatment in mice with multiple myeloma also reduced tumor burden and increased T-cell function (Guillerey et al. 2018), indicating that blocking of TIGIT could also hold promise for the treatment of other B-cell malignancies including CLL.

Last, another question which arises from the identification of $CD8^+$ T_{EX} $CD39^+$ cells in this work is whether they constitute a potential biomarker for response to immune checkpoint blockade therapies, as stratification criteria for identifying CLL patients who could benefit from these therapies have not yet been established. In recent work evaluating the clinical response to PD-1 blockade in non-small-cell lung cancer and melanoma patients, the presence of $CD8^+$ T-cells expressing elevated levels of PD-1 or PD-1 and CTLA-4, respectively, was reported to be predictive of a response to the therapy (Daud et al. 2016; Thommen et al. 2018). Additionally, in another melanoma cohort, the presence of $EOMES^+$ $CD69^+$ $CD8^+$ T_{EM} was indicative of a response to both αPD-1 monotherapy or combined αPD-1 and αCTLA-4 therapy (Gide et al. 2019). Since the frequency of $CD8^+$ T_{EX} $CD39^+$ cells significantly varied between CLL patients, their abundance could have some prognostic power for categorizing patients who would respond to immune checkpoint blockade. Hence, future investigations should focus on the immune composition of pre-treatment LNs samples and its association with response to therapy.

5.8 Conclusion

The current work aimed to comprehensively describe the phenotype, distribution and function of T-cells in CLL patients based on integrative single-cell RNA-seq and mass cytometry analyses of LNs, PB, and BM samples from CLL patients and healthy controls. The central finding is that CLL LNs constitute a distinct niche where clonally-expanded $CD8^+$ T_{EM} cells become more abundant with tumor development, and T-cells with an exhausted state accumulate. In this nodal microenvironment, CLL cells establish a cross-talk with different T-cell subsets, receiving and inducing both pro-survival and inhibitory signals. Moreover, an EOMES-dependent role of $CD8^+$ T_{EM} in controlling CLL progression was determined using the TCL1 mouse model. Finally, T_R1 cells were newly described in CLL patients, and their dependency on EOMES and IL-10 receptor signaling for regulating CLL development in TCL1 mice was demonstrated. Altogether, these data help characterizing the phenotypical changes in the $CD8^+$ T-cell compartment of CLL at an unprecedented resolution and significantly advance our understanding of the disease's pathomechanisms.

6 Appendix

6.1 Profiling of rs9880772 SNP in samples of CLL patients using Sanger Sequencing

DNA from 13 LNs samples analyzed by mass cytometry was isolated using the QIAamp DNA Micro Kit (Qiagen, 56304) following the instructions provided by the manufacturer. Next, 100 ng of DNA were mixed with 0.5mM of forward (5'-GTCTTTATCACTACTAGCAACATGC-3') and reverse (5'-GCACGACCTTTGCTCCTTTT-3') primers and 1X Prima Amp Hot Start Master Mix (Steinbenner Laborsysteme, SL-9714-10ml). The PCR reaction was run with the following protocol:

Step	Temperature	Time (hh:mm:ss)
1	96 °C	00:02:00
2	96 °C	00:00:30
3	51 °C	00:00:15
4	60 °C	00:04:00
5	Go to Step 2, 24x (25 cycles)	
6	15 °C	Hold

Samples were subsequently run on a 2 % agarose gel, and amplified bands were cut and cleaned using the QIAquick PCR Purification Kit (Qiagen, 28104). Purified samples were submitted to Sanger sequencing with the aforementioned primers.

The presence of the rs9880772 SNP (G>A) was examined in all 13 samples. The results are indicated in Table S12.

Table S12: Analysis of rs9880772 genotype in samples of CLL patients.

Risk allele	Non-risk allele
HD4	BC1
	BC2
	BC3
	BC4
	BC5
	BC10
	HD1
	HD2
	HD3
	HD5
	HD6
	HD7

Note: The region of the *EOMES* gene spanning rs9880772 SNP was amplified with gene-specific primers and Sanger-sequenced. 13 CLL samples were classified according to allele presence (G>A / G>C).

6.2 Supplementary patient information

Information regarding viral infection positivity at the time of sample collection was available for samples of CLL patients obtained from the Hospital Clínic (Barcelona) (Table S13). Immunohistochemical staining and *in situ* hybridization (EBERs) methods were used for EBV and CMV, respectively.

Table S13: Detection of CMV- and EBV-positive cells in CLL patient samples.

Patient ID	EBV	CMV
BC1	NA	CMV+
BC10	EBV-	CMV+
BC2	NA	NA
BC3	EBV+	CMV+
BC4	EBV-	CMV-
BC5	EBV+	NA
BC6	NA	CMV+
BC7	NA	NA
BC8	NA	CMV low (2004)
BC9	NA	CMV-

Note: NA = not available, EBV = Epstein-Barr-virus, CMV = cytomegalovirus.

7 List of Publications

Llaó Cid L, Roessner PM, Chapaprieta V, Roider T, Bordas M, Öztürk S, Hanna BS, Izcue A, Dietrich S, Colomer D, Stilgenbauer S, Martín-Subero JI, Seiffert M. EOMES is essential for anti-tumor activity of CD8+ T-cells in chronic lymphocytic leukemia. *Leukemia* (under revision).

Aydin E, Faehling S, Saleh M, **Llaó Cid L**, Seiffert M, Roessner PM. PI3K signaling in the tumor microenvironment: What needs to be considered when treating CLL with PI3K inhibigtors? *Frontiers in Immunology* (under revision) (2020).

Hanna BS, **Llaó Cid L**, Iskar M, Roessner PM, Klett L, Öztürk S, Mack N, Kalter V, Colomer D, Campo E, Bloehdorn J, Stilgenbauer S, Dietrich S, Schmidt M, Gabriel R, Rippe K, Zapatka M, Feuerer M, Lichter P, Seiffert M. IL-10 receptor signaling alters chromatin accessibility in CD8+ T-cells preventing their exhaustion and immune escape in chronic lymphocytic leukemia. *Immunity* (under revision).

Roessner PM*, **Llaó Cid L***, Lupar E*, Roider T, Bordas M, Schifflers C, Gaupel AC, Kilpert F, Krötschel M, Arnold SJ, Sellner L, Stilgenbauer S, Dietrich S, Lichter P, Izcue A, Seiffert M. EOMES and IL-10 regulate anti-tumor activity of T regulatory type 1 CD4+ T-cells in chronic lymphocytic leukemia. *Leukemia* (accepted) (2020). *These authors contributed equally to this work.

Llaó Cid L, Hanna BS, Iskar M, Roessner PM, Öztürk S, Lichter P, Seiffert M. CD8+ T-cells of CLL-bearing mice acquire a transcriptional program of T-cell activation and exhaustion. *Leuk Lymphoma* (2020).

Roessner PM, Hanna BS, Öztürk S, Schulz R, **Llaó Cid L**, Yazdanparast H, Scheffold A, Colomer D, Stilgenbauer S, Lichter P, Seiffert M. TBET-expressing Th1 $CD4^+$ T cells accumulate in chronic lymphocytic leukaemia without affecting disease progression in Eμ-TCL1 mice. *Br J Haematol*. (2020).

Haderk, F, Schulz, R, Iskar, M, **Llaó Cid, L**, Worst T, Willmund KV, Schulz A, Warnken U, Seiler J, Benner A, Nessling M, Zenz T, Göbel M, Dürig J, Diederichs S, Paggetti J, Moussay E, Stilgenbauer S, Zapatka M, Lichter P, Seiffert M. Tumor-derived exosomes modulate PD-L1 expression in monocytes. *Sci Immunol* (2017).

8 References

Aandahl EM, Sandberg JK, Beckerman KP, Tasken K, Moretto WJ, Nixon DF. 2003. CD7 is a differentiation marker that identifies multiple CD8 T cell effector subsets. *J Immunol* **170**: 2349-2355.

Aguirre-Ghiso JA. 2007. Models, mechanisms and clinical evidence for cancer dormancy. *Nat Rev Cancer* **7**: 834-846.

Ahearne MJ, Willimott S, Pinon L, Kennedy DB, Miall F, Dyer MJ, Wagner SD. 2013. Enhancement of CD154/IL4 proliferation by the T follicular helper (Tfh) cytokine, IL21 and increased numbers of circulating cells resembling Tfh cells in chronic lymphocytic leukaemia. *Br J Haematol* **162**: 360-370.

Akdis M, Verhagen J, Taylor A, Karamloo F, Karagiannidis C, Crameri R, Thunberg S, Deniz G, Valenta R, Fiebig H et al. 2004. Immune responses in healthy and allergic individuals are characterized by a fine balance between allergen-specific T regulatory 1 and T helper 2 cells. *J Exp Med* **199**: 1567-1575.

Alfei F, Zehn D. 2017. T Cell Exhaustion: An Epigenetically Imprinted Phenotypic and Functional Makeover. *Trends Mol Med* **23**: 769-771.

Allsup DJ, Kamiguti AS, Lin K, Sherrington PD, Matrai Z, Slupsky JR, Cawley JC, Zuzel M. 2005. B-cell receptor translocation to lipid rafts and associated signaling differ between prognostically important subgroups of chronic lymphocytic leukemia. *Cancer Res* **65**: 7328-7337.

Aoki T, Chong LC, Takata K, Milne K, Hav M, Colombo A, Chavez EA, Nissen M, Wang X, Miyata-Takata T et al. 2020. Single-Cell Transcriptome Analysis Reveals Disease-Defining T-cell Subsets in the Tumor Microenvironment of Classic Hodgkin Lymphoma. *Cancer Discov* **10**: 406-421.

Arimura Y, Kato H, Dianzani U, Okamoto T, Kamekura S, Buonfiglio D, Miyoshi-Akiyama T, Uchiyama T, Yagi J. 2002. A co-stimulatory molecule on activated T cells, H4/ICOS, delivers specific signals in T(h) cells and regulates their responses. *Int Immunol* **14**: 555-566.

Arruga F, Serra S, Vitale N, Guerra G, Papait A, Gyau BB, Tito F, Efremov D, Vaisitti T, Deaglio S. 2020. Targeting of the A2A adenosine receptor counteracts immunosuppression in vivo in a mouse model of chronic lymphocytic leukemia. *Haematologica* doi:10.3324/haematol.2019.242016.

Austen B, Skowronska A, Baker C, Powell JE, Gardiner A, Oscier D, Majid A, Dyer M, Siebert R, Taylor AM et al. 2007. Mutation status of the residual ATM allele is an important determinant of the cellular response to chemotherapy and survival in patients with chronic lymphocytic leukemia containing an 11q deletion. *J Clin Oncol* **25**: 5448-5457.

Azizi E, Carr AJ, Plitas G, Cornish AE, Konopacki C, Prabhakaran S, Nainys J, Wu K, Kiseliovas V, Setty M et al. 2018. Single-Cell Map of Diverse Immune Phenotypes in the Breast Tumor Microenvironment. *Cell* **174**: 1293-1308 e1236.

Bacchetta R, Bigler M, Touraine JL, Parkman R, Tovo PA, Abrams J, de Waal Malefyt R, de Vries JE, Roncarolo MG. 1994. High levels of interleukin 10 production in vivo are associated with tolerance in SCID patients transplanted with HLA mismatched hematopoietic stem cells. *J Exp Med* **179**: 493-502.

Bade B, Boettcher HE, Lohrmann J, Hink-Schauer C, Bratke K, Jenne DE, Virchow JC, Jr., Luttmann W. 2005. Differential expression of the granzymes A, K and M and perforin in human peripheral blood lymphocytes. *Int Immunol* **17**: 1419-1428.

Badoux X, Bueso-Ramos C, Harris D, Li P, Liu Z, Burger J, O'Brien S, Ferrajoli A, Keating MJ, Estrov Z. 2011. Cross-talk between chronic lymphocytic leukemia cells and bone marrow endothelial cells: role of signal transducer and activator of transcription 3. *Hum Pathol* **42**: 1989-2000.

Bagaev DV, Vroomans RMA, Samir J, Stervbo U, Rius C, Dolton G, Greenshields-Watson A, Attaf M, Egorov ES, Zvyagin IV et al. 2020. VDJdb in 2019: database extension, new analysis infrastructure and a T-cell receptor motif compendium. *Nucleic Acids Res* **48**: D1057-D1062.

Bagnara D, Kaufman MS, Calissano C, Marsilio S, Patten PE, Simone R, Chum P, Yan XJ, Allen SL, Kolitz JE et al. 2011. A novel adoptive transfer model of chronic lymphocytic leukemia suggests a key role for T lymphocytes in the disease. *Blood* **117**: 5463-5472.

Bai M, Zheng Y, Liu H, Su B, Zhan Y, He H. 2017. CXCR5(+) CD8(+) T cells potently infiltrate pancreatic tumors and present high functionality. *Exp Cell Res* **361**: 39-45.

Baitsch L, Baumgaertner P, Devevre E, Raghav SK, Legat A, Barba L, Wieckowski S, Bouzourene H, Deplancke B, Romero P et al. 2011. Exhaustion of tumor-specific CD8(+) T cells in metastases from melanoma patients. *J Clin Invest* **121**: 2350-2360.

Baliakas P, Hadzidimitriou A, Sutton LA, Rossi D, Minga E, Villamor N, Larrayoz M, Kminkova J, Agathangelidis A, Davis Z et al. 2015. Recurrent mutations refine prognosis in chronic lymphocytic leukemia. *Leukemia* **29**: 329-336.

Bancroft GJ, Schreiber RD, Unanue ER. 1991. Natural immunity: a T-cell-independent pathway of macrophage activation, defined in the scid mouse. *Immunol Rev* **124**: 5-24.

Banerjee A, Gordon SM, Intlekofer AM, Paley MA, Mooney EC, Lindsten T, Wherry EJ, Reiner SL. 2010. Cutting edge: The transcription factor eomesodermin enables CD8+ T cells to compete for the memory cell niche. *J Immunol* **185**: 4988-4992.

Baumgarth N. 2017. A Hard(y) Look at B-1 Cell Development and Function. *J Immunol* **199**: 3387-3394.

Beekman R, Chapaprieta V, Russinol N, Vilarrasa-Blasi R, Verdaguer-Dot N, Martens JHA, Duran-Ferrer M, Kulis M, Serra F, Javierre BM et al. 2018. The reference epigenome and regulatory chromatin landscape of chronic lymphocytic leukemia. *Nat Med* **24**: 868-880.

Bengsch B, Ohtani T, Khan O, Setty M, Manne S, O'Brien S, Gherardini PF, Herati RS, Huang AC, Chang KM et al. 2018. Epigenomic-Guided Mass Cytometry Profiling Reveals Disease-Specific Features of Exhausted CD8 T Cells. *Immunity* **48**: 1029-1045 e1025.

Bergmann C, Strauss L, Wang Y, Szczepanski MJ, Lang S, Johnson JT, Whiteside TL. 2008. T regulatory type 1 cells in squamous cell carcinoma of the head and neck: mechanisms of suppression and expansion in advanced disease. *Clin Cancer Res* **14**: 3706-3715.

Berndt SI Camp NJ Skibola CF Vijai J Wang Z Gu J Nieters A Kelly RS Smedby KE Monnereau A et al. 2016. Meta-analysis of genome-wide association studies discovers multiple loci for chronic lymphocytic leukemia. *Nat Commun* **7**: 10933.

Berndt SI Skibola CF Joseph V Camp NJ Nieters A Wang Z Cozen W Monnereau A Wang SS Kelly RS et al. 2013. Genome-wide association study identifies multiple risk loci for chronic lymphocytic leukemia. *Nat Genet* **45**: 868-876.

Bertilaccio MT, Simonetti G, Dagklis A, Rocchi M, Rodriguez TV, Apollonio B, Mantovani A, Ponzoni M, Ghia P, Garlanda C et al. 2011. Lack of TIR8/SIGIRR triggers progression of chronic lymphocytic leukemia in mouse models. *Blood* **118**: 660-669.

Beyer M, Kochanek M, Darabi K, Popov A, Jensen M, Endl E, Knolle PA, Thomas RK, von Bergwelt-Baildon M, Debey S et al. 2005. Reduced frequencies and suppressive function of CD4+CD25hi regulatory T cells in patients with chronic lymphocytic leukemia after therapy with fludarabine. *Blood* **106**: 2018-2025.

Bhattacharya N, Reichenzeller M, Caudron-Herger M, Haebe S, Brady N, Diener S, Nothing M, Dohner H, Stilgenbauer S, Rippe K et al. 2015. Loss of cooperativity of secreted CD40L and increased dose-response to IL4 on CLL cell viability correlates with enhanced activation of NF-kB and STAT6. *Int J Cancer* **136**: 65-73.

Biancotto A, Dagur PK, Fuchs JC, Wiestner A, Bagwell CB, McCoy JP, Jr. 2012. Phenotypic complexity of T regulatory subsets in patients with B-chronic lymphocytic leukemia. *Mod Pathol* **25**: 246-259.

Bichi R, Shinton SA, Martin ES, Koval A, Calin GA, Cesari R, Russo G, Hardy RR, Croce CM. 2002. Human chronic lymphocytic leukemia modeled in mouse by targeted TCL1 expression. *Proc Natl Acad Sci U S A* **99**: 6955-6960.

Binder M, Lechenne B, Ummanni R, Scharf C, Balabanov S, Trusch M, Schluter H, Braren I, Spillner E, Trepel M. 2010. Stereotypical chronic lymphocytic leukemia B-cell receptors recognize survival promoting antigens on stromal cells. *PLoS One* **5**: e15992.

Binet JL, Auquier A, Dighiero G, Chastang C, Piguet H, Goasguen J, Vaugier G, Potron G, Colona P, Oberling F et al. 1981. A new prognostic classification of chronic lymphocytic leukemia derived from a multivariate survival analysis. *Cancer* **48**: 198-206.

Binsky I, Haran M, Starlets D, Gore Y, Lantner F, Harpaz N, Leng L, Goldenberg DM, Shvidel L, Berrebi A et al. 2007. IL-8 secreted in a macrophage migration-inhibitory factor- and CD74-dependent manner regulates B cell chronic lymphocytic leukemia survival. *Proc Natl Acad Sci U S A* **104**: 13408-13413.

Bissell MJ, Hines WC. 2011. Why don't we get more cancer? A proposed role of the microenvironment in restraining cancer progression. *Nat Med* **17**: 320-329.

Blanco G, Vardi A, Puiggros A, Gomez-Llonin A, Muro M, Rodriguez-Rivera M, Stalika E, Abella E, Gimeno E, Lopez-Sanchez M et al. 2018. Restricted T cell receptor repertoire in CLL-like monoclonal B cell lymphocytosis and early stage CLL. *Oncoimmunology* **7**: e1432328.

Blank CU, Haining WN, Held W, Hogan PG, Kallies A, Lugli E, Lynn RC, Philip M, Rao A, Restifo NP et al. 2019. Defining 'T cell exhaustion'. *Nat Rev Immunol* **19**: 665-674.

Blattman JN, Wherry EJ, Ha SJ, van der Most RG, Ahmed R. 2009. Impact of epitope escape on PD-1 expression and CD8 T-cell exhaustion during chronic infection. *J Virol* **83**: 4386-4394.

Brack C, Hirama M, Lenhard-Schuller R, Tonegawa S. 1978. A complete immunoglobulin gene is created by somatic recombination. *Cell* **15**: 1-14.

Bresin A, D'Abundo L, Narducci MG, Fiorenza MT, Croce CM, Negrini M, Russo G. 2016. TCL1 transgenic mouse model as a tool for the study of therapeutic targets and microenvironment in human B-cell chronic lymphocytic leukemia. *Cell Death Dis* **7**: e2071.

Brockmann L, Gagliani N, Steglich B, Giannou AD, Kempski J, Pelczar P, Geffken M, Mfarrej B, Huber F, Herkel J et al. 2017. IL-10 Receptor Signaling Is Essential for TR1 Cell Function In Vivo. *J Immunol* **198**: 1130-1141.

Bronte V, Zanovello P. 2005. Regulation of immune responses by L-arginine metabolism. *Nat Rev Immunol* **5**: 641-654.

Brooks DG, Ha SJ, Elsaesser H, Sharpe AH, Freeman GJ, Oldstone MB. 2008. IL-10 and PD-L1 operate through distinct pathways to suppress T-cell activity during persistent viral infection. *Proc Natl Acad Sci U S A* **105**: 20428-20433.

Brooks DG, Trifilo MJ, Edelmann KH, Teyton L, McGavern DB, Oldstone MB. 2006. Interleukin-10 determines viral clearance or persistence in vivo. *Nat Med* **12**: 1301-1309.

Bruggner RV, Bodenmiller B, Dill DL, Tibshirani RJ, Nolan GP. 2014. Automated identification of stratifying signatures in cellular subpopulations. *Proc Natl Acad Sci U S A* **111**: E2770-2777.

Brummelman J, Mazza EMC, Alvisi G, Colombo FS, Grilli A, Mikulak J, Mavilio D, Alloisio M, Ferrari F, Lopci E et al. 2018. High-dimensional single cell analysis identifies stem-like cytotoxic CD8(+) T cells infiltrating human tumors. *J Exp Med* **215**: 2520-2535.

Brusa D, Serra S, Coscia M, Rossi D, D'Arena G, Laurenti L, Jaksic O, Fedele G, Inghirami G, Gaidano G et al. 2013. The PD-1/PD-L1 axis contributes to T-cell dysfunction in chronic lymphocytic leukemia. *Haematologica* **98**: 953-963.

Buggins AG, Patten PE, Richards J, Thomas NS, Mufti GJ, Devereux S. 2008. Tumor-derived IL-6 may contribute to the immunological defect in CLL. *Leukemia* **22**: 1084-1087.

Burger JA. 2011. Nurture versus nature: the microenvironment in chronic lymphocytic leukemia. *Hematology Am Soc Hematol Educ Program* **2011**: 96-103.

Burger JA. 2020. Treatment of Chronic Lymphocytic Leukemia. *N Engl J Med* **383**: 460-473.

Burger JA, Burger M, Kipps TJ. 1999. Chronic lymphocytic leukemia B cells express functional CXCR4 chemokine receptors that mediate spontaneous migration beneath bone marrow stromal cells. *Blood* **94**: 3658-3667.

Burger JA, Chiorazzi N. 2013. B cell receptor signaling in chronic lymphocytic leukemia. *Trends Immunol* **34**: 592-601.

Burger JA, Quiroga MP, Hartmann E, Burkle A, Wierda WG, Keating MJ, Rosenwald A. 2009. High-level expression of the T-cell chemokines CCL3 and CCL4 by chronic lymphocytic

leukemia B cells in nurselike cell cocultures and after BCR stimulation. *Blood* **113**: 3050-3058.

Burger JA, Tsukada N, Burger M, Zvaifler NJ, Dell'Aquila M, Kipps TJ. 2000. Blood-derived nurse-like cells protect chronic lymphocytic leukemia B cells from spontaneous apoptosis through stromal cell-derived factor-1. *Blood* **96**: 2655-2663.

Burkle A, Niedermeier M, Schmitt-Graff A, Wierda WG, Keating MJ, Burger JA. 2007. Overexpression of the CXCR5 chemokine receptor, and its ligand, CXCL13 in B-cell chronic lymphocytic leukemia. *Blood* **110**: 3316-3325.

Burnet FM. 1970. The concept of immunological surveillance. *Prog Exp Tumor Res* **13**: 1-27.

Burnet M. 1957. Cancer: a biological approach. III. Viruses associated with neoplastic conditions. IV. Practical applications. *Br Med J* **1**: 841-847.

Buschle M, Campana D, Carding SR, Richard C, Hoffbrand AV, Brenner MK. 1993. Interferon gamma inhibits apoptotic cell death in B cell chronic lymphocytic leukemia. *J Exp Med* **177**: 213-218.

Butler A, Hoffman P, Smibert P, Papalexi E, Satija R. 2018. Integrating single-cell transcriptomic data across different conditions, technologies, and species. *Nat Biotechnol* **36**: 411-420.

Butler JM, Kobayashi H, Rafii S. 2010. Instructive role of the vascular niche in promoting tumour growth and tissue repair by angiocrine factors. *Nat Rev Cancer* **10**: 138-146.

Byrd JC, Brown JR, O'Brien S, Barrientos JC, Kay NE, Reddy NM, Coutre S, Tam CS, Mulligan SP, Jaeger U et al. 2014. Ibrutinib versus ofatumumab in previously treated chronic lymphoid leukemia. *N Engl J Med* **371**: 213-223.

Caligaris-Cappio F. 1996. B-chronic lymphocytic leukemia: a malignancy of anti-self B cells. *Blood* **87**: 2615-2620.

Calin GA, Cimmino A, Fabbri M, Ferracin M, Wojcik SE, Shimizu M, Taccioli C, Zanesi N, Garzon R, Aqeilan RI et al. 2008. MiR-15a and miR-16-1 cluster functions in human leukemia. *Proc Natl Acad Sci U S A* **105**: 5166-5171.

Cambier JC, Gauld SB, Merrell KT, Vilen BJ. 2007. B-cell anergy: from transgenic models to naturally occurring anergic B cells? *Nat Rev Immunol* **7**: 633-643.

Campregher C, Luciani MG, Gasche C. 2008. Activated neutrophils induce an hMSH2-dependent G2/M checkpoint arrest and replication errors at a (CA)13-repeat in colon epithelial cells. *Gut* **57**: 780-787.

Canale FP, Ramello MC, Nunez N, Araujo Furlan CL, Bossio SN, Gorosito Serran M, Tosello Boari J, Del Castillo A, Ledesma M, Sedlik C et al. 2018. CD39 Expression Defines Cell Exhaustion in Tumor-Infiltrating CD8(+) T Cells. *Cancer Res* **78**: 115-128.

Catakovic K, Gassner FJ, Ratswohl C, Zaborsky N, Rebhandl S, Schubert M, Steiner M, Gutjahr JC, Pleyer L, Egle A et al. 2017. TIGIT expressing CD4+T cells represent a tumor-supportive T cell subset in chronic lymphocytic leukemia. *Oncoimmunology* **7**: e1371399.

Catovsky D, Miliani E, Okos A, Galton DA. 1974. Clinical significance of T-cells in chronic lymphocytic leukaemia. *Lancet* **2**: 751-752.

Cerhan JR, Slager SL. 2015. Familial predisposition and genetic risk factors for lymphoma. *Blood* **126**: 2265-2273.

Chauvin JM, Pagliano O, Fourcade J, Sun Z, Wang H, Sander C, Kirkwood JM, Chen TH, Maurer M, Korman AJ et al. 2015. TIGIT and PD-1 impair tumor antigen-specific CD8(+) T cells in melanoma patients. *J Clin Invest* **125**: 2046-2058.

Cheever MA, Allison JP, Ferris AS, Finn OJ, Hastings BM, Hecht TT, Mellman I, Prindiville SA, Viner JL, Weiner LM et al. 2009. The prioritization of cancer antigens: a national cancer institute pilot project for the acceleration of translational research. *Clin Cancer Res* **15**: 5323-5337.

Chen J, Lopez-Moyado IF, Seo H, Lio CJ, Hempleman LJ, Sekiya T, Yoshimura A, Scott-Browne JP, Rao A. 2019. NR4A transcription factors limit CAR T cell function in solid tumours. *Nature* **567**: 530-534.

Chen SS, Chang BY, Chang S, Tong T, Ham S, Sherry B, Burger JA, Rai KR, Chiorazzi N. 2016. BTK inhibition results in impaired CXCR4 chemokine receptor surface

expression, signaling and function in chronic lymphocytic leukemia. *Leukemia* **30**: 833-843.

Chevrier S, Crowell HL, Zanotelli VRT, Engler S, Robinson MD, Bodenmiller B. 2018. Compensation of Signal Spillover in Suspension and Imaging Mass Cytometry. *Cell Syst* **6**: 612-620 e615.

Chevrier S, Levine JH, Zanotelli VRT, Silina K, Schulz D, Bacac M, Ries CH, Ailles L, Jewett MAS, Moch H et al. 2017. An Immune Atlas of Clear Cell Renal Cell Carcinoma. *Cell* **169**: 736-749 e718.

Chigrinova E, Rinaldi A, Kwee I, Rossi D, Rancoita PM, Strefford JC, Oscier D, Stamatopoulos K, Papadaki T, Berger F et al. 2013. Two main genetic pathways lead to the transformation of chronic lymphocytic leukemia to Richter syndrome. *Blood* **122**: 2673-2682.

Chiorazzi N, Ferrarini M. 2011. Cellular origin(s) of chronic lymphocytic leukemia: cautionary notes and additional considerations and possibilities. *Blood* **117**: 1781-1791.

Christopoulos P, Pfeifer D, Bartholome K, Follo M, Timmer J, Fisch P, Veelken H. 2011. Definition and characterization of the systemic T-cell dysregulation in untreated indolent B-cell lymphoma and very early CLL. *Blood* **117**: 3836-3846.

Chu CC, Catera R, Hatzi K, Yan XJ, Zhang L, Wang XB, Fales HM, Allen SL, Kolitz JE, Rai KR et al. 2008. Chronic lymphocytic leukemia antibodies with a common stereotypic rearrangement recognize nonmuscle myosin heavy chain IIA. *Blood* **112**: 5122-5129.

Chu F, Li HS, Liu X, Cao J, Ma W, Ma Y, Weng J, Zhu Z, Cheng X, Wang Z et al. 2019. CXCR5(+)CD8(+) T cells are a distinct functional subset with an antitumor activity. *Leukemia* **33**: 2640-2653.

Chung W, Eum HH, Lee HO, Lee KM, Lee HB, Kim KT, Ryu HS, Kim S, Lee JE, Park YH et al. 2017. Single-cell RNA-seq enables comprehensive tumour and immune cell profiling in primary breast cancer. *Nat Commun* **8**: 15081.

Clark WH, Jr., Elder DE, Guerry Dt, Braitman LE, Trock BJ, Schultz D, Synnestvedt M, Halpern AC. 1989. Model predicting survival in stage I melanoma based on tumor progression. *J Natl Cancer Inst* **81**: 1893-1904.

Colotta F, Allavena P, Sica A, Garlanda C, Mantovani A. 2009. Cancer-related inflammation, the seventh hallmark of cancer: links to genetic instability. *Carcinogenesis* **30**: 1073-1081.

Cols M, Barra CM, He B, Puga I, Xu W, Chiu A, Tam W, Knowles DM, Dillon SR, Leonard JP et al. 2012. Stromal endothelial cells establish a bidirectional crosstalk with chronic lymphocytic leukemia cells through the TNF-related factors BAFF, APRIL, and CD40L. *J Immunol* **188**: 6071-6083.

Coussens LM, Tinkle CL, Hanahan D, Werb Z. 2000. MMP-9 supplied by bone marrow-derived cells contributes to skin carcinogenesis. *Cell* **103**: 481-490.

Crotty S. 2011. Follicular helper CD4 T cells (TFH). *Annu Rev Immunol* **29**: 621-663.

Crowther-Swanepoel D, Broderick P, Di Bernardo MC, Dobbins SE, Torres M, Mansouri M, Ruiz-Ponte C, Enjuanes A, Rosenquist R, Carracedo A et al. 2010. Common variants at 2q37.3, 8q24.21, 15q21.3 and 16q24.1 influence chronic lymphocytic leukemia risk. *Nat Genet* **42**: 132-136.

Cruz-Guilloty F, Pipkin ME, Djuretic IM, Levanon D, Lotem J, Lichtenheld MG, Groner Y, Rao A. 2009. Runx3 and T-box proteins cooperate to establish the transcriptional program of effector CTLs. *J Exp Med* **206**: 51-59.

Csanaky G, Vass JA, Milosevits J, Ocsovszki I, Szomor A, Schmelczer M. 1994. Expression and function of L-selectin molecules (LECAM-1) in B-cell chronic lymphocytic leukemia. *Haematologica* **79**: 132-136.

Cuni S, Perez-Aciego P, Perez-Chacon G, Vargas JA, Sanchez A, Martin-Saavedra FM, Ballester S, Garcia-Marco J, Jorda J, Durantez A. 2004. A sustained activation of PI3K/NF-kappaB pathway is critical for the survival of chronic lymphocytic leukemia B cells. *Leukemia* **18**: 1391-1400.

Curtsinger JM, Valenzuela JO, Agarwal P, Lins D, Mescher MF. 2005. Type I IFNs provide a third signal to CD8 T cells to stimulate clonal expansion and differentiation. *J Immunol* **174**: 4465-4469.

D'Arena G, Laurenti L, Minervini MM, Deaglio S, Bonello L, De Martino L, De Padua L, Savino L, Tarnani M, De Feo V et al. 2011. Regulatory T-cell number is increased in chronic lymphocytic leukemia patients and correlates with progressive disease. *Leuk Res* **35**: 363-368.

Dal Bo M, Rossi FM, Rossi D, Deambrogi C, Bertoni F, Del Giudice I, Palumbo G, Nanni M, Rinaldi A, Kwee I et al. 2011. 13q14 deletion size and number of deleted cells both influence prognosis in chronic lymphocytic leukemia. *Genes Chromosomes Cancer* **50**: 633-643.

Damle RN, Wasil T, Fais F, Ghiotto F, Valetto A, Allen SL, Buchbinder A, Budman D, Dittmar K, Kolitz J et al. 1999. Ig V gene mutation status and CD38 expression as novel prognostic indicators in chronic lymphocytic leukemia. *Blood* **94**: 1840-1847.

Damm F, Mylonas E, Cosson A, Yoshida K, Della Valle V, Mouly E, Diop M, Scourzic L, Shiraishi Y, Chiba K et al. 2014. Acquired initiating mutations in early hematopoietic cells of CLL patients. *Cancer Discov* **4**: 1088-1101.

Dancescu M, Rubio-Trujillo M, Biron G, Bron D, Delespesse G, Sarfati M. 1992. Interleukin 4 protects chronic lymphocytic leukemic B cells from death by apoptosis and upregulates Bcl-2 expression. *J Exp Med* **176**: 1319-1326.

Das M, Zhu C, Kuchroo VK. 2017. Tim-3 and its role in regulating anti-tumor immunity. *Immunol Rev* **276**: 97-111.

Daud AI, Loo K, Pauli ML, Sanchez-Rodriguez R, Sandoval PM, Taravati K, Tsai K, Nosrati A, Nardo L, Alvarado MD et al. 2016. Tumor immune profiling predicts response to anti-PD-1 therapy in human melanoma. *J Clin Invest* **126**: 3447-3452.

Daussy C, Faure F, Mayol K, Viel S, Gasteiger G, Charrier E, Bienvenu J, Henry T, Debien E, Hasan UA et al. 2014. T-bet and Eomes instruct the development of two distinct natural killer cell lineages in the liver and in the bone marrow. *J Exp Med* **211**: 563-577.

de la Fuente MT, Casanova B, Moyano JV, Garcia-Gila M, Sanz L, Garcia-Marco J, Silva A, Garcia-Pardo A. 2002. Engagement of alpha4beta1 integrin by fibronectin induces in vitro resistance of B chronic lymphocytic leukemia cells to fludarabine. *J Leukoc Biol* **71**: 495-502.

De Obaldia ME, Bhandoola A. 2015. Transcriptional regulation of innate and adaptive lymphocyte lineages. *Annu Rev Immunol* **33**: 607-642.

de Totero D, Reato G, Mauro F, Cignetti A, Ferrini S, Guarini A, Gobbi M, Grossi CE, Foa R. 1999. IL4 production and increased CD30 expression by a unique CD8+ T-cell subset in B-cell chronic lymphocytic leukaemia. *Br J Haematol* **104**: 589-599.

de Visser KE, Eichten A, Coussens LM. 2006. Paradoxical roles of the immune system during cancer development. *Nat Rev Cancer* **6**: 24-37.

de Waal Malefyt R, Abrams J, Bennett B, Figdor CG, de Vries JE. 1991. Interleukin 10(IL-10) inhibits cytokine synthesis by human monocytes: an autoregulatory role of IL-10 produced by monocytes. *J Exp Med* **174**: 1209-1220.

de Weerdt I, Hofland T, de Boer R, Dobber JA, Dubois J, van Nieuwenhuize D, Mobasher M, de Boer F, Hoogendoorn M, Velders GA et al. 2019. Distinct immune composition in lymph node and peripheral blood of CLL patients is reshaped during venetoclax treatment. *Blood Adv* **3**: 2642-2652.

Deaglio S, Malavasi F. 2009. Chronic lymphocytic leukemia microenvironment: shifting the balance from apoptosis to proliferation. *Haematologica* **94**: 752-756.

Deaglio S, Vaisitti T, Bergui L, Bonello L, Horenstein AL, Tamagnone L, Boumsell L, Malavasi F. 2005. CD38 and CD100 lead a network of surface receptors relaying positive signals for B-CLL growth and survival. *Blood* **105**: 3042-3050.

Decker T, Bogner C, Oelsner M, Peschel C, Ringshausen I. 2010. Antiapoptotic effect of interleukin-2 (IL-2) in B-CLL cells with low and high affinity IL-2 receptors. *Ann Hematol* **89**: 1125-1132.

Del Giudice I, Chiaretti S, Tavolaro S, De Propris MS, Maggio R, Mancini F, Peragine N, Santangelo S, Marinelli M, Mauro FR et al. 2009. Spontaneous regression of chronic lymphocytic leukemia: clinical and biologic features of 9 cases. *Blood* **114**: 638-646.

Dennis KL, Blatner NR, Gounari F, Khazaie K. 2013. Current status of interleukin-10 and regulatory T-cells in cancer. *Curr Opin Oncol* **25**: 637-645.

Desfrancois J, Derre L, Corvaisier M, Le Mevel B, Catros V, Jotereau F, Gervois N. 2009. Increased frequency of nonconventional double positive CD4CD8 alphabeta T cells in human breast pleural effusions. *Int J Cancer* **125**: 374-380.

Desfrancois J, Moreau-Aubry A, Vignard V, Godet Y, Khammari A, Dreno B, Jotereau F, Gervois N. 2010. Double positive CD4CD8 alphabeta T cells: a new tumor-reactive population in human melanomas. *PLoS One* **5**: e8437.

Di Bernardo MC, Crowther-Swanepoel D, Broderick P, Webb E, Sellick G, Wild R, Sullivan K, Vijayakrishnan J, Wang Y, Pittman AM et al. 2008. A genome-wide association study identifies six susceptibility loci for chronic lymphocytic leukemia. *Nat Genet* **40**: 1204-1210.

Dighiero G, Maloum K, Desablens B, Cazin B, Navarro M, Leblay R, Leporrier M, Jaubert J, Lepeu G, Dreyfus B et al. 1998. Chlorambucil in indolent chronic lymphocytic leukemia. French Cooperative Group on Chronic Lymphocytic Leukemia. *N Engl J Med* **338**: 1506-1514.

Ding W, LaPlant BR, Call TG, Parikh SA, Leis JF, He R, Shanafelt TD, Sinha S, Le-Rademacher J, Feldman AL et al. 2017. Pembrolizumab in patients with CLL and Richter transformation or with relapsed CLL. *Blood* **129**: 3419-3427.

Ding W, Nowakowski GS, Knox TR, Boysen JC, Maas ML, Schwager SM, Wu W, Wellik LE, Dietz AB, Ghosh AK et al. 2009. Bi-directional activation between mesenchymal stem cells and CLL B-cells: implication for CLL disease progression. *Br J Haematol* **147**: 471-483.

Doering TA, Crawford A, Angelosanto JM, Paley MA, Ziegler CG, Wherry EJ. 2012. Network analysis reveals centrally connected genes and pathways involved in CD8+ T cell exhaustion versus memory. *Immunity* **37**: 1130-1144.

Dohner H, Fischer K, Bentz M, Hansen K, Benner A, Cabot G, Diehl D, Schlenk R, Coy J, Stilgenbauer S et al. 1995. p53 gene deletion predicts for poor survival and non-response to therapy with purine analogs in chronic B-cell leukemias. *Blood* **85**: 1580-1589.

Dohner H, Stilgenbauer S, Benner A, Leupolt E, Krober A, Bullinger L, Dohner K, Bentz M, Lichter P. 2000. Genomic aberrations and survival in chronic lymphocytic leukemia. *N Engl J Med* **343**: 1910-1916.

Dong S, Guinn D, Dubovsky JA, Zhong Y, Lehman A, Kutok J, Woyach JA, Byrd JC, Johnson AJ. 2014. IPI-145 antagonizes intrinsic and extrinsic survival signals in chronic lymphocytic leukemia cells. *Blood* **124**: 3583-3586.

Dorfman DM, Shahsafaei A. 2011. CD200 (OX-2 membrane glycoprotein) is expressed by follicular T helper cells and in angioimmunoblastic T-cell lymphoma. *Am J Surg Pathol* **35**: 76-83.

Dreger P, Dohner H, Ritgen M, Bottcher S, Busch R, Dietrich S, Bunjes D, Cohen S, Schubert J, Hegenbart U et al. 2010. Allogeneic stem cell transplantation provides durable disease control in poor-risk chronic lymphocytic leukemia: long-term clinical and MRD results of the German CLL Study Group CLL3X trial. *Blood* **116**: 2438-2447.

Dubovsky JA, Beckwith KA, Natarajan G, Woyach JA, Jaglowski S, Zhong Y, Hessler JD, Liu TM, Chang BY, Larkin KM et al. 2013. Ibrutinib is an irreversible molecular inhibitor of ITK driving a Th1-selective pressure in T lymphocytes. *Blood* **122**: 2539-2549.

Dudley ME, Wunderlich JR, Robbins PF, Yang JC, Hwu P, Schwartzentruber DJ, Topalian SL, Sherry R, Restifo NP, Hubicki AM et al. 2002. Cancer regression and autoimmunity in patients after clonal repopulation with antitumor lymphocytes. *Science* **298**: 850-854.

Duhen T, Duhen R, Montler R, Moses J, Moudgil T, de Miranda NF, Goodall CP, Blair TC, Fox BA, McDermott JE et al. 2018. Co-expression of CD39 and CD103 identifies tumor-reactive CD8 T cells in human solid tumors. *Nat Commun* **9**: 2724.

Dunn GP, Bruce AT, Ikeda H, Old LJ, Schreiber RD. 2002. Cancer immunoediting: from immunosurveillance to tumor escape. *Nat Immunol* **3**: 991-998.

Dvorak HF. 1986. Tumors: wounds that do not heal. Similarities between tumor stroma generation and wound healing. *N Engl J Med* **315**: 1650-1659.

E J, Yan F, Kang Z, Zhu L, Xing J, Yu E. 2018. CD8(+)CXCR5(+) T cells in tumor-draining lymph nodes are highly activated and predict better prognosis in colorectal cancer. *Hum Immunol* **79**: 446-452.

Efremova M, Vento-Tormo M, Teichmann SA, Vento-Tormo R. 2020. CellPhoneDB: inferring cell-cell communication from combined expression of multi-subunit ligand-receptor complexes. *Nat Protoc* **15**: 1484-1506.

Egeblad M, Werb Z. 2002. New functions for the matrix metalloproteinases in cancer progression. *Nat Rev Cancer* **2**: 161-174.

Ejrnaes M, Filippi CM, Martinic MM, Ling EM, Togher LM, Crotty S, von Herrath MG. 2006. Resolution of a chronic viral infection after interleukin-10 receptor blockade. *J Exp Med* **203**: 2461-2472.

Elinav E, Nowarski R, Thaiss CA, Hu B, Jin C, Flavell RA. 2013. Inflammation-induced cancer: crosstalk between tumours, immune cells and microorganisms. *Nat Rev Cancer* **13**: 759-771.

Elston L, Fegan C, Hills R, Hashimdeen SS, Walsby E, Henley P, Pepper C, Man S. 2020. Increased frequency of CD4(+) PD-1(+) HLA-DR(+) T cells is associated with disease progression in CLL. *Br J Haematol* **188**: 872-880.

Epstein NA, Fatti LP. 1976. Prostatic carcinoma: some morphological features affecting prognosis. *Cancer* **37**: 2455-2465.

Ernst J, Kellis M. 2012. ChromHMM: automating chromatin-state discovery and characterization. *Nat Methods* **9**: 215-216.

Fabbri G, Dalla-Favera R. 2016. The molecular pathogenesis of chronic lymphocytic leukaemia. *Nat Rev Cancer* **16**: 145-162.

Fabbri G, Khiabanian H, Holmes AB, Wang J, Messina M, Mullighan CG, Pasqualucci L, Rabadan R, Dalla-Favera R. 2013. Genetic lesions associated with chronic lymphocytic leukemia transformation to Richter syndrome. *J Exp Med* **210**: 2273-2288.

Facciabene A, Motz GT, Coukos G. 2012. T-regulatory cells: key players in tumor immune escape and angiogenesis. *Cancer Res* **72**: 2162-2171.

Facciotti F, Gagliani N, Haringer B, Alfen JS, Penatti A, Maglie S, Paroni M, Iseppon A, Moro M, Crosti MC et al. 2016. IL-10-producing forkhead box protein 3-negative regulatory T cells inhibit B-cell responses and are involved in systemic lupus erythematosus. *J Allergy Clin Immunol* **137**: 318-321 e315.

Fayad L, Keating MJ, Reuben JM, O'Brien S, Lee BN, Lerner S, Kurzrock R. 2001. Interleukin-6 and interleukin-10 levels in chronic lymphocytic leukemia: correlation with phenotypic characteristics and outcome. *Blood* **97**: 256-263.

Ferrer G, Montserrat E. 2018. Critical molecular pathways in CLL therapy. *Mol Med* **24**: 9.

Fesnak AD, June CH, Levine BL. 2016. Engineered T cells: the promise and challenges of cancer immunotherapy. *Nat Rev Cancer* **16**: 566-581.

Fluckiger AC, Rossi JF, Bussel A, Bryon P, Banchereau J, Defrance T. 1992. Responsiveness of chronic lymphocytic leukemia B cells activated via surface Igs or CD40 to B-cell tropic factors. *Blood* **80**: 3173-3181.

Foa R, Massaia M, Cardona S, Tos AG, Bianchi A, Attisano C, Guarini A, di Celle PF, Fierro MT. 1990. Production of tumor necrosis factor-alpha by B-cell chronic lymphocytic leukemia cells: a possible regulatory role of TNF in the progression of the disease. *Blood* **76**: 393-400.

Folkman J. 1974. Tumor angiogenesis. *Adv Cancer Res* **19**: 331-358.

Folkman J, Watson K, Ingber D, Hanahan D. 1989. Induction of angiogenesis during the transition from hyperplasia to neoplasia. *Nature* **339**: 58-61.

Forconi F, Moss P. 2015. Perturbation of the normal immune system in patients with CLL. *Blood* **126**: 573-581.

Forconi F, Potter KN, Wheatley I, Darzentas N, Sozzi E, Stamatopoulos K, Mockridge CI, Packham G, Stevenson FK. 2010. The normal IGHV1-69-derived B-cell repertoire contains stereotypic patterns characteristic of unmutated CLL. *Blood* **115**: 71-77.

Furman RR, Asgary Z, Mascarenhas JO, Liou HC, Schattner EJ. 2000. Modulation of NF-kappa B activity and apoptosis in chronic lymphocytic leukemia B cells. *J Immunol* **164**: 2200-2206.

Furman RR, Sharman JP, Coutre SE, Cheson BD, Pagel JM, Hillmen P, Barrientos JC, Zelenetz AD, Kipps TJ, Flinn I et al. 2014. Idelalisib and rituximab in relapsed chronic lymphocytic leukemia. *N Engl J Med* **370**: 997-1007.

Furusawa A, Reiser J, Sadashivaiah K, Simpson H, Banerjee A. 2018. Eomesodermin Increases Survival and IL-2 Responsiveness of Tumor-specific CD8+ T Cells in an Adoptive Transfer Model of Cancer Immunotherapy. *J Immunother* **41**: 53-63.

Gabrilovich DI, Ishida T, Nadaf S, Ohm JE, Carbone DP. 1999. Antibodies to vascular endothelial growth factor enhance the efficacy of cancer immunotherapy by improving endogenous dendritic cell function. *Clin Cancer Res* **5**: 2963-2970.

Gabrilovich DI, Nagaraj S. 2009. Myeloid-derived suppressor cells as regulators of the immune system. *Nat Rev Immunol* **9**: 162-174.

Gagliani N, Magnani CF, Huber S, Gianolini ME, Pala M, Licona-Limon P, Guo B, Herbert DR, Bulfone A, Trentini F et al. 2013. Coexpression of CD49b and LAG-3 identifies human and mouse T regulatory type 1 cells. *Nat Med* **19**: 739-746.

Galletti G, Scielzo C, Barbaglio F, Rodriguez TV, Riba M, Lazarevic D, Cittaro D, Simonetti G, Ranghetti P, Scarfo L et al. 2016. Targeting Macrophages Sensitizes Chronic Lymphocytic Leukemia to Apoptosis and Inhibits Disease Progression. *Cell Rep* **14**: 1748-1760.

Garcia-Barchino MJ, Sarasquete ME, Panizo C, Morscio J, Martinez A, Alcoceba M, Fresquet V, Gonzalez-Farre B, Paiva B, Young KH et al. 2018. Richter transformation driven by Epstein-Barr virus reactivation during therapy-related immunosuppression in chronic lymphocytic leukaemia. *J Pathol* **245**: 61-73.

Gaspal FM, McConnell FM, Kim MY, Gray D, Kosco-Vilbois MH, Raykundalia CR, Botto M, Lane PJ. 2006. The generation of thymus-independent germinal centers depends on CD40 but not on CD154, the T cell-derived CD40-ligand. *Eur J Immunol* **36**: 1665-1673.

Gasser S, Orsulic S, Brown EJ, Raulet DH. 2005. The DNA damage pathway regulates innate immune system ligands of the NKG2D receptor. *Nature* **436**: 1186-1190.

Gassner FJ, Zaborsky N, Catakovic K, Rebhandl S, Huemer M, Egle A, Hartmann TN, Greil R, Geisberger R. 2015. Chronic lymphocytic leukaemia induces an exhausted T cell phenotype in the TCL1 transgenic mouse model. *Br J Haematol* **170**: 515-522.

Gatti RA, Good RA. 1971. Occurrence of malignancy in immunodeficiency diseases. A literature review. *Cancer* **28**: 89-98.

Gattinoni L, Speiser DE, Lichterfeld M, Bonini C. 2017. T memory stem cells in health and disease. *Nat Med* **23**: 18-27.

Gaudio E, Spizzo R, Paduano F, Luo Z, Efanov A, Palamarchuk A, Leber AS, Kaou M, Zanesi N, Bottoni A et al. 2012. Tcl1 interacts with Atm and enhances NF-kappaB activation in hematologic malignancies. *Blood* **119**: 180-187.

Gehrke I, Gandhirajan RK, Poll-Wolbeck SJ, Hallek M, Kreuzer KA. 2011. Bone marrow stromal cell-derived vascular endothelial growth factor (VEGF) rather than chronic lymphocytic leukemia (CLL) cell-derived VEGF is essential for the apoptotic resistance of cultured CLL cells. *Mol Med* **17**: 619-627.

Genovese G, Kahler AK, Handsaker RE, Lindberg J, Rose SA, Bakhoum SF, Chambert K, Mick E, Neale BM, Fromer M et al. 2014. Clonal hematopoiesis and blood-cancer risk inferred from blood DNA sequence. *N Engl J Med* **371**: 2477-2487.

Ghiotto F, Fais F, Valetto A, Albesiano E, Hashimoto S, Dono M, Ikematsu H, Allen SL, Kolitz J, Rai KR et al. 2004. Remarkably similar antigen receptors among a subset of patients with chronic lymphocytic leukemia. *J Clin Invest* **113**: 1008-1016.

Giannoni P, Pietra G, Travaini G, Quarto R, Shyti G, Benelli R, Ottaggio L, Mingari MC, Zupo S, Cutrona G et al. 2014. Chronic lymphocytic leukemia nurse-like cells express hepatocyte growth factor receptor (c-MET) and indoleamine 2,3-dioxygenase and display features of immunosuppressive type 2 skewed macrophages. *Haematologica* **99**: 1078-1087.

Giannopoulos K, Schmitt M, Wlasiuk P, Chen J, Bojarska-Junak A, Kowal M, Rolinski J, Dmoszynska A. 2008. The high frequency of T regulatory cells in patients with B-cell chronic lymphocytic leukemia is diminished through treatment with thalidomide. *Leukemia* **22**: 222-224.

Gide TN, Quek C, Menzies AM, Tasker AT, Shang P, Holst J, Madore J, Lim SY, Velickovic R, Wongchenko M et al. 2019. Distinct Immune Cell Populations Define Response to Anti-PD-1 Monotherapy and Anti-PD-1/Anti-CTLA-4 Combined Therapy. *Cancer Cell* **35**: 238-255 e236.

Giesen C, Wang HA, Schapiro D, Zivanovic N, Jacobs A, Hattendorf B, Schuffler PJ, Grolimund D, Buhmann JM, Brandt S et al. 2014. Highly multiplexed imaging of tumor tissues with subcellular resolution by mass cytometry. *Nat Methods* **11**: 417-422.

Girardi M, Oppenheim DE, Steele CR, Lewis JM, Glusac E, Filler R, Hobby P, Sutton B, Tigelaar RE, Hayday AC. 2001. Regulation of cutaneous malignancy by gammadelta T cells. *Science* **294**: 605-609.

Goldin LR, Bjorkholm M, Kristinsson SY, Turesson I, Landgren O. 2009. Elevated risk of chronic lymphocytic leukemia and other indolent non-Hodgkin's lymphomas among relatives of patients with chronic lymphocytic leukemia. *Haematologica* **94**: 647-653.

Gong S, Osei ES, Kaplan D, Chen YH, Meyerson H. 2015. CD317 is over-expressed in B-cell chronic lymphocytic leukemia, but not B-cell acute lymphoblastic leukemia. *Int J Clin Exp Pathol* **8**: 1613-1621.

Gonnord P, Costa M, Abreu A, Peres M, Ysebaert L, Gadat S, Valitutti S. 2019. Multiparametric analysis of CD8(+) T cell compartment phenotype in chronic lymphocytic leukemia reveals a signature associated with progression toward therapy. *Oncoimmunology* **8**: e1570774.

Gonzalez-Rodriguez AP, Contesti J, Huergo-Zapico L, Lopez-Soto A, Fernandez-Guizan A, Acebes-Huerta A, Gonzalez-Huerta AJ, Gonzalez E, Fernandez-Alvarez C, Gonzalez S. 2010. Prognostic significance of CD8 and CD4 T cells in chronic lymphocytic leukemia. *Leuk Lymphoma* **51**: 1829-1836.

Gorby C, Sotolongo Bellon J, Wilmes S, Warda W, Pohler E, Fyfe PK, Cozzani A, Ferrand C, Walter MR, Mitra S et al. 2020. Engineered IL-10 variants elicit potent immunomodulatory effects at low ligand doses. *Sci Signal* **13**.

Gordon SM, Chaix J, Rupp LJ, Wu J, Madera S, Sun JC, Lindsten T, Reiner SL. 2012. The transcription factors T-bet and Eomes control key checkpoints of natural killer cell maturation. *Immunity* **36**: 55-67.

Gorgun G, Holderried TA, Zahrieh D, Neuberg D, Gribben JG. 2005. Chronic lymphocytic leukemia cells induce changes in gene expression of CD4 and CD8 T cells. *J Clin Invest* **115**: 1797-1805.

Gorgun G, Ramsay AG, Holderried TA, Zahrieh D, Le Dieu R, Liu F, Quackenbush J, Croce CM, Gribben JG. 2009. E(mu)-TCL1 mice represent a model for immunotherapeutic reversal of chronic lymphocytic leukemia-induced T-cell dysfunction. *Proc Natl Acad Sci U S A* **106**: 6250-6255.

Goronzy JJ, Fang F, Cavanagh MM, Qi Q, Weyand CM. 2015. Naive T cell maintenance and function in human aging. *J Immunol* **194**: 4073-4080.

Gothert JR, Eisele L, Klein-Hitpass L, Weber S, Zesewitz ML, Sellmann L, Roth A, Pircher H, Duhrsen U, Durig J. 2013. Expanded CD8+ T cells of murine and human CLL are driven into a senescent KLRG1+ effector memory phenotype. *Cancer Immunol Immunother* **62**: 1697-1709.

Goto T, Kennel SJ, Abe M, Takishita M, Kosaka M, Solomon A, Saito S. 1994. A novel membrane antigen selectively expressed on terminally differentiated human B cells. *Blood* **84**: 1922-1930.

Granziero L, Circosta P, Scielzo C, Frisaldi E, Stella S, Geuna M, Giordano S, Ghia P, Caligaris-Cappio F. 2003. CD100/Plexin-B1 interactions sustain proliferation and survival of normal and leukemic CD5+ B lymphocytes. *Blood* **101**: 1962-1969.

Gregori S, Tomasoni D, Pacciani V, Scirpoli M, Battaglia M, Magnani CF, Hauben E, Roncarolo MG. 2010. Differentiation of type 1 T regulatory cells (Tr1) by tolerogenic DC-10 requires the IL-10-dependent ILT4/HLA-G pathway. *Blood* **116**: 935-944.

Greten FR, Eckmann L, Greten TF, Park JM, Li ZW, Egan LJ, Kagnoff MF, Karin M. 2004. IKKbeta links inflammation and tumorigenesis in a mouse model of colitis-associated cancer. *Cell* **118**: 285-296.

Grewal IS, Flavell RA. 1998. CD40 and CD154 in cell-mediated immunity. *Annu Rev Immunol* **16**: 111-135.

Gribben JG, Zahrieh D, Stephans K, Bartlett-Pandite L, Alyea EP, Fisher DC, Freedman AS, Mauch P, Schlossman R, Sequist LV et al. 2005. Autologous and allogeneic stem cell transplantations for poor-risk chronic lymphocytic leukemia. *Blood* **106**: 4389-4396.

Grivennikov SI, Greten FR, Karin M. 2010. Immunity, inflammation, and cancer. *Cell* **140**: 883-899.

Grosselin K, Durand A, Marsolier J, Poitou A, Marangoni E, Nemati F, Dahmani A, Lameiras S, Reyal F, Frenoy O et al. 2019. High-throughput single-cell ChIP-seq identifies heterogeneity of chromatin states in breast cancer. *Nat Genet* **51**: 1060-1066.

Groux H, O'Garra A, Bigler M, Rouleau M, Antonenko S, de Vries JE, Roncarolo MG. 1997. A CD4+ T-cell subset inhibits antigen-specific T-cell responses and prevents colitis. *Nature* **389**: 737-742.

Gruarin P, Maglie S, De Simone M, Haringer B, Vasco C, Ranzani V, Bosotti R, Noddings JS, Larghi P, Facciotti F et al. 2019. Eomesodermin controls a unique differentiation program in human IL-10 and IFN-gamma coproducing regulatory T cells. *Eur J Immunol* **49**: 96-111.

Guillerey C, Harjunpaa H, Carrie N, Kassem S, Teo T, Miles K, Krumeich S, Weulersse M, Cuisinier M, Stannard K et al. 2018. TIGIT immune checkpoint blockade restores CD8(+) T-cell immunity against multiple myeloma. *Blood* **132**: 1689-1694.

Guillot B, Portales P, Thanh AD, Merlet S, Dereure O, Clot J, Corbeau P. 2005. The expression of cytotoxic mediators is altered in mononuclear cells of patients with melanoma and increased by interferon-alpha treatment. *Br J Dermatol* **152**: 690-696.

Guo X, Zhang Y, Zheng L, Zheng C, Song J, Zhang Q, Kang B, Liu Z, Jin L, Xing R et al. 2018. Global characterization of T cells in non-small-cell lung cancer by single-cell sequencing. *Nat Med* **24**: 978-985.

Gupta PK, Godec J, Wolski D, Adland E, Yates K, Pauken KE, Cosgrove C, Ledderose C, Junger WG, Robson SC et al. 2015. CD39 Expression Identifies Terminally Exhausted CD8+ T Cells. *PLoS Pathog* **11**: e1005177.

Haderk F, Schulz R, Iskar M, Cid LL, Worst T, Willmund KV, Schulz A, Warnken U, Seiler J, Benner A et al. 2017. Tumor-derived exosomes modulate PD-L1 expression in monocytes. *Sci Immunol* **2**.

Hahne F, LeMeur N, Brinkman RR, Ellis B, Haaland P, Sarkar D, Spidlen J, Strain E, Gentleman R. 2009. flowCore: a Bioconductor package for high throughput flow cytometry. *BMC Bioinformatics* **10**: 106.

Hall AM, Vickers MA, McLeod E, Barker RN. 2005. Rh autoantigen presentation to helper T cells in chronic lymphocytic leukemia by malignant B cells. *Blood* **105**: 2007-2015.

Halle S, Halle O, Forster R. 2017. Mechanisms and Dynamics of T Cell-Mediated Cytotoxicity In Vivo. *Trends Immunol* **38**: 432-443.

Hallek M, Cheson BD, Catovsky D, Caligaris-Cappio F, Dighiero G, Dohner H, Hillmen P, Keating M, Montserrat E, Chiorazzi N et al. 2018. iwCLL guidelines for diagnosis, indications for treatment, response assessment, and supportive management of CLL. *Blood* **131**: 2745-2760.

Hallek M, Wanders L, Ostwald M, Busch R, Senekowitsch R, Stern S, Schick HD, Kuhn-Hallek I, Emmerich B. 1996. Serum beta(2)-microglobulin and serum thymidine kinase are independent predictors of progression-free survival in chronic lymphocytic leukemia and immunocytoma. *Leuk Lymphoma* **22**: 439-447.

Hamblin TJ. 2010. The TCL1 mouse as a model for chronic lymphocytic leukemia. *Leuk Res* **34**: 135-136.

Hamblin TJ, Davis Z, Gardiner A, Oscier DG, Stevenson FK. 1999. Unmutated Ig V(H) genes are associated with a more aggressive form of chronic lymphocytic leukemia. *Blood* **94**: 1848-1854.

Hanahan D, Coussens LM. 2012. Accessories to the crime: functions of cells recruited to the tumor microenvironment. *Cancer Cell* **21**: 309-322.

Hanahan D, Weinberg RA. 2011. Hallmarks of cancer: the next generation. *Cell* **144**: 646-674.

Hanna BS, McClanahan F, Yazdanparast H, Zaborsky N, Kalter V, Rossner PM, Benner A, Durr C, Egle A, Gribben JG et al. 2016. Depletion of CLL-associated patrolling monocytes and macrophages controls disease development and repairs immune dysfunction in vivo. *Leukemia* **30**: 570-579.

Hanna BS, Roessner PM, Yazdanparast H, Colomer D, Campo E, Kugler S, Yosifov D, Stilgenbauer S, Schmidt M, Gabriel R et al. 2019. Control of chronic lymphocytic leukemia development by clonally-expanded CD8(+) T-cells that undergo functional exhaustion in secondary lymphoid tissues. *Leukemia* **33**: 625-637.

Hanna BS, Yazdanparast H, Demerdash Y, Roessner PM, Schulz R, Lichter P, Stilgenbauer S, Seiffert M. 2020. Combining ibrutinib and checkpoint blockade improves CD8+ T-cell function and control of chronic lymphocytic leukemia in Em-TCL1 mice. *Haematologica* doi:10.3324/haematol.2019.238154.

Hashimoto M, Kamphorst AO, Im SJ, Kissick HT, Pillai RN, Ramalingam SS, Araki K, Ahmed R. 2018. CD8 T Cell Exhaustion in Chronic Infection and Cancer: Opportunities for Interventions. *Annu Rev Med* **69**: 301-318.

Hayakawa K, Formica AM, Brill-Dashoff J, Shinton SA, Ichikawa D, Zhou Y, Morse HC, 3rd, Hardy RR. 2016. Early generated B1 B cells with restricted BCRs become chronic lymphocytic leukemia with continued c-Myc and low Bmf expression. *J Exp Med* **213**: 3007-3024.

Hayakawa Y, Kelly JM, Westwood JA, Darcy PK, Diefenbach A, Raulet D, Smyth MJ. 2002. Cutting edge: tumor rejection mediated by NKG2D receptor-ligand interaction is dependent upon perforin. *J Immunol* **169**: 5377-5381.

Heinemann C, Heink S, Petermann F, Vasanthakumar A, Rothhammer V, Doorduijn E, Mitsdoerffer M, Sie C, Prazeres da Costa O, Buch T et al. 2014. IL-27 and IL-12 oppose pro-inflammatory IL-23 in CD4+ T cells by inducing Blimp1. *Nat Commun* **5**: 3770.

Hendriks J, Gravestein LA, Tesselaar K, van Lier RA, Schumacher TN, Borst J. 2000. CD27 is required for generation and long-term maintenance of T cell immunity. *Nat Immunol* **1**: 433-440.

Herishanu Y, Katz BZ, Lipsky A, Wiestner A. 2013. Biology of chronic lymphocytic leukemia in different microenvironments: clinical and therapeutic implications. *Hematol Oncol Clin North Am* **27**: 173-206.

Herishanu Y, Perez-Galan P, Liu D, Biancotto A, Pittaluga S, Vire B, Gibellini F, Njuguna N, Lee E, Stennett L et al. 2011. The lymph node microenvironment promotes B-cell receptor signaling, NF-kappaB activation, and tumor proliferation in chronic lymphocytic leukemia. *Blood* **117**: 563-574.

Herling M, Patel KA, Khalili J, Schlette E, Kobayashi R, Medeiros LJ, Jones D. 2006. TCL1 shows a regulated expression pattern in chronic lymphocytic leukemia that correlates with molecular subtypes and proliferative state. *Leukemia* **20**: 280-285.

Herling M, Patel KA, Weit N, Lilienthal N, Hallek M, Keating MJ, Jones D. 2009. High TCL1 levels are a marker of B-cell receptor pathway responsiveness and adverse outcome in chronic lymphocytic leukemia. *Blood* **114**: 4675-4686.

Herndon TM, Chen SS, Saba NS, Valdez J, Emson C, Gatmaitan M, Tian X, Hughes TE, Sun C, Arthur DC et al. 2017. Direct in vivo evidence for increased proliferation of CLL cells in lymph nodes compared to bone marrow and peripheral blood. *Leukemia* **31**: 1340-1347.

Herve M, Xu K, Ng YS, Wardemann H, Albesiano E, Messmer BT, Chiorazzi N, Meffre E. 2005. Unmutated and mutated chronic lymphocytic leukemias derive from self-reactive B cell precursors despite expressing different antibody reactivity. *J Clin Invest* **115**: 1636-1643.

Hinz S, Trauzold A, Boenicke L, Sandberg C, Beckmann S, Bayer E, Walczak H, Kalthoff H, Ungefroren H. 2000. Bcl-XL protects pancreatic adenocarcinoma cells against CD95- and TRAIL-receptor-mediated apoptosis. *Oncogene* **19**: 5477-5486.

Hodge-Dufour J, Noble PW, Horton MR, Bao C, Wysoka M, Burdick MD, Strieter RM, Trinchieri G, Pure E. 1997. Induction of IL-12 and chemokines by hyaluronan requires adhesion-dependent priming of resident but not elicited macrophages. *J Immunol* **159**: 2492-2500.

Hodi FS, O'Day SJ, McDermott DF, Weber RW, Sosman JA, Haanen JB, Gonzalez R, Robert C, Schadendorf D, Hassel JC et al. 2010. Improved survival with ipilimumab in patients with metastatic melanoma. *N Engl J Med* **363**: 711-723.

Hofbauer JP, Heyder C, Denk U, Kocher T, Holler C, Trapin D, Asslaber D, Tinhofer I, Greil R, Egle A. 2011. Development of CLL in the TCL1 transgenic mouse model is associated with severe skewing of the T-cell compartment homologous to human CLL. *Leukemia* **25**: 1452-1458.

Hofland T, de Weerdt I, Ter Burg H, de Boer R, Tannheimer S, Tonino SH, Kater AP, Eldering E. 2019. Dissection of the Effects of JAK and BTK Inhibitors on the Functionality of Healthy and Malignant Lymphocytes. *J Immunol* **203**: 2100-2109.

Holler C, Pinon JD, Denk U, Heyder C, Hofbauer S, Greil R, Egle A. 2009. PKCbeta is essential for the development of chronic lymphocytic leukemia in the TCL1 transgenic mouse model: validation of PKCbeta as a therapeutic target in chronic lymphocytic leukemia. *Blood* **113**: 2791-2794.

Howlader N NA, Krapcho M, Miller D, Brest A, Yu M, Ruhl J, Tatalovich Z, Mariotto A, Lewis DR, Chen HS, Feuer EJ, Cronin KA. 2017. SEER Cancer Statistics Review, 1975-2017. National Cancer Institute. Bethesda, MD.

Hu H, Wu X, Jin W, Chang M, Cheng X, Sun SC. 2011. Noncanonical NF-kappaB regulates inducible costimulator (ICOS) ligand expression and T follicular helper cell development. *Proc Natl Acad Sci U S A* **108**: 12827-12832.

Huang AY, Golumbek P, Ahmadzadeh M, Jaffee E, Pardoll D, Levitsky H. 1994. Role of bone marrow-derived cells in presenting MHC class I-restricted tumor antigens. *Science* **264**: 961-965.

Hutloff A, Dittrich AM, Beier KC, Eljaschewitsch B, Kraft R, Anagnostopoulos I, Kroczek RA. 1999. ICOS is an inducible T-cell co-stimulator structurally and functionally related to CD28. *Nature* **397**: 263-266.

Ilander M, Kreutzman A, Rohon P, Melo T, Faber E, Porkka K, Vakkila J, Mustjoki S. 2014. Enlarged memory T-cell pool and enhanced Th1-type responses in chronic myeloid leukemia patients who have successfully discontinued IFN-alpha monotherapy. *PLoS One* **9**: e87794.

Im SJ, Hashimoto M, Gerner MY, Lee J, Kissick HT, Burger MC, Shan Q, Hale JS, Lee J, Nasti TH et al. 2016. Defining CD8+ T cells that provide the proliferative burst after PD-1 therapy. *Nature* **537**: 417-421.

Intlekofer AM, Banerjee A, Takemoto N, Gordon SM, Dejong CS, Shin H, Hunter CA, Wherry EJ, Lindsten T, Reiner SL. 2008. Anomalous type 17 response to viral infection by CD8+ T cells lacking T-bet and eomesodermin. *Science* **321**: 408-411.

Intlekofer AM, Takemoto N, Wherry EJ, Longworth SA, Northrup JT, Palanivel VR, Mullen AC, Gasink CR, Kaech SM, Miller JD et al. 2005. Effector and memory CD8+ T cell fate coupled by T-bet and eomesodermin. *Nat Immunol* **6**: 1236-1244.

Ishikawa J, Kaisho T, Tomizawa H, Lee BO, Kobune Y, Inazawa J, Oritani K, Itoh M, Ochi T, Ishihara K et al. 1995. Molecular cloning and chromosomal mapping of a bone marrow stromal cell surface gene, BST2, that may be involved in pre-B-cell growth. *Genomics* **26**: 527-534.

Istaces N, Splittgerber M, Lima Silva V, Nguyen M, Thomas S, Le A, Achouri Y, Calonne E, Defrance M, Fuks F et al. 2019. EOMES interacts with RUNX3 and BRG1 to promote innate memory cell formation through epigenetic reprogramming. *Nat Commun* **10**: 3306.

Iwai Y, Ishida M, Tanaka Y, Okazaki T, Honjo T, Minato N. 2002. Involvement of PD-L1 on tumor cells in the escape from host immune system and tumor immunotherapy by PD-L1 blockade. *Proc Natl Acad Sci U S A* **99**: 12293-12297.

Jaiswal S, Fontanillas P, Flannick J, Manning A, Grauman PV, Mar BG, Lindsley RC, Mermel CH, Burtt N, Chavez A et al. 2014. Age-related clonal hematopoiesis associated with adverse outcomes. *N Engl J Med* **371**: 2488-2498.

Jemal A, Siegel R, Xu J, Ward E. 2010. Cancer statistics, 2010. *CA Cancer J Clin* **60**: 277-300.

Jia B, Zhao C, Rakszawski KL, Claxton DF, Ehmann WC, Rybka WB, Mineishi S, Wang M, Shike H, Bayerl MG et al. 2019. Eomes(+)T-bet(low) CD8(+) T Cells Are Functionally Impaired and Are Associated with Poor Clinical Outcome in Patients with Acute Myeloid Leukemia. *Cancer Res* **79**: 1635-1645.

Jin HT, Anderson AC, Tan WG, West EE, Ha SJ, Araki K, Freeman GJ, Kuchroo VK, Ahmed R. 2010. Cooperation of Tim-3 and PD-1 in CD8 T-cell exhaustion during chronic viral infection. *Proc Natl Acad Sci U S A* **107**: 14733-14738.

Jitschin R, Braun M, Buttner M, Dettmer-Wilde K, Bricks J, Berger J, Eckart MJ, Krause SW, Oefner PJ, Le Blanc K et al. 2014. CLL-cells induce IDOhi CD14+HLA-DRlo myeloid-derived suppressor cells that inhibit T-cell responses and promote TRegs. *Blood* **124**: 750-760.

Johnston RJ, Comps-Agrar L, Hackney J, Yu X, Huseni M, Yang Y, Park S, Javinal V, Chiu H, Irving B et al. 2014. The immunoreceptor TIGIT regulates antitumor and antiviral CD8(+) T cell effector function. *Cancer Cell* **26**: 923-937.

Kalluri R, Zeisberg M. 2006. Fibroblasts in cancer. *Nat Rev Cancer* **6**: 392-401.

Kamanaka M, Kim ST, Wan YY, Sutterwala FS, Lara-Tejero M, Galan JE, Harhaj E, Flavell RA. 2006. Expression of interleukin-10 in intestinal lymphocytes detected by an interleukin-10 reporter knockin tiger mouse. *Immunity* **25**: 941-952.

Kao C, Oestreich KJ, Paley MA, Crawford A, Angelosanto JM, Ali MA, Intlekofer AM, Boss JM, Reiner SL, Weinmann AS et al. 2011. Transcription factor T-bet represses expression of the inhibitory receptor PD-1 and sustains virus-specific CD8+ T cell responses during chronic infection. *Nat Immunol* **12**: 663-671.

Karin M, Greten FR. 2005. NF-kappaB: linking inflammation and immunity to cancer development and progression. *Nat Rev Immunol* **5**: 749-759.

Kataoka T, Schroter M, Hahne M, Schneider P, Irmler M, Thome M, Froelich CJ, Tschopp J. 1998. FLIP prevents apoptosis induced by death receptors but not by perforin/granzyme B, chemotherapeutic drugs, and gamma irradiation. *J Immunol* **161**: 3936-3942.

Kern C, Cornuel JF, Billard C, Tang R, Rouillard D, Stenou V, Defrance T, Ajchenbaum-Cymbalista F, Simonin PY, Feldblum S et al. 2004. Involvement of BAFF and APRIL in the resistance to apoptosis of B-CLL through an autocrine pathway. *Blood* **103**: 679-688.

Khan O, Giles JR, McDonald S, Manne S, Ngiow SF, Patel KP, Werner MT, Huang AC, Alexander KA, Wu JE et al. 2019. TOX transcriptionally and epigenetically programs CD8(+) T cell exhaustion. *Nature* **571**: 211-218.

Kikushige Y, Ishikawa F, Miyamoto T, Shima T, Urata S, Yoshimoto G, Mori Y, Iino T, Yamauchi T, Eto T et al. 2011. Self-renewing hematopoietic stem cell is the primary target in pathogenesis of human chronic lymphocytic leukemia. *Cancer Cell* **20**: 246-259.

Kim N, Kim HK, Lee K, Hong Y, Cho JH, Choi JW, Lee JI, Suh YL, Ku BM, Eum HH et al. 2020. Single-cell RNA sequencing demonstrates the molecular and cellular reprogramming of metastatic lung adenocarcinoma. *Nat Commun* **11**: 2285.

King C, Tangye SG, Mackay CR. 2008. T follicular helper (TFH) cells in normal and dysregulated immune responses. *Annu Rev Immunol* **26**: 741-766.

Kipps TJ, Stevenson FK, Wu CJ, Croce CM, Packham G, Wierda WG, O'Brien S, Gribben J, Rai K. 2017. Chronic lymphocytic leukaemia. *Nat Rev Dis Primers* **3**: 16096.

Kiselev VY, Andrews TS, Hemberg M. 2019. Challenges in unsupervised clustering of single-cell RNA-seq data. *Nat Rev Genet* **20**: 273-282.

Kitada S, Zapata JM, Andreeff M, Reed JC. 1999. Bryostatin and CD40-ligand enhance apoptosis resistance and induce expression of cell survival genes in B-cell chronic lymphocytic leukaemia. *Br J Haematol* **106**: 995-1004.

Kitchen SG, Jones NR, LaForge S, Whitmire JK, Vu BA, Galic Z, Brooks DG, Brown SJ, Kitchen CM, Zack JA. 2004. CD4 on CD8(+) T cells directly enhances effector function and is a target for HIV infection. *Proc Natl Acad Sci U S A* **101**: 8727-8732.

Klein U, Dalla-Favera R. 2008. Germinal centres: role in B-cell physiology and malignancy. *Nat Rev Immunol* **8**: 22-33.

Klein U, Lia M, Crespo M, Siegel R, Shen Q, Mo T, Ambesi-Impiombato A, Califano A, Migliazza A, Bhagat G et al. 2010. The DLEU2/miR-15a/16-1 cluster controls B cell proliferation and its deletion leads to chronic lymphocytic leukemia. *Cancer Cell* **17**: 28-40.

Klein U, Rajewsky K, Kuppers R. 1998. Human immunoglobulin (Ig)M+IgD+ peripheral blood B cells expressing the CD27 cell surface antigen carry somatically mutated variable region genes: CD27 as a general marker for somatically mutated (memory) B cells. *J Exp Med* **188**: 1679-1689.

Klein U, Tu Y, Stolovitzky GA, Mattioli M, Cattoretti G, Husson H, Freedman A, Inghirami G, Cro L, Baldini L et al. 2001. Gene expression profiling of B cell chronic lymphocytic leukemia reveals a homogeneous phenotype related to memory B cells. *J Exp Med* **194**: 1625-1638.

Kocher T, Asslaber D, Zaborsky N, Flenady S, Denk U, Reinthaler P, Ablinger M, Geisberger R, Bauer JW, Seiffert M et al. 2016. CD4+ T cells, but not non-classical monocytes, are dispensable for the development of chronic lymphocytic leukemia in the TCL1-tg murine model. *Leukemia* **30**: 1409-1413.

Kowalewski DJ, Schuster H, Backert L, Berlin C, Kahn S, Kanz L, Salih HR, Rammensee HG, Stevanovic S, Stickel JS. 2015. HLA ligandome analysis identifies the underlying specificities of spontaneous antileukemia immune responses in chronic lymphocytic leukemia (CLL). *Proc Natl Acad Sci U S A* **112**: E166-175.

Kulis M, Heath S, Bibikova M, Queiros AC, Navarro A, Clot G, Martinez-Trillos A, Castellano G, Brun-Heath I, Pinyol M et al. 2012. Epigenomic analysis detects widespread gene-body DNA hypomethylation in chronic lymphocytic leukemia. *Nat Genet* **44**: 1236-1242.

Kurtova AV, Balakrishnan K, Chen R, Ding W, Schnabl S, Quiroga MP, Sivina M, Wierda WG, Estrov Z, Keating MJ et al. 2009. Diverse marrow stromal cells protect CLL cells from spontaneous and drug-induced apoptosis: development of a reliable and reproducible system to assess stromal cell adhesion-mediated drug resistance. *Blood* **114**: 4441-4450.

Kurtulus S, Madi A, Escobar G, Klapholz M, Nyman J, Christian E, Pawlak M, Dionne D, Xia J, Rozenblatt-Rosen O et al. 2019. Checkpoint Blockade Immunotherapy Induces Dynamic Changes in PD-1(-)CD8(+) Tumor-Infiltrating T Cells. *Immunity* **50**: 181-194 e186.

Labanieh L, Majzner RG, Mackall CL. 2018. Programming CAR-T cells to kill cancer. *Nat Biomed Eng* **2**: 377-391.

Lagneaux L, Delforge A, Bernier M, Stryckmans P, Bron D. 1998. TGF-beta activity and expression of its receptors in B-cell chronic lymphocytic leukemia. *Leuk Lymphoma* **31**: 99-106.

Lahnemann D, Koster J, Szczurek E, McCarthy DJ, Hicks SC, Robinson MD, Vallejos CA, Campbell KR, Beerenwinkel N, Mahfouz A et al. 2020. Eleven grand challenges in single-cell data science. *Genome Biol* **21**: 31.

Lampson BL, Kasar SN, Matos TR, Morgan EA, Rassenti L, Davids MS, Fisher DC, Freedman AS, Jacobson CA, Armand P et al. 2016. Idelalisib given front-line for treatment of chronic lymphocytic leukemia causes frequent immune-mediated hepatotoxicity. *Blood* **128**: 195-203.

Landau DA, Carter SL, Stojanov P, McKenna A, Stevenson K, Lawrence MS, Sougnez C, Stewart C, Sivachenko A, Wang L et al. 2013. Evolution and impact of subclonal mutations in chronic lymphocytic leukemia. *Cell* **152**: 714-726.

Landau DA, Tausch E, Taylor-Weiner AN, Stewart C, Reiter JG, Bahlo J, Kluth S, Bozic I, Lawrence M, Bottcher S et al. 2015. Mutations driving CLL and their evolution in progression and relapse. *Nature* **526**: 525-530.

Lavin Y, Kobayashi S, Leader A, Amir ED, Elefant N, Bigenwald C, Remark R, Sweeney R, Becker CD, Levine JH et al. 2017. Innate Immune Landscape in Early Lung Adenocarcinoma by Paired Single-Cell Analyses. *Cell* **169**: 750-765 e717.

Lawrence MS, Stojanov P, Polak P, Kryukov GV, Cibulskis K, Sivachenko A, Carter SL, Stewart C, Mermel CH, Roberts SA et al. 2013. Mutational heterogeneity in cancer and the search for new cancer-associated genes. *Nature* **499**: 214-218.

Le J, Park JE, Ha VL, Luong A, Branciamore S, Rodin AS, Gogoshin G, Li F, Loh YE, Camacho V et al. 2020. Single-Cell RNA-Seq Mapping of Human Thymopoiesis Reveals Lineage Specification Trajectories and a Commitment Spectrum in T Cell Development. *Immunity* **52**: 1105-1118 e1109.

Le KS, Ame-Thomas P, Tarte K, Gondois-Rey F, Granjeaud S, Orlanducci F, Foucher ED, Broussais F, Bouabdallah R, Fest T et al. 2018. CXCR5 and ICOS expression identifies a CD8 T-cell subset with TFH features in Hodgkin lymphomas. *Blood Adv* **2**: 1889-1900.

Le Roy C, Deglesne PA, Chevallier N, Beitar T, Eclache V, Quettier M, Boubaya M, Letestu R, Levy V, Ajchenbaum-Cymbalista F et al. 2012. The degree of BCR and NFAT activation predicts clinical outcomes in chronic lymphocytic leukemia. *Blood* **120**: 356-365.

Leach DR, Krummel MF, Allison JP. 1996. Enhancement of antitumor immunity by CTLA-4 blockade. *Science* **271**: 1734-1736.

LeBien TW. 2000. Fates of human B-cell precursors. *Blood* **96**: 9-23.

Lee AYS, Korner H. 2019. The CCR6-CCL20 axis in humoral immunity and T-B cell immunobiology. *Immunobiology* **224**: 449-454.

Levings MK, Sangregorio R, Galbiati F, Squadrone S, de Waal Malefyt R, Roncarolo MG. 2001. IFN-alpha and IL-10 induce the differentiation of human type 1 T regulatory cells. *J Immunol* **166**: 5530-5539.

Li H, van der Leun AM, Yofe I, Lubling Y, Gelbard-Solodkin D, van Akkooi ACJ, van den Braber M, Rozeman EA, Haanen J, Blank CU et al. 2019. Dysfunctional CD8 T Cells Form a Proliferative, Dynamically Regulated Compartment within Human Melanoma. *Cell* **176**: 775-789 e718.

Li J, He Y, Hao J, Ni L, Dong C. 2018. High Levels of Eomes Promote Exhaustion of Anti-tumor CD8(+) T Cells. *Front Immunol* **9**: 2981.

Li MO, Wan YY, Sanjabi S, Robertson AK, Flavell RA. 2006. Transforming growth factor-beta regulation of immune responses. *Annu Rev Immunol* **24**: 99-146.

Lia M, Carette A, Tang H, Shen Q, Mo T, Bhagat G, Dalla-Favera R, Klein U. 2012. Functional dissection of the chromosome 13q14 tumor-suppressor locus using transgenic mouse lines. *Blood* **119**: 2981-2990.

Lipponen PK, Eskelinen MJ, Jauhiainen K, Harju E, Terho R. 1992. Tumour infiltrating lymphocytes as an independent prognostic factor in transitional cell bladder cancer. *Eur J Cancer* **29A**: 69-75.

Lotz M, Ranheim E, Kipps TJ. 1994. Transforming growth factor beta as endogenous growth inhibitor of chronic lymphocytic leukemia B cells. *J Exp Med* **179**: 999-1004.

Lupar E, Brack M, Garnier L, Laffont S, Rauch KS, Schachtrup K, Arnold SJ, Guery JC, Izcue A. 2015. Eomesodermin Expression in CD4+ T Cells Restricts Peripheral Foxp3 Induction. *J Immunol* **195**: 4742-4752.

Maaten Lvd, Hinton G. 2008. Visualizing data using t-SNE. *Journal of machine learning research* **9**: 2579-2605.

MacMicking J, Xie QW, Nathan C. 1997. Nitric oxide and macrophage function. *Annu Rev Immunol* **15**: 323-350.

Maffei R, Bulgarelli J, Fiorcari S, Bertoncelli L, Martinelli S, Guarnotta C, Castelli I, Deaglio S, Debbia G, De Biasi S et al. 2013. The monocytic population in chronic lymphocytic leukemia shows altered composition and deregulation of genes involved in phagocytosis and inflammation. *Haematologica* **98**: 1115-1123.

Maffei R, Fiorcari S, Bulgarelli J, Martinelli S, Castelli I, Deaglio S, Debbia G, Fontana M, Coluccio V, Bonacorsi G et al. 2012. Physical contact with endothelial cells through beta1- and beta2- integrins rescues chronic lymphocytic leukemia cells from spontaneous and drug-induced apoptosis and induces a peculiar gene expression profile in leukemic cells. *Haematologica* **97**: 952-960.

Magen A, Nie J, Ciucci T, Tamoutounour S, Zhao Y, Mehta M, Tran B, McGavern DB, Hannenhalli S, Bosselut R. 2019. Single-Cell Profiling Defines Transcriptomic Signatures Specific to Tumor-Reactive versus Virus-Responsive CD4(+) T Cells. *Cell Rep* **29**: 3019-3032 e3016.

Magnani CF, Alberigo G, Bacchetta R, Serafini G, Andreani M, Roncarolo MG, Gregori S. 2011. Killing of myeloid APCs via HLA class I, CD2 and CD226 defines a novel mechanism of suppression by human Tr1 cells. *Eur J Immunol* **41**: 1652-1662.

Mahauad-Fernandez WD, DeMali KA, Olivier AK, Okeoma CM. 2014. Bone marrow stromal antigen 2 expressed in cancer cells promotes mammary tumor growth and metastasis. *Breast Cancer Res* **16**: 493.

Maier T, Guell M, Serrano L. 2009. Correlation of mRNA and protein in complex biological samples. *FEBS Lett* **583**: 3966-3973.

Majzner RG, Mackall CL. 2019. Clinical lessons learned from the first leg of the CAR T cell journey. *Nat Med* **25**: 1341-1355.

Man K, Gabriel SS, Liao Y, Gloury R, Preston S, Henstridge DC, Pellegrini M, Zehn D, Berberich-Siebelt F, Febbraio MA et al. 2017. Transcription Factor IRF4 Promotes CD8(+) T Cell Exhaustion and Limits the Development of Memory-like T Cells during Chronic Infection. *Immunity* **47**: 1129-1141 e1125.

Mansouri L, Sutton LA, Ljungstrom V, Bondza S, Arngarden L, Bhoi S, Larsson J, Cortese D, Kalushkova A, Plevova K et al. 2015. Functional loss of IkappaBepsilon leads to NF-kappaB deregulation in aggressive chronic lymphocytic leukemia. *J Exp Med* **212**: 833-843.

Martinez GJ, Pereira RM, Aijo T, Kim EY, Marangoni F, Pipkin ME, Togher S, Heissmeyer V, Zhang YC, Crotty S et al. 2015. The transcription factor NFAT promotes exhaustion of activated CD8(+) T cells. *Immunity* **42**: 265-278.

Martinez-Torres AC, Quiney C, Attout T, Boullet H, Herbi L, Vela L, Barbier S, Chateau D, Chapiro E, Nguyen-Khac F et al. 2015. CD47 agonist peptides induce programmed cell death in refractory chronic lymphocytic leukemia B cells via PLCgamma1 activation: evidence from mice and humans. *PLoS Med* **12**: e1001796.

Martinez-Usatorre A, Donda A, Zehn D, Romero P. 2018. PD-1 Blockade Unleashes Effector Potential of Both High- and Low-Affinity Tumor-Infiltrating T Cells. *J Immunol* **201**: 792-803.

Matsuzaki J, Gnjatic S, Mhawech-Fauceglia P, Beck A, Miller A, Tsuji T, Eppolito C, Qian F, Lele S, Shrikant P et al. 2010. Tumor-infiltrating NY-ESO-1-specific CD8+ T cells are negatively regulated by LAG-3 and PD-1 in human ovarian cancer. *Proc Natl Acad Sci U S A* **107**: 7875-7880.

Matzinger P. 1994. Tolerance, danger, and the extended family. *Annu Rev Immunol* **12**: 991-1045.

Mayr C, Bund D, Schlee M, Bamberger M, Kofler DM, Hallek M, Wendtner CM. 2006. MDM2 is recognized as a tumor-associated antigen in chronic lymphocytic leukemia by CD8+ autologous T lymphocytes. *Exp Hematol* **34**: 44-53.

Mazzoni A, Maggi L, Siracusa F, Ramazzotti M, Rossi MC, Santarlasci V, Montaini G, Capone M, Rossettini B, De Palma R et al. 2019. Eomes controls the development of Th17-derived (non-classic) Th1 cells during chronic inflammation. *Eur J Immunol* **49**: 79-95.

McAdam AJ, Chang TT, Lumelsky AE, Greenfield EA, Boussiotis VA, Duke-Cohan JS, Chernova T, Malenkovich N, Jabs C, Kuchroo VK et al. 2000. Mouse inducible costimulatory molecule (ICOS) expression is enhanced by CD28 costimulation and regulates differentiation of CD4+ T cells. *J Immunol* **165**: 5035-5040.

McClanahan F, Hanna B, Miller S, Clear AJ, Lichter P, Gribben JG, Seiffert M. 2015a. PD-L1 checkpoint blockade prevents immune dysfunction and leukemia development in a mouse model of chronic lymphocytic leukemia. *Blood* **126**: 203-211.

McClanahan F, Riches JC, Miller S, Day WP, Kotsiou E, Neuberg D, Croce CM, Capasso M, Gribben JG. 2015b. Mechanisms of PD-L1/PD-1-mediated CD8 T-cell dysfunction in the context of aging-related immune defects in the Emicro-TCL1 CLL mouse model. *Blood* **126**: 212-221.

McGranahan N, Furness AJ, Rosenthal R, Ramskov S, Lyngaa R, Saini SK, Jamal-Hanjani M, Wilson GA, Birkbak NJ, Hiley CT et al. 2016. Clonal neoantigens elicit T cell immunoreactivity and sensitivity to immune checkpoint blockade. *Science* **351**: 1463-1469.

McLane LM, Abdel-Hakeem MS, Wherry EJ. 2019. CD8 T Cell Exhaustion During Chronic Viral Infection and Cancer. *Annu Rev Immunol* **37**: 457-495.

Medzhitov R. 2008. Origin and physiological roles of inflammation. *Nature* **454**: 428-435.

Melchers F. 2015. Checkpoints that control B cell development. *J Clin Invest* **125**: 2203-2210.

Messmer BT, Messmer D, Allen SL, Kolitz JE, Kudalkar P, Cesar D, Murphy EJ, Koduru P, Ferrarini M, Zupo S et al. 2005. In vivo measurements document the dynamic cellular kinetics of chronic lymphocytic leukemia B cells. *J Clin Invest* **115**: 755-764.

Methot SP, Di Noia JM. 2017. Molecular Mechanisms of Somatic Hypermutation and Class Switch Recombination. *Adv Immunol* **133**: 37-87.

Meyaard L, Adema GJ, Chang C, Woollatt E, Sutherland GR, Lanier LL, Phillips JH. 1997. LAIR-1, a novel inhibitory receptor expressed on human mononuclear leukocytes. *Immunity* **7**: 283-290.

Miles B, Miller SM, Folkvord JM, Levy DN, Rakasz EG, Skinner PJ, Connick E. 2016. Follicular Regulatory CD8 T Cells Impair the Germinal Center Response in SIV and Ex Vivo HIV Infection. *PLoS Pathog* **12**: e1005924.

Miller BC, Sen DR, Al Abosy R, Bi K, Virkud YV, LaFleur MW, Yates KB, Lako A, Felt K, Naik GS et al. 2019. Subsets of exhausted CD8(+) T cells differentially mediate tumor control and respond to checkpoint blockade. *Nat Immunol* **20**: 326-336.

Miragaia RJ, Gomes T, Chomka A, Jardine L, Riedel A, Hegazy AN, Whibley N, Tucci A, Chen X, Lindeman I et al. 2019. Single-Cell Transcriptomics of Regulatory T Cells Reveals Trajectories of Tissue Adaptation. *Immunity* **50**: 493-504 e497.

Mok CL, Gil-Gomez G, Williams O, Coles M, Taga S, Tolaini M, Norton T, Kioussis D, Brady HJ. 1999. Bad can act as a key regulator of T cell apoptosis and T cell development. *J Exp Med* **189**: 575-586.

Monserrat J, Sanchez MA, de Paz R, Diaz D, Mur S, Reyes E, Prieto A, de la Hera A, Martinez AC, Alvarez-Mon M. 2014. Distinctive patterns of naive/memory subset distribution and cytokine expression in CD4 T lymphocytes in ZAP-70 B-chronic lymphocytic patients. *Cytometry B Clin Cytom* **86**: 32-43.

Motta M, Rassenti L, Shelvin BJ, Lerner S, Kipps TJ, Keating MJ, Wierda WG. 2005. Increased expression of CD152 (CTLA-4) by normal T lymphocytes in untreated patients with B-cell chronic lymphocytic leukemia. *Leukemia* **19**: 1788-1793.

Mumprecht S, Schurch C, Schwaller J, Solenthaler M, Ochsenbein AF. 2009. Programmed death 1 signaling on chronic myeloid leukemia-specific T cells results in T-cell exhaustion and disease progression. *Blood* **114**: 1528-1536.

Nabhan C, Rosen ST. 2014. Chronic lymphocytic leukemia: a clinical review. *JAMA* **312**: 2265-2276.

Naing A, Papadopoulos KP, Autio KA, Ott PA, Patel MR, Wong DJ, Falchook GS, Pant S, Whiteside M, Rasco DR et al. 2016. Safety, Antitumor Activity, and Immune Activation of Pegylated Recombinant Human Interleukin-10 (AM0010) in Patients With Advanced Solid Tumors. *J Clin Oncol* **34**: 3562-3569.

Naito Y, Saito K, Shiiba K, Ohuchi A, Saigenji K, Nagura H, Ohtani H. 1998. CD8+ T cells infiltrated within cancer cell nests as a prognostic factor in human colorectal cancer. *Cancer Res* **58**: 3491-3494.

Nascimbeni M, Shin EC, Chiriboga L, Kleiner DE, Rehermann B. 2004. Peripheral CD4(+)CD8(+) T cells are differentiated effector memory cells with antiviral functions. *Blood* **104**: 478-486.

Neumann C, Heinrich F, Neumann K, Junghans V, Mashreghi MF, Ahlers J, Janke M, Rudolph C, Mockel-Tenbrinck N, Kuhl AA et al. 2014. Role of Blimp-1 in programing Th effector cells into IL-10 producers. *J Exp Med* **211**: 1807-1819.

Nganga VK, Palmer VL, Naushad H, Kassmeier MD, Anderson DK, Perry GA, Schabla NM, Swanson PC. 2013. Accelerated progression of chronic lymphocytic leukemia in Emu-TCL1 mice expressing catalytically inactive RAG1. *Blood* **121**: 3855-3866, S3851-3816.

Ni G, Wang T, Walton S, Zhu B, Chen S, Wu X, Wang Y, Wei MQ, Liu X. 2015. Manipulating IL-10 signalling blockade for better immunotherapy. *Cell Immunol* **293**: 126-129.

Niemann CU, Herman SE, Maric I, Gomez-Rodriguez J, Biancotto A, Chang BY, Martyr S, Stetler-Stevenson M, Yuan CM, Calvo KR et al. 2016. Disruption of in vivo Chronic Lymphocytic Leukemia Tumor-Microenvironment Interactions by Ibrutinib--Findings from an Investigator-Initiated Phase II Study. *Clin Cancer Res* **22**: 1572-1582.

Nishio M, Endo T, Tsukada N, Ohata J, Kitada S, Reed JC, Zvaifler NJ, Kipps TJ. 2005. Nurselike cells express BAFF and APRIL, which can promote survival of chronic lymphocytic leukemia cells via a paracrine pathway distinct from that of SDF-1alpha. *Blood* **106**: 1012-1020.

Noguchi M, Ropars V, Roumestand C, Suizu F. 2007. Proto-oncogene TCL1: more than just a coactivator for Akt. *FASEB J* **21**: 2273-2284.

Novak M, Prochazka V, Turcsanyi P, Papajik T. 2015. Numbers of CD8+PD-1+ and CD4+PD-1+ Cells in Peripheral Blood of Patients with Chronic Lymphocytic Leukemia Are Independent of Binet Stage and Are Significantly Higher Compared to Healthy Volunteers. *Acta Haematol* **134**: 208-214.

Nozawa H, Chiu C, Hanahan D. 2006. Infiltrating neutrophils mediate the initial angiogenic switch in a mouse model of multistage carcinogenesis. *Proc Natl Acad Sci U S A* **103**: 12493-12498.

Nunes C, Wong R, Mason M, Fegan C, Man S, Pepper C. 2012. Expansion of a CD8(+)PD-1(+) replicative senescence phenotype in early stage CLL patients is associated with inverted CD4:CD8 ratios and disease progression. *Clin Cancer Res* **18**: 678-687.

O'Brien S, Kantarjian H, Beran M, Robertson LE, Koller C, Lerner S, Keating MJ. 1995. Interferon maintenance therapy for patients with chronic lymphocytic leukemia in remission after fludarabine therapy. *Blood* **86**: 1298-1300.

O'Flanagan CH, Campbell KR, Zhang AW, Kabeer F, Lim JLP, Biele J, Eirew P, Lai D, McPherson A, Kong E et al. 2019. Dissociation of solid tumor tissues with cold active protease for single-cell RNA-seq minimizes conserved collagenase-associated stress responses. *Genome Biol* **20**: 210.

O'Shea JJ, Murray PJ. 2008. Cytokine signaling modules in inflammatory responses. *Immunity* **28**: 477-487.

Oakes CC, Seifert M, Assenov Y, Gu L, Przekopowitz M, Ruppert AS, Wang Q, Imbusch CD, Serva A, Koser SD et al. 2016. DNA methylation dynamics during B cell maturation underlie a continuum of disease phenotypes in chronic lymphocytic leukemia. *Nat Genet* **48**: 253-264.

Okamura T, Sumitomo S, Morita K, Iwasaki Y, Inoue M, Nakachi S, Komai T, Shoda H, Miyazaki J, Fujio K et al. 2015. TGF-beta3-expressing CD4+CD25(-)LAG3+ regulatory T cells control humoral immune responses. *Nat Commun* **6**: 6329.

Okazaki IM, Kotani A, Honjo T. 2007. Role of AID in tumorigenesis. *Adv Immunol* **94**: 245-273.

Ono M, Torisu H, Fukushi J, Nishie A, Kuwano M. 1999. Biological implications of macrophage infiltration in human tumor angiogenesis. *Cancer Chemother Pharmacol* **43 Suppl**: S69-71.

Orchard JA, Ibbotson RE, Davis Z, Wiestner A, Rosenwald A, Thomas PW, Hamblin TJ, Staudt LM, Oscier DG. 2004. ZAP-70 expression and prognosis in chronic lymphocytic leukaemia. *Lancet* **363**: 105-111.

Orsini E, Guarini A, Chiaretti S, Mauro FR, Foa R. 2003. The circulating dendritic cell compartment in patients with chronic lymphocytic leukemia is severely defective and unable to stimulate an effective T-cell response. *Cancer Res* **63**: 4497-4506.

Os A, Burgler S, Ribes AP, Funderud A, Wang D, Thompson KM, Tjonnfjord GE, Bogen B, Munthe LA. 2013. Chronic lymphocytic leukemia cells are activated and proliferate in response to specific T helper cells. *Cell Rep* **4**: 566-577.

Ouillette P, Collins R, Shakhan S, Li J, Li C, Shedden K, Malek SN. 2011. The prognostic significance of various 13q14 deletions in chronic lymphocytic leukemia. *Clin Cancer Res* **17**: 6778-6790.

Overgaard NH, Jung JW, Steptoe RJ, Wells JW. 2015. CD4+/CD8+ double-positive T cells: more than just a developmental stage? *J Leukoc Biol* **97**: 31-38.

Ozaki S, Kosaka M, Wakatsuki S, Abe M, Koishihara Y, Matsumoto T. 1997. Immunotherapy of multiple myeloma with a monoclonal antibody directed against a plasma cell-specific antigen, HM1.24. *Blood* **90**: 3179-3186.

Ozturk S, Roessner PM, Schulze-Edinghausen L, Yazdanparast H, Kalter V, Lichter P, Hanna BS, Seiffert M. 2019. Rejection of adoptively transferred Emicro-TCL1 chronic lymphocytic leukemia cells in C57BL/6 substrains or knockout mouse lines. *Leukemia* **33**: 1514-1539.

Pahler JC, Tazzyman S, Erez N, Chen YY, Murdoch C, Nozawa H, Lewis CE, Hanahan D. 2008. Plasticity in tumor-promoting inflammation: impairment of macrophage recruitment evokes a compensatory neutrophil response. *Neoplasia* **10**: 329-340.

Paley MA, Kroy DC, Odorizzi PM, Johnnidis JB, Dolfi DV, Barnett BE, Bikoff EK, Robertson EJ, Lauer GM, Reiner SL et al. 2012. Progenitor and terminal subsets of CD8+ T cells cooperate to contain chronic viral infection. *Science* **338**: 1220-1225.

Palma M, Gentilcore G, Heimersson K, Mozaffari F, Nasman-Glaser B, Young E, Rosenquist R, Hansson L, Osterborg A, Mellstedt H. 2017. T cells in chronic lymphocytic leukemia display dysregulated expression of immune checkpoints and activation markers. *Haematologica* **102**: 562-572.

Panayiotidis P, Jones D, Ganeshaguru K, Foroni L, Hoffbrand AV. 1996. Human bone marrow stromal cells prevent apoptosis and support the survival of chronic lymphocytic leukaemia cells in vitro. *Br J Haematol* **92**: 97-103.

Parikh SA. 2018. Chronic lymphocytic leukemia treatment algorithm 2018. *Blood Cancer J* **8**: 93.

Pascutti MF, Jak M, Tromp JM, Derks IA, Remmerswaal EB, Thijssen R, van Attekum MH, van Bochove GG, Luijks DM, Pals ST et al. 2013. IL-21 and CD40L signals from autologous T cells can induce antigen-independent proliferation of CLL cells. *Blood* **122**: 3010-3019.

Pasikowska M, Walsby E, Apollonio B, Cuthill K, Phillips E, Coulter E, Longhi MS, Ma Y, Yallop D, Barber LD et al. 2016. Phenotype and immune function of lymph node and peripheral blood CLL cells are linked to transendothelial migration. *Blood* **128**: 563-573.

Pauken KE, Sammons MA, Odorizzi PM, Manne S, Godec J, Khan O, Drake AM, Chen Z, Sen DR, Kurachi M et al. 2016. Epigenetic stability of exhausted T cells limits durability of reinvigoration by PD-1 blockade. *Science* **354**: 1160-1165.

Paul Y. 2020. Clonal Evolution Dynamics and Tumor Microenvironment Composition of Chronic Lymphocytic Leukemia. pp. 66 - 116, Heidelberg.

Pedroza-Gonzalez A, Zhou G, Vargas-Mendez E, Boor PP, Mancham S, Verhoef C, Polak WG, Grunhagen D, Pan Q, Janssen H et al. 2015. Tumor-infiltrating plasmacytoid dendritic cells promote immunosuppression by Tr1 cells in human liver tumors. *Oncoimmunology* **4**: e1008355.

Pekarsky Y, Koval A, Hallas C, Bichi R, Tresini M, Malstrom S, Russo G, Tsichlis P, Croce CM. 2000. Tcl1 enhances Akt kinase activity and mediates its nuclear translocation. *Proc Natl Acad Sci U S A* **97**: 3028-3033.

Pekarsky Y, Palamarchuk A, Maximov V, Efanov A, Nazaryan N, Santanam U, Rassenti L, Kipps T, Croce CM. 2008. Tcl1 functions as a transcriptional regulator and is directly involved in the pathogenesis of CLL. *Proc Natl Acad Sci U S A* **105**: 19643-19648.

Pekarsky Y, Santanam U, Cimmino A, Palamarchuk A, Efanov A, Maximov V, Volinia S, Alder H, Liu CG, Rassenti L et al. 2006. Tcl1 expression in chronic lymphocytic leukemia is regulated by miR-29 and miR-181. *Cancer Res* **66**: 11590-11593.

Penn I, Starzl TE. 1970. Malignant lymphomas in transplantation patients: a review of the world experience. *Int Z Klin Pharmakol Ther Toxikol* **3**: 49-54.

Perry C, Hazan-Halevy I, Kay S, Cipok M, Grisaru D, Deutsch V, Polliack A, Naparstek E, Herishanu Y. 2012. Increased CD39 expression on CD4(+) T lymphocytes has clinical and prognostic significance in chronic lymphocytic leukemia. *Ann Hematol* **91**: 1271-1279.

Pflug N, Bahlo J, Shanafelt TD, Eichhorst BF, Bergmann MA, Elter T, Bauer K, Malchau G, Rabe KG, Stilgenbauer S et al. 2014. Development of a comprehensive prognostic index for patients with chronic lymphocytic leukemia. *Blood* **124**: 49-62.

Piao W, Xiong Y, Famulski K, Brinkman CC, Li L, Toney N, Wagner C, Saxena V, Simon T, Bromberg JS. 2019. Author Correction: Regulation of T cell afferent lymphatic migration by targeting LTbetaR-mediated non-classical NFkappaB signaling. *Nat Commun* **10**: 2927.

Pieper K, Grimbacher B, Eibel H. 2013. B-cell biology and development. *J Allergy Clin Immunol* **131**: 959-971.

Pikarsky E, Porat RM, Stein I, Abramovitch R, Amit S, Kasem S, Gutkovich-Pyest E, Urieli-Shoval S, Galun E, Ben-Neriah Y. 2004. NF-kappaB functions as a tumour promoter in inflammation-associated cancer. *Nature* **431**: 461-466.

Pipkin ME, Sacks JA, Cruz-Guilloty F, Lichtenheld MG, Bevan MJ, Rao A. 2010. Interleukin-2 and inflammation induce distinct transcriptional programs that promote the differentiation of effector cytolytic T cells. *Immunity* **32**: 79-90.

Podhorecka M, Dmoszynska A, Rolinski J, Wasik E. 2002. T type 1/type 2 subsets balance in B-cell chronic lymphocytic leukemia--the three-color flow cytometry analysis. *Leuk Res* **26**: 657-660.

Ponader S, Chen SS, Buggy JJ, Balakrishnan K, Gandhi V, Wierda WG, Keating MJ, O'Brien S, Chiorazzi N, Burger JA. 2012. The Bruton tyrosine kinase inhibitor PCI-32765 thwarts chronic lymphocytic leukemia cell survival and tissue homing in vitro and in vivo. *Blood* **119**: 1182-1189.

Porter DL, Hwang WT, Frey NV, Lacey SF, Shaw PA, Loren AW, Bagg A, Marcucci KT, Shen A, Gonzalez V et al. 2015. Chimeric antigen receptor T cells persist and induce sustained remissions in relapsed refractory chronic lymphocytic leukemia. *Sci Transl Med* **7**: 303ra139.

Pot C, Jin H, Awasthi A, Liu SM, Lai CY, Madan R, Sharpe AH, Karp CL, Miaw SC, Ho IC et al. 2009. Cutting edge: IL-27 induces the transcription factor c-Maf, cytokine IL-21, and the costimulatory receptor ICOS that coordinately act together to promote differentiation of IL-10-producing Tr1 cells. *J Immunol* **183**: 797-801.

Puente XS, Bea S, Valdes-Mas R, Villamor N, Gutierrez-Abril J, Martin-Subero JI, Munar M, Rubio-Perez C, Jares P, Aymerich M et al. 2015. Non-coding recurrent mutations in chronic lymphocytic leukaemia. *Nature* **526**: 519-524.

Puente XS, Pinyol M, Quesada V, Conde L, Ordonez GR, Villamor N, Escaramis G, Jares P, Bea S, Gonzalez-Diaz M et al. 2011. Whole-genome sequencing identifies recurrent mutations in chronic lymphocytic leukaemia. *Nature* **475**: 101-105.

Pulte D, Furman RR, Broekman MJ, Drosopoulos JH, Ballard HS, Olson KE, Kizer JR, Marcus AJ. 2011. CD39 expression on T lymphocytes correlates with severity of disease in patients with chronic lymphocytic leukemia. *Clin Lymphoma Myeloma Leuk* **11**: 367-372.

Puram SV, Tirosh I, Parikh AS, Patel AP, Yizhak K, Gillespie S, Rodman C, Luo CL, Mroz EA, Emerick KS et al. 2017. Single-Cell Transcriptomic Analysis of Primary and Metastatic Tumor Ecosystems in Head and Neck Cancer. *Cell* **171**: 1611-1624 e1624.

Qi H. 2016. T follicular helper cells in space-time. *Nat Rev Immunol* **16**: 612-625.

Quesada V, Conde L, Villamor N, Ordonez GR, Jares P, Bassaganyas L, Ramsay AJ, Bea S, Pinyol M, Martinez-Trillos A et al. 2011. Exome sequencing identifies recurrent mutations of the splicing factor SF3B1 gene in chronic lymphocytic leukemia. *Nat Genet* **44**: 47-52.

Quesada V, Ramsay AJ, Lopez-Otin C. 2012. Chronic lymphocytic leukemia with SF3B1 mutation. *N Engl J Med* **366**: 2530.

Quintana FJ, Basso AS, Iglesias AH, Korn T, Farez MF, Bettelli E, Caccamo M, Oukka M, Weiner HL. 2008. Control of T(reg) and T(H)17 cell differentiation by the aryl hydrocarbon receptor. *Nature* **453**: 65-71.

Rahemtullah A, Reichard KK, Preffer FI, Harris NL, Hasserjian RP. 2006. A double-positive CD4+CD8+ T-cell population is commonly found in nodular lymphocyte predominant Hodgkin lymphoma. *Am J Clin Pathol* **126**: 805-814.

Rai KR, Sawitsky A, Cronkite EP, Chanana AD, Levy RN, Pasternack BS. 1975. Clinical staging of chronic lymphocytic leukemia. *Blood* **46**: 219-234.

Rajasagi M, Shukla SA, Fritsch EF, Keskin DB, DeLuca D, Carmona E, Zhang W, Sougnez C, Cibulskis K, Sidney J et al. 2014. Systematic identification of personal tumor-specific neoantigens in chronic lymphocytic leukemia. *Blood* **124**: 453-462.

Ramsay AG, Clear AJ, Fatah R, Gribben JG. 2012. Multiple inhibitory ligands induce impaired T-cell immunologic synapse function in chronic lymphocytic leukemia that can be blocked with lenalidomide: establishing a reversible immune evasion mechanism in human cancer. *Blood* **120**: 1412-1421.

Ramsay AG, Johnson AJ, Lee AM, Gorgun G, Le Dieu R, Blum W, Byrd JC, Gribben JG. 2008. Chronic lymphocytic leukemia T cells show impaired immunological synapse formation that can be reversed with an immunomodulating drug. *J Clin Invest* **118**: 2427-2437.

Rassenti LZ, Huynh L, Toy TL, Chen L, Keating MJ, Gribben JG, Neuberg DS, Flinn IW, Rai KR, Byrd JC et al. 2004. ZAP-70 compared with immunoglobulin heavy-chain gene mutation status as a predictor of disease progression in chronic lymphocytic leukemia. *N Engl J Med* **351**: 893-901.

Rau FC, Dieter J, Luo Z, Priest SO, Baumgarth N. 2009. B7-1/2 (CD80/CD86) direct signaling to B cells enhances IgG secretion. *J Immunol* **183**: 7661-7671.

Redondo-Munoz J, Escobar-Diaz E, Samaniego R, Terol MJ, Garcia-Marco JA, Garcia-Pardo A. 2006. MMP-9 in B-cell chronic lymphocytic leukemia is up-regulated by alpha4beta1 integrin or CXCR4 engagement via distinct signaling pathways, localizes to podosomes, and is involved in cell invasion and migration. *Blood* **108**: 3143-3151.

Reittie JE, Yong KL, Panayiotidis P, Hoffbrand AV. 1996. Interleukin-6 inhibits apoptosis and tumour necrosis factor induced proliferation of B-chronic lymphocytic leukaemia. *Leuk Lymphoma* **22**: 83-90, follow 186, color plate VI.

Rendeiro AF, Krausgruber T, Fortelny N, Zhao F, Penz T, Farlik M, Schuster LC, Nemc A, Tasnady S, Reti M et al. 2020. Chromatin mapping and single-cell immune profiling define the temporal dynamics of ibrutinib response in CLL. *Nat Commun* **11**: 577.

Ribas A, Wolchok JD. 2018. Cancer immunotherapy using checkpoint blockade. *Science* **359**: 1350-1355.

Riches JC, Davies JK, McClanahan F, Fatah R, Iqbal S, Agrawal S, Ramsay AG, Gribben JG. 2013. T cells from CLL patients exhibit features of T-cell exhaustion but retain capacity for cytokine production. *Blood* **121**: 1612-1621.

Riches JC, Gribben JG. 2013. Understanding the immunodeficiency in chronic lymphocytic leukemia: potential clinical implications. *Hematol Oncol Clin North Am* **27**: 207-235.

Rilke F, Colnaghi MI, Cascinelli N, Andreola S, Baldini MT, Bufalino R, Della Porta G, Menard S, Pierotti MA, Testori A. 1991. Prognostic significance of HER-2/neu expression in breast cancer and its relationship to other prognostic factors. *Int J Cancer* **49**: 44-49.

Ringshausen I, Dechow T, Schneller F, Weick K, Oelsner M, Peschel C, Decker T. 2004. Constitutive activation of the MAPkinase p38 is critical for MMP-9 production and survival of B-CLL cells on bone marrow stromal cells. *Leukemia* **18**: 1964-1970.

Rodriguez PC, Ochoa AC. 2008. Arginine regulation by myeloid derived suppressor cells and tolerance in cancer: mechanisms and therapeutic perspectives. *Immunol Rev* **222**: 180-191.

Roessner PM, Cid LL, Lupar E, Roider T, Bordas M, Schifflers C, Gaupel A-C, Kilpert F, Krötschel M, Arnold SJ et al. 2020a. EOMES and IL-10 regulate anti-tumor activity of PD-1⁺ CD4⁺ T-cells in B-cell Non-Hodgkin lymphoma. *bioRxiv* doi:10.1101/2020.03.09.983098: 2020.2003.2009.983098.

Roessner PM, Hanna BS, Ozturk S, Schulz R, Llao Cid L, Yazdanparast H, Scheffold A, Colomer D, Stilgenbauer S, Lichter P et al. 2020b. TBET-expressing Th1 CD4(+) T cells accumulate in chronic lymphocytic leukaemia without affecting disease progression in Emicro-TCL1 mice. *Br J Haematol* **189**: 133-145.

Roider T, Seufert J, Uvarovskii A, Frauhammer F, Bordas M, Abedpour N, Stolarczyk M, Mallm JP, Herbst SA, Bruch PM et al. 2020. Dissecting intratumour heterogeneity of nodal B-cell lymphomas at the transcriptional, genetic and drug-response levels. *Nat Cell Biol* **22**: 896-906.

Romano M, Fanelli G, Albany CJ, Giganti G, Lombardi G. 2019. Past, Present, and Future of Regulatory T Cell Therapy in Transplantation and Autoimmunity. *Front Immunol* **10**: 43.

Romano MF, Lamberti A, Tassone P, Alfinito F, Costantini S, Chiurazzi F, Defrance T, Bonelli P, Tuccillo F, Turco MC et al. 1998. Triggering of CD40 antigen inhibits fludarabine-induced apoptosis in B chronic lymphocytic leukemia cells. *Blood* **92**: 990-995.

Roncarolo MG, Gregori S, Bacchetta R, Battaglia M. 2014. Tr1 cells and the counter-regulation of immunity: natural mechanisms and therapeutic applications. *Curr Top Microbiol Immunol* **380**: 39-68.

Roncarolo MG, Gregori S, Bacchetta R, Battaglia M, Gagliani N. 2018. The Biology of T Regulatory Type 1 Cells and Their Therapeutic Application in Immune-Mediated Diseases. *Immunity* **49**: 1004-1019.

Roncarolo MG, Yssel H, Touraine JL, Betuel H, De Vries JE, Spits H. 1988. Autoreactive T cell clones specific for class I and class II HLA antigens isolated from a human chimera. *J Exp Med* **167**: 1523-1534.

Rosenberg SA, Yang JC, Sherry RM, Kammula US, Hughes MS, Phan GQ, Citrin DE, Restifo NP, Robbins PF, Wunderlich JR et al. 2011. Durable complete responses in heavily pretreated patients with metastatic melanoma using T-cell transfer immunotherapy. *Clin Cancer Res* **17**: 4550-4557.

Rosenwald A, Alizadeh AA, Widhopf G, Simon R, Davis RE, Yu X, Yang L, Pickeral OK, Rassenti LZ, Powell J et al. 2001. Relation of gene expression phenotype to immunoglobulin mutation genotype in B cell chronic lymphocytic leukemia. *J Exp Med* **194**: 1639-1647.

Rossi D, Terzi-di-Bergamo L, De Paoli L, Cerri M, Ghilardi G, Chiarenza A, Bulian P, Visco C, Mauro FR, Morabito F et al. 2015. Molecular prediction of durable remission after first-line fludarabine-cyclophosphamide-rituximab in chronic lymphocytic leukemia. *Blood* **126**: 1921-1924.

Russo G, Isobe M, Gatti R, Finan J, Batuman O, Huebner K, Nowell PC, Croce CM. 1989. Molecular analysis of a t(14;14) translocation in leukemic T-cells of an ataxia telangiectasia patient. *Proc Natl Acad Sci U S A* **86**: 602-606.

Sade-Feldman M, Yizhak K, Bjorgaard SL, Ray JP, de Boer CG, Jenkins RW, Lieb DJ, Chen JH, Frederick DT, Barzily-Rokni M et al. 2018. Defining T Cell States Associated with Response to Checkpoint Immunotherapy in Melanoma. *Cell* **175**: 998-1013 e1020.

Sadik A, Somarribas Patterson LF, Ozturk S, Mohapatra SR, Panitz V, Secker PF, Pfander P, Loth S, Salem H, Prentzell MT et al. 2020. IL4I1 Is a Metabolic Immune Checkpoint that Activates the AHR and Promotes Tumor Progression. *Cell* **182**: 1252-1270 e1234.

Sahin U, Tureci O. 2018. Personalized vaccines for cancer immunotherapy. *Science* **359**: 1355-1360.

Sandberg JK, Fast NM, Nixon DF. 2001. Functional heterogeneity of cytokines and cytolytic effector molecules in human CD8+ T lymphocytes. *J Immunol* **167**: 181-187.

Sarrabayrouse G, Corvaisier M, Ouisse LH, Bossard C, Le Mevel B, Potiron L, Meurette G, Gervois N, Jotereau F. 2011. Tumor-reactive CD4+ CD8alphabeta+ CD103+ alphabetaT cells: a prevalent tumor-reactive T-cell subset in metastatic colorectal cancers. *Int J Cancer* **128**: 2923-2932.

Satpathy AT, Granja JM, Yost KE, Qi Y, Meschi F, McDermott GP, Olsen BN, Mumbach MR, Pierce SE, Corces MR et al. 2019. Massively parallel single-cell chromatin landscapes of human immune cell development and intratumoral T cell exhaustion. *Nat Biotechnol* **37**: 925-936.

Schaffner C, Stilgenbauer S, Rappold GA, Dohner H, Lichter P. 1999. Somatic ATM mutations indicate a pathogenic role of ATM in B-cell chronic lymphocytic leukemia. *Blood* **94**: 748-753.

Schatz DG, Oettinger MA, Baltimore D. 1989. The V(D)J recombination activating gene, RAG-1. *Cell* **59**: 1035-1048.

Schetter AJ, Heegaard NH, Harris CC. 2010. Inflammation and cancer: interweaving microRNA, free radical, cytokine and p53 pathways. *Carcinogenesis* **31**: 37-49.

Schietinger A, Philip M, Krisnawan VE, Chiu EY, Delrow JJ, Basom RS, Lauer P, Brockstedt DG, Knoblaugh SE, Hammerling GJ et al. 2016. Tumor-Specific T Cell Dysfunction Is a Dynamic Antigen-Driven Differentiation Program Initiated Early during Tumorigenesis. *Immunity* **45**: 389-401.

Schreiber RD, Old LJ, Smyth MJ. 2011. Cancer immunoediting: integrating immunity's roles in cancer suppression and promotion. *Science* **331**: 1565-1570.

Schreiber RD, Pace JL, Russell SW, Altman A, Katz DH. 1983. Macrophage-activating factor produced by a T cell hybridoma: physiochemical and biosynthetic resemblance to gamma-interferon. *J Immunol* **131**: 826-832.

Schulz A, Toedt G, Zenz T, Stilgenbauer S, Lichter P, Seiffert M. 2011. Inflammatory cytokines and signaling pathways are associated with survival of primary chronic lymphocytic leukemia cells in vitro: a dominant role of CCL2. *Haematologica* **96**: 408-416.

Schwanhausser B, Busse D, Li N, Dittmar G, Schuchhardt J, Wolf J, Chen W, Selbach M. 2011. Global quantification of mammalian gene expression control. *Nature* **473**: 337-342.

Scielzo C, Bertilaccio MT, Simonetti G, Dagklis A, ten Hacken E, Fazi C, Muzio M, Caiolfa V, Kitamura D, Restuccia U et al. 2010. HS1 has a central role in the trafficking and homing of leukemic B cells. *Blood* **116**: 3537-3546.

Scurr M, Ladell K, Besneux M, Christian A, Hockey T, Smart K, Bridgeman H, Hargest R, Phillips S, Davies M et al. 2014. Highly prevalent colorectal cancer-infiltrating LAP(+) Foxp3(-) T cells exhibit more potent immunosuppressive activity than Foxp3(+) regulatory T cells. *Mucosal Immunol* **7**: 428-439.

Secchiero P, Tiribelli M, Barbarotto E, Celeghini C, Michelutti A, Masolini P, Fanin R, Zauli G. 2005. Aberrant expression of TRAIL in B chronic lymphocytic leukemia (B-CLL) cells. *J Cell Physiol* **205**: 246-252.

Seifert M, Sellmann L, Bloehdorn J, Wein F, Stilgenbauer S, Durig J, Kuppers R. 2012. Cellular origin and pathophysiology of chronic lymphocytic leukemia. *J Exp Med* **209**: 2183-2198.

Seiffert M, Schulz A, Ohl S, Dohner H, Stilgenbauer S, Lichter P. 2010. Soluble CD14 is a novel monocyte-derived survival factor for chronic lymphocytic leukemia cells, which is induced by CLL cells in vitro and present at abnormally high levels in vivo. *Blood* **116**: 4223-4230.

Serrano D, Monteiro J, Allen SL, Kolitz J, Schulman P, Lichtman SM, Buchbinder A, Vinciguerra VP, Chiorazzi N, Gregersen PK. 1997. Clonal expansion within the CD4+CD57+ and CD8+CD57+ T cell subsets in chronic lymphocytic leukemia. *J Immunol* **158**: 1482-1489.

Shanafelt TD, Geyer SM, Bone ND, Tschumper RC, Witzig TE, Nowakowski GS, Zent CS, Call TG, Laplant B, Dewald GW et al. 2008. CD49d expression is an independent predictor of overall survival in patients with chronic lymphocytic leukaemia: a prognostic parameter with therapeutic potential. *Br J Haematol* **140**: 537-546.

Shankaran V, Ikeda H, Bruce AT, White JM, Swanson PE, Old LJ, Schreiber RD. 2001. IFNgamma and lymphocytes prevent primary tumour development and shape tumour immunogenicity. *Nature* **410**: 1107-1111.

Shapiro-Shelef M, Calame K. 2005. Regulation of plasma-cell development. *Nat Rev Immunol* **5**: 230-242.

Sharma P, Allison JP. 2015. The future of immune checkpoint therapy. *Science* **348**: 56-61.

Sharma S, Rai KR. 2019. Chronic lymphocytic leukemia (CLL) treatment: So many choices, such great options. *Cancer* **125**: 1432-1440.

Sheil AG. 1986. Cancer after transplantation. *World J Surg* **10**: 389-396.

Shinkai Y, Rathbun G, Lam KP, Oltz EM, Stewart V, Mendelsohn M, Charron J, Datta M, Young F, Stall AM et al. 1992. RAG-2-deficient mice lack mature lymphocytes owing to inability to initiate V(D)J rearrangement. *Cell* **68**: 855-867.

Shukla V, Ma S, Hardy RR, Joshi SS, Lu R. 2013. A role for IRF4 in the development of CLL. *Blood* **122**: 2848-2855.

Siddiqui I, Schaeuble K, Chennupati V, Fuertes Marraco SA, Calderon-Copete S, Pais Ferreira D, Carmona SJ, Scarpellino L, Gfeller D, Pradervand S et al. 2019. Intratumoral Tcf1(+)PD-1(+)CD8(+) T Cells with Stem-like Properties Promote Tumor Control in Response to Vaccination and Checkpoint Blockade Immunotherapy. *Immunity* **50**: 195-211 e110.

Simonetti G, Bertilaccio MT, Ghia P, Klein U. 2014. Mouse models in the study of chronic lymphocytic leukemia pathogenesis and therapy. *Blood* **124**: 1010-1019.

Simoni Y, Becht E, Fehlings M, Loh CY, Koo SL, Teng KWW, Yeong JPS, Nahar R, Zhang T, Kared H et al. 2018. Bystander CD8(+) T cells are abundant and phenotypically distinct in human tumour infiltrates. *Nature* **557**: 575-579.

Slack GW. 2016. The Pathology of Reactive Lymphadenopathies: A Discussion of Common Reactive Patterns and Their Malignant Mimics. *Arch Pathol Lab Med* **140**: 881-892.

Slager SL, Skibola CF, Di Bernardo MC, Conde L, Broderick P, McDonnell SK, Goldin LR, Croft N, Holroyd A, Harris S et al. 2012. Common variation at 6p21.31 (BAK1) influences the risk of chronic lymphocytic leukemia. *Blood* **120**: 843-846.

Smyth MJ, Cretney E, Takeda K, Wiltrout RH, Sedger LM, Kayagaki N, Yagita H, Okumura K. 2001. Tumor necrosis factor-related apoptosis-inducing ligand (TRAIL) contributes to interferon gamma-dependent natural killer cell protection from tumor metastasis. *J Exp Med* **193**: 661-670.

Smyth MJ, Dunn GP, Schreiber RD. 2006. Cancer immunosurveillance and immunoediting: the roles of immunity in suppressing tumor development and shaping tumor immunogenicity. *Adv Immunol* **90**: 1-50.

Song Z, Zhang T, Li G, Tang Y, Luo Y, Yu G. 2018. Tr1 responses are elevated in asymptomatic H. pylori-infected individuals and are functionally impaired in H. pylori-gastric cancer patients. *Exp Cell Res* **367**: 251-256.

Speedy HE, Beekman R, Chapaprieta V, Orlando G, Law PJ, Martin-Garcia D, Gutierrez-Abril J, Catovsky D, Bea S, Clot G et al. 2019. Insight into genetic predisposition to chronic lymphocytic leukemia from integrative epigenomics. *Nat Commun* **10**: 3615.

Speedy HE, Di Bernardo MC, Sava GP, Dyer MJ, Holroyd A, Wang Y, Sunter NJ, Mansouri L, Juliusson G, Smedby KE et al. 2014. A genome-wide association study identifies multiple susceptibility loci for chronic lymphocytic leukemia. *Nat Genet* **46**: 56-60.

Speiser DE, Utzschneider DT, Oberle SG, Munz C, Romero P, Zehn D. 2014. T cell differentiation in chronic infection and cancer: functional adaptation or exhaustion? *Nat Rev Immunol* **14**: 768-774.

Spencer SD, Di Marco F, Hooley J, Pitts-Meek S, Bauer M, Ryan AM, Sordat B, Gibbs VC, Aguet M. 1998. The orphan receptor CRF2-4 is an essential subunit of the interleukin 10 receptor. *J Exp Med* **187**: 571-578.

Stall AM, Farinas MC, Tarlinton DM, Lalor PA, Herzenberg LA, Strober S, Herzenberg LA. 1988. Ly-1 B-cell clones similar to human chronic lymphocytic leukemias routinely develop in older normal mice and young autoimmune (New Zealand Black-related) animals. *Proc Natl Acad Sci U S A* **85**: 7312-7316.

Stamatopoulos K, Agathangelidis A, Rosenquist R, Ghia P. 2017. Antigen receptor stereotypy in chronic lymphocytic leukemia. *Leukemia* **31**: 282-291.

Stamatopoulos K, Belessi C, Moreno C, Boudjograh M, Guida G, Smilevska T, Belhoul L, Stella S, Stavroyianni N, Crespo M et al. 2007. Over 20% of patients with chronic lymphocytic leukemia carry stereotyped receptors: Pathogenetic implications and clinical correlations. *Blood* **109**: 259-270.

Stankovic T, Skowronska A. 2014. The role of ATM mutations and 11q deletions in disease progression in chronic lymphocytic leukemia. *Leuk Lymphoma* **55**: 1227-1239.

Stein JV, Lopez-Fraga M, Elustondo FA, Carvalho-Pinto CE, Rodriguez D, Gomez-Caro R, De Jong J, Martinez AC, Medema JP, Hahne M. 2002. APRIL modulates B and T cell immunity. *J Clin Invest* **109**: 1587-1598.

Stevenson FK, Krysov S, Davies AJ, Steele AJ, Packham G. 2011. B-cell receptor signaling in chronic lymphocytic leukemia. *Blood* **118**: 4313-4320.

Stilgenbauer S, Zenz T, Winkler D, Buhler A, Schlenk RF, Groner S, Busch R, Hensel M, Duhrsen U, Finke J et al. 2009. Subcutaneous alemtuzumab in fludarabine-refractory chronic lymphocytic leukemia: clinical results and prognostic marker analyses from the CLL2H study of the German Chronic Lymphocytic Leukemia Study Group. *J Clin Oncol* **27**: 3994-4001.

Strati P, Abruzzo LV, Wierda WG, O'Brien S, Ferrajoli A, Keating MJ. 2015. Second cancers and Richter transformation are the leading causes of death in patients with trisomy 12 chronic lymphocytic leukemia. *Clin Lymphoma Myeloma Leuk* **15**: 420-427.

Strati P, Shanafelt TD. 2015. Monoclonal B-cell lymphocytosis and early-stage chronic lymphocytic leukemia: diagnosis, natural history, and risk stratification. *Blood* **126**: 454-462.

Street SE, Cretney E, Smyth MJ. 2001. Perforin and interferon-gamma activities independently control tumor initiation, growth, and metastasis. *Blood* **97**: 192-197.

Strid J, Roberts SJ, Filler RB, Lewis JM, Kwong BY, Schpero W, Kaplan DH, Hayday AC, Girardi M. 2008. Acute upregulation of an NKG2D ligand promotes rapid reorganization of a local immune compartment with pleiotropic effects on carcinogenesis. *Nat Immunol* **9**: 146-154.

Stuart T, Butler A, Hoffman P, Hafemeister C, Papalexi E, Mauck WM, 3rd, Hao Y, Stoeckius M, Smibert P, Satija R. 2019. Comprehensive Integration of Single-Cell Data. *Cell* **177**: 1888-1902 e1821.

Suvas S, Singh V, Sahdev S, Vohra H, Agrewala JN. 2002. Distinct role of CD80 and CD86 in the regulation of the activation of B cell and B cell lymphoma. *J Biol Chem* **277**: 7766-7775.

Swerdlow SH. 2017. *WHO classification of tumours of haematopoietic and lymphoid tissues*.

Swerdlow SH, Campo E, Pileri SA, Harris NL, Stein H, Siebert R, Advani R, Ghielmini M, Salles GA, Zelenetz AD et al. 2016. The 2016 revision of the World Health Organization classification of lymphoid neoplasms. *Blood* **127**: 2375-2390.

Szabo PA, Levitin HM, Miron M, Snyder ME, Senda T, Yuan J, Cheng YL, Bush EC, Dogra P, Thapa P et al. 2019. Single-cell transcriptomics of human T cells reveals tissue and activation signatures in health and disease. *Nat Commun* **10**: 4706.

Taghiloo S, Allahmoradi E, Tehrani M, Hossein-Nataj H, Shekarriz R, Janbabaei G, Abediankenari S, Asgarian-Omran H. 2017. Frequency and functional characterization of exhausted CD8(+) T cells in chronic lymphocytic leukemia. *Eur J Haematol* **98**: 622-631.

Tai YT, Horton HM, Kong SY, Pong E, Chen H, Cemerski S, Bernett MJ, Nguyen DH, Karki S, Chu SY et al. 2012. Potent in vitro and in vivo activity of an Fc-engineered humanized anti-HM1.24 antibody against multiple myeloma via augmented effector function. *Blood* **119**: 2074-2082.

Takai A, Toyoshima T, Uemura M, Kitawaki Y, Marusawa H, Hiai H, Yamada S, Okazaki IM, Honjo T, Chiba T et al. 2009. A novel mouse model of hepatocarcinogenesis triggered by AID causing deleterious p53 mutations. *Oncogene* **28**: 469-478.

Takeda K, Hayakawa Y, Smyth MJ, Kayagaki N, Yamaguchi N, Kakuta S, Iwakura Y, Yagita H, Okumura K. 2001. Involvement of tumor necrosis factor-related apoptosis-inducing ligand in surveillance of tumor metastasis by liver natural killer cells. *Nat Med* **7**: 94-100.

Tang J, Zha J, Guo X, Shi P, Xu B. 2017. CXCR5(+)CD8(+) T cells present elevated capacity in mediating cytotoxicity toward autologous tumor cells through interleukin 10 in diffuse large B-cell lymphoma. *Int Immunopharmacol* **50**: 146-151.

Teijaro JR, Ng C, Lee AM, Sullivan BM, Sheehan KC, Welch M, Schreiber RD, de la Torre JC, Oldstone MB. 2013. Persistent LCMV infection is controlled by blockade of type I interferon signaling. *Science* **340**: 207-211.

Ten Hacken E, Burger JA. 2016. Microenvironment interactions and B-cell receptor signaling in Chronic Lymphocytic Leukemia: Implications for disease pathogenesis and treatment. *Biochim Biophys Acta* **1863**: 401-413.

Terabe M, Berzofsky JA. 2004. Immunoregulatory T cells in tumor immunity. *Curr Opin Immunol* **16**: 157-162.

The BLUEPRINT Consortium. 2016. Blueprint Epigenome. Vol 2020.

Thomas S, Prendergast GC. 2016. Cancer Vaccines: A Brief Overview. *Methods Mol Biol* **1403**: 755-761.

Thommen DS, Koelzer VH, Herzig P, Roller A, Trefny M, Dimeloe S, Kiialainen A, Hanhart J, Schill C, Hess C et al. 2018. A transcriptionally and functionally distinct PD-1(+) CD8(+)

T cell pool with predictive potential in non-small-cell lung cancer treated with PD-1 blockade. *Nat Med* **24**: 994-1004.

Tibbitt CA, Stark JM, Martens L, Ma J, Mold JE, Deswarte K, Oliynyk G, Feng X, Lambrecht BN, De Bleser P et al. 2019. Single-Cell RNA Sequencing of the T Helper Cell Response to House Dust Mites Defines a Distinct Gene Expression Signature in Airway Th2 Cells. *Immunity* **51**: 169-184 e165.

Tinoco R, Alcalde V, Yang Y, Sauer K, Zuniga EI. 2009. Cell-intrinsic transforming growth factor-beta signaling mediates virus-specific CD8+ T cell deletion and viral persistence in vivo. *Immunity* **31**: 145-157.

Tirosh I, Izar B, Prakadan SM, Wadsworth MH, 2nd, Treacy D, Trombetta JJ, Rotem A, Rodman C, Lian C, Murphy G et al. 2016. Dissecting the multicellular ecosystem of metastatic melanoma by single-cell RNA-seq. *Science* **352**: 189-196.

Tobin G, Thunberg U, Karlsson K, Murray F, Laurell A, Willander K, Enblad G, Merup M, Vilpo J, Juliusson G et al. 2004. Subsets with restricted immunoglobulin gene rearrangement features indicate a role for antigen selection in the development of chronic lymphocytic leukemia. *Blood* **104**: 2879-2885.

Topalian SL, Hodi FS, Brahmer JR, Gettinger SN, Smith DC, McDermott DF, Powderly JD, Carvajal RD, Sosman JA, Atkins MB et al. 2012. Safety, activity, and immune correlates of anti-PD-1 antibody in cancer. *N Engl J Med* **366**: 2443-2454.

Torisu H, Ono M, Kiryu H, Furue M, Ohmoto Y, Nakayama J, Nishioka Y, Sone S, Kuwano M. 2000. Macrophage infiltration correlates with tumor stage and angiogenesis in human malignant melanoma: possible involvement of TNFalpha and IL-1alpha. *Int J Cancer* **85**: 182-188.

Totterman TH, Carlsson M, Simonsson B, Bengtsson M, Nilsson K. 1989. T-cell activation and subset patterns are altered in B-CLL and correlate with the stage of the disease. *Blood* **74**: 786-792.

Tree TI, Lawson J, Edwards H, Skowera A, Arif S, Roep BO, Peakman M. 2010. Naturally arising human CD4 T-cells that recognize islet autoantigens and secrete interleukin-10 regulate proinflammatory T-cell responses via linked suppression. *Diabetes* **59**: 1451-1460.

Trentin L, Cerutti A, Zambello R, Sancretta R, Tassinari C, Facco M, Adami F, Rodeghiero F, Agostini C, Semenzato G. 1996. Interleukin-15 promotes the growth of leukemic cells of patients with B-cell chronic lymphoproliferative disorders. *Blood* **87**: 3327-3335.

Troeger A, Johnson AJ, Wood J, Blum WG, Andritsos LA, Byrd JC, Williams DA. 2012. RhoH is critical for cell-microenvironment interactions in chronic lymphocytic leukemia in mice and humans. *Blood* **119**: 4708-4718.

Tsukada N, Burger JA, Zvaifler NJ, Kipps TJ. 2002. Distinctive features of "nurselike" cells that differentiate in the context of chronic lymphocytic leukemia. *Blood* **99**: 1030-1037.

Turtle CJ, Hay KA, Hanafi LA, Li D, Cherian S, Chen X, Wood B, Lozanski A, Byrd JC, Heimfeld S et al. 2017. Durable Molecular Remissions in Chronic Lymphocytic Leukemia Treated With CD19-Specific Chimeric Antigen Receptor-Modified T Cells After Failure of Ibrutinib. *J Clin Oncol* **35**: 3010-3020.

Tzankov A, Dirnhofer S. 2018. A pattern-based approach to reactive lymphadenopathies. *Semin Diagn Pathol* **35**: 4-19.

Utzschneider DT, Charmoy M, Chennupati V, Pousse L, Ferreira DP, Calderon-Copete S, Danilo M, Alfei F, Hofmann M, Wieland D et al. 2016. T Cell Factor 1-Expressing Memory-like CD8(+) T Cells Sustain the Immune Response to Chronic Viral Infections. *Immunity* **45**: 415-427.

van der Leun AM, Thommen DS, Schumacher TN. 2020. CD8(+) T cell states in human cancer: insights from single-cell analysis. *Nat Rev Cancer* **20**: 218-232.

Van Gassen S, Callebaut B, Van Helden MJ, Lambrecht BN, Demeester P, Dhaene T, Saeys Y. 2015. FlowSOM: Using self-organizing maps for visualization and interpretation of cytometry data. *Cytometry A* **87**: 636-645.

van Gent R, Kater AP, Otto SA, Jaspers A, Borghans JA, Vrisekoop N, Ackermans MA, Ruiter AF, Wittebol S, Eldering E et al. 2008. In vivo dynamics of stable chronic lymphocytic

leukemia inversely correlate with somatic hypermutation levels and suggest no major leukemic turnover in bone marrow. *Cancer Res* **68**: 10137-10144.

Vardi A, Agathangelidis A, Sutton LA, Ghia P, Rosenquist R, Stamatopoulos K. 2014. Immunogenetic studies of chronic lymphocytic leukemia: revelations and speculations about ontogeny and clinical evolution. *Cancer Res* **74**: 4211-4216.

Vardi A, Vlachonikola E, Karypidou M, Stalika E, Bikos V, Gemenetzi K, Maramis C, Siorenta A, Anagnostopoulos A, Pospisilova S et al. 2017. Restrictions in the T-cell repertoire of chronic lymphocytic leukemia: high-throughput immunoprofiling supports selection by shared antigenic elements. *Leukemia* **31**: 1555-1561.

Vento-Tormo R, Efremova M, Botting RA, Turco MY, Vento-Tormo M, Meyer KB, Park JE, Stephenson E, Polanski K, Goncalves A et al. 2018. Single-cell reconstruction of the early maternal-fetal interface in humans. *Nature* **563**: 347-353.

Vesely MD, Kershaw MH, Schreiber RD, Smyth MJ. 2011. Natural innate and adaptive immunity to cancer. *Annu Rev Immunol* **29**: 235-271.

Victora GD, Nussenzweig MC. 2012. Germinal centers. *Annu Rev Immunol* **30**: 429-457.

Vincent AM, Cawley JC, Burthem J. 1996. Integrin function in chronic lymphocytic leukemia. *Blood* **87**: 4780-4788.

Vinuesa CG, Linterman MA, Yu D, MacLennan IC. 2016. Follicular Helper T Cells. *Annu Rev Immunol* **34**: 335-368.

Vogler M, Butterworth M, Majid A, Walewska RJ, Sun XM, Dyer MJ, Cohen GM. 2009. Concurrent up-regulation of BCL-XL and BCL2A1 induces approximately 1000-fold resistance to ABT-737 in chronic lymphocytic leukemia. *Blood* **113**: 4403-4413.

Wagner J, Rapsomaniki MA, Chevrier S, Anzeneder T, Langwieder C, Dykgers A, Rees M, Ramaswamy A, Muenst S, Soysal SD et al. 2019. A Single-Cell Atlas of the Tumor and Immune Ecosystem of Human Breast Cancer. *Cell* **177**: 1330-1345 e1318.

Wan YY, Flavell RA. 2005. Identifying Foxp3-expressing suppressor T cells with a bicistronic reporter. *Proc Natl Acad Sci U S A* **102**: 5126-5131.

Wang L, Lawrence MS, Wan Y, Stojanov P, Sougnez C, Stevenson K, Werner L, Sivachenko A, DeLuca DS, Zhang L et al. 2011. SF3B1 and other novel cancer genes in chronic lymphocytic leukemia. *N Engl J Med* **365**: 2497-2506.

Wang W, Nishioka Y, Ozaki S, Jalili A, Abe S, Kakiuchi S, Kishuku M, Minakuchi K, Matsumoto T, Sone S. 2009. HM1.24 (CD317) is a novel target against lung cancer for immunotherapy using anti-HM1.24 antibody. *Cancer Immunol Immunother* **58**: 967-976.

Wang Y, Liu J, Burrows PD, Wang JY. 2020. B Cell Development and Maturation. *Adv Exp Med Biol* **1254**: 1-22.

Wardemann H, Yurasov S, Schaefer A, Young JW, Meffre E, Nussenzweig MC. 2003. Predominant autoantibody production by early human B cell precursors. *Science* **301**: 1374-1377.

Wattel E, Preudhomme C, Hecquet B, Vanrumbeke M, Quesnel B, Dervite I, Morel P, Fenaux P. 1994. p53 mutations are associated with resistance to chemotherapy and short survival in hematologic malignancies. *Blood* **84**: 3148-3157.

Wculek SK, Cueto FJ, Mujal AM, Melero I, Krummel MF, Sancho D. 2020. Dendritic cells in cancer immunology and immunotherapy. *Nat Rev Immunol* **20**: 7-24.

Weulersse M, Asrir A, Pichler AC, Lemaitre L, Braun M, Carrie N, Joubert MV, Le Moine M, Do Souto L, Gaud G et al. 2020. Eomes-Dependent Loss of the Co-activating Receptor CD226 Restrains CD8(+) T Cell Anti-tumor Functions and Limits the Efficacy of Cancer Immunotherapy. *Immunity* **53**: 824-839 e810.

Wherry EJ. 2011. T cell exhaustion. *Nat Immunol* **12**: 492-499.

Wherry EJ, Ahmed R. 2004. Memory CD8 T-cell differentiation during viral infection. *J Virol* **78**: 5535-5545.

Wherry EJ, Ha SJ, Kaech SM, Haining WN, Sarkar S, Kalia V, Subramaniam S, Blattman JN, Barber DL, Ahmed R. 2007. Molecular signature of CD8+ T cell exhaustion during chronic viral infection. *Immunity* **27**: 670-684.

Wierz M, Pierson S, Guyonnet L, Viry E, Lequeux A, Oudin A, Niclou SP, Ollert M, Berchem G, Janji B et al. 2018. Dual PD1/LAG3 immune checkpoint blockade limits tumor

development in a murine model of chronic lymphocytic leukemia. *Blood* **131**: 1617-1621.

Wikenheiser DJ, Stumhofer JS. 2016. ICOS Co-Stimulation: Friend or Foe? *Front Immunol* **7**: 304.

Wilkerson MD, Hayes DN. 2010. ConsensusClusterPlus: a class discovery tool with confidence assessments and item tracking. *Bioinformatics* **26**: 1572-1573.

Williams MA, Bevan MJ. 2007. Effector and memory CTL differentiation. *Annu Rev Immunol* **25**: 171-192.

Wilson EB, Yamada DH, Elsaesser H, Herskovitz J, Deng J, Cheng G, Aronow BJ, Karp CL, Brooks DG. 2013. Blockade of chronic type I interferon signaling to control persistent LCMV infection. *Science* **340**: 202-207.

Woyach JA, Smucker K, Smith LL, Lozanski A, Zhong Y, Ruppert AS, Lucas D, Williams K, Zhao W, Rassenti L et al. 2014. Prolonged lymphocytosis during ibrutinib therapy is associated with distinct molecular characteristics and does not indicate a suboptimal response to therapy. *Blood* **123**: 1810-1817.

Wu J, Xu X, Lee EJ, Shull AY, Pei L, Awan F, Wang X, Choi JH, Deng L, Xin HB et al. 2016a. Phenotypic alteration of CD8+ T cells in chronic lymphocytic leukemia is associated with epigenetic reprogramming. *Oncotarget* **7**: 40558-40570.

Wu T, Ji Y, Moseman EA, Xu HC, Manglani M, Kirby M, Anderson SM, Handon R, Kenyon E, Elkahloun A et al. 2016b. The TCF1-Bcl6 axis counteracts type I interferon to repress exhaustion and maintain T cell stemness. *Sci Immunol* **1**.

Yan H, Zhang P, Kong X, Hou X, Zhao L, Li T, Yuan X, Fu H. 2017. Primary Tr1 cells from metastatic melanoma eliminate tumor-promoting macrophages through granzyme B- and perforin-dependent mechanisms. *Tumour Biol* **39**: 1010428317697554.

Yan XJ, Albesiano E, Zanesi N, Yancopoulos S, Sawyer A, Romano E, Petlickovski A, Efremov DG, Croce CM, Chiorazzi N. 2006. B cell receptors in TCL1 transgenic mice resemble those of aggressive, treatment-resistant human chronic lymphocytic leukemia. *Proc Natl Acad Sci U S A* **103**: 11713-11718.

Yao C, Sun HW, Lacey NE, Ji Y, Moseman EA, Shih HY, Heuston EF, Kirby M, Anderson S, Cheng J et al. 2019. Single-cell RNA-seq reveals TOX as a key regulator of CD8(+) T cell persistence in chronic infection. *Nat Immunol* **20**: 890-901.

Yin S, Gambe RG, Sun J, Martinez AZ, Cartun ZJ, Regis FFD, Wan Y, Fan J, Brooks AN, Herman SEM et al. 2019. A Murine Model of Chronic Lymphocytic Leukemia Based on B Cell-Restricted Expression of Sf3b1 Mutation and Atm Deletion. *Cancer Cell* **35**: 283-296 e285.

Yoshinaga SK, Whoriskey JS, Khare SD, Sarmiento U, Guo J, Horan T, Shih G, Zhang M, Coccia MA, Kohno T et al. 1999. T-cell co-stimulation through B7RP-1 and ICOS. *Nature* **402**: 827-832.

Yoshinaga SK, Zhang M, Pistillo J, Horan T, Khare SD, Miner K, Sonnenberg M, Boone T, Brankow D, Dai T et al. 2000. Characterization of a new human B7-related protein: B7RP-1 is the ligand to the co-stimulatory protein ICOS. *Int Immunol* **12**: 1439-1447.

Yosifov DY, Wolf C, Stilgenbauer S, Mertens D. 2019. From Biology to Therapy: The CLL Success Story. *Hemasphere* **3**: e175.

Yost KE, Satpathy AT, Wells DK, Qi Y, Wang C, Kageyama R, McNamara KL, Granja JM, Sarin KY, Brown RA et al. 2019. Clonal replacement of tumor-specific T cells following PD-1 blockade. *Nat Med* **25**: 1251-1259.

Younes A, Brody J, Carpio C, Lopez-Guillermo A, Ben-Yehuda D, Ferhanoglu B, Nagler A, Ozcan M, Avivi I, Bosch F et al. 2019. Safety and activity of ibrutinib in combination with nivolumab in patients with relapsed non-Hodgkin lymphoma or chronic lymphocytic leukaemia: a phase 1/2a study. *Lancet Haematol* **6**: e67-e78.

Yu D, Ye L. 2018. A Portrait of CXCR5(+) Follicular Cytotoxic CD8(+) T cells. *Trends Immunol* **39**: 965-979.

Yu H, Pardoll D, Jove R. 2009. STATs in cancer inflammation and immunity: a leading role for STAT3. *Nat Rev Cancer* **9**: 798-809.

Yukawa M, Jagannathan S, Vallabh S, Kartashov AV, Chen X, Weirauch MT, Barski A. 2020. AP-1 activity induced by co-stimulation is required for chromatin opening during T cell activation. *J Exp Med* **217**.

Zaborsky N, Gassner FJ, Hopner JP, Schubert M, Hebenstreit D, Stark R, Asslaber D, Steiner M, Geisberger R, Greil R et al. 2019. Exome sequencing of the TCL1 mouse model for CLL reveals genetic heterogeneity and dynamics during disease development. *Leukemia* **33**: 957-968.

Zapata JM, Krajewska M, Morse HC, 3rd, Choi Y, Reed JC. 2004. TNF receptor-associated factor (TRAF) domain and Bcl-2 cooperate to induce small B cell lymphoma/chronic lymphocytic leukemia in transgenic mice. *Proc Natl Acad Sci U S A* **101**: 16600-16605.

Zemmour D, Zilionis R, Kiner E, Klein AM, Mathis D, Benoist C. 2018. Single-cell gene expression reveals a landscape of regulatory T cell phenotypes shaped by the TCR. *Nat Immunol* **19**: 291-301.

Zenz T, Mertens D, Kuppers R, Dohner H, Stilgenbauer S. 2010. From pathogenesis to treatment of chronic lymphocytic leukaemia. *Nat Rev Cancer* **10**: 37-50.

Zhang F, Zhou X, DiSpirito JR, Wang C, Wang Y, Shen H. 2014. Epigenetic manipulation restores functions of defective CD8(+) T cells from chronic viral infection. *Mol Ther* **22**: 1698-1706.

Zhang J, Marotel M, Fauteux-Daniel S, Mathieu AL, Viel S, Marcais A, Walzer T. 2018a. T-bet and Eomes govern differentiation and function of mouse and human NK cells and ILC1. *Eur J Immunol* **48**: 738-750.

Zhang L, Yu X, Zheng L, Zhang Y, Li Y, Fang Q, Gao R, Kang B, Zhang Q, Huang JY et al. 2018b. Lineage tracking reveals dynamic relationships of T cells in colorectal cancer. *Nature* **564**: 268-272.

Zhang P, Lee JS, Gartlan KH, Schuster IS, Comerford I, Varelias A, Ullah MA, Vuckovic S, Koyama M, Kuns RD et al. 2017. Eomesodermin promotes the development of type 1 regulatory T (TR1) cells. *Sci Immunol* **2**.

Zhang Y, Huang S, Gong D, Qin Y, Shen Q. 2010. Programmed death-1 upregulation is correlated with dysfunction of tumor-infiltrating CD8+ T lymphocytes in human non-small cell lung cancer. *Cell Mol Immunol* **7**: 389-395.

Zheng C, Zheng L, Yoo JK, Guo H, Zhang Y, Guo X, Kang B, Hu R, Huang JY, Zhang Q et al. 2017. Landscape of Infiltrating T Cells in Liver Cancer Revealed by Single-Cell Sequencing. *Cell* **169**: 1342-1356 e1316.

Zhu J, Paul WE. 2008. CD4 T cells: fates, functions, and faults. *Blood* **112**: 1557-1569.

Zhu J, Yamane H, Paul WE. 2010. Differentiation of effector CD4 T cell populations (*). *Annu Rev Immunol* **28**: 445-489.

Zurli V, Wimmer G, Cattaneo F, Candi V, Cencini E, Gozzetti A, Raspadori D, Campoccia G, Sanseviero F, Bocchia M et al. 2017. Ectopic ILT3 controls BCR-dependent activation of Akt in B-cell chronic lymphocytic leukemia. *Blood* **130**: 2006-2017.

9 Acknowledgments

This project would not have come to a conclusion without the valuable contribution of many people, whom I would like to acknowledge accordingly.

First, I would like to express my deepest gratitude to Dr. Martina Seiffert, for her direct supervision and ongoing support throughout my PhD studies. Her tremendous knowledge coupled with her excellent guidance, constructive input and trust were of immense help for the development of this work. Moreover, her honesty and positive spirit crucially foster a fantastic working atmosphere in the team. To me, she represents a role model, whose high standards on both a scientific and a professional level, I aim to follow in my future career.

I would also like to extend my sincere thanks to Prof. Dr. Peter Lichter, for giving me the opportunity to perform my PhD work in his Division and thus be part of this team of outstanding scientists. He was always willing to share scientific and strategic advice, for which I am truly thankful for.

It was a great pleasure to join forces with Dr. Yashna Paul and later Dr. Murat Iskar to bring the single-cell project to life. I highly appreciate their enthusiastic commitment and invaluable bioinformatic expertise, which were essential for the development of the project. At the same time, I would like to thank Dr. Marc Zapatka for his patience and essential contributions to the project.

Furthermore, I would like to further thank our collaborators Prof. Dr. Elias Campo, Dr. Dolors Colomer, Dr. José Ignacio Martín, and Dr. Vicente Chapaprieta from the Hospital Clínic of Barcleona, and Dr. Sascha Dietrich and Dr. Tobias Roider from the University Clinic of Heidelberg, not only for the precious samples and analyses they provided, but also for their wholehearted and knowledgeable discussions. Of equal importance was the time and effort invested by Dr. Marina Wierz, Dr. Jérôme Paggetti, and Dr. Etienne Moussay from the Luxembourg Institute of Heath, as well as Dr. Ekaterina Lupar and Dr. Ana Izcue from the Max-Plank Institute in Freiburg in the single-cell and T_R1 projects, respectively. It was a pleasure to stablish such fruitful collaborations with all of them.

I would like to offer my special thanks to Prof. Dr. Stefan Wiemann, and Dr. Sascha Dietrich for their valuable input and scientific discussions as part of my Thesis Advisory Committee. Likewise, I would like to thank Prof. Dr. Stefan Wiemann, Dr. Michael Milsom, and Prof. Dr.

Rüdiger Hell for their willingness to evaluate and discuss my PhD thesis as part of my examination committee.

With respect to the scientific and practical support, I would like to emphasize the contribution of Verena Kalter, Norman Mack and Sybille Ohl who efficiently provided essential technical assistance during the course of this project. Similarly, I highly value the role of Frauke Devens, Petra Schröter, Magdalena Schlotter, Andrea Wittmann, and Achim Stephan for their eagerness to assist and efficiently manage the laboratory; and the skillful and essential IT support provided by Michael Hain. I would like to further thank Dr. Jan-Philipp Mallm, Dr. Michelle Liberio and Katharina Bauer from the ScOpenLab for their incredible support with the single-cell RNA-seq experiments. Equally important was the role of Dr. Steffen Schmitt, Dr. Marcus Eich, Klaus Hexel, Tobias Rubner, Florian Blum, and Daniel Sanzio Gimenes da Cruz from the Flow Cytometry Core Facility in providing very valuable flow cytometry and sorting trainings, and in maintaining such a high-standard facility; as well as the DKFZ Animal Facility for their relevant work in everyday care and breeding of mice. I would like to also thank Dr. Angela Schulz and the rest of the team from the High Throughput Sequencing Core Facility at the DKFZ, for providing excellent advice and services.

I am very grateful to all the present and previous CLL group members Dr. Philipp Rößner, Dr. Selcen Ötürk, Dr. Lena Jassowicz, Dr. Bola Hanna, Dr. Ralph Schulz, Dr. Lavinia Arseni, Dr. Ebru Aydin, Marie Bordas, Mariana Coelho Mendes Martines, Dr. Franziska Haderk, Dr. Ibrahim Murathan Sektioglu, Dr. Haniyeh Yazdanparast, Cansu Eris, Lok Lam Ngai, Ramy Girgis, and Dr. Ann-Christin Gaupel for their generous contributions to this work, both at the practical and theoretical level, and for their supportive and cheerful attitude all along. I also would like to thank all current and former members of the B060/ B06X divisions, including Michael Periscke, Jasmin Mangei, Dr. Liliana Francois Martín del Campo, Dr. Lidia Silva, Dr. Niclas Kneisel, Theresa Schmid, Dr. Yashna Paul, Milena Simovic, Umar Khalid, Karol Urbanek, Dr. Manasi Ratnaparkhe, Dr. Christian Aichmüller, Dr. Emma Phlips, Tolga Lokumcu, Dr. Himanshu Soni, Pavle Boskovic, Ka Hou Man, and Yuan Peng, for contributing to make every moment in the laboratory not only enlightening and of high scientific value, but also fun and memorable.

I would like to thank Christoph Schifflers and Mariam Mamdouh Shafik Saleh for crucially contributing to this work with their genuine interest and hardworking attitude. It was a privilege and great pleasure to supervise them during their master studies, which also represented an instructive experience for me.

9 Acknowledgments

I would also like to thank my friends, Michael Persicke, Franziska Haderk, Lidia Silva, Jasmin Mangei, Liliana Francois Martín del Campo, Marie Bordas, Christoph Schifflers, Mariam Mamdouh Shafik Saleh, Manuel Rodriguez-Paredes, Nicole Colaianni, Ona Sociats, Carla Codina, Jaume Fortuny, Anna Llorens, and Ricard Argelaguet, who were a source of inspiration and numerous joyful moments that made these last almost-four-and-a-half years a truly delightful and enriching experience.

I would like to thank my family for their love and unwavering support: als meus pares Josep Ramón i Sabina, als meus germans Marina, Cecília i Gabriel, i al Fer, vull agrair-los l'escalf i l'amor transmès en cada pas del camí. Gràcies per ajudar-me a encarar els obstacles amb una actitud positiva i compartir l'alegria de cada propòsit aconseguit. A més, m 'agradaria estendre aquest agraïment a la resta de la meva família, pel seu suport incondicional i per fer-se sentir sempre a la vora.

And last, my deepest thanks to Florian Köhler, who not only substantially contributed to this work with his constructive criticism and thoughtful advice, but also lit up every single day of these last four years with his enthusiastic, loving, and adventurous nature. Thank you for running with me through every winding forest path, steeper climb, and mountain trail that life brings, and for all those routes that are yet come to come.